

August 2015

Design and Synthesis of Polybetaines for Nonfouling Applications

Katherine A. Gibney
Polymer Science and Engineering

Follow this and additional works at: https://scholarworks.umass.edu/dissertations_2

Recommended Citation

Gibney, Katherine A., "Design and Synthesis of Polybetaines for Nonfouling Applications" (2015). *Doctoral Dissertations*. 356.

https://scholarworks.umass.edu/dissertations_2/356

This Campus-Only Access for Five (5) Years is brought to you for free and open access by the Dissertations and Theses at ScholarWorks@UMass Amherst. It has been accepted for inclusion in Doctoral Dissertations by an authorized administrator of ScholarWorks@UMass Amherst. For more information, please contact scholarworks@library.umass.edu.

DESIGN AND SYNTHESIS OF POLYBETAINES FOR NONFOULING
APPLICATIONS

A Dissertation Presented

by

KATHERINE A. GIBNEY

Submitted to the Graduate School of the
University of Massachusetts Amherst in partial fulfillment
of the requirements for the degree of

DOCTOR OF PHILOSOPHY

May 2015

Polymer Science and Engineering

DESIGN AND SYNTHESIS OF POLYBETAINES FOR NONFOULING
APPLICATIONS

A Dissertation Presented

by

KATHERINE A. GIBNEY

Approved as to style and content by:

Gregory N. Tew, Chair

Kenneth R. Carter, Member

Richard W. Vachet, Member

David A. Hoagland, Department Head
Polymer Science and Engineering

DEDICATION

*To my parents –
who have only ever wanted the best for us in this world, and expected us to make it a
better place*

ACKNOWLEDGEMENTS

First and foremost, I want to thank my advisor Prof. Gregory Tew. His support and guidance have been invaluable over the past five years. Likewise, my committee members Prof. Ken Carter and Prof. Richard Vachet have not only taken the time to be on my committee but also forced me to think about my science critically. I truly believe I have grown as a scientist during my time here and I am forever grateful for all their help.

I also want to thank my undergraduate advisor Prof. Kenichi Kuroda and his lab members (now Professor) Edmund Palermo and Dr. Iva Sovadinova. Not only were they unbelievably supportive and welcoming when I first started working in lab, they helped guide me to a career in science. Even after I embarked on the next step, they remained incredibly supportive. They are wonderful scientists and people, and I feel lucky to have known them.

The PSE staff has been amazing. Weiguo, Jack, Sekar, Steve, Lisa and Maria were amazing sources of knowledge and support. Likewise, I would like to acknowledge my collaborators through the ONR, specifically Zhan Chen's group (Yuwei Liu and Chuan Leng) at the University of Michigan and Shane Stafslie at North Dakota State University for their scientific knowledge and ability, and (more than a little) patience.

Of course, the Tew group members have been amazing collaborators, mentors, friends and a *de facto* support group. Brittany, Joel, Madhura, Ilker, Coralie, Kelly and Nick: thank you for seeing me off and I wish you all the best. I sincerely hope that in my time sharing a lab with you I was able to provide some help and guidance. Cathy, my classmate and groupmate, you were always at least a step ahead of me and having such a great friend in the group to celebrate and commiserate with was priceless. Tew group

members past: Mike, Melissa, Hitesh, Jun, Yongping, Ozgul, Semra, Raj, Fede, Bob, Abhi, Jing, Ke, and Yan – I learned so much from all of you, tangibly and intangibly. I hope our paths cross again in the future. Semra, you have been incredibly supportive of me and I am forever in your debt. And of course, I want to thank Trouble who made life so much easier and so much more exciting.

Graduate school is a difficult undertaking. It can be (and more often than not is) a painful, frustrating process. Having good friends makes the ride a little easier though. Andrew and Neith, Cathy and Travis, Isaac, Ray, Brittany, Dan, and Yana: you all made life bearable during the rough patches and even more fun the rest of the time. Former lab partners Irem and Varun: it was a great experience being able to work with you that first semester when everything seemed scary and overwhelming, and an even better experience becoming friends. The incoming class of 2009 was small but amazing. Again, I hope all of our paths cross again and I know that everyone is going on to great things. I met so many interesting people throughout my time in PSE and I am honored to have had that experience.

I'm sure they know this already, but I need to say that my family has been the single greatest source of support during my time in graduate school. Through the especially difficult times they provided a shoulder to cry on and tough love. My parents, to their credit, never said they wanted their children to be doctors or lawyers or any of that. They did, however, want my sister and me to go forward and contribute something great to this world. I hope to be able to live up to that.

ABSTRACT

DESIGN AND SYNTHESIS OF POLYBETAINES FOR NONFOULING APPLICATIONS

MAY 2015

KATHERINE A. GIBNEY, B.S.c, UNIVERSITY OF MICHIGAN ANN ARBOR

M.S., UNIVERSITY OF MASSACHUSETTS AMHERST

Ph.D., UNIVERSITY OF MASSACHUSETTS AMHERST

Directed by: Professor Gregory N. Tew

Polybetaines represent a unique class of charged polymers. These polymers contain both a positive and negative charge on each repeat unit so that the polymer itself is charge-neutral. The highly polar nature of the betaine gives rise to biocompatibility and strong hydration, making polybetaines attractive biomaterials. Ring-opening metathesis polymerization's utility in polymerizing charged monomers opened up a new avenue to obtain polybetaines. Dual-functional polybetaines obtained by ring-opening the imide group of cationic oxanorbornene-based polymers were previously described. Here, that chemistry is expanded upon to create a broad library of new betaines. First, the ring-opening reaction in oxanorbornene imides is explored in-depth so that it can be developed into an efficient set of post-polymerization functionalization reactions. New betaines based on the oxanorbornene scaffold are then synthesized, taking advantage of this dual-functional chemistry. A range of well-defined, amphiphilic betaines that contain alkyl, benzyl and fluorinated moieties are obtained in this way. Additionally, the more traditional linear carboxybetaine and sulfobetaine structures are incorporated into the oxanorbornene imide backbone as well. These materials then allow us to study the

structure-property relationships between the diverse betaine chemistries and their surface and nonfouling properties.

TABLE OF CONTENTS

	Page
ACKNOWLEDGEMENTS	v
ABSTRACT	vii
LIST OF TABLES	xii
LIST OF FIGURES	xiii
CHAPTER	
1. AN OVERVIEW OF POLYBETAINES	1
1.1 Introduction	1
1.2 Properties of Charged Polymers	1
1.3 Polybetaine Synthesis	5
1.4 Biofouling	7
1.5 Nonfouling Strategies	10
1.5.1 Hydrophilic Materials	10
1.5.2 Amphiphilic materials	12
1.6 Oxanorbornene-based Betaines	16
1.7 Scope of the Thesis	17
1.8 References	19
2. RING-OPENING IN NORBORNENE-BASED IMIDES	26
2.1 Introduction	26
2.2 Ring-opening Properties of Poly(oxanorbornene imide)s	27
2.3 ¹ H NMR Spectroscopy Characterization of Ring-opened Oxanorbornene imides	32
2.4 Characterization of Poly1	36
2.4.1 Solution Properties of Poly1(Am)	39
2.5 Amine-catalyzed ring-opening	42
2.5.1 Characterization of Poly2	43
2.6 Characterization of Unsubstituted Imide Poly7 Ring-opening	46
2.7 Experimental Procedures	49

2.8	Conclusions.....	54
2.9	References.....	54
3.	SYNTHESIS OF POLYBETAINES BY RING-OPENING METATHESIS POLYMERIZATION	57
3.1	Introduction.....	57
3.2	General Approach	58
3.3	Monomer Synthesis	60
	3.3.1 Hydrophilic Dual-functional and Linear betaines.....	60
	3.3.2 Amphiphilic dual-functional betaines.....	64
3.4	Polymer synthesis	69
3.5	Experiment Procedures	71
3.6	Conclusions.....	87
3.7	References.....	87
4.	NORBORNENE-BASED POLYMERS FOR SURFACE MODIFICATION	90
4.1	Introduction.....	90
4.2	General Approach	91
4.3	Polymer Synthesis and Characterization	93
4.4	Surface Functionalization and Coating Characterization	97
4.5	Protein Adsorption.....	101
4.6	PDMS Functionalization.....	107
4.7	Experimental Procedures	110
4.8	Conclusions.....	114
4.9	References.....	115
5.	NONFOULING PROPERTIES OF HYDROPHILIC BETAINES: EFFECT OF INTERCHARGE DISTANCE.....	117
5.1	Introduction.....	117
5.2	General Approach	117
5.3	Coating Preparation and Characterization	119
	5.3.1 Polymer Synthesis.....	119
	5.3.2 Surface Characterization	121
5.4	Protein Adsorption.....	128
5.5	Experimental Procedures	134
5.6	Conclusions.....	141
5.7	References.....	142

6.	NONFOULING PROPERTIES OF AMPHIPHILIC BETAINES: EFFECT OF HYDROPHOBIC SUBSTITUENTS	144
	6.1 Introduction.....	144
	6.2 General Approach	144
	6.3.1 Polymer Synthesis.....	146
	6.3.2 Surface Characterization	148
	6.4 Protein Adsorption	154
	6.5 Sum Frequency Generation Spectroscopy	165
	6.6 Experimental Procedures	171
	6.7 Conclusions.....	178
	6.8 References.....	179
7.	CHARGED HYDROGELS FROM NORBORNENE-BASED POLYMERS	181
	7.1 Introduction.....	181
	7.2 Hydrogel Synthesis	182
	7.2.1 Polymer Precursor Synthesis	182
	7.2.2 Gelation.....	183
	7.3 Gel Characterization	187
	7.3.1 Network Chemistry	187
	7.3.2 Swelling Properties and Water Uptake	188
	7.4 Experimental Procedures	192
	7.5 Conclusions.....	194
	7.6 References.....	195
	BIBLIOGRAPHY.....	197

LIST OF TABLES

Table		Page
2.1.	Ring-opening reactions for a selection of functionalized oxanorbornene imides with sodium hydroxide and n-butylamine.....	29
2.2.	Ring-opening reactions in water-miscible organic solvents.	30
3.1.	Summary of linear betaine structures.	61
3.2.	Summary of amphiphilic dual-functional betaine structures.	65
4.1.	Compositional characterization of random and block polymers by NMR spectroscopy.....	94
4.2.	Surface properties of random and block copolymers.	101
4.3.	Experimental parameters to prepare functionalized PDMS surfaces	108
5.1.	Composition and molecular weight characterization of hydrophilic polymers by NMR spectroscopy.....	121
5.2.	Surface properties of hydrophilic zwitterionic coatings	125
6.1.	Summary of amphiphilic dual-functional betaine structures.	146
6.2.	Composition and molecular weight characterization of amphiphilic polymers by NMR spectroscopy.....	147
6.3.	Surface properties of amphiphilic zwitterionic coatings	154
7.1.	Attempted gelation conditions between Poly1-4 and PAA	185

LIST OF FIGURES

Figure	Page
1.1.	General structures of charged polymers: (a) polyelectrolyte; (b) polyzwitterion; (c) polyampholyte; (d) polybetaine.2
1.2.	Solution properties of charged polymers: (a) cationic polymer exhibiting the polyelectrolyte effect; (b) zwitterionic polymer exhibiting the antipolyelectrolyte effect; (c) schematic representation of polyzwitterions' charge shielding in an aqueous electrolyte solution.3
1.3.	Zwitterionic structures: (a) phosphorylcholine, (b) carboxybetaine, and (c) sulfobetaine.4
1.4.	Stepwise colonization process of a marine foulant. (Reproduced from Bixler <i>et al</i> , Phil. Trans. R. Soc. A, 2012.)8
1.5.	Examples of foulants: (a) adsorbed protein on an explanted device (reproduced from Mosquera <i>et al</i> , Rev Esp Cardiol., 2011); (b) bacterial biofilm (reproduced from http://dujs.dartmouth.edu/fall-2009/biofilms-bacteria); and (c) adult barnacles (reproduced from Callow <i>et al</i> , Nat. Commun., 2011).8
1.6.	Schematic representation of an ambiguous nonfouling amphiphilic surface where the green domains represent hydrophobic segments and the blue domains represent hydrophilic segments. (Reproduced from Callow <i>et al</i> , Nat. Commun., 2011.)13
1.7.	Representative amphiphilic polymer and surfaces for nonfouling applications: (a) Styrenic block copolymer containing a PEGylated/fluorinated side chain (reproduced from Krishnan <i>et al</i> , Langmuir, 2006); (b) AFM images of a surface-active block copolymer (i) in air and (ii) in water, undergoing characteristic rearrangement (reproduced from Martinelli <i>et al</i> , Langmuir, 2008).14
1.8.	Structures of dual-functional (right image) and linear (left image) oxanorbornene-based polybetaines. (Reproduced from Colak <i>et al</i> , Langmuir, 2012.)16
2.1.	Schematic representation of poly(oxanorbornene imide) ring-opening in the presence of sodium hydroxide and primary amines.28

2.2.	General conditions for the synthesis and ring-opening of poly(oxanorbornene imide)s to create carboxylate- and diamide-containing polymers: (i) Grubbs' 3 rd generation catalyst, solvent, 20 minutes, room temperature; (ii) ethyl vinyl ether, 1 hour; (iii) 0.1 M NaOH, 1 hour; (iv) n-butylamine (excess), THF/H ₂ O, 1 hour, room temperature.	32
2.3.	NMR spectra of the model oxanorbornene imide monomer 2 demonstrating hydroxide and amine reactivity: (a) monomer as synthesized (in DMSO-d ₆); (b) ring-opened monomer containing both carboxylate and amide functional groups (in 0.1 M NaOD); (c) purified diamide monomer after reaction with n-butylamine (in DMSO-d ₆); and (d) corresponding carbon spectra of (b) and (c) showing the characteristic (i) carboxylate and amide peaks and (ii) unequivocal amide peaks.	33
2.4.	¹ H NMR spectra in D ₂ O of (a) the as-prepared cationic imide polymer Poly1_{n=20} and (b) the base-treated zwitterionic polymer Poly1(Am)_{n=20} . The complete upfield shift of the methylene protons <i>D</i> to <i>D'</i> confirm quantitative conversion.	35
2.5.	¹ H NMR spectra in DMSO-d ₆ of (a) the as-prepared imide polymer Poly2_{n=20} and (b) the butylamine-treated polymer Poly2(Am)_{n=20} . The complete upfield shift of the methylene protons <i>D</i> to <i>D'</i> confirm quantitative conversion.	36
2.6.	FT-IR spectra of Poly1_{n=20} (black line) and Poly1(Am)_{n=20} (green line). Dotted vertical line indicates characteristic imide resonance at 1707 cm ⁻¹	37
2.7.	GPC traces of Poly1_{n=10} (black line) and Poly1(Am)_{n=10} (green line) in 2,2,2-trifluoroethanol with 20 mM NaTFA as the eluent, relative to PMMA standards. Spectra show retention of monomodal distribution after base treatment.	38
2.8.	Dynamic light scattering data from Poly1_{n=230} and Poly1(Am)_{n=230} in 0.1 M NaBr, where (■) represent the cationic imide form and (○) represent the ring-opened zwitterionic form. (a) Representative diameter distributions at 90° by number weight, with peak maxima observed at approximately 10 and 24 nm for Poly1_{n=230} and Poly1(Am)_{n=230} , respectively. (b) Γ vs. q^2 plots.	41
2.9.	Effect of primary amine on the conversion to the ring-opened form of 1 as a function of the initial ratio of reactants. Conversion was calculated by ¹ H NMR spectroscopy.	43

2.10.	Characterization of the conversion from Poly2_{n=20} to Poly2(dAm)_{n=20} by n-butylamine. (a) FT-IR spectra (b) GPC traces for Poly2_{n=20} (black line) and Poly2(dAm)_{n=20} (blue line). GPC traces were obtained in DMF with 0.01 M LiCl as the eluent, relative to PMMA standards.	45
2.11.	Ring-opening reaction of poly(oxanorbornene imide) Poly7 in the presence of sodium hydroxide. (a) Reaction scheme and structures showing the progression from the imide form (black) to partial ring-opening (red) to full conversion to the amide and carboxylate groups (blue) after exposure to 0.1 M NaOH; (b) FT-IR spectra of Poly7 showing the ring-opening reaction progression. Dotted vertical line indicates characteristic imide resonance at 1707 cm ⁻¹	47
3.1.	Synthesis of cationic precursor and zwitterionic oxanorbornene imide-based monomers. (a) (i) <i>N,N</i> -dimethylalkyldiamine, methanol/tetrahydrofuran, 60 °C (1 hour) to 50 °C, overnight; (ii) dimethylsulfate, tetrahydrofuran, 0 °C to room temperature, 4 hours; (b) (i) <i>N,N</i> -dimethylethylenediamine, methanol/tetrahydrofuran, 60 °C (1 hour) to 50 °C, overnight; (ii) R-X, tetrahydrofuran or acetonitrile, 50 °C, 48 hours.	59
3.2.	Synthesis of linear carboxy- and sulfobetaines: (a) (i) THF, 50 °C, 48 hours; (ii) THF, room temperature, overnight; (iii) 5.0 M HCl (aq), 30 minutes; (b) (i) acetonitrile, 1 wt % 1,3-dinitrobenzene, 50 °C, 48 hours.	62
3.3.	Representative FT-IR spectra of the cationic precursor Carboxy(+) and the deprotected zwitterionic Carboxy(ZI) monomers.	63
3.4.	Synthesis of hydrophobe precursors. (a) (i) 4-toluenesulfonyl chloride, triethylamine, THF, 0 °C – room temperature, 3 hours; (b) trifluoromethanesulfonic anhydride, pyridine, DCM/dioxane, 30 minutes.	66
3.5.	Representative NMR spectra in MeOD-d ₄ of monomer Amph(+h) . (a) ¹ H NMR and (b) ¹⁹ F NMR spectra (TFA used as standard).	68
3.6.	Representative polymerization conditions for the C₁(+) , Carboxy(+) , Sulfo(ZI) , and Amph(+) series: (i) Grubbs' 3 rd generation catalyst, TFE/CH ₂ Cl ₂ , room temperature, 15-35 minutes; (ii) ethyl vinyl ether, room temperature, 1 hour.	69

3.7.	Kinetics for the homopolymerizations by ROMP of monomer Amph(+) h , where [Amph(+) h] ₀ 80 mM and [monomer] ₀ : [catalyst] ₀ = 50:1. (a) Conversion as a function of time as calculated from ¹ H NMR spectra; (b) First-order time conversion with linear fit; (c) Representative GPC trace after 8 minutes (~70% conversion). 2,2,2-trifluoroethanol + 0.1% NaTFA was used as the eluent, with molecular weights calculated relative to PMMA standards.	70
4.1.	Schematic representation of random and block copolymers containing zwitterionic and siloxane-containing side chains for surface modification.	92
4.2.	Synthesis of model sulfobetaine polymers for surface modification. (a) Random copolymers: (i) 5-(bicycloheptenyl)-triethoxysilane, G3, CH ₂ Cl ₂ /TFE, room temperature, 30 minutes; (ii) ethyl vinyl ether, room temperature, 1 hour; (b) Block copolymers: (i) G3, CH ₂ Cl ₂ /TFE, room temperature, 15 minutes; (ii) 5-(bicycloheptenyl)-triethoxysilane, CH ₂ Cl ₂ , room temperature, 10 minutes; (iii) ethyl vinyl ether, room temperature, 1 hour.	93
4.3.	Representative NMR spectra of (a) rP[Sulfo(ZI)b] _{30,6} in D ₂ O/NaBr; (b) bP[Sulfo(ZI)b] _{30,6} in D ₂ O/NaBr; and (c) bP[Sulfo(ZI)b] _{30,6} in TFE-d ₃ . Arrows indicate -Si(OCH ₂ CH ₃) ₃ peak shifts.	95
4.4.	General procedure for coating preparation on silicon wafers.	97
4.5.	AFM tapping mode height images of (a) rP[Sulfo(ZI)b] _{33,3} ; (b) rP[Sulfo(ZI)b] _{30,6} ; and (c) rP[Sulfo(ZI)b] _{18,18} . All images represent a 1 μm x 1 μm x 7.5 nm area.	98
4.6.	AFM tapping mode height images of (a) bP[Sulfo(ZI)b] _{33,3} ; (b) bP[Sulfo(ZI)b] _{30,6} ; (c) bP[Sulfo(ZI)b] _{18,18} ; and (d) bP[Sulfo(ZI)b] _{70,10} . All images represent a 1 μm x 1 μm x 30 nm area.	99
4.7.	Fibrinogen adsorption on (a) random, and (b) block copolymer surfaces. A silica surface (shaded bar) was used as a control. Error bars represent ± standard deviation, based on at least 3 independent measurements.	103
4.8.	AFM height images of (a) 1:1 rP[Sulfo(ZI)b] _{30,6} : bP[Sulfo(ZI)b] _{70,10} ; and (b) 7:3 rP[Sulfo(ZI)b] _{30,6} : bP[Sulfo(ZI)b] _{70,10} . All images represent a 1 μm x 1 μm x 5 nm area.	105
4.9.	Fibrinogen adsorption on random copolymer, block copolymer and mixed surfaces. A silica surface (shaded bar) was used as a control. Error bars represent ± standard deviation, based on at least 3 independent measurements.	106

4.10.	Grazing angle FT-IR spectra of PDMS substrate (top line, magenta), and oxidized PDMS functionalized with rP[Sulfo(ZI)b]_{30,6} (bottom line, black). Dotted lines highlight characteristic imide frequencies at 1779 cm ⁻¹ and 1704 cm ⁻¹	107
4.11.	Surface characteristics of functionalized PDMS by (a) AFM and (b) optical microscopy images. The AFM image represents a 1 μm x 1 μm x 5 nm area.	109
5.1.	Polymers used to study the effect of charge distribution on oxanorbornene-based (a) dual-functional betaines, (b) carboxybetaines, and (c) sulfobetaines.	118
5.2.	Polymerization of the C₁(ZI) , Carboxy(ZI) , and Sulfo(ZI) series and representative post-polymerization functionalization reactions: (a) (i) Grubbs' 3 rd generation catalyst, TFE/CH ₂ Cl ₂ , room temperature, 30 minutes; (ii) excess ethyl vinyl ether, room temperature, 1 hour; (b) (i) 0.1 M NaOH, 20 minutes; (c) (i) HCl (g), overnight.....	120
5.3.	Representative FT-IR spectra of the cured and post-functionalized (a) rP[C₁(ZI)] , (b) rP[Carboxy(ZI)] and (c) rP[Sulfo(ZI)] surfaces. Characteristic peaks corresponding to imide (1707 cm ⁻¹), amide (1580 cm ⁻¹), carboxylic acid (1650/1630 and 1390 cm ⁻¹) and sulfonate (1395 and 1187 cm ⁻¹) functional groups are marked with the dotted lines.....	124
5.4.	Representative tapping mode AFM height (top) and phase (bottom) images of (a) rP[Sulfo(ZI)a] and (b) rP[Sulfo(ZI)b] surfaces. Images represent a 1 μm x 1 μm area, where the z axis is 5 nm for the height images.	126
5.5.	Fibrinogen adsorption as measured by ellipsometry for the (a) rP[C₁(ZI)] series; (b) rP[Carboxy(ZI)] series; and (c) rP[Sulfo(ZI)] series. Controls are indicated by the shaded bars. Error bars represent ± standard deviation, based on at least 3 independent measurements.	129
5.6.	Fibrinogen adsorption vs. alkyl spacer length (m or n) for rP[C₁(ZI)] (green diamonds) and rP[Carboxy(ZI)] (red squares) surfaces.	131
5.7.	Fibrinogen adsorption vs. advancing water contact angle for rP[C₁(ZI)] (green diamonds), rP[Carboxy(ZI)] (red squares), and rP[Sulfo(ZI)] (blue circles) surfaces.....	132
6.1.	Polymers used to study the effect of amphiphilic structure on oxanorbornene-based dual-functional polybetaines: (a) hydrocarbon hydrophobic groups; and (b) fluorinated hydrophobic groups.	145

6.2.	Polymerization of the Amph(ZI) series and representative post-polymerization functionalization reactions: (a) (i) Grubbs' 3 rd generation catalyst, TFE/CH ₂ Cl ₂ , room temperature, 40 minutes; (ii) excess ethyl vinyl ether, room temperature, 1 hour; (b) (i) 1:1 0.2 M NaOH:DMF, 20 minutes.....	147
6.3.	Representative FT-IR spectrum of rP[Amph(ZI)c] . The blue arrow highlights a weak peak corresponding to the imide carbonyl group at approximately 1700 cm ⁻¹	148
6.4.	XPS spectra of (a) sP[Amph(ZI)c] and (b) sP[Amph(ZI)l] . A representative fluorine peak is highlighted in (b)	149
6.5.	Tapping-mode AFM height images of zwitterionic, amphiphilic surfaces: (a) rP[Amph(ZI)a] ; (b) rP[Amph(ZI)b] ; (c) rP[Amph(ZI)c] ; (d) rP[Amph(ZI)d] ; (e) rP[Amph(ZI)e] ; (f) rP[Amph(ZI)f] ; (g) rP[Amph(ZI)g] ; (h) rP[Amph(ZI)h] ; (i) rP[Amph(ZI)i] ; (j) rP[Amph(ZI)j] ; (k) rP[Amph(ZI)k] ; and (l) rP[Amph(ZI)l] . Images (a)-(i) and (k)-(l) represent a 1 μm x 1 μm x 5 nm area. Image (j) represents a 1 μm x 1 μm x 30 nm area.	151
6.6.	Tapping-mode AFM height (top) and phase (bottom) images of zwitterionic, amphiphilic surfaces: (a) rP[Amph(ZI)c] , and (b) rP[Amph(ZI)l]	152
6.7.	Nonfouling properties of rP[Amph(ZI)a] , rP[Amph(ZI)b] , and rP[Amph(ZI)c] : (a) fibrinogen adsorption, and (b) fibrinogen adsorption as a function of advancing water contact angle. Controls are indicated by the shaded bars. Error bars represent ± standard deviation, based on at least 3 independent measurements.....	156
6.8.	Nonfouling properties of rP[Amph(ZI)b] , rP[Amph(ZI)g] , rP[Amph(ZI)d] , rP[Amph(ZI)h] , rP[Amph(ZI)c] , and rP[Amph(ZI)l] : (a) fibrinogen adsorption, (b) fibrinogen adsorption as a function of advancing water contact angle, (c) fibrinogen adsorption as a function of surface free energy, and (d) advancing water contact angle (open black bars) and surface free energy by surface (solid blue bars). Nonfluorinated surfaces are indicated by the shaded bars. Error bars represent ± standard deviation, based on at least 3 independent measurements.....	159

6.9.	Nonfouling properties of rP[Amph(ZI)d] , rP[Amph(ZI)e] , rP[Amph(ZI)f] , rP[Amph(ZI)g] , rP[Amph(ZI)h] , and rP[Amph(ZI)i] : (a) fibrinogen adsorption, (b) fibrinogen adsorption as a function of advancing water contact angle, (c) fibrinogen adsorption as a function of surface free energy, and (d) advancing water contact angle (open black bars) and surface free energy by surface (solid blue bars). Asymmetrically substituted benzyl surfaces are indicated by the shaded bars. Error bars represent \pm standard deviation, based on at least 3 independent measurements.....	162
6.10.	Fibrinogen adsorption as a function of (a) advancing water contact and (b) surface free energy for the Amph(ZI) series.....	164
6.11.	Structures of dual-functional betaines studied by SFG spectroscopy: (a) rP[Amph(ZI)b] , (b) rP[Amph(ZI)j] , and (c) rP[OEG(ZI)]	165
6.12.	SFG spectra of rP[OEG(ZI)] (black line), rP[Amph(ZI)b] (red line), and rP[Amph(ZI)j] (blue line) (a) in air, and (b) in D ₂ O. The peak at 2975 cm ⁻¹ corresponding to the quaternary amine group is highlighted with a dotted line. (Reproduced from Leng <i>et al.</i> , ACS Macro Letters, 2013.)	167
6.13.	SFG spectra of rP[Amph(ZI)j] in air (black line) and in D ₂ O (red line) for the (a) C-F and (b) -C=O functional groups. (Reproduced from Leng <i>et al.</i> , ACS Macro Letters, 2013.).....	168
7.1.	Synthesis of poly(oxanorbornene imide) polymer precursors. (a) (i) Grubbs' 3 rd generation catalyst, TFE/CH ₂ Cl ₂ , room temperature, 30 minutes; (ii) ethyl vinyl ether, room temperature, 1 hour; (b) (i) 1:1 CH ₂ Cl ₂ :TFA, room temperature, overnight.	183
7.2.	General gelation reaction between Poly1-4 and PAA in water.	184
7.3.	Resulting gels from (a) Poly2/PAA and (b) Poly3/PAA	186
7.4.	Representative IR spectrum of a dehydrated Poly2/PAA gel. Frequencies corresponding to imide groups (fine dotted line) and amide and carboxylate groups (bold dotted lines) are marked for clarity.	187
7.5.	Swelling ratios of an SBMA control gel, and Poly2/PAA , Poly3/PAA , and Poly4/PAA gels (1/1.5 mol/mol) at varying salt concentrations. Error bars represent \pm standard deviation based on at least three samples, when available.....	189

CHAPTER 1

AN OVERVIEW OF POLYBETAINES

1.1 Introduction

Charged molecules are seen throughout the natural world and are often vital components of biological systems, such as the cellular membrane.¹ Nature itself creates well-defined charged macromolecules and biopolymers such as proteins and polypeptides. Synthetic charged molecules and polymers are of great interest both for biological applications, and industrial and materials applications.²⁻⁵ Polyzwitterions are a unique class of charged polymers that contain both positive and negative charges, but are overall net neutral.^{2,3} These polymers are largely biocompatible and water-soluble, thus their use in biological applications. With the advent of more advanced and facile polymerization techniques, zwitterionic chemistries can be expanded to widen their applicability and gain access to new material properties.

1.2 Properties of Charged Polymers

Charged polymers can be divided into two general groups: polyelectrolytes and polyzwitterions.^{2,3} Polyelectrolytes (Figure 1.1a) contain one type of charged moiety, either cationic or anionic. These polymers have an overall net charge, determined by their chemical structure. In contrast, polyzwitterions (Figure 1.1b) contain both cationic *and* anionic groups, and can be further differentiated based on the configuration of the charges. In polyampholytes, the opposite charges are sequestered on separate repeat units (Figure 1.1c), whereas in polybetaines each repeat unit contains a positive and negative

charge (Figure 1.1d). While polybetaines are intrinsically charge-neutral, polyampholytes may have an overall net charge or a localized net charge based on the sequence of the repeat units. Depending on the nature of the charged functional groups, a polymer may transition between an electrolyte and neutral or between an electrolyte and a zwitterion based on the environment.

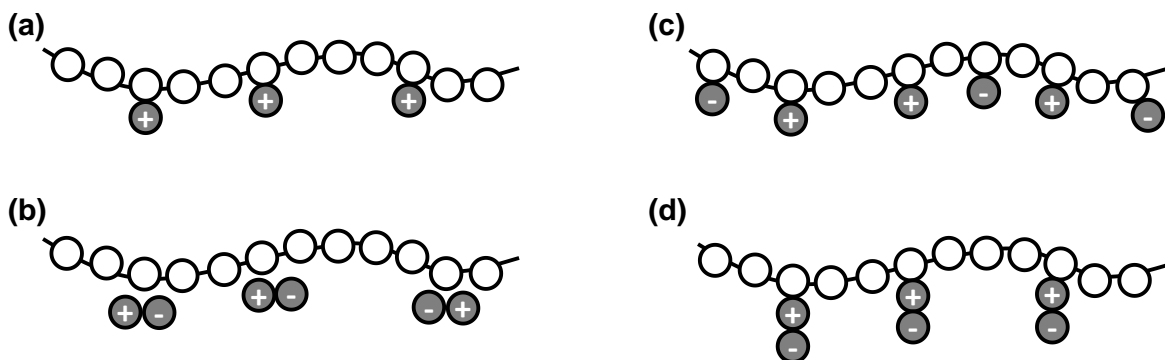


Figure 1.1: General structures of charged polymers: **(a)** polyelectrolyte; **(b)** polyzwitterion; **(c)** polyampholyte; **(d)** polybetaine.

Charged polymers possess unique solution properties due to their polar functional groups and connectivity.^{2,3} While the polymer chemistry and architecture dictates the precise behavior of a given polymer in solution, the *polyelectrolyte effect* (Figure 1.2a) and *antipolyelectrolyte effect* (Figure 1.2b) describe most charged polymers' behavior in aqueous solutions. As might be expected, polyelectrolytes are freely soluble in deionized water. The charged moieties are highly hydrated in aqueous solutions, and intra- and intermolecular Coulombic repulsions between the charged groups drive the polymer to take on an extended chain conformation. Certain polyzwitterions, such as those containing phosphatidylcholine betaines, behave similarly as well.⁶ Small molecule electrolytes in solution, however, shield the electrostatic interactions between charged

groups. Without the additional repulsive forces, the polymer chains take on a collapsed conformation and at high enough salt concentrations can precipitate out of solution. This phenomenon is dubbed the polyelectrolyte effect. Many polyelectrolytes, on the other hand, exhibit the antipolyelectrolyte effect. In this case, the strong intra- and intermolecular interactions between the betaine groups cause the polymer chains to aggregate. In an electrolyte solution, the polymers' charged groups are shielded from one another and the chains swell (Figure 1.2c).

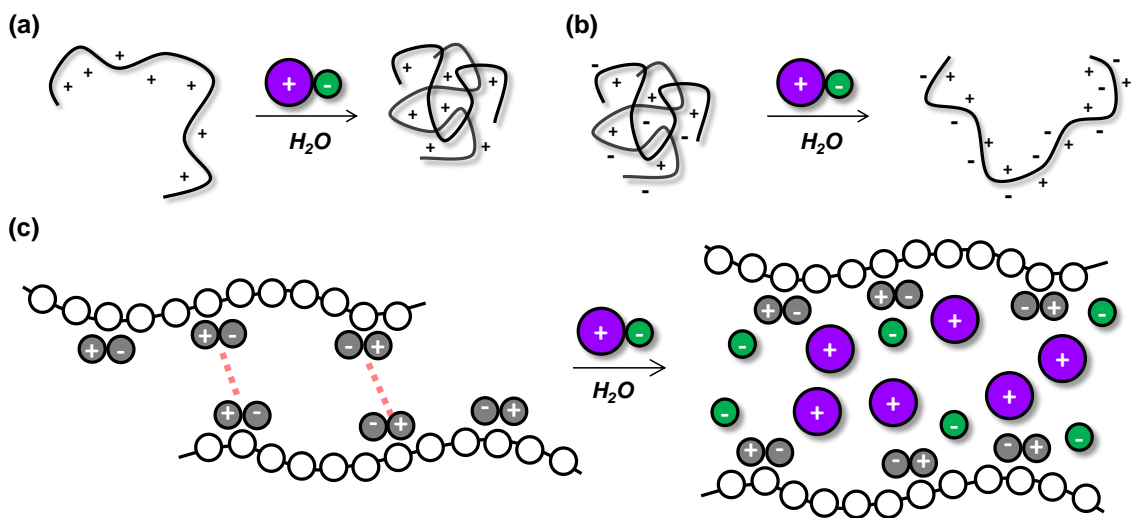


Figure 1.2: Solution properties of charged polymers: **(a)** cationic polymer exhibiting the polyelectrolyte effect; **(b)** zwitterionic polymer exhibiting the antipolyelectrolyte effect; **(c)** schematic representation of polyelectrolytes' charge shielding in an aqueous electrolyte solution.

Polyelectrolytes and polyelectrolytes are further differentiated from one another, and from non-charged polymers, by their solubility in organic solvents as well. Many polyelectrolytes are largely soluble in both protic and aprotic polar organic solvents, including: methanol, ethanol, DMSO and DMF. This solubility in organics, especially volatile organics, has important implications for synthesis and applications, as discussed later. Most polyelectrolytes, however, are largely insoluble in organic solvents especially

at higher molecular weights. An important exception is 2,2,2-trifluoroethanol (TFE). TFE is a good solvent for polyzwitterions, even better than high ionic strength aqueous solutions.²

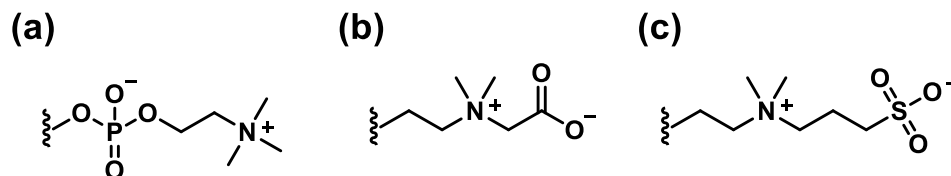


Figure 1.3: Zwitterionic structures: (a) phosphorylcholine, (b) carboxybetaine, and (c) sulfobetaine.

Common zwitterionic structures are given in Figure 1.3.^{2,4} While these linearly configured betaines are often utilized in synthetic systems, they are direct analogues of naturally occurring charged groups found in peptides and amino acids.² In these betaines, the cationic group is a quaternary amine and the anionic group varies. Other quaternary amines can be used as well, including pyridine- and imidazole-derived cations. These subtle structural differences, however, can have important ramifications. The phosphorylcholine (PC) group (Figure 1.3a) is unique among these betaines in that its polymers typically exhibit the polyelectrolyte effect as opposed to the antipolyelectrolyte effect.⁶ The carboxybetaine moiety (Figure 1.3b) is pH-sensitive: by protonating and deprotonating the carboxylic acid, the structure can transition between cationic and zwitterionic. In fact, this property can be utilized in responsive systems. The sulfobetaine group (Figure 1.3c) is zwitterionic regardless of the environmental conditions.

1.3 Polybetaine Synthesis

Zwitterionic functional groups have been incorporated into synthetic polymers in a variety of ways.²⁻⁴ Methacrylic phosphorylcholine (PC)-based polymers, for example, are among the most thoroughly studied polybetaines.⁶⁻⁸ This group of polymers has been expanded to include a variety of backbone chemistries such as PC-polyolefins and polyesters,⁹⁻¹¹ demonstrating the versatility of this biomimetic functionality. More recently, a large body of research has been devoted to the synthesis and applications of acrylate- and acrylamide-based carboxybetaines and sulfobetaines.⁴ Free radical polymerization is very tolerant of zwitterionic monomers.²⁻⁴ Controlled radical polymerization techniques such as ATRP and RAFT have been used as well, with good results.¹²⁻¹⁹ Solubility was sometimes an issue in these systems, but conditions could usually be optimized to obtain polymers in aqueous or organic solutions. In fact, surface-initiated ATRP, both aqueous and organic, has been used extensively to synthesize polycarboxybetaine and polysulfobetaine brushes for nonfouling applications.¹⁶⁻¹⁹

Due to their highly polar functional groups, zwitterionic monomers can interfere with certain polymerization techniques, such as anionic polymerization.²⁻⁴ This issue can be overcome by post-polymerization functionalization reactions. Group transfer polymerization (GTP) was used to polymerize the 2-(dimethylamino)ethyl methacrylate, which was then reacted with 1,3-butane sultone to give the betaine.²⁰ This functionalization reaction was incomplete however, and the resulting polymer contained some residual cationic groups. Alternatively, a polyester with a pendant alkyne group was synthesized by ring-opening polymerization from a lactone.¹¹ Using click chemistry, the polymer was then quantitatively functionalized with PC groups. Likewise,

zwitterionic poly(oxazolines) were recently synthesized by polymerizing oxazolines with pendant alkene groups, which were then functionalized with sulfobetaine moieties by thiol-ene chemistry.²¹ In both these examples, well-defined polybetaines were obtained by polymerization methods that are incompatible with zwitterionic groups by choosing efficient, high-yielding post-polymerization functionalization reactions. Ideally, however, the polymerization technique should be fully compatible with the zwitterionic moieties to avoid an extra synthetic step.

Ring-opening metathesis polymerization is a facile method for obtaining well-defined polymers under generally mild conditions, with the correct choice of catalyst and monomer.²² Ruthenium-based catalysts particularly are stable and easy to handle, and frequently enable controlled polymerizations.²³ It was shown that cationic norbornene and oxanorbornene imide monomers could be polymerized in a controlled manner by Grubbs' 1st generation catalyst in a TFE/CH₂Cl₂ mixture.²⁴⁻²⁷ Interestingly, the counterion had an appreciable effect on the polymerization kinetics.²⁶ In the case of iodide, the reaction was impeded completely. Subsequently, sulfobetaine and carboxybetaine monomers were polymerized by ROMP with good control.^{25,27} ROMP-based polybetaines with cyclooctene backbones that gave different material properties have since been synthesized as well.⁹⁻¹⁰

Although Grubbs' catalysts were mostly compatible with tertiary and quaternary amine groups,^{22,24-27} amines and carboxylic acids complexed with the catalyst and interfered with the polymerization.²⁷⁻³² To obtain charged polymers containing those groups, the amine needed to be protected and the carboxylate group needed to be fully protonated or protected.^{27,32} Despite these drawbacks, ROMP was still an attractive

method for polybetaines because of its speed (certain polymerization reactions could take as little as a few minutes), wide variety of available monomer chemistries and ease of use.

1.4 Biofouling

Among many biologically relevant applications, polyzwitterions have shown especially high efficacy as nonfouling materials.³³ *Biofouling* is the accumulation of organic and biological material on a foreign surface submerged in an aqueous environment.³³⁻⁴⁴ The fouling process is often modelled as hierarchical, with less complex foulants giving rise to more complex organisms until the surface has been colonized.^{34,38,42} As with many biologically oriented systems, this model is an oversimplification of the true natural phenomenon, however it is useful to visualize the process.

In the first step, solute (water) molecules interact with the surface.^{34,38} Hydrophilic surfaces, or those that contain highly hydrated functional groups, can induce long-range ordering in the water molecules extending from the surface.⁵ It is thought that this ordered water layer is more difficult to disturb or displace than the loosely correlated water layer that forms around more hydrophobic surfaces.^{5,33-38,43} As such, this stage is dictated by surface chemistry, as well as the nature of the aqueous environment. Next, macromolecules such as proteins and lipopolysaccharides form a conditioning layer on the surface.^{34-38,43} Irreversible protein adsorption arises from electrostatic and hydrophobic interactions. Attraction to the surface causes the protein to denature and expose its hydrophobic domains to the underlying substrate, where adhesion occurs.

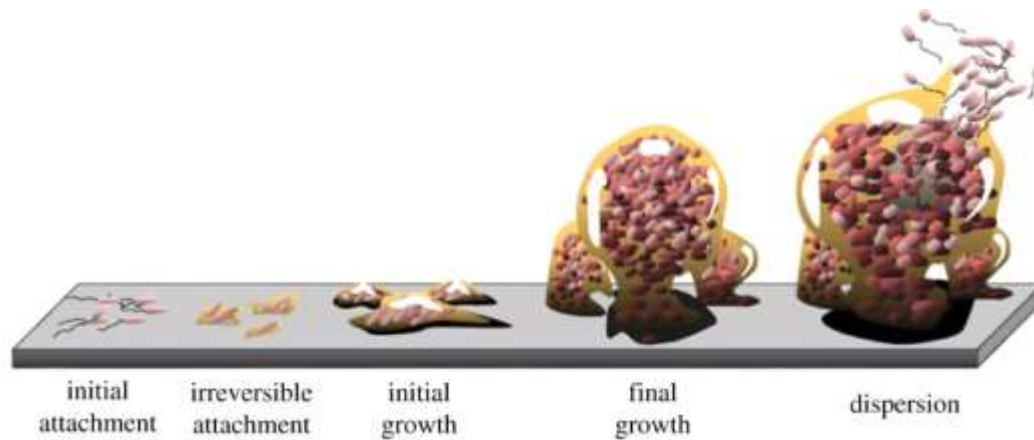


Figure 1.4: Stepwise colonization process of a marine foulant. (Reproduced from Bixler *et al*, Phil. Trans. R. Soc. A, 2012.)

Protein adsorption in and of itself can be detrimental, especially in biomedical devices.⁴² In many cases, however, the adsorbed protein layer acts as a so-called conditioning layer.^{33,38} After the protein has been deposited, larger organisms such as bacteria or spores begin to settle on and colonize the surface. This process can occur quickly, within minutes of the surface's exposure to the aqueous environment. Figure 1.4 shows this process stage-by-stage, from the initial attachment stage through colonization and dispersion. Once the organisms have attached to the surface, they are extremely difficult to displace, which highlights the need to arrest the process in its earliest stages.

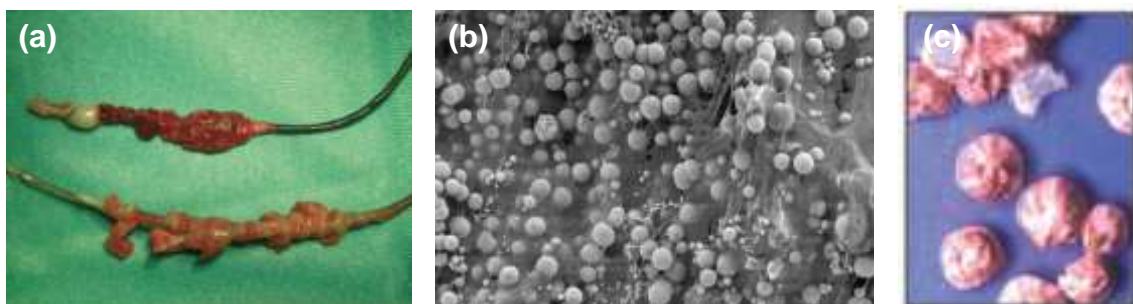


Figure 1.5: Examples of foulants: **(a)** adsorbed protein on an explanted device (reproduced from Mosquera *et al*, Rev Esp Cardiol., 2011); **(b)** bacterial biofilm (reproduced from <http://dujs.dartmouth.edu/fall-2009/biofilms-bacteria>); and **(c)** adult barnacles (reproduced from Callow *et al*, Nat. Commun., 2011).

Biofouling, especially marine biofouling, is an extremely difficult problem to combat.^{37,38,44} For one, foulants encompass a range of length scales, from macromolecules and proteins (Figure 1.5a) to single-celled organisms like bacteria (Figure 1.5b) to multicellular organisms like barnacles (Figure 1.5c) and other marine animals.³⁸ The nature of the foulants can vary from location to location. Foulants, especially macrofoulants, employ a range of adhesion mechanisms as well.³⁸ Finding a material that can deal with all these issues in an effective manner is an overwhelming challenge. Compounding these difficulties is the poorly understood nature of many organisms' adhesion mechanisms as well as the biofouling process in general.

In many cases, foulants have a detrimental effect on the underlying material. Devices such as sensors or implants can become coated in proteinaceous material and lose efficacy or integrity.^{34,46} Bacterial and fungal biofilms have been shown to cause infection and, in extreme cases, death.³⁹⁻⁴¹ It has been estimated that billions of dollars are spent annually in the health care and military fields to combat problems directly related to biofouling, including extended hospital stays and increased fuel costs from drag on naval ships.^{38,39} Whether for biomedical, environmental, or industrial uses, nonfouling materials must be highly efficient over long time scales and robust enough to stand up to harsh environments such as extreme pH or high salinity, while also being non-toxic or minimally toxic.^{37,38,44} The nonfouling efficiency is especially significant as only 0.1 ng/mm² of adsorbed protein was found to trigger the adhesion of more substantial foulants such as platelets on a substrate.⁴²

1.5 Nonfouling Strategies

Many strategies have been developed to combat biofouling. Biocidal methods, while effective, have been largely phased out due to their adverse effects.³⁸ Engineered topographies such as the Sharklet and artificial lotus leaf topographies have also shown great promise as nonfouling or foul-release materials.^{38,44} These materials are outside the scope of this section, however, so only chemical approaches will be discussed below.

1.5.1 Hydrophilic Materials

Biological fouling is thought to occur mainly due to hydrophobic and electrostatic interactions between proteinaceous materials and surfaces.^{33-38,43,45} Strongly hydrophilic surfaces support a highly structured, tightly bound water layer that shields the underlying surface from interacting with proteins and other macromolecules, preventing denaturation and irreversible adhesion. Hydrophilic surfaces with a net charge, however, can promote fouling through electrostatic interactions. With those parameters in mind, it was found that hydrophilic oligo(ethylene oxide) self-assembled monolayers (OEG SAMs) were highly efficient at resisting nonspecific protein adsorption.^{47,48} OEG-based materials were not only highly hydrophilic but also environmentally benign. Their efficiency was dependent on the OEG segments' conformations: when the chains crystallized, the surface dehydrated and protein adsorption increased.⁴⁸

The high surface coverage of the SAMs created impressive nonfouling surfaces, however they were impractical for large surface areas and real-life applications. Polymer brushes were then explored as alternatives. It was found that densely grafted, surface-initiated PEG brushes resisted protein adsorption as well as, if not better than, the OEG SAMs.⁴⁹ The high graft density ensured that the surface was appropriately shielded from

hydrophobic interactions with proteinaceous material. The importance of surface coverage has been corroborated with many different polymers, including zwitterions and polyols.⁵⁰⁻⁵² While PEG has long been a standard nonfouling treatment, it suffers from a lack of intrinsic functional groups for surface modification. More importantly, PEG is subject to degradation in biologically relevant environments, which limits its use to short-term applications. Other hydrophilic uncharged polymers such as glycerol-based polyols⁵⁰ and polysaccharides,⁵³ which are more stable and more conducive to surface functionalization than PEG, have been successfully explored as nonfouling materials as well.

As polymerization methods were developed that were better equipped to handle charged monomers in a controlled manner, zwitterionic materials emerged as promising nonfouling candidates due to their strong surface hydration (hydrophilicity) coupled with charge neutrality.^{33,38,43,44} Additionally, many polybetaines exhibited increased resistance to degradation when compared to ethylene oxide-based materials.⁴³ Zwitterions have been employed in a variety of ways to create nonfouling materials, such as self-assembled monolayers, monolayers, gels, bulk coatings, and polymer brushes.^{16-1933,37,43,54-64} With the advent of controlled radical polymerization techniques, surface-initiated polymerization could be used to create zwitterionic brushes with a higher degree of surface coverage as compared to grafting-to techniques. Using various polymerization techniques, (meth)acrylate- or acrylamide-based PC, carboxybetaine, and sulfobetaine bulk or brush surfaces could be made and then studied as nonfouling coatings.

Many of these surfaces exhibited low degrees of protein adsorption ($< 0.1 \text{ ng/mm}^2$), as well as resistance against bacteria, macrophage, and platelet fouling.^{16-1933,37,43,54-64} In

fact, polycarboxybetaine brushes were found to resist fouling from blood plasma.⁶⁴ Highly dense zwitterionic brushes out-performed PEG- and monolayer-based coatings, demonstrating the advantage of a polyzwitterion approach.³³ As with the PEG- and polyol-based materials, graft density or surface coverage was paramount to achieving superlow-fouling capabilities.⁵¹ Betaines were also preferred over ampholytes or mixed-charge surface because they ensured charged neutrality throughout the material.³³ As many betaines are biomimetic, these polymers are also typically biocompatible.

1.5.2 Amphiphilic materials

Based on our current understanding of biofouling, it seems counterintuitive that amphiphilic materials containing both hydrophilic and hydrophobic components could be used for nonfouling applications. And yet, a number of novel amphiphilic chemistries have shown great promise as robust, efficient nonfouling materials.^{33,38,44} Figure 1.6 shows a schematic representation of a bulk amphiphilic, or ‘ambiguous’, material, where the colors represent the phase-separated hydrophilic and hydrophobic domains.

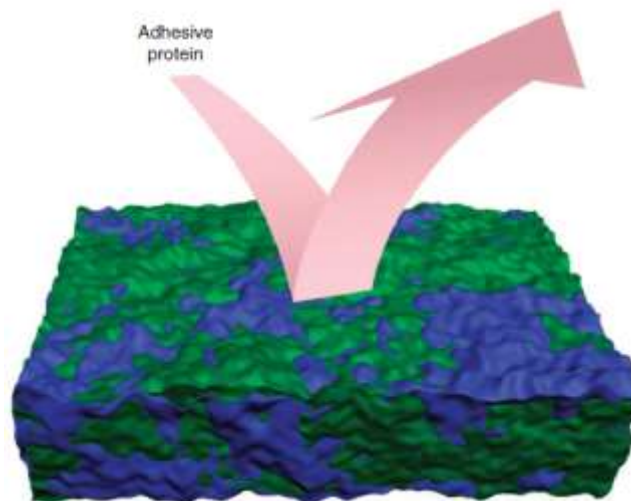


Figure 1.6: Schematic representation of an ambiguous nonfouling amphiphilic surface where the green domains represent hydrophobic segments and the blue domains represent hydrophilic segments. (Reproduced from Callow *et al*, Nat. Commun., 2011.)

Some of the earliest amphiphilic nonfouling materials embraced the ambiguous character of these surfaces.^{38,65-67} Hyperbranched fluoropolymer-PEG composite coatings were created by condensation polymerization of 3,5-bis[(pentafluorobenzyl)oxy]-benzyl alcohols or similar molecules and oligo(ethylene oxide) diols. The hyperbranched structure prevented the components from completely separating but allowed them to rearrange and restructure in different environments. These surfaces were difficult to characterize, however it was found that they had low surface energy, dynamic surfaces, and resisted protein adsorption, lipopolysaccharide adsorption and fouling from marine organisms.

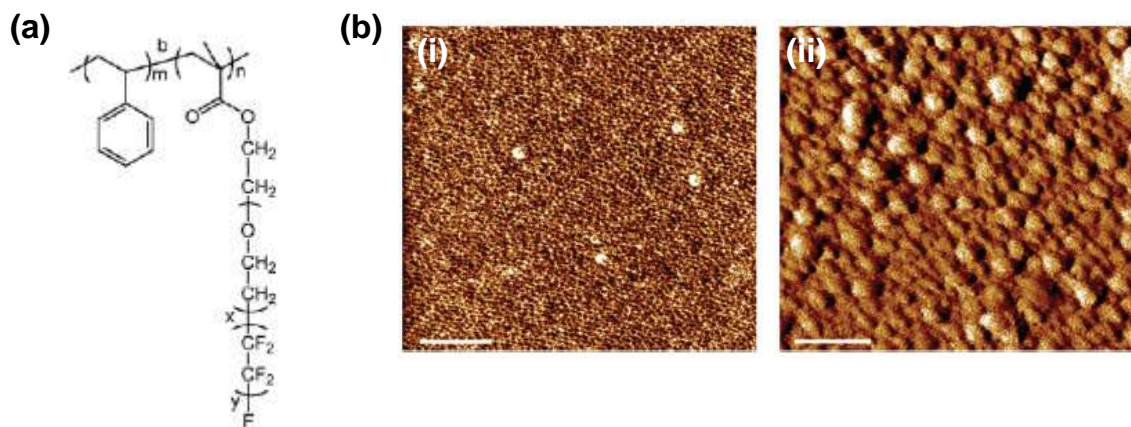


Figure 1.7: Representative amphiphilic polymer and surfaces for nonfouling applications: **(a)** Styrenic block copolymer containing a PEGylated/fluorinated side chain (reproduced from Krishnan *et al*, Langmuir, 2006); **(b)** AFM images of a surface-active block copolymer (i) in air and (ii) in water, undergoing characteristic rearrangement (reproduced from Martinelli *et al*, Langmuir, 2008).

Dynamic surface features tended to be a general characteristic of these amphiphilic materials, regardless of their specific chemistry.^{38,44} Surface-active block copolymers (SABCs) were another class of amphiphilic materials that were studied in-depth as nonfouling materials. Figure 1.7a shows a representative SABC, where the hydrophobic styrene block was used to adhere the polymer to a surface while the methacrylate block imparted the surface-active properties.⁶⁸ It was observed that the PEG/fluorinated side chain reoriented itself based on the environment. In water, the PEG section was present at the interface while the fluorinated tail retreated to the bulk; in air, the fluorinated tail extended out from the surface. The orientation of the hydrophilic and hydrophobic components in different environments has been confirmed by surface-sensitive analytical techniques such as NEXAFS.⁶⁹ Surface properties like roughness (Figure 1.7b and c) as determined by AFM⁷⁰ and water contact angle hysteresis are also indicators of dynamic surfaces.

A variety of SABCs have been synthesized that vary the backbone and incorporate the hydrophilic and hydrophobic side chains into the backbone through different functionalities.^{44,68,69} The use controlled polymerization techniques like anionic polymerization and efficient post-polymerization functionalization chemistries like thiol-ene addition created well-defined polymers to better understand the surface properties of these amphiphilic materials. Other notable amphiphilic materials include co-cured diacrylate perfluoroether/PEG networks.⁷¹ The polymer precursors were miscible prior to crosslinking, which allowed a macroscopically homogeneous network to form. Again it was found that these networks underwent dynamic rearrangement when placed in water. By varying the network components and the curing conditions, materials were obtained that resisted *Ulva* spore settlement to an appreciable degree. It was interesting to note that the amphiphilic materials for nonfouling applications contained a wide variety of chemistries and creative uses of materials, however the hydrophilic component was almost exclusively PEG. Based on the amphiphilic materials' success at reducing biofouling, introducing new hydrophilic components seemed like an interesting avenue to pursue.

1.6 Oxanorbornene-based Betaines

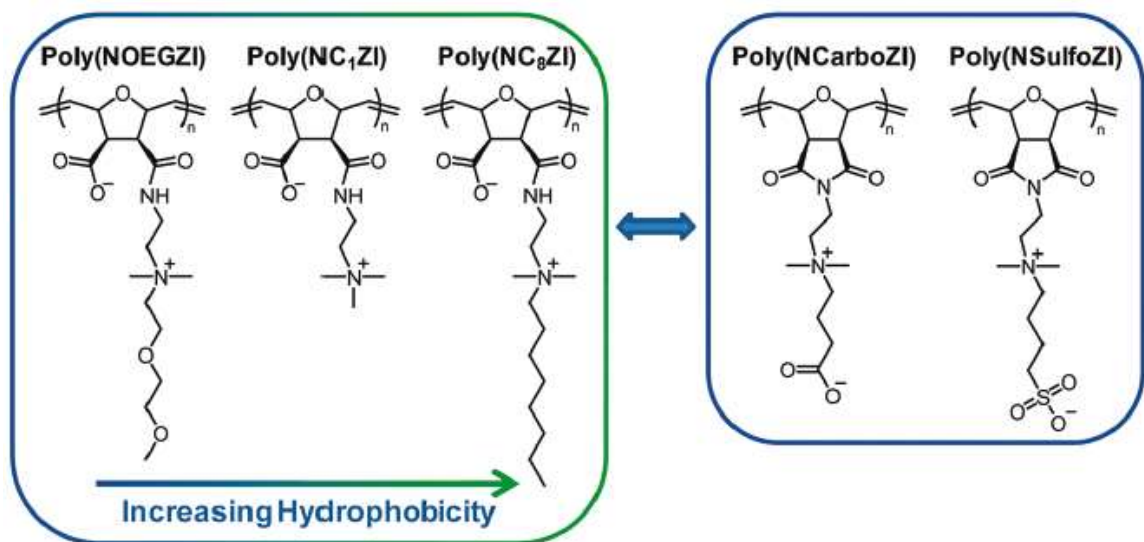


Figure 1.8: Structures of dual-functional (right image) and linear (left image) oxanorbornene-based polybetaines. (Reproduced from Colak *et al*, Langmuir, 2012.)

ROMP had been known to tolerate quaternary amines and sulfobetaines, making it an attractive method to synthesize certain polyelectrolytes and polybetaines.²⁴⁻²⁷ The oxanorbornene imide, specifically, polymerized in a controlled manner. Originally, ROMP-based betaines were pursued as nonfouling materials to determine if antibiofouling performance could still be achieved with an oxanorbornene backbone. Subsequently, the fortuitous discovery was made that the *N*-substituted imide ring-opened under basic conditions to form two side chains: a carboxylic acid and an amide containing the *N* substituent.^{27,72,73} When the side chain contained a cationic group, this ring-opening reaction resulted in a betaine with the charge sequestered on separate arms within the repeat unit. This reaction allowed for the facile incorporation of anionic carboxylate groups into ROMP polymers, where the carboxylic acid was known to

interact with the catalyst. More importantly, a new class of dual-functional betaines could be obtained by this reaction.

As shown in Figure 1.8, the quaternary amine could contain a multitude of chemically diverse side chains, including hydrophilic oligo(ethylene oxide) and hydrophobic hydrocarbon chains, so that the polymers' overall hydrophilicity or hydrophobicity could be tuned. In addition to the linear carboxybetaine and sulfobetaine chemistries, these polymers were used as nonfouling coatings. Envisaged as foundational materials to study the effects of hydrophilicity and polymer backbone on nonfouling properties, these polymers actually performed reasonably well. The **Poly(NOEGZI)** surface, for instance, was highly wettable (advancing water contact angle $\approx 30^\circ$) and resisted fibrinogen adsorption down to 0.04 ng/mm^2 .⁷²

When the dual-functional betaines contained a lipophobic perfluoroalkane side chain, fibrinogen adsorption was reduced down to 0.03 ng/mm^2 .⁷³ This result was in contrast to the similarly hydrophobic octyl side chain, where $\Gamma_{\text{Fibrinogen}} \approx 4 \text{ ng/mm}^2$. In this way it was shown that the oxanorbornene imide synthetic platform could accommodate diverse chemistries, which in turn resulted in tunable surface properties.

1.7 Scope of the Thesis

The following chapters of this thesis encompass the design and synthesis of oxanorbornene imide-based polybetaines. This chemistry expands on the dual-functional structures that were previously synthesized and explored as nonfouling materials (Figure 1.8).^{72,73} Structure-property relationships are then explored between this library of polymers and their nonfouling performance.

Chapter 2 characterizes the imide ring-opening reaction that enables the dual-functional betaine chemistry. A variety of oxanorbornene imide molecules are screened to determine the limits of the ring-opening reaction. Ring-opened polymers are also characterized.

Chapter 3 describes the synthesis of a large library of oxanorbornene-based betaines. Linear as well as dual-functional polybetaines are synthesized. Carboxybetaine and sulfobetaine moieties are included, where the intercharge distance is varied. A set of dual-functional betaines where the intercharge distance is varied is synthesized as well for a direct comparison between the dual-functional and linear chemistries. Finally, a set of amphiphilic betaines is synthesized, which include both hydrocarbon and fluorinated moieties. The modular nature of the oxanorbornene imide backbone allows for a diverse set of novel betaines to be synthesized with the same backbone, so that they can be studied as model nonfouling materials.

The synthesis of polymers for surface functionalization is described in Chapter 4. Here, copolymers containing triethoxysilane repeat units are used to create robust coatings for nonfouling applications. A sulfobetaine monomer is used as the model zwitterionic component. The composition of the polymers is varied both to study the structure-property relationships between the polymer and the resulting coatings, as well as to optimize the coatings so that they can be used to study nonfouling properties in the subsequent chapters.

Chapters 5 and 6 deal with the nonfouling properties of the polybetaines outlined in Chapter 3. In Chapter 5, the hydrophilic betaines (carboxybetaine, sulfobetaine and methyl dual-functional) are compared. Their structures allow us to study the effects of

intercharge distance as well as zwitterionic chemistry on the nonfouling properties of these bulk coatings. Chapter 6 describes the nonfouling properties of the amphiphilic dual-functional series. In both chapters, the surface properties of the coatings are thoroughly characterized. Nonfouling performance is measured by fibrinogen adsorption as measured by ellipsometry.

Finally, in Chapter 7, preliminary work on hydrogels that are obtained from oxanorbornene imide polymers is discussed. Gelation occurs in the presence of poly(oxanorbornene imide)s and a multifunctional primary amine, in this case poly(allylamine). These hydrogels represent a novel material application for these charged ROMP polymers and another unique application of the ring-opening reaction described in Chapter 2.

1.8 References

- (1) Alberts, B.; Johnson, A.; Lewis, J.; Raff, M.; Roberts, K.; Walter, P. *Molecular Biology of the Cell*. 4th Ed. Garland Science, New York, **2002**.
- (2) Lowe, A. B.; McCormick, C. L. Synthesis and Solution Properties of Zwitterionic Polymers. *Chem. Rev.* **2002**, *102*, 4177-41895.
- (3) Kudaibergenov, S.; Jaeger, W.; Laschewsky, A. Polymeric Betaines: Synthesis, Characterization and Application. *Adv. Polym. Sci.* **2006**, *201*, 157-224.
- (4) Laschewsky, A. Structures and Synthesis of Zwitterionic Polymers. *Polymers* **2014**, *6*, 1544-1601.
- (5) Kane, R. S.; Deschatelets, R.; Whitesides, G. M. Kosmotropes Form the Basis of Protein-Resistant Surfaces. *Langmuir* **2003**, *19*, 2388-2391.
- (6) Lewis, A. L. Phosphorycholine-based polymers and their use in the prevention of biofouling. *Colloids Surf., B* **2000**, *18*, 261-275.

- (7) Ueda, T.; Oshida, H.; Kurita, K.; Ishihara, K.; Nakabayashi, N. Preparation of 2-Methacryloyloxyethyl Phosphorylcholine Copolymers with Alkyl Methacrylates and Their Blood Compatibility. *Polym. J.* **1992**, *24*, 1259-1269.
- (8) Page, SM.; Parelkar, S.; Gerasimenko, A.; Shin, DY.; Peyton, S.; Emrick, T. Promoting cell adhesion on slippery phosphorylcholine hydrogel surfaces. *J. Mater. Chem. B* **2014**, *2*, 620-624.
- (9) Kratz, K.; Breitenkamp, K.; Hule, R.; Pochan, D.; Emrick, T. PC-Polyolefins: Synthesis and Assembly Behavior in Water. *Macromolecules* **2009**, *42*, 3227-3229.
- (10) Kratz, K.; Xie, W.; Lee, A.; Freeman, BD.; Emrick, T. Phosphorylcholine-Substituted ROMP Polyolefin Coatings Provide Fouling Resistance to Membrane Materials. *Macromol. Mater. Eng.* **2011**, *296*, 1142-1148.
- (11) Cooper, B. M.; Chan-Seng, D.; Samanta, D.; Zhang, X.F.; Parelkar, S.; Emrick, T. Polyester-graft-phosphorylcholine prepared by ring-opening polymerization and click chemistry. *Chem. Commun.* **2009**, *7*, 815-817.
- (12) Yu, B.; Lowe, A. B.; Ishihara, K. RAFT Synthesis and Stimulus-Induced Self-Assembly in Water of Copolymers Based on the Biocompatible Monomer 2-(Methacryloyloxy)ethyl Phosphorylcholine. *Biomacromolecules* **2009**, *10*, 950-958.
- (13) Polzer, F.; Heigl, J.; Schneider, C.; Ballauff, M.; Borisov, O. Synthesis and Analysis of Zwitterionic Spherical Polyelectrolyte Brushes in Aqueous Solution. *Macromolecules* **2011**, *44*, 1654-1660.
- (14) Zhang, Z.; Cheng, G.; Carr, L. R.; Vaisocherova, H.; Chen, S.; Jiang, S. The hydrolysis of cationic polycarboxybetaine esters to zwitterionic polycarboxybetaines with controlled properties.
- (15) Rodriguez-Emmenegger, C.; Schmidt, B. V. K. J.; Sedlakova, Z.; Subr, V.; Alles, A. B.; Brynda, D.; Barner-Kowollik, C. Low Temperature Aqueous Living/Controlled (RAFT) Polymerization of Carboxybetaine Methacrylamide up to High Molecular Weights. *Macromol. Rapid Commun.* **2011**, *32*, 958-965.
- (16) Zhang, Z.; Chen, S.; Chang, Y.; Jiang, S. Surface Grafted Sulfobetaine Polymers via Atom Transfer Radical Polymerization as Superlow Fouling Coatings. *J. Phys. Chem. B* **2006**, *110*, 10799-10804.
- (17) Zhang, Z.; Chao, T.; Chen, S.; Jiang, S. Superlow Fouling Sulfobetaine and Carboxybetaine Polymers on Glass Slides. *Langmuir* **2006**, *22*, 10072-10077.
- (18) Zhang, Z.; Chen, S.; Jiang, S. Dual-Functional Biomimetic Materials: Nonfouling Poly(carboxybetaine) with Active Functional Groups for Protein Immobilization. *Biomacromolecules* **2006**, *7*, 3311-3315.

- (19) Zhang, Z.; Vaisocherova, H.; Cheng, G.; Yang, W.; Xue, H.; Jiang, S. Nonfouling Behavior of Polycarboxybetaine-Grafted Surfaces: Structural and Environmental Effects. *Biomacromolecules* **2008**, *9*, 2686-2692.
- (20) Lowe, A. B.; Billingham, N. C.; Armes, S. P. Synthesis of polybetaines with narrow molecular mass distribution and controlled architecture. *Chem. Comm.* **1996**, 1555-1556.
- (21) Tauhardt, L.; Pretzel, D.; Kempe, K.; Gottschaldt, M.; Pohlers, D.; Schubert, U. S. Zwitterionic poly(2-oxazoline)s as promising candidates for blood contacting applications. *Polym. Chem.* **2014**, *5*, 5751-5764.
- (22) Bielawski, C. W.; Grubbs, R. H. Living ring-opening metathesis polymerization. *Prog. Polym. Sci.* **2007**, *32*, 1-29.
- (23) Love, J. A.; Morgan, J. P.; Trnka, T. M.; Grubbs, R. H. A Practical and Highly Active Ruthenium-Based Catalyst that Effects the Cross Metathesis of Acrylonitrile. *Angew. Chem. Int. Ed.* **2002**, *41*, 4035-4037.
- (24) Rankin, D. A.; P'Pool, S. J.; Schanz, H-J.; Lowe, A. B. The Controlled Homogeneous Organic Solution Polymerization of New Hydrophilic Cationic *exo*-7-Oxanorbornenes via ROMP with RuCl₂(PCy₃)₂CHPh in a Novel 2,2,2-Trifluoroethanol/Methylene Chloride Solvent Mixture. *J. Polym. Sci., Part A: Polym. Chem.* **2007**, *45*, 2113-2128.
- (25) Rankin, D. A.; Lowe, A. B. New Well-Defined Polymeric Betaines: First Report Detailing the Synthesis and ROMP of Salt-Responsive Sulfopropylbetaine- and Carboxyethylbetaine-*exo*-7-oxanorbornene Monomers. *Macromolecules* **2008**, *41*, 614-622.
- (26) Rankin, D. A.; Schanz, H-J. Effect of the Halide Counterion in the ROMP of *exo*-Benzyl-[2-(3,5-dioxo-10-oxa-4-azatricyclo[5.2.1.0^{2,6}]dec-8-en-4-yl)ethyl]dimethylammonium Bromide/Chloride. *Macromol. Chem. Phys.* **2007**, *208*, 2389-2395.
- (27) Colak, S.; Tew, G. N. Synthesis and Solution Properties of Norbornene Based Polybetaines. *Macromolecules* **2008**, *41*, 8436-8440.
- (28) Harrison, D. B.; Feast, W. J. Aqueous ring-opening metathesis polymerizations of heteropolycyclic carboxylic acids with transition-metal chlorides. *Polymer* **1991**, *32*, 558-563.
- (29) Schitter, R. M. E.; Jocham, D.; Stelzer, F.; Moszner, N.; Völkel, T. J. New routes to polyelectrolytes and reactive polymers via ROMP. *J. Appl. Polym. Sci.* **2000**, *78*, 47-60.

- (30) Ahmed, S. R.; Bullock, S. E.; Cresce, S. V.; Kofinas, P. Polydispersity control in ring opening metathesis polymerization of amphiphilic norbornene diblock copolymers. *Polymer* **2003**, *44*, 4943-4948.
- (31) Stubenrauch, K.; Fritz-Popovski, G.; Ingolic, E.; Grogger, W.; Glatter, O.; Stelzer, F.; Trimmel, G. Microphase Separation Study of Amphiphilic ROMP Block Copolymers by SAXS and TEM. *Macromolecules* **2007**, *40*, 4592-4600.
- (32) Lienkamp, K.; Kins, C. F.; Alfred, S. F.; Madkour, A. E.; Tew, G. N. Water-Soluble Polymers from Acid-Functionalized Norbornenes. *J. Polym. Sci.: Part A* **2009**, *47*, 1266-1273.
- (33) Chen, S.; Jiang, S. A New Avenue to Nonfouling Materials. *Adv. Mater.* **2008**, *20*, 335-338.
- (34) Bixler, G. D.; Bhushan, B. Biofouling: lessons from nature. *Phil. Trans. R. Soc. A* **370**, 2381-2417.
- (35) Chen, S.; Li, L.; Zhao, C.; Zheng, J. Surface hydration: Principles and applications toward low-fouling/nonfouling biomaterials. *Polymer* **2012**, *51*, 5283-5293.
- (36) Song, W.; Mano, J. F. Interactions between cells or proteins and surfaces exhibiting extreme wettabilities. *Soft Matter* **2013**, *9*, 2985-2999.
- (37) Banerjee, I.; Pangule, R. C.; Kane, R. S. Antifouling Coatings: Recent Developments in the Design of Surfaces That Prevent Fouling by Proteins, Bacteria, and Marine Organisms. *Adv. Mater.* **2011**, *23*, 690-718.
- (38) Callow, J. A.; Callow, M. E. Trends in the development of environmentally friendly fouling-resistant marine coatings. *Nat. Commun.* **2011**, DOI: 10.1038/ncomms1251.
- (39) Darouiche, R. O. Treatment of infections associated with surgical implants. *New Engl. J. Med.* **2004**, *350*, 1422-1429.
- (40) Page, K.; Wilson, M.; Parkin, I. P. Antimicrobial surfaces and their potential in reducing the role of the inanimate environment in the incidence of hospital-acquired infections. *J. Mater. Chem.* **2009**, *19*, 3819-3831.
- (41) Lynch, A. S.; Robertson, G. T. Bacterial and Fungal Biofilm Infections. *Annu. Rev. Med.* **2008**, *59*, 415-428.
- (42) Tsai, W. B.; Grunkemeier, J. M.; Horbett, T. A. Human plasma fibrinogen adsorption and platelet adhesion to polystyrene. *J. Biomed. Mater. Res.* **1999**, *44*, 130-139.

- (43) Ostuni, E.; Chapman, R. G.; Holmlin, R. E.; Takayama, S.; Whitesides, G. M. A survey of Structure-Property Relationships of Surfaces that Resist the Adsorption of Protein. *Langmuir* **2001**, *17*, 5605–5620.
- (44) Grozea, C. M.; Walker, G. C. Approaches in designing non-toxic polymer surfaces to deter marine biofouling. *Soft Matter* **2009**, *5*, 4088-4100.
- (45) Worz, A.; Berchtold, B.; Moosmann, K.; Prucker, O.; Ruhe, J. Protein-resistant polymer surfaces. *J. Mater. Chem.* **2012**, *22*, 19547-19561.
- (46) Mosquera, V. X.; Perez-Alvarez, L.; Ricoy-Martinez, E.; Mosquera-Perez, I.; Castro-Beira, A.; Cuenca-Castillo, J.J. Initial Experience With Excimer Laser-Assisted Pacemaker and Defibrillator Lead Extraction. *Rev Esp Cardiol.* **2011**, *64*, 824-827.
- (47) Prime, K. L.; Whitesides, G. M. Adsorption of proteins onto surfaces containing end-attached oligo(ethylene oxide): a model system using self-assembled monolayers. *J. Am. Chem. Soc.* **1993**, *115*, 10714-10721.
- (48) Harder, P.; Grunze, M.; Dahint, R.; Whitesides, G. M.; Laibinis, P. E. Molecular Conformation in Oligo(ethylene glycol)-Terminated Self-Assembled Monolayers on Gold and Silver Surfaces Determine Their Ability to Resist Protein Adsorption. *J. Phys. Chem. B* **1998**, *102*, 426-436.
- (49) Hucknall, A.; Rangarajan, S.; Chilkoti, A. In Pursuit of Zero: Polymer Brushes that Resist the Adsorption of Proteins. *Adv. Mater.* **2009**, *21*, 2441-2446.
- (50) Gunkel, G.; Weinhart, M.; Becherer, T.; Haag, R.; Huck, W. T. S. Effect of Polymer Brush Architecture on Antibiofouling Properties. *Biomacromolecules* **2011**, *12*, 4169-4172.
- (51) Huang, C-J.; Li, Y.; Krause, J. B.; Brault, N. D.; Jiang, S. Internal Architecture of Zwitterionic Polymer Brushes Regulates Nonfouling Properties. *Macromol. Rapid Commun.* **2012**, *33*, 1003-1007.
- (52) Toomey, R.; Tirrell, M. Functional polymer brushes in aqueous media from self-assembled and surface-initiated polymers. *Annu. Rev. Phys. Chem.* **2008**, *59*, 493-517.
- (53) Mussard, W.; Kebir, N.; Kriegel, I.; Esteve, M.; Semetey. Facile and Efficient Control of Bioadhesion on Poly(dimethylsiloxane) by Using a Biomimetic Approach. *Angew. Chem. Int. Ed.* **2011**, *50*, 10871-10874.
- (54) Estephan, Z. G.; Schlenoff, P. S.; Schlenoff, J. B. Zwitteration as an Alternative to PEGylation. *Langmuir* **2011**, *27*, 6794-6800.

- (55) Ishihara, K.; Aragaki, R.; Ueda, T.; Watanabe, A.; Nakabayashi, N. Reduced thrombogenicity of polymers having phospholipid polar groups. *J. Biomed. Mater. Res.* **1990**, *24*, 1069-1077.
- (56) Ueda, T.; Watanabe, A.; Ishihara, K.; Nakabayashi, N. Protein adsorption on biomedical polymers with a phosphorylcholine moiety adsorbed with phospholipid. *J. Biomater. Sci., Polym. Ed.* **1992**, *3*, 185-194.
- (57) Ishihara, K.; Ziats, N. P.; Tierney, B. P.; Nakabayashi, N.; Anderson, J. M. Protein adsorption from human plasma is reduced on phospholipid polymers. *J. Biomed. Mater. Res.* **1991**, *25*, 1397-1407.
- (58) Ueda, T.; Oshida, H.; Kurita, K.; Ishihara, K.; Nakabayashi, N. Preparation of 2-Methacryloyloxyethyl Phosphorylcholine Copolymers with Alkyl Methacrylates and Their Blood Compatibility. *Polym. J.* **1992**, *24*, 1259-1269.
- (59) Ishihara, K.; Oshida, H.; Endo, Y.; Ueda, T.; Watanabe, A.; Nakabayashi, N. Hemocompatibility of human whole blood on polymers with a phospholipid polar group and its mechanism. *J. Biomed. Mater. Res.* **1992**, *26*, 1543-1552.
- (60) Xu, Y.; Takai, M.; Konno, T.; Ishihara, K. Microfluidic flow control on charged phospholipid polymer interface. *Lab Chip* **2007**, *7*, 199-206.
- (61) Lowe, A. B.; Vamvakaki, M.; Wassall, M.A.; Wong, L.; Billingham, N. C.; Armes, S. P.; Lloyd, A.W. Well-defined sulfobetaine-based statistical copolymers as potential antibioadherent coatings. *J. Biomed. Mater. Res.* **2000**, *52*, 88-94.
- (62) Chang, Y.; Liao, S.; Higuchi, A.; Ruaan, R.; Chu, C.; Chen, W. A Highly Stable Nonbiofouling Surface with Well-Packed Grafted Zwitterionic Polysulfobetaine for Plasma Protein Repulsion. *Langmuir* **2008**, *24*, 5453-5458.
- (63) Wang, D. A.; Williams, C. G.; Li, Q. A.; Sharma, B.; Elisseeff, J. H. Synthesis and characterization of a novel degradable phosphate-containing hydrogel. *Biomaterials* **2003**, *24*, 3969-3980.
- (64) Rodriguez Emmenegger, C.; Brynda, E.; Riedel, T.; Sedlakova, Z.; Housak, M.; Alles, A. B. Interaction of Blood Plasma with Antifouling Surfaces. *Langmuir* **2009**, *25*, 6328-6333.
- (65) Bartels, J. W.; Cheng, C.; Powell, K. T.; Xu, J.; Wooley, K. L. Hyperbranched Fluoropolymers and their Hybridization into Complex Amphiphilic Crosslinked Copolymer Networks. *Macromol. Chem. Phys.* **2007**, *208*, 1676-1687.
- (66) Gudipati, C. S.; Finlay, J. A.; Callow, J. A.; Callow, M. E.; Wooley, K. L. The Antifouling and Fouling-Release Performance of Hyperbranched Fluoropolymer

(HBFP)–Poly(ethylene glycol) (PEG) Composite Coatings Evaluated by Adsorption of Biomacromolecules and the Green Fouling Alga *Ulva*. *Langmuir* **2005**, *21*, 3044–3053.

(67) Gudipati, C. S.; Greenlief, C. M.; Johnson, J. A.; Prayongpan, P.; Wooley, K. L. Hyperbranched Fluoropolymer (HBFP) and Linear Poly(ethylene glycol) (PEG) Based Amphiphilic Crosslinked Networks as Efficient Anti-fouling Coatings: An insight into the surface compositions, topographies and morphologies. *J. Polym. Sci., Part A: Polym. Chem.* **2004**, *42*, 6193-6208.

(68) Krishnan, S.; Ayothi, R.; Hexemer, A.; Finlay, J. A.; Sohn, K. E.; Perry, R.; Ober, C. K.; Kramer, E. J.; Callow, M. E., Callow, J. A.; Fischer, D. A. Anti-biofouling Properties of Comblike Block Copolymers with Amphiphilic Side Chains. *Langmuir* **2006**, *22*, 5075–5086.

(69) Dimitriou, M. D.; Zhou, Z.; Yoo, H-S.; Killops, K. L.; Finlay, J. A.; Cone, G.; Sundaram, H, A.; Lynd, N. A.; Barteau, K. P.; Campos, L. M.; Fischer, D. A.; Callow, M. E.; Callow, J. A.; Ober, C. K.; Hawker, C. J.; Kramer, E. J. A General Approach to Controlling the Surface Composition of Poly(ethylene oxide)-Based Block Copolymers for Antifouling Coatings. *Langmuir* **2011**, *27*, 13762-13772.

(70) Martinelli, E. Nanostructured films of amphiphilic fluorinated block copolymers for fouling release application. *Langmuir* **2008**, *24*, 13138–13147.

(71) Wang, Y.; Finlay, J. A.; Betts, D. E.; Merkel, T. J.; Luft, J. C.; Callow, M. E.; Callow, J. A.; DeSimone, J. M. Amphiphilic Co-networks with Moisture-Induced Surface Segregation for High-Performance Nonfouling Coatings. *Langmuir* **2011**, *27*, 10365-10369.

(72) Colak, S.; Tew, G. N. Dual-Functional ROMP-Based Betaines: Effect of Hydrophilicity and Backbone Structure on Nonfouling Properties. *Langmuir* **2012**, *28*, 666-675.

(73) Colak, S.; Tew, G. N. Amphiphilic Polybetaines: The Effect of Side-Chain Hydrophobicity on Protein Adsorption. *Biomacromolecules* **2012**, *13*, 1233-1239.

CHAPTER 2

RING-OPENING IN NORBORNENE-BASED IMIDES

2.1 Introduction

Chapter 2 details the ring-opening reaction of oxanorbornene imides in the presence of an aqueous base. The use of both sodium hydroxide and n-butylamine as the base were explored. Both types of bases induced ring-opening of the imide to form an amide side chain as well as a carboxylate group. It was also discovered that when excess butylamine was used, the primary amine inserted itself into the imide to create two amide side chains. This reaction potentially allowed for hydrophobic moieties to be incorporated into the polymer through an amide linkage. Ring-opening of the imide group in a range of *N*-substituted oxanorbornene imide monomers and polymers was confirmed by both NMR and IR spectroscopy. Two model poly(oxanorbornene imide)s, one with a hydrophilic cationic substituent and one with a hydrophobic benzyl substituent, were synthesized to fully characterize both the amide and diamide ring-opening reactions in polymers. These ring-opening reactions were both fast and quantitative, making them efficient post-polymerization functionalization methods. Furthermore, the well-defined molecular weights and low PDIs of the precursor polymers were maintained post-functionalization. These reactions constituted a new set of post-polymerization reactions for poly(oxanorbornene imides) to obtain chemistries that have historically been problematic to achieve directly by ROMP, as well as a new synthetic platform for functionalizing ROMP-based materials.

2.2 Ring-opening Properties of Poly(oxanorbornene imide)s

We previously reported on the synthesis and applications of oxanorbornene imide-based polybetaines¹⁻⁴ – zwitterionic polymers where both a positive and negative charge are present on each repeat unit.^{5,6} ROMP was initially selected to synthesize a set of polybetaines due to its demonstrated compatibility with sulfobetaine and quaternary ammonium moieties.⁷⁻¹⁰ During a stability test, it was first observed that the imide group of *N*-substituted oxanorbornene imide monomers containing a quaternary amine appeared to ring-open in aqueous NaOH solutions.¹ This phenomenon was then utilized to create a set of dual-functional polybetaines.^{3,4}

The ring-opening reaction of sterically hindered imide groups has been observed in aromatic and small molecule aliphatic systems.^{11,12} The phthalimide protecting group is labile under basic, nucleophilic conditions, but typically requires harsh basic conditions to ring-open.¹³ *N*-substituted succinimides are known to ring-open in the presence of nucleophiles,¹⁴ with a preference towards amines. The dual carbonyl groups in a cyclic structure activate the imide group towards nucleophilic attack, and substitutions on the nitrogen and around the ring further influence reactivity. To the best of our knowledge, the initial report from our lab was the first published reference of the phenomenon in aliphatic, polymeric systems.^{1,3,4} Regardless, imides are traditionally thought to be stable under a variety of conditions, and are frequently used because of their tolerance to pH changes.

We subsequently discovered that this ring-opening reaction happened consistently with any imide-containing polymer under similar conditions (Figure 2.1). Additionally, it was found that the imide ring-opened when a primary alkyl amine was used as a base in

the presence of water. While this reaction was not altogether surprising, primary amines also ring-opened and inserted into the imide backbone to form an amide, similar to succinimide reactivity with amines. As outlined in Figure 2.1, a second pendant group was added post-polymerization into each repeat unit by this aminolysis reaction.

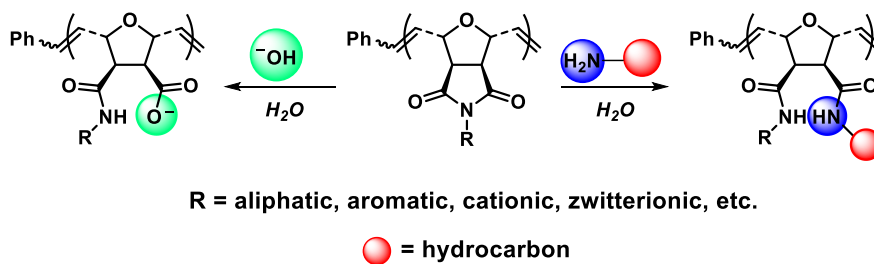


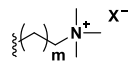
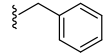
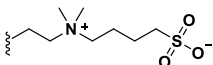
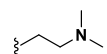
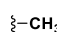
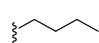
Figure 2.1: Schematic representation of poly(oxanorbornene imide) ring-opening in the presence of sodium hydroxide and primary amines.

To determine if the reactions outlined in Figure 2.1 were general properties of this imide system, we studied a library of oxanorbornene imide-based monomers and polymers. As shown in Table 1, a wide variety of oxanorbornene imide monomers and their corresponding polymers were screened under basic conditions to determine their ring-opening propensities. The R-groups ranged from hydrophilic (**1**, **3-4**) to hydrophobic (**2**, **5-7**), and included charged and uncharged, as well as aliphatic and aromatic moieties. Monomers were polymerized in the same manner as shown in Figure 1, where a short degree of polymerization of 20 was used to aid solubility and characterization of the ring-opened products. Whenever possible, NMR spectroscopy was used to confirm the ring-opening reactions.

With the exception of the unsubstituted oxanorbornene imide **7** (discussed later in the chapter), all monomers and their resulting polymers ring-opened under basic conditions. In the case of the polymers, slightly longer reaction times (an hour as opposed to minutes) and more dilute conditions were required to ensure near-quantitative

conversion. The slight change in reactivity was most likely due to steric hindrance along the backbone and the reduced solubility of the polymers compared to their monomers. These reactions occurred in the presence of permanently charged groups (**1**, **3**), implying that charge stabilization between the R group and the resulting anionic acid did not ultimately affect the ability of the imide to ring-open. Hydrophobic monomers and polymers, and those that were partially soluble (**4**) also ring-opened. In the case of hydrophobic monomers, their conversion to an electrolyte after ring-opening to form an acid was accompanied by increased solubility in aqueous solutions. This effect was present in the hydrophobic polymers but to a more limited extent. Ring-opening of the imide group, therefore, was determined to be a general property of this system.

Table 2.1: Ring-opening reactions for a selection of functionalized oxanorbornene imides with sodium hydroxide and n-butylamine.

R	NaOH treatment ^a		n-butylamine treatment ^d	
	monomer	polymer	monomer	polymer
1 	+	+	+ ^e	+
2 	+	+ ^b	+	+
3 	+	+	+ ^e	+ ^e
4 	+	N. D. ^c	+ ^e	N. D. ^c
5 	+	+ ^b	+	+
6 	+	+ ^b	+	+
7 H	-	+ ^b	-	N. D. ^c

(+) = ring-opening; (-) = no ring-opening; ^a as determined by ¹H and ¹³C NMR spectroscopy in 0.1 M NaOD unless otherwise specified; ^b as determined by ¹H and ¹³C NMR spectroscopy in 1:1 0.2 M NaOD:DMSO-d₆; ^c N. D. = not determined; ^d as determined by FT-IR after purification unless otherwise specified; ^e as determined by ¹H and ¹³C NMR spectroscopy in D₂O.

While water was necessary for the ring-opening reactions to occur, it was not always a good solvent for oxanorbornene imide-based monomers or polymers, especially those without charged side chains. A variety of organic cosolvents were screened to determine if they could be used to solubilize the imide in an aqueous solution and not interfere with the ring-opening reactions, as shown in Table 2.2. Methanol, TFE, THF, DMSO, and DMF were selected because of their miscibility with water as well as their demonstrated ability to solvate a range of oxanorbornene imide-based monomers and polymers. Monomer **1** ($m = 1$) was used to test methanol and TFE while monomers **2** and **6** was used to screen the remaining solvents. It was found that the sodium hydroxide-mediated ring-opening reactions proceeded as expected in 1:1 ratios of the listed organic solvents and water. Ring-opening in the presence of butylamine proceeded as expected for all the organic solvents *except* DMF, which appeared to inhibit the reaction. Even when the reaction solution was heated at 50 °C for up to 48 hours, there was no evidence of ring-opening by either NMR or IR spectroscopy.

Table 2.2: Ring-opening reactions in water-miscible organic solvents.

Solvent	NaOH treatment	n-butylamine treatment
Methanol	+	+
2,2,2-trifluoroethanol (TFE)	+	+
Tetrahydrofuran (THF)	+	+
Dimethylsulfoxide (DMSO)	+	+
<i>N,N</i> -dimethylformamide (DMF)	+	-

(+) = ring-opening; (-) = no ring-opening

Two model sets of molecules (Figure 2.2) were selected for more in-depth characterization. The R-groups, a quaternary amine (**1**) and a benzyl group (**2**), were specifically chosen to span the range from hydrophilic to hydrophobic, as well as to incorporate charged and aromatic moieties, which are not only beneficial to a number of applications but also demonstrate the range of these reactions. As shown in Figure 2.2, both **1** and **2** were polymerized using Grubbs' 3rd generation catalyst, where the degree of polymerization was determined by the ratio of monomer to catalyst. The isolated polymer was then treated with aqueous solutions of either sodium hydroxide (**Poly1(Am)**) or n-butylamine (**Poly2(dAm)**). In the case of hydrophobic monomers and polymers, THF was used as a co-solvent with water to ensure full solubility. These general conditions were used for the polymerization and ring-opening of all other monomers and polymers discussed in this chapter. In the nomenclature for this chapter, monomers are referred to by their number as denoted in Table 2.1; polymers are given the prefix **Poly**; molecules in the ring-opened form are given the suffix (**Am**) (single amide); and molecules with two amide side chains are given the suffix (**dAm**) (diamide).

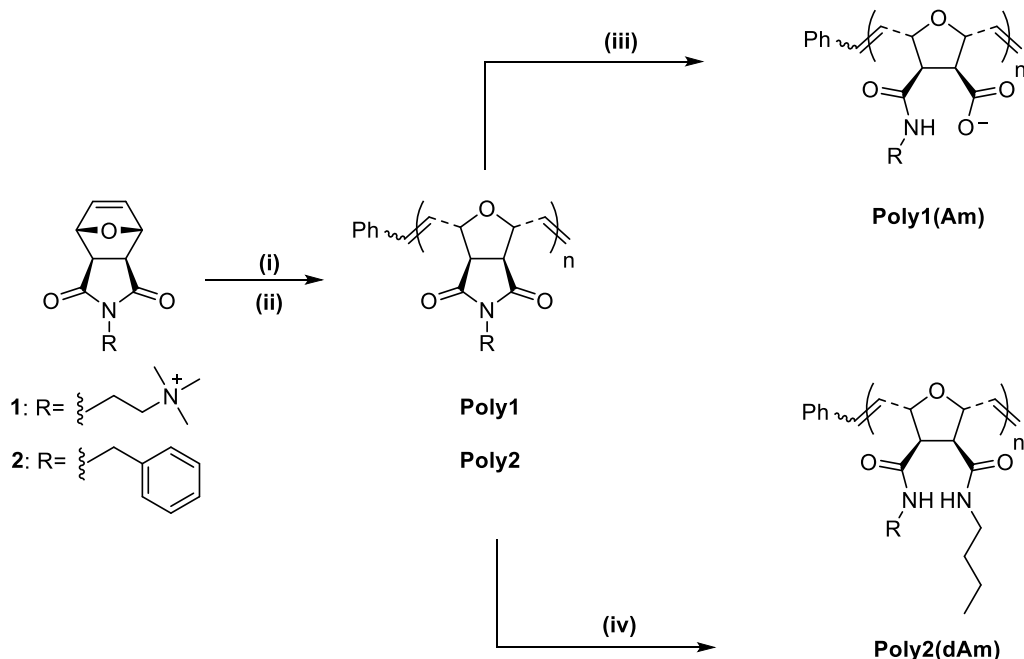


Figure 2.2: General conditions for the synthesis and ring-opening of poly(oxanorbornene imide)s to create carboxylate- and diamide-containing polymers: **(i)** Grubbs' 3rd generation catalyst, solvent, 20 minutes, room temperature; **(ii)** ethyl vinyl ether, 1 hour; **(iii)** 0.1 M NaOH, 1 hour; **(iv)** n-butylamine (excess), THF/H₂O, 1 hour, room temperature.

2.3 ¹H NMR Spectroscopy Characterization of Ring-opened Oxanorbornene imides

It was found that the imide and ring-opened amide or diamide forms of the oxanorbornene imide monomers exhibited unique, well-defined shifts in their NMR spectra that facilitated characterizing the resulting ring-opened product for this class of molecules. Representative spectra for **2** are given in Figure 2.3, where the monomer alone is shown for clarity. Of particular interest were the alkene and methine bridgehead-adjacent protons of the oxanorbornene segment, as they exhibited the most obvious shifts between the imide and ring-opened forms. The imide starting material had well-defined singlets in the proton NMR spectrum at 6.57, 5.18, and 3.00 ppm, which corresponded to protons A, B, and C as labelled in Figure 2.3a. Notably, these peaks do not exhibit appreciable splitting (see inset), due to the weak coupling constants of the adjacent

protons. When **2** was placed in a basic solution of NaOD for several hours to allow for quantitative ring-opening (Figure 2.3b), a new set of peaks appeared in the spectrum that were indicative of a loss of symmetry. The A and B protons from the alkene and methine groups in the imide monomer both shifted upfield and become two doublets corresponding to the A' and A'' (6.38 and 6.31 ppm) and B' and B'' (5.04 and 4.93 ppm) protons in **2(Am)** (see inset). The spectrum in Figure 2.3b was obtained in D₂O/NaOD as opposed to DMSO-d₆ to observe the ring-opening reaction *in situ*.

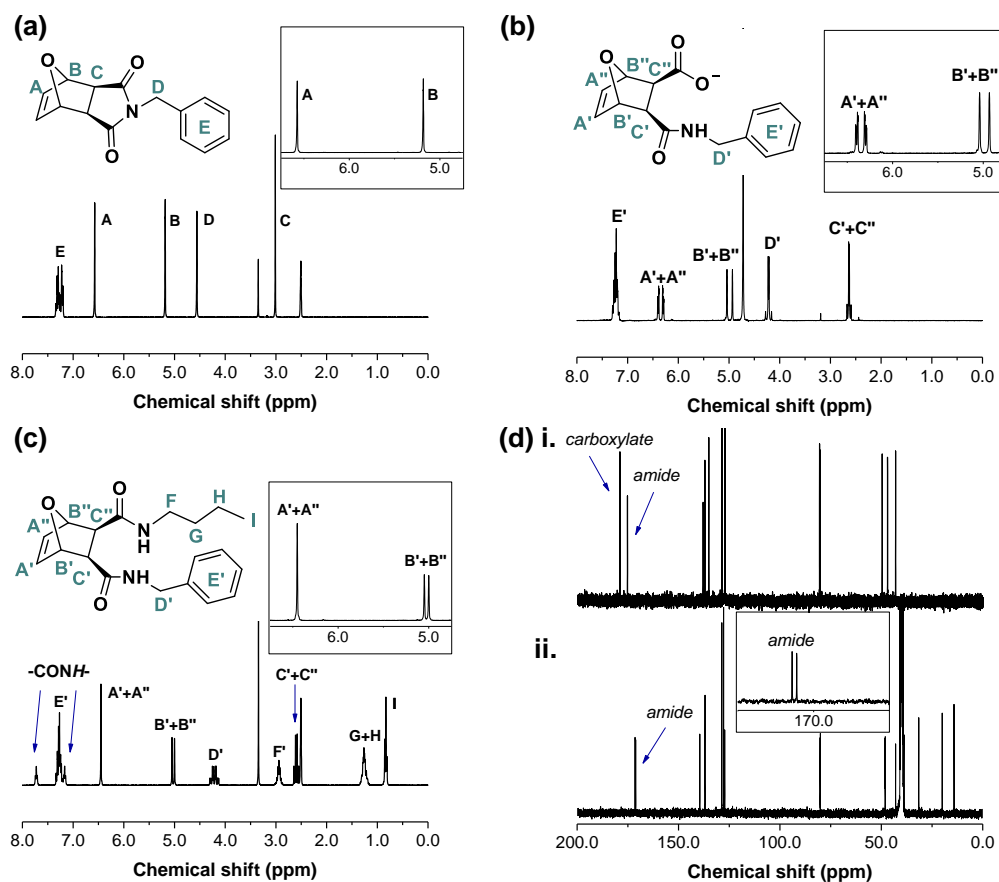


Figure 2.3: NMR spectra of the model oxanorbornene imide monomer **2** demonstrating hydroxide and amine reactivity: **(a)** monomer as synthesized (in DMSO-d₆); **(b)** ring-opened monomer containing both carboxylate and amide functional groups (in 0.1 M NaOD); **(c)** purified diamide monomer after reaction with n-butylamine (in DMSO-d₆); and **(d)** corresponding carbon spectra of (b) and (c) showing the characteristic **(i)** carboxylate and amide peaks and **(ii)** unequivalent amide peaks.

To more easily confirm the formation of the diamide after the addition of n-butylamine to **2**, the imide monomer was reacted with butylamine in the presence of water and purified prior to obtaining NMR spectra. Due to the limited solubility of **2(dAm)**, the spectrum shown in Figure 2.3c was again obtained in DMSO-d₆. As with **2(Am)**, the diamide **2(dAm)** showed the characteristic upfield shift of the alkene and methine protons and the appearance of A' and A'' (6.45 and 6.44 ppm) and B' and B'' (5.05 and 5.00 ppm) (see inset). Furthermore, the presence of peaks at 2.95, 1.26, and 0.83 ppm corresponding to protons F-I proved that n-butylamine was incorporated into **2(dAm)** to form the diamide. In fact, the two unique amide protons were visible in DMSO-d₆, appearing at 7.73 ppm (benzyl arm) and 7.16 ppm (butyl arm). The formation of an amide and carboxylate group in **2(Am)** and two amides in **2(dAm)** was also confirmed by their ¹³C NMR spectra (Figure 2.3d). While two clearly resolved peaks at 179.0 and 175.3 ppm corresponding to the carboxylate and amide carbonyl carbons respectively were visible in Figure 2.3d(i), two adjacent peaks at 171.4 and 171.1 ppm were observed in the amide region in Figure 2.3d(ii), as expected for the non-equivalent amide groups in **2(dAm)**. Ring-opening was confirmed for the given monomers in Table 2.1 in this manner when applicable.

Quantitative ring-opening of the **Poly1_{n=20}** was again demonstrated by ¹H NMR spectroscopy (Figure 2.4). In this case, the polymer was treated with base and purified by dialysis. The lyophilized ring-opened product **Poly1(Am)_{n=20}** was then analyzed by NMR spectroscopy. As seen with the monomers, the alkene backbone protons (A) and the methylene protons directly adjacent to the imide (D) shifted upfield (A' and D') after

ring-opening. Furthermore, there was no evidence of the quaternary ammonium group degrading under basic conditions in the several minutes that it took for the imide to be fully consumed.

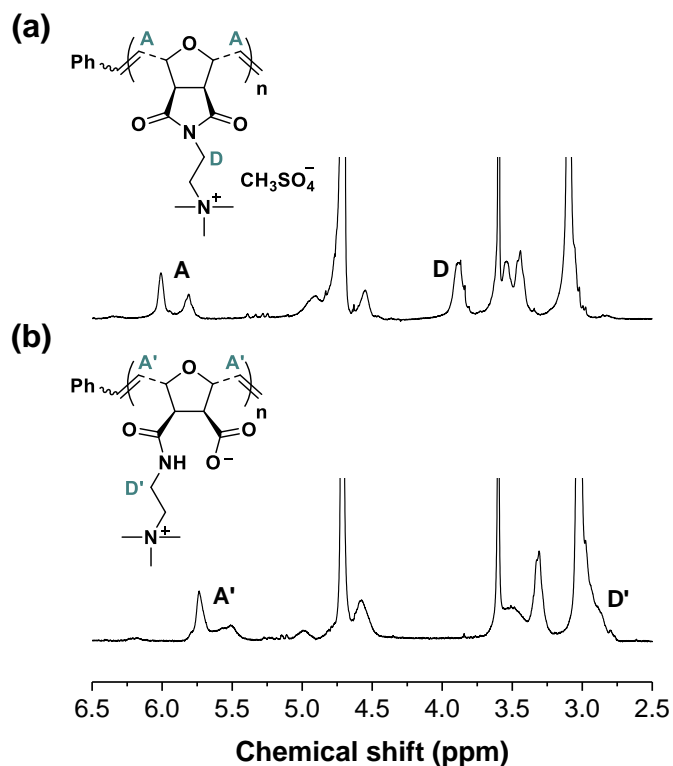


Figure 2.4: ^1H NMR spectra in D_2O of (a) the as-prepared cationic imide polymer **Poly1**_{n=20} and (b) the base-treated zwitterionic polymer **Poly1(Am)**_{n=20}. The complete upfield shift of the methylene protons *D* to *D'* confirm quantitative conversion.

The ^1H NMR spectra of **Poly2** and **Poly2(dAm)** (Figure 2.5a and b) confirmed that the butyl moiety had been incorporated into the polymer, and that the benzyl and butyl groups were present in a 1:1 ratio based on integration of the alkyl peaks and aromatic peaks. When the reaction was allowed to stir for long periods of time at $50\text{ }^\circ\text{C}$ in the presence of excess *n*-butylamine, the ratio of butyl groups to benzyl groups increased based on the peak integrations in the NMR spectra. This result was attributed to transamidation reactions where the benzyl groups were displaced by butylamine. The

lower resolution of the **Poly2(dAm)** spectrum in Figure 2.5b is due to the decreased solubility of the diamide polymer in organic solvents, which is discussed later in the chapter.

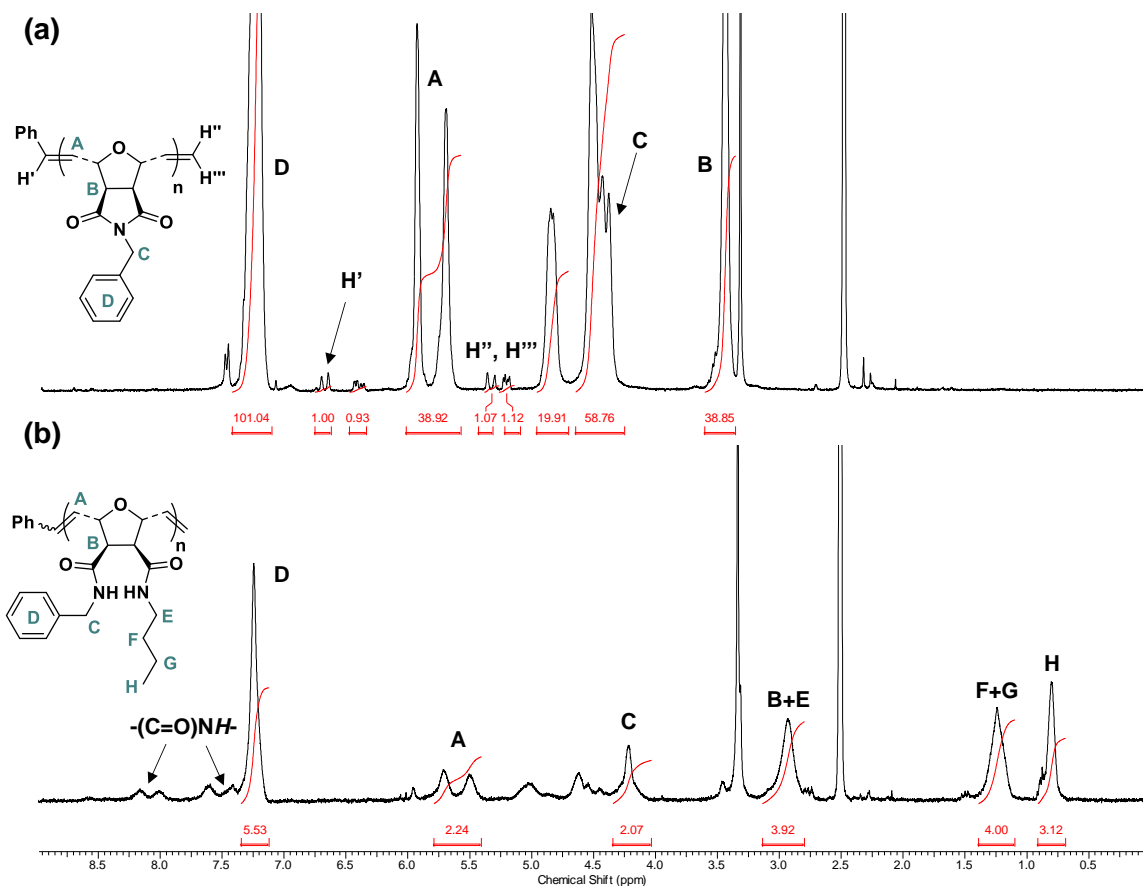


Figure 2.5. ^1H NMR spectra in DMSO-d_6 of (a) the as-prepared imide polymer **Poly2**_{n=20} and (b) the butylamine-treated polymer **Poly2(Am)**_{n=20}. The complete upfield shift of the methylene protons *D* to *D'* confirm quantitative conversion.

2.4 Characterization of Poly1

When R was cationic, as in the case of **Poly1**, the conversion of the imide to an amide and carboxylate effectively formed a zwitterion.^{3,5,6} While the ^1H NMR spectrum was a clear indication that the polymer's structure had changed, it did not decisively confirm that these structural changes were due to a reaction with the imide group. For this, FT-IR spectroscopy was employed to positively identify the functional groups present in

the precursor polymer and their conversion in the product. Figure 2.6 shows the spectra of **Poly1** (black line) and **Poly1(Am)** (green line). The vertical dotted line indicates the most intense C=O stretching frequency at 1707 cm^{-1} corresponding to the imide group. Whereas this peak was prominently featured in the spectrum of **Poly1**, it disappeared in the ring-opened product's spectrum. New resonances at 1565 cm^{-1} (C=O stretching, carboxylate), and 1659 and 3336 cm^{-1} (C=O and N-H stretching, amide) confirmed the presence of the expected carboxylate and amide groups in **Poly1(Am)**. NMR and IR corroborated the quantitative nature of this reaction, and the complete conversion of cationic **Poly1** to the zwitterionic form **Poly1(Am)**.

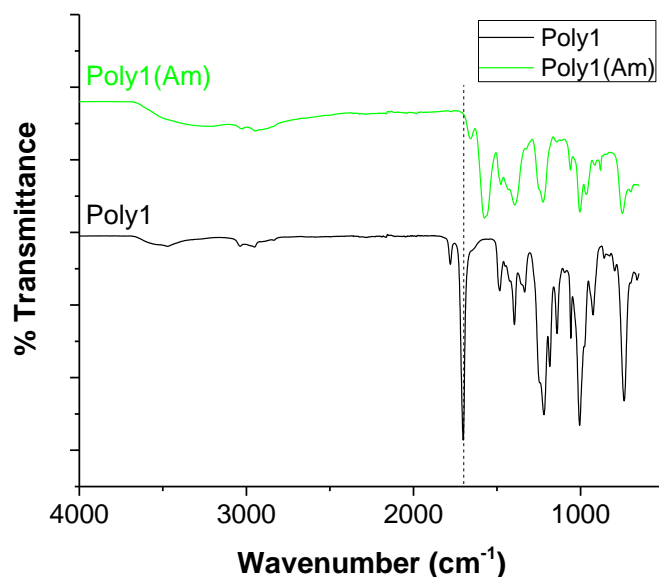


Figure 2.6: FT-IR spectra of **Poly1**_{n=20} (black line) and **Poly1(Am)**_{n=20} (green line). Dotted vertical line indicates characteristic imide resonance at 1707 cm^{-1} .

One advantage of ROMP is its ability to synthesize well-defined, low PDI (<1.1) polymers under mild conditions from a wide range monomers;¹⁵ however, certain functional groups, such as the anionic carboxylate, can complex with the catalyst and arrest

polymerization.^{1,8,9} Methods to avoid these complications include fully neutralizing the acid prior to polymerization or utilizing a protecting group such as a *tert*-butyl ester that is cleaved post-polymerization.^{1,3,9} This ring-opening reaction is essentially an alternative method for incorporating carboxylic acids into an oxanorbornene backbone. We showed above that the reaction in polymers is fast and quantitative; however, it was still unclear if the base treatment inadvertently interfered with the polymers' molecular weights or distributions. The GPC traces in Figure 2.7 showed that both **Poly1**_{n=20} and **Poly1(Am)**_{n=20} maintained similar distributions and retention times, implying that the ring-opening reaction did not significantly affect the polymer backbone through adverse reactions.

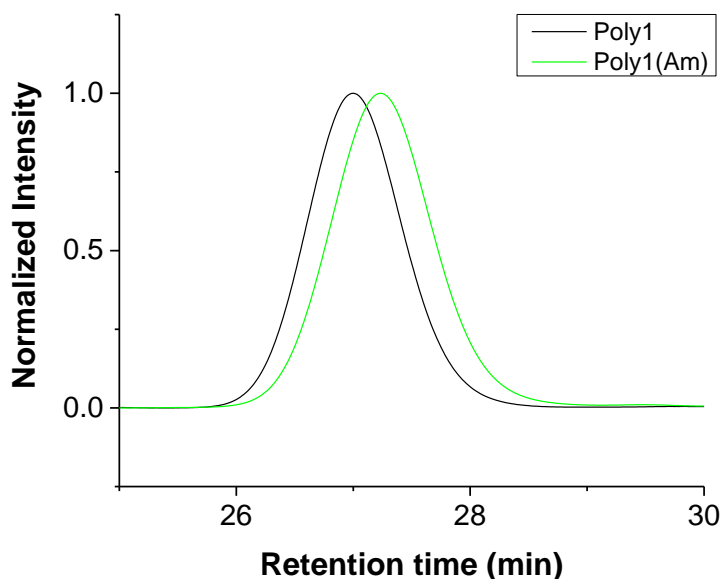


Figure 2.7: GPC traces of **Poly1**_{n=10} (black line) and **Poly1(Am)**_{n=10} (green line) in 2,2,2-trifluoroethanol with 20 mM NaTFA as the eluent, relative to PMMA standards. Spectra show retention of monomodal distribution after base treatment.

A molecular weight of 7 kDa for **Poly1**_{n=20} was confirmed by end-group analysis. The number average molecular weights (M_n) of **Poly1**_{n=20} and **Poly1(Am)**_{n=20} were given by GPC as 23 and 20 kDa, respectively, relative to PMMA standards. The discrepancy

between the theoretical and apparent molecular weights from GPC was attributed to the differences in solution properties and hydrodynamic radii between the PMMA standards and our oxanorbornene-based polymers, as well as the potential for interactions between the charged polymers and the stationary phase. Likewise, the longer retention time of the ring-opened polymer is thought to be a result of inadequately screened electrostatic interactions⁵ within the system as opposed to a true significant difference between the polymers. While GPC, especially in TFE, is not a reliable method for determining the molecular weight of these polymers, it ultimately shows that the ring-opened polymers maintained their relative distribution and low PDI (1.04). The well-defined structure of these ring-opened carboxylate-containing polymers, by a relatively straightforward synthetic method, makes this ring-opening reaction an interesting alternative for the incorporation of acid groups into an oxanorbornene backbone.

2.4.1 Solution Properties of Poly1(Am)

Polymeric betaines are overall charge-neutral, and many possess unique solution properties such as high solubility in salt water but low solubility in pure water, a phenomenon known as the anti-polyelectrolyte effect.⁵ Sulfobetaine, carboxybetaine and phosphorylcholine groups are the most common zwitterionic moieties to be incorporated into polymers, where the quaternary ammonium cation and various anions are both contained within each repeat unit and, more specifically, within the same side chain.⁵ The betaines that result from the ring-opening of a cationic oxanorbornene precursor, such as **Poly1(Am)**, are thus unique in that each repeat unit contains both charges; however, the charges are sequestered on separate arms of the repeat unit.

While the surface properties for dual-functional polybetaines like **Poly1(Am)** were well-established, their solution properties had not yet been investigated. We hoped to determine if the ring-opened polybetaine behaved similarly to polycarboxybetaines, which are structural isomers of **Poly1(Am)**, and if any unique characteristics such as aggregation were observed. Qualitatively, it was observed that **Poly1(Am)** crashed out of aqueous solution during dialysis and that it was no longer soluble in pure water or dilute solutions, unlike its precursor polymers. Dynamic light scattering (DLS) was used to observe the behavior of **Poly1_{n=230}** and **Poly1(Am)_{n=230}** in an aqueous solution of 0.1 M NaBr (Figure 2.8), where the salt concentration was selected due to its previously demonstrated ability to effectively solubilize oxanorbornene-based polybetaines and polyelectrolytes. Higher molecular weight polymers (83 kDa, based on conversion from NMR spectroscopy) were used to obtain better quality scattering data. A representative plot of the diameter distributions in solution as measured at 90° is given in Figure 2.8a, where the closed squares represent **Poly1_{n=230}** and the open circles represent **Poly1(Am)_{n=230}**. Although several relaxation times were observed for each polymer, only one significant size population existed for both **Poly1_{n=230}** and **Poly1(Am)_{n=230}**, where the diameters corresponding to the peak maxima were 10 nm and 24 nm, respectively.

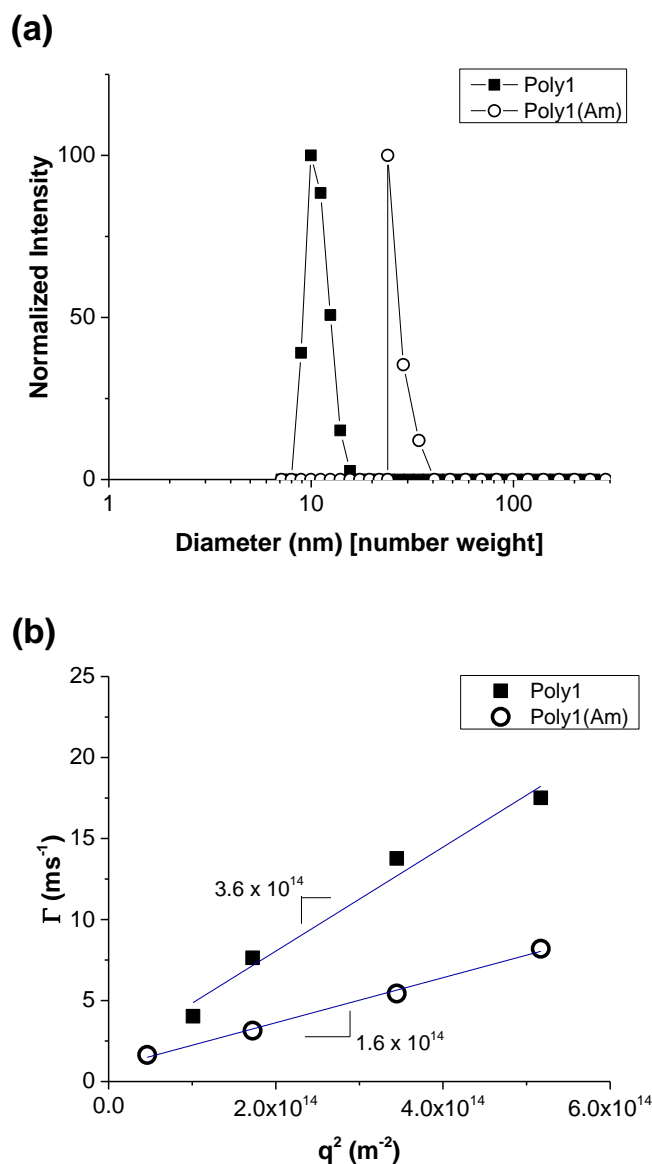


Figure 2.8: Dynamic light scattering data from **Poly1**_{n=230} and **Poly1(Am)**_{n=230} in 0.1 M NaBr, where (■) represent the cationic imide form and (○) represent the ring-opened zwitterionic form. **(a)** Representative diameter distributions at 90° by number weight, with peak maxima observed at approximately 10 and 24 nm for **Poly1**_{n=230} and **Poly1(Am)**_{n=230}, respectively. **(b)** Γ vs. q^2 plots.

For a more robust analysis of the polymers' behavior in solution, Γ vs. q^2 plots (Figure 2.8b) were generated. The linear fits of the slopes gave the diffusion coefficients $D = 3.64 \times 10^{-14}$ and $1.59 \times 10^{-14} \text{ m}^2/\text{ms}$ for **Poly1**_{n=230} and **Poly1(Am)**_{n=230}, respectively.² The hydrodynamic radii (R_h) were then calculated by the Stokes-Einstein equation² to be

5.6 and 11 nm for **Poly1**_{n=230} and **Poly1(Am)**_{n=230}, respectively. These R_h values are reasonable based on those calculated for other water-soluble polymers with oxanorbornene backbones and comparable molecular weights.^{1,9} The single population for each polymer implies that the polymers are molecularly dissolved in solution. Likewise, calculated hydrodynamic radii on the order of nanometers implies that the species in solution are polymer chains and not large aggregates. At this ionic strength, it was expected that the charges on the zwitterionic polymer were screened such that the polymer took on an extended chain conformation due to decreased inter- and intramolecular interactions.^{5,6,9} Thus, the diameter of **Poly1(Am)** was greater than that of **Poly1**, which would be expected to slightly shrink in an electrolyte solution due to the polyelectrolyte effect.

2.5 Amine-catalyzed ring-opening

In an analogous reaction to that discussed above, primary amines were found to catalyze the ring-opening reaction as well. Based on NMR studies with monomer **1** and n-butylamine in D₂O, ring-opening which formed a carboxylic acid and amide arm occurred when the amine was reacted with excess or stoichiometric amounts of monomer due to the change in pH (Figure 2.9). This reaction occurred quickly, within the time it took to prepare an NMR sample. Conversion to the ring-opened form increased linearly as the ratio of monomer to amine increased, with a slight excess of amine necessary for full conversion. The pK_a of n-butylamine is 10.59, making it weakly basic.¹⁶ When other amines such as isopropylamine ($pK_a = 10.63$) and benzylamine ($pK_a = 9.34$) were used, a decrease in reactivity was observed with increasing acidity.¹⁷ At a ratio of 3:4 [amine]:[monomer], for instance, n-butylamine resulted in 70% conversion, whereas isopropylamine and benzylamine resulted in 60% and 50% conversion, respectively. This

trend of instantaneous conversion followed with basicity of the amine, as expected. All amines behaved similarly when the system was allowed to react for longer time periods (up to 24 hours), suggesting that the basicity of the amine mostly affected the rate of reaction. It was found that while both aliphatic and aromatic amines could induce ring-opening, deactivated amines such as 1H,1H-perfluorooctylamine would not react, even at extended reaction times and with the addition of heat.

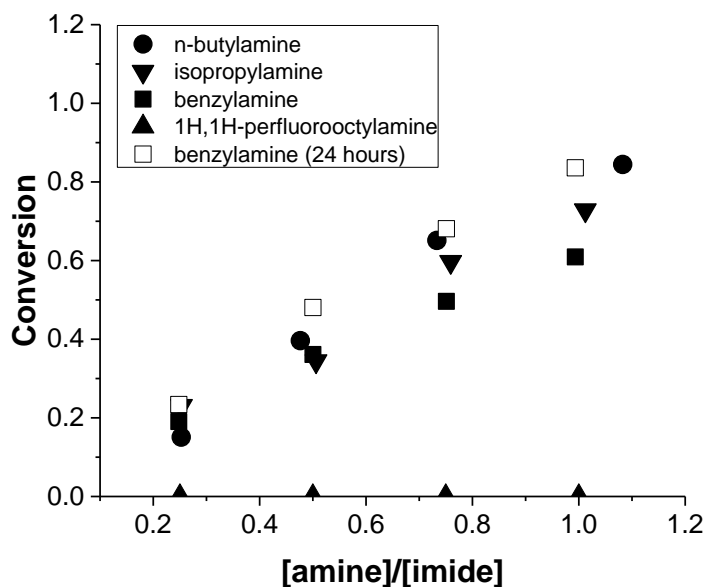


Figure 2.9: Effect of primary amine on the conversion to the ring-opened form of 1 as a function of the initial ratio of reactants. Conversion was calculated by ^1H NMR spectroscopy.

2.5.1 Characterization of Poly2

When a several-fold excess of amine was used, the imide was converted to two amide groups where the amine was incorporated into the monomer as a secondary side chain, for example in **Poly2(dAm)** (Figure 2.2). This reaction opened up a new synthetic avenue for post-polymerization functionalization. Ring-opening the imide monomer provided a facile method to obtain diamide monomers, a feat which is challenging with

other synthetic methods due to side reactions. More problematic was the inability of the diamide monomers to be readily polymerized by Grubbs' catalysts. The amide linkage for functional groups is desirable due to its increased stability over ester groups under aqueous conditions, as well as the potential for hydrogen bonding. Ring-opening of the substituted imide post-polymerization allowed for well-defined diamide polymers to be synthesized.

To demonstrate the range of this reaction, the hydrophobic **Poly2** with an aromatic side chain was used as a model system. The imide precursor polymer was fully dissolved in a minimum amount of THF and an equal volume of n-butylamine was added. Water was then added dropwise in equal volume. Again, the reaction was fast and quantitative, with full conversion in a matter of minutes. In the case of volatile amines like butylamine, the polymer could be recovered by evaporating off the solvent, otherwise the polymer was recovered by precipitation. IR spectra of reactant **Poly2** (black line) and product **Poly2(dAm)** (blue line) are given in Figure 2.10. The imide carbonyl stretching resonance, marked with the dotted vertical line, was prominent in the spectrum of **Poly2**. Peaks corresponding to the amide groups appeared at 1649 and 3293 cm^{-1} in the spectrum of **Poly2(dAm)** while the peak at 1707 cm^{-1} had disappeared, indicating complete consumption of the imide groups along the polymer backbone. A sharp peak at 2931 cm^{-1} corresponding to a new alkyl side chain also appeared. No acid resonance was observed, which implied that each repeat unit had been converted to the diamide form as opposed to the amide/acid form.

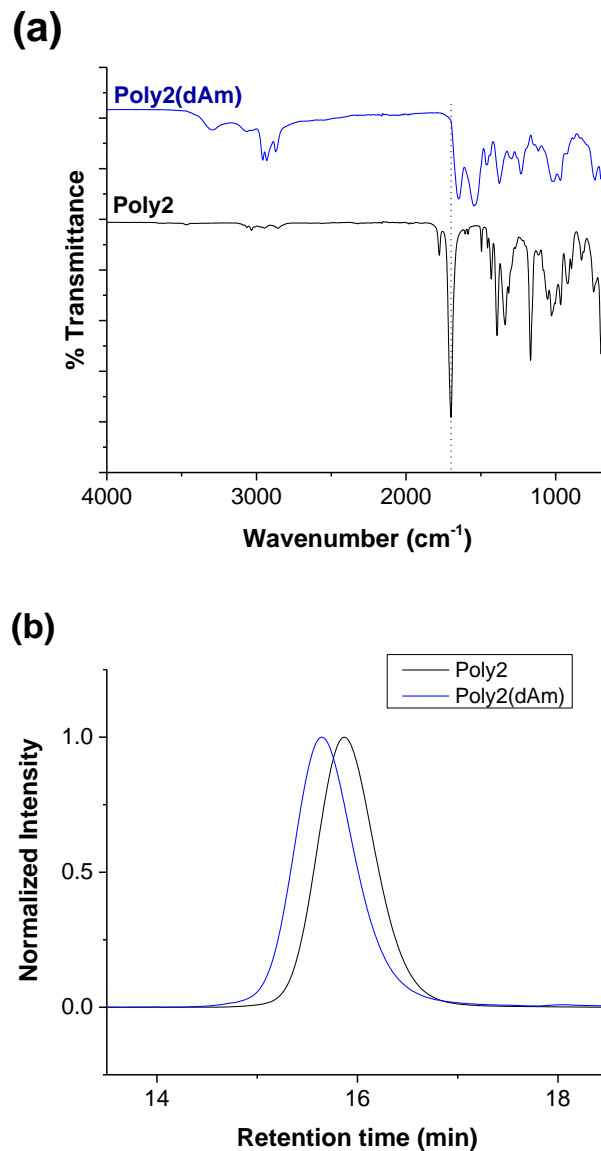


Figure 2.10: Characterization of the conversion from **Poly2_{n=20}** to **Poly2(dAm)_{n=20}** by n-butylamine. **(a)** FT-IR spectra **(b)** GPC traces for **Poly2_{n=20}** (black line) and **Poly2(dAm)_{n=20}** (blue line). GPC traces were obtained in DMF with 0.01 M LiCl as the eluent, relative to PMMA standards.

Previous attempts at polymerizing these diamide oxanobornene monomers yielded either oligomers or poorly controlled polymers; however, the GPC traces for **Poly2_{n=20}** and **Poly2(dAm)_{n=20}** in Fig. 6b show that both the imide precursor polymer and the diamide product were monomodal with low polydispersities (PDI < 1.1). The longer retention time

of **Poly2(dAm)_{n=20}** corresponds to the increased molecular weight due to the incorporation of the butyl group. Clearly, the well-defined nature of **Poly2** was preserved during the ring-opening reaction, demonstrating the efficacy of this reaction as a post-polymerization functionalization method. It should be noted that while **Poly2** was freely soluble in chloroform, THF, and other organic solvents, **Poly2(dAm)** was only fully soluble in DMF. In fact, **Poly2(dAm)** would form a cloudy emulsion with water at high dilutions. The polymer then aggregated upon the addition of guanidine hydrochloride, possibly indicating that hydrogen bonding between the amide groups is responsible for the polymer's decreased solubility in organics.

2.6 Characterization of Unsubstituted Imide Poly7 Ring-opening

In Table 2.1, a notable exception among the monomers was clear: the unsubstituted oxanorbornene imide **7** (R=H) did not ring-open under basic hydroxide or amine conditions. When first placed in 0.1 M NaOD, the monomer was initially insoluble. After approximately 10 minutes a clear, homogeneous solution was obtained; however, there was no evidence in the NMR spectra of ring-opening. No ring-opening was observed when the reaction time and the base concentration of the solution (up to 1.0 M NaOH) was further increased. Based on the monomer's gradual dissolution in aqueous media, it was thought that the imide was deprotonated under basic conditions. The pK_a of succinimide is near 9,¹⁷ so monomer **7** was assumed to be weakly acidic as well, and thus deprotonated under these reaction conditions where the pH of the sodium hydroxide solution was approximately 11. After deprotonation, the increased delocalized electron density across the imide group could be expected to greatly decrease its electrophilicity, thereby inhibiting ring-opening.

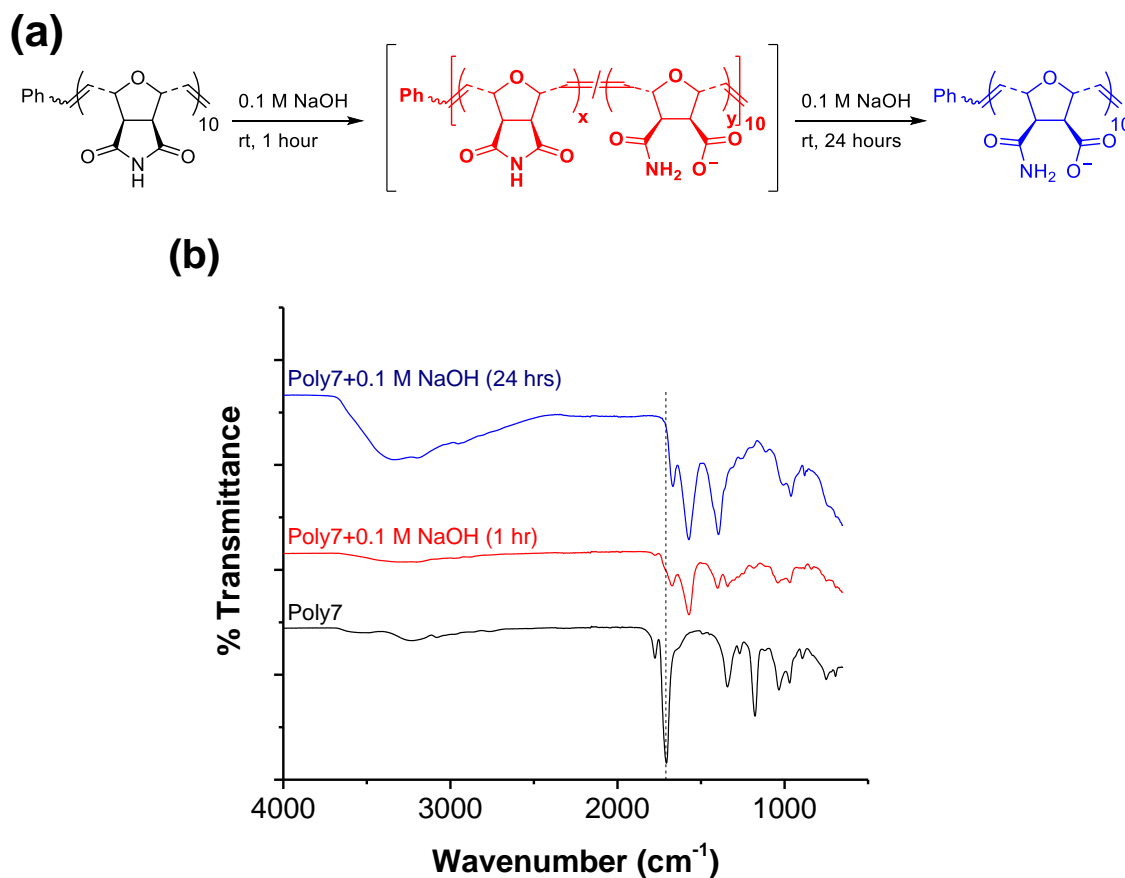


Figure 2.11: Ring-opening reaction of poly(oxanorbornene imide) **Poly7** in the presence of sodium hydroxide. **(a)** Reaction scheme and structures showing the progression from the imide form (black) to partial ring-opening (red) to full conversion to the amide and carboxylate groups (blue) after exposure to 0.1 M NaOH; **(b)** FT-IR spectra of **Poly7** showing the ring-opening reaction progression. Dotted vertical line indicates characteristic imide resonance at 1707 cm^{-1} .

To our surprise, however, **Poly7** ring-opened after polymerization (Figure 2.11). Due to the general insolubility of **Poly7** in many organic solvents, only a short polymer (DP = 10) was synthesized as a model to aid in characterization. Even at low molecular weights, **Poly7** was only partially insoluble in both NaOD solutions and DMSO/NaOD solutions, so *in situ* NMR characterization was inconclusive. The isolated polymer after ring-opening was largely insoluble in polar organic and aqueous solvents as well, so in this case the most powerful characterization method was IR spectroscopy. It was found that

when **Poly7**_{n=10} was stirred in a dilute solution of 0.1 M NaOH for one hour, a portion of its imide groups had ring-opened (Figure 2.11a), and after 24 hours all imide groups had been consumed.

Figure 2.11b shows the reaction progression as monitored by IR spectroscopy, where the black line represented **Poly7**_{n=10} as-prepared, the red line after 1 hour in NaOH, and the blue line after 24 hours. The dotted vertical line highlights the characteristic imide peak at 1707 cm⁻¹, which weakened after 1 hour and disappeared after 24 hours. After 24 hours, peaks at 1576, 1669, and 3339 cm⁻¹ indicated the presence of amide and carboxylate groups in the product, as expected from the ring-opening reaction. The broadness of the peak from 2900 to 3700 cm⁻¹ suggests the presence of hydrogen bonding or retained water within the sample. Conversion of the imide repeat units to the ring-opened forms was considered to be quantitative within the resolution of the spectra.

Ring strain was ruled out as the dominant driving force behind the ring-opening of **Poly7**, because the imide ring-opened after polymerization where ring strain was assumed to be less than in the monomer. Unfortunately, the limited solubility of **Poly7** also made it extremely difficult to quantitatively measure the pK_a and other solution properties of the polymer before or after ring-opening. While monomer **7** was freely soluble in a range of polar and chlorinated solvents including acetone and dichloromethane, **Poly7** was only soluble in DMSO and DMF; after ring-opening, the polymer was only partially soluble in DMSO, DMF and an organic/aqueous mixture. It is known that polymerization of an acidic monomer results in an increase of the acidic group's pK_a, such as in the case of acrylic acid and poly(acrylic acid).⁷ The titration of a similarly acidic, oxanorbornene diacid polymer had demonstrated the same phenomenon, where the pK_a increased from 5.3 to 6.1

for the monomer and polymer, respectively.⁷ The acidity of the imide group was thus expected to decrease after polymerization as well. It is feasible that the increased basicity of the imide proton increased the electrophilicity of the carbonyl groups and/or decreased the likelihood of deprotonation, both of which would make the imide more susceptible to nucleophilic attack and subsequent ring-opening. While it was interesting that **Poly7** but not monomer **7** ring-opened, the resulting polymer's insolubility in both aqueous and organic solutions limits many potential applications.

2.7 Experimental Procedures

2.7.1 Materials

All reagents were purchased from either Sigma-Aldrich, Alfa Aesar, Acros Organics or Fisher Scientific in the highest purity available and used as received, unless otherwise noted. 1,3-dinitrobenzene was obtained from Avocado Research Chemicals and used as received. Sodium deuterioxide (40 wt % in deuterium oxide) was purchased from Cambridge Isotopes. Tetrahydrofuran (THF, Fisher Scientific, HPLC grade) was distilled from sodium/benzophenone under nitrogen and dichloromethane (CH₂Cl₂, Fisher Scientific, ACS grade) was distilled from CaH₂ under nitrogen immediately prior to use. 2,2,2-trifluoroethanol (TFE, 99+%) was purchased from Alfa Aesar and used as received. Grubbs' 3rd generation catalyst (G3) was synthesized according to a previously published procedure.¹⁹ Spectra/Por® 6 dialysis membranes were purchased from Spectrum Medical Industries.

2.7.2 Instrumentation and methodology

Nuclear magnetic resonance (NMR) spectra were obtained on a Bruker DPX-300 NMR spectrometer. Abbreviations for assignments are as follows: s: singlet; t: triplet; q: quartet; m: multiplet; comp: overlapping non-equivalent peaks; br: broad.

Mass spectral data were obtained at the University of Massachusetts, Mass Spectrometry Facility from a JEOL JMS 700 instrument (JEOL, Peabody, MA).

Gel permeation chromatography (GPC) traces in 2,2,2-trifluoroethanol (TFE) were obtained on an Agilent 1260 series system with a refractive index detector. A HFIP gel guard column (7 mm x 50 mm) and 3 HFIP gel columns (7mm x 300 mm) were connected in series. The columns were incubated at 40 °C. TFE with 20 mM NaTFA was used as the eluent at a flow rate of 1.0 mL/min. Methanol was used as the flow marker. Molecular weight was calculated relative to poly(methyl methacrylate) standards.

GPC traces in N,N-dimethylformamide (DMF) were obtained using a Polymer Laboratories PL-GPC50 instrument with two 5 mm mixed-D columns, a 5 mm guard column, and a Knauer RI detector. DMF with 0.01 M LiCl was used as the eluent at a flow rate of 1.0 mL/min. The system was calibrated against poly(methyl methacrylate), with toluene as the flow marker.

Fourier transform infrared (FT-IR) spectra were recorded by a PerkinElmer Spectrum 100 spectrometer with a universal ATR sampling accessory and ZnSe crystal.

Dynamic light scattering data was obtained on a Brookhaven BI-200 SM research goniometer system, equipped with an argon laser ($\lambda = 637$ nm) and a photomultiplier detector, with a TurboCorr digital correlator for signal processing. BI-DLSW control software was supplied by the manufacturer. Polymer samples were prepared by stirring

the purified polymers in 0.1 M NaBr for 72 hours, then filtering through a 0.45 μm PES Restek syringe filter immediately prior to analysis. Samples were measured at four angles: 45°, 60°, 90°, and 120°.

2.7.3 Synthesis

2.7.3.1 Monomer synthesis

Oxanorbornene imide-based monomers were synthesized according to previously published procedures. **1**: ref. 3; **2**: ref. 19; **3**: ref. 1; **4**: ref. 8; **5**: ref. 20; **6**: ref. 19; **7**: ref. 21.

2.7.3.2 General polymerization procedures

Charged monomers 1, 3: Monomer (**1** or **3**) and G3 were weighed into separate clean, dry Schlenk flasks under N_2 . The monomer was then dissolved in 3 mL 2,2,2-trifluoroethanol and the catalyst was dissolved in 2 mL dry CH_2Cl_2 . Both solutions were subjected to 3 freeze-pump-thaw cycles and warmed to room temperature. Using a nitrogen-purged syringe, the monomer solution was added to the catalyst solution. The polymerization was allowed to proceed for 30 minutes at room temperature under N_2 . To quench the reaction, 1.5 mL ethyl vinyl ether was added and the solution was stirred for an additional hour. The polymer was then precipitated out into anhydrous diethyl ether, isolated by vacuum filtration and dried under high vacuum overnight. Yields were greater than 90% for all polymers.

Uncharged monomers 2, 4-7: Monomer (**2, 4-7**) (0.3 g, 0.83 mmol, 30 equivalents) and G3 (0.024 g, 0.028 mmol, 1 equivalent) weighed into separate clean, dry Schlenk flasks under N_2 . The monomer and catalyst were then dissolved in dissolved in 2 mL dry CH_2Cl_2 each. Both solutions were subjected to 3 freeze-pump-thaw cycles and

warmed to room temperature. Using a nitrogen-purged syringe, the monomer solution was added to the catalyst solution. The polymerization was allowed to proceed for 30 minutes at room temperature under N₂. To quench the reaction, 1.5 mL ethyl vinyl ether was added and the solution was stirred for an additional hour. The polymer was then precipitated out into anhydrous diethyl ether, isolated by vacuum filtration and dried under high vacuum overnight. Yields were greater than 90% for all polymers.

2.7.3.3 General ring-opening procedures

Sodium hydroxide ring-opening NMR experimental procedure: 0.1 M sodium deuterioxide (NaOD) was prepared by serially diluting stock sodium deuterioxide as purchased. Monomer or polymer at a concentration of 10.0 mg/mL was allowed to fully dissolve in the NMR solvent. Spectra were collected immediately after dissolution.

Synthesis of Poly1(Am): Approximately 0.1 g polymer was dissolved in 20 mL 0.1 M NaOH and allowed to stir for 1 hour. The solution was then dialyzed against RO water (MWCO = 2000 Da or 8000 Da) until the conductivity of the water reached 0.1 μ S. Polymer was isolated as a white powder by lyophilization.

Synthesis of 2(dAm): 0.1 g of **1** was dissolved in a minimum amount of 1:1 THF:n-butylamine. An equal volume of water was then added dropwise. Within several minutes, an off-white precipitate had formed. The reaction was allowed to stir overnight. The precipitate was filtered, washed with excess water and THF, and dried overnight under vacuum.

Synthesis of Poly2(dAm): Approximately 0.1 g polymer was dissolved in 10 mL THF, then 5 mL n-butylamine was added. Dropwise, 5 mL water was added to the vigorously stirring solution. The homogenous reaction was allowed to stir for 1 hour,

then the organic solvents were removed under reduced pressure. Excess water was added to precipitate out the polymer. The polymer was filtered, washed with excess THF, and dried overnight under vacuum. In cases where an emulsion formed (lower molecular weights), the product was isolated by centrifugation.

2.7.4 Characterization

Poly1: ^1H NMR (300MHz, D_2O): δ (ppm) = 3.10 (br, 9H), 3.45 (br, 2H), 3.52 (br, 2H), 3.59 (s, 3H, CH_3SO_4^-), 3.87 (br, 2H), 4.57 (br, 1H), 4.92 (br, 1H), 5.81 (br, 1H), 6.01 (br, 1H).

Poly2: ^1H NMR (300MHz, DMSO-d_6): δ (ppm) = 3.47 (br, 2H, $-\text{CH}-\text{C}=\text{O}$), 4.46 (br m, 3H, $-\text{CH}_2-(\text{C}_6\text{H}_5)$ and $-\text{C}-\text{CH}-\text{O}-$), 4.85 (br, 1H, $-\text{C}-\text{CH}-\text{O}-$), 5.72 (br, 1H, $-\text{CH}=\text{CH}-$), 5.95 (br, 1H, $-\text{CH}=\text{CH}-$), 7.25 (br, 5H, $-\text{CH}_2-(\text{C}_6\text{H}_5)$).

Poly1(Am): ^1H NMR (300MHz, 0.1 M NaOD): δ (ppm) = 2.88 (br, 2H), 3.04 (br, 9H), 3.31 (br, 2H), 3.49 (br, 2H), 3.61 (s, 3H, CH_3SO_4^-), 4.59 (br, 1H), 4.98 (br, 1H), 5.49 (br, 1H), 5.74 (br, 1H).

2(dAm): ^1H NMR (300MHz, DMSO-d_6): δ (ppm) = 0.83 (m, 3H, $-\text{CH}_2-\text{CH}_2-\text{CH}_2-\text{CH}_3$), 1.26 (m, 4H, $-\text{CH}_2-\text{CH}_2-\text{CH}_2-\text{CH}_3$), 2.55 (d, 1H, $-\text{CH}-\text{C}=\text{O}$), 2.62 (d, 1H, $-\text{CH}-\text{C}=\text{O}$), 2.93 (m, 2H, $-\text{CH}_2-\text{CH}_2-\text{CH}_2-\text{CH}_3$), 4.16 (m, 1H, $-\text{CH}_2-(\text{C}_6\text{H}_5)$), 4.27 (m, 1H, $-\text{CH}_2-(\text{C}_6\text{H}_5)$), 5.00 (s, 1H, $-\text{C}-\text{CH}-\text{O}-$), 5.05 (s, 1H, $-\text{C}-\text{CH}-\text{O}-$), 6.45 (br, 2H, $-\text{CH}=\text{CH}-$), 7.17 (t, $J = 5.46$ Hz, 1H, $-(\text{C}=\text{O})-\text{NH}-$), 7.27 (br, 5H, $-\text{CH}_2-(\text{C}_6\text{H}_5)$), 7.73 (t, $J = 5.65$, 1H, $-(\text{C}=\text{O})-\text{NH}-$).

Poly2(dAm): ^1H NMR (300MHz, DMSO-d_6): δ (ppm) = 0.80 (br, 3H, $-\text{CH}_2-\text{CH}_2-\text{CH}_2-\text{CH}_3$), 1.24 (br, 4H, $-\text{CH}_2-\text{CH}_2-\text{CH}_2-\text{CH}_3$), 2.93 (m, 4H, $-\text{CH}_2-\text{CH}_2-\text{CH}_2-\text{CH}_3$ and $-\text{CH}-\text{C}=\text{O}$), 4.21 (br, 2H, $-\text{CH}_2-(\text{C}_6\text{H}_5)$), 4.62 (br, 1H, $-\text{C}-\text{CH}-\text{O}-$), 5.03 (br, 1H, $-\text{C}-\text{CH}-\text{O}-$), 5.51

(br, 1H, -CH=CH-), 5.71 (br, 1H, -CH=CH-), 7.24 (br, 5H, -CH₂-(C₆H₅)), 7.52 (m, 1H, -(C=O)-NH-), 8.09 (m, 1H, -(C=O)-NH-).

2.8 Conclusions

Poly(oxanorbornene imide)s are popular synthetic platforms for ROMP polymers, due to their modular nature, facile and controlled polymerization, and stability. Previously it had been observed that the imide would ring-open when exposed to an aqueous sodium hydroxide solution. It was shown here that all *N*-substituted oxanorbornene imides ring-opened in the presence of a base. Either sodium hydroxide or organic primary amines could catalyze this reaction. When an excess of amine was used, a diamide structure was formed, where the amine incorporated itself into the polymer as a new side chain. Consequently, poly(oxanorbornene imide)s could be functionalized post-polymerization to incorporate carboxylate and amide groups into the polymer. The quantitative nature and short time scale of the ring-opening made these reactions attractive alternatives to other post-polymerization functionalization methods. We proved that the resulting polymers maintained their well-defined molecular weight distributions and low PDIs. It was further envisioned that these post-polymerization functionalization reactions can be used to create many novel polymeric materials.

2.9 References

- (1) Colak, S.; Tew, G. N. Synthesis and Solution Properties of Norbornene Based Polybetaines. *Macromolecules* **2008**, *41*, 8436-8440.
- (2) Maddikeri, R. R.; Colak, S.; Gido, S. P.; Tew, G. N. Zwitterionic Polymersomes in an Ionic Liquid: Room Temperature TEM characterization. *Biomacromolecules* **2011**, *12*, 3412-3417.

- (3) Colak, S.; Tew, G. N. Dual-Functional ROMP-Based Betaines: Effect of Hydrophilicity and Backbone Structure on Nonfouling Properties. *Langmuir* **2012**, *28*, 666-675.
- (4) Colak, S.; Tew, G. N. Amphiphilic Polybetaines: The Effect of Side-Chain Hydrophobicity on Protein Adsorption. *Biomacromolecules* **2012**, *13*, 1233-1239.
- (5) Lowe, A. B.; McCormick, C. L. Synthesis and Solution Properties of Zwitterionic Polymers. *Chem. Rev.* **2002**, *102*, 4177-41895.
- (6) Kudaibergenov, S.; Jaeger, W.; Laschewsky, A. Polymeric Betaines: Synthesis, Characterization and Application. *Adv. Polym. Sci.* **2006**, *201*, 157-224.
- (7) Lienkamp, K.; Kins, C. F.; Alfred, S. F.; Madkour, A. E.; Tew, G. N. Water-Soluble Polymers from Acid-Functionalized Norbornenes. *J. Polym. Sci.: Part A* **2009**, *47*, 1266-1273.
- (8) Rankin, D. A.; P'Pool, S.J.; Schanz, H-J.; Lowe, A. B. The Controlled Homogeneous Organic Solution Polymerization of New Hydrophilic Cationic *exo*-7-Oxanorbornenes via ROMP with RuCl₂(PCy₃)₂CHPh in a Novel 2,2,2-Trifluoroethanol/Methylene Chloride Solvent Mixture. *J. Polym. Sci.: Part A* **2007**, *45*, 2113-2128.
- (9) Rankin, D. A.; Lowe, A. B. New Well-Defined Polymeric Betaines: First Report Detailing the Synthesis and ROMP of Salt-Responsive Sulfopropylbetaine- and Carboxyethylbetaine-*exo*-7-oxanorbornene Monomers. *Macromolecules* **2008**, *41*, 614-622.
- (10) Rankin, D. A.; Schanz, H-J. Effect of the Halide Counterion in the ROMP of *exo*-Benzyl-[2-(3,5-dioxo-10-oxa-4-azatricyclo[5.2.1.0^{2,6}]dec-8-en-4-yl)ethyl]dimethylammonium Bromide/Chloride. *Macromol. Chem. Phys.* **2007**, *208*, 2389-2395.
- (11) Su, S. C. K.; Shafer, J. A. Effect of the imidazole group on the hydrolysis of N-[2-(4-imidazolyl)ethyl] phthalimide. *J. Org. Chem.* **1969**, *34*, 2911-2915.
- (12) González-Vera, J. A.; García-López, M. T.; Herranz, R. Regioselective Base-Promoted Nucleophilic Ring Opening of Spirocyclic 2,6-Dioxopiperazines: Synthesis of *N*-(1-Carboxycyclohexyl)amino Acid Derivatives. *Eur. J. Org. Chem.* **2007**, 548-554.
- (13) Green, T. W.; Wuts, P. G. M. *Protective Groups in Organic Synthesis*. Wiley-Interscience, New York, **1999**, 564-566, 740-743.
- (14) Katritzky, A. R.; Yao, J.; Qi, M.; Chou, Y.; Sikora, D. J.; Davis, S. Ring opening reactions of succinimides. *Heterocycles* **1998**, *48*, 2677-2691.

- (15) Bielawski, C. W.; Grubbs, R. H. Living ring-opening metathesis polymerization. *Prog. Polym. Sci.* **2007**, *32*, 1-29.
- (16) Hall, H. K. Correlation of the Base Strengths of Amines. *J. Am. Chem. Soc.* **1957**, *79*, 5441-5444.
- (17) *Merck Index*, 12th Edition, 9040.
- (18) Love, J. A.; Morgan, J. P.; Trnka, T. M.; Grubbs, R. H. A Practical and Highly Active Ruthenium-Based Catalyst that Effects the Cross Metathesis of Acrylonitrile. *Angew. Chem. Int. Ed.* **2002**, *41*, 4035-4037.
- (19) Som, A.; Tezgel, A. O.; Gabriel, G. J.; Tew, G. N. Self Activation in De Novo Designed Mimics of Cell-Penetrating Peptides. *Angew Chem., Int. Ed.*, **2011**, *50*, 6147-6150.
- (20) Matson, J. B.; Grubbs, R. H. ROMP-ATRP Block Copolymers Prepared from Monotelechelic Poly(oxa)norbornenes Using a Difunctional Terminating Agent. *Macromolecules* **2008**, *41*, 5626.
- (21) Kim, G.-C.; Jeong, J.-G.; Lee, N.-J.; Ha, C.-S.; Cho, W.-J. Synthesis and biological activities of endo-3,6-epoxy-1,2,3,6-tetrahydrophthalimide and its polymers. *Journal of Applied Polymer Science* **1997**, *64*, 2605-2612.

CHAPTER 3
SYNTHESIS OF POLYBETAINES BY RING-OPENING METATHESIS
POLYMERIZATION

3.1 Introduction

In this chapter, the synthesis of a library of novel oxanorbornene imide-based polybetaines is discussed. A ROMP-based platform was initially chosen because of its demonstrated ability to tolerate charged groups and the controlled structure of the resulting polymers.¹⁻⁴ The modular nature of the oxanorbornene imide monomer allowed for easy incorporation of a wide variety of zwitterionic chemistries into the same polymer backbone. Two broad classes of zwitterions were designed and synthesized: linear betaines and dual-functional betaines, both of which contained quaternary amines as the cationic group. The linear betaines encompassed the **Carboxy(ZI)** and **Sulfo(ZI)** series, which contained carboxylate and sulfonate anions, respectively. The dual-functional betaines were obtained by the ring-opening reaction described in Chapter 2. A cationic precursor was converted to a betaine by treating the polymer with sodium hydroxide to form the anionic carboxylate group. The **C₁(ZI)** dual-functional series contained a quaternary ammonium group while the alkyl chain between the cationic group and the backbone was increased from an ethyl to a hexyl group. Enabled by the unique dual-functional chemistry afforded by the imide backbone, a series of amphiphilic betaines (**Amph(ZI)**) was synthesized that contained a range of hydrocarbon and fluorinated hydrophobes. The controlled nature of these unique molecules' polymerization by Grubbs' 3rd generation catalyst was also confirmed. This chapter lays the synthetic

groundwork for foundational polybetaines that will be studied in subsequent chapters as nonfouling materials.

3.2 General Approach

Despite the breadth of literature that exists for polyzwitterions from radical polymerization techniques, most (methy)acrylate/acrylamide-based zwitterionic chemistry lacks structural diversity.^{5,6} Based on our knowledge of oxanorbornene-based polymers and ROMP (Chapter 2), we saw an opportunity to synthesize a wide range of structurally diverse polybetaines by utilizing this polymer chemistry. ROMP is known to be largely tolerant of charged functional groups and thus well-defined polymers could be obtained under relatively mild reaction conditions.¹⁻⁴ Norbornene-based monomers that incorporate a range of charged side chain chemistries are also relatively easy to synthesize.^{7,8} The oxanorbornene imide backbone was of particular interest. As discussed in Chapter 2, the imide ring-opened under strongly basic conditions, which allowed for the creation of dual-functional zwitterions. These betaines contained a carboxylate group, formed when the imide group ring-opened after treatment with sodium hydroxide, and a quaternary amine that carried an additional functional group.

Previously, oxanorbornene-based sulfobetaines and carboxybetaines had been synthesized and tested as potential nonfouling coatings.⁷ Novel dual-functional oxanorbornene-based polybetaines containing hydrophilic, hydrophobic and lipophobic (fluorinated) side chains were synthesized as well.⁸ These polymers served as foundational materials by allowing for tunable hydrophilicity and oleophobicity, properties that have traditionally been thought of as the largest contributors to nonfouling performance. Based on the promising nonfouling properties of the initial oxanorbornene-

based polybetaines and the ease with which a library of polymers could be generated, we looked to expand upon the available zwitterionic chemistries.

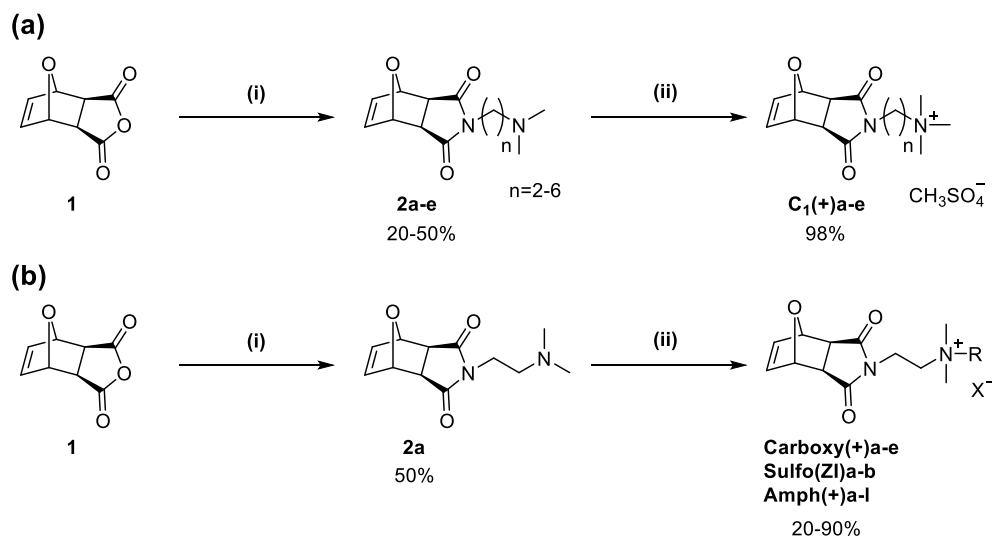


Figure 3.1. Synthesis of cationic precursor and zwitterionic oxanorbornene imide-based monomers. **(a)** (i) *N,N*-dimethylalkyldiamine, methanol/tetrahydrofuran, 60 °C (1 hour) to 50 °C, overnight; (ii) dimethylsulfate, tetrahydrofuran, 0 °C to room temperature, 4 hours; **(b)** (i) *N,N*-dimethylethylenediamine, methanol/tetrahydrofuran, 60 °C (1 hour) to 50 °C, overnight; (ii) R-X, tetrahydrofuran or acetonitrile, 50 °C, 48 hours.

The synthetic procedures to obtain the monomers discussed hereafter are outlined in Figure 3.1. In the nomenclature used from here onward, **C₁**, **Carboxy**, **Sulfo** and **Amph** refer to the dual-functional methyl, carboxybetaine, sulfobetaine and dual-functional amphiphilic series respectively; (+) denotes the cationic precursor form of the dual-functional and carboxybetaine monomers and polymers; **(ZI)** denotes the zwitterionic monomers and polymers; and the prefix **P** denotes the final polymer form. All monomers began with a common building block, the Diels-Alder adduct *exo* oxanorbornene anhydride **1** (Figure 3.1a). The *exo* isomer was necessary to achieve fast reaction times, quantitative conversion and controlled molecular weights during polymerization with Grubbs' 3rd generation catalyst. From there, a simple condensation

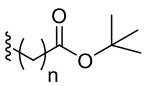
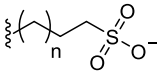
reaction with the appropriate *N,N*-dimethylalkyldiamine gave the tertiary amine-functionalized **2**. The alkyl spacer separating the imide group and the tertiary amine was varied from 2 to 6 carbons, based on the commercial availability of the amine reagents. The simplest cationic monomer could then be obtained by quaternizing the tertiary amine with dimethylsulfate. Linear betaine (**Carboxy** and **Sulfo**) and amphiphilic dual-functional (**Amph**) monomers were obtained by reacted **2a** with the appropriate electrophile (Figure 3.1b).

3.3 Monomer Synthesis

3.3.1 Hydrophilic Dual-functional and Linear betaines

The **C₁** series was obtained by condensation reaction between an anhydride and a diamine.¹ Alternatively, **2** could be obtained by a Mitsunobu reaction between *exo* oxanorbornene imide and a (dimethylamino)alcohol.⁴ While these reactions are often high yielding, the stoichiometric amounts of triphenylphosphine and DIAD are difficult to remove from the final product.⁹ Furthermore, when a Mitsunobu reaction was attempted between *exo* oxanorbornene imide and 4-(dimethylamino)butanol, no expected product was obtained. Instead, an intramolecular reaction occurred within the 4-(dimethylamino)butanol to form a cyclic amine. While the condensation reactions were near-quantitative, yields were typically low due to the aqueous work-up for **C₁(+)b-e**. The exception was **C₁(+)a**, which could be easily recrystallized to give a 50% or greater yield.

Table 3.1: Summary of linear betaine structures.

Polymer	R	X	n
Carboxy(+)a-e		Br	1-5
Sulfo(ZI)a-b		N/A	1-2

As mentioned before, however, this chemical platform was so attractive because of its versatility. Any number of electrophiles could be used to quaternize the tertiary amine group, resulting in a variety of R groups (Figure 3.1b). Most of these monomers were obtained under similar conditions, where the cationic or zwitterionic product precipitated out of organic solvent for easy purification. For simplicity's sake, when $R \neq \text{CH}_3$, n was held constant at 2 carbons, or an ethylene spacer (**2a**). Table 3.1 presents the full range of side chain chemistries that were incorporated into the carboxybetaine and sulfobetaine monomers. In the case of these linear zwitterions, the alkyl spacers between the quaternary amines and the anionic carboxylate or sulfonate groups were varied from 1 to 5 and 3 to 4 carbons, respectively. In addition to creating a library of various zwitterions, the **C₁**, **Carboxy**, and **Sulfo** series would later allow us to study the effect of interchange distance (the distance between positive and negative charges within the zwitterionic functional group) on the nonfouling properties of these polymers.

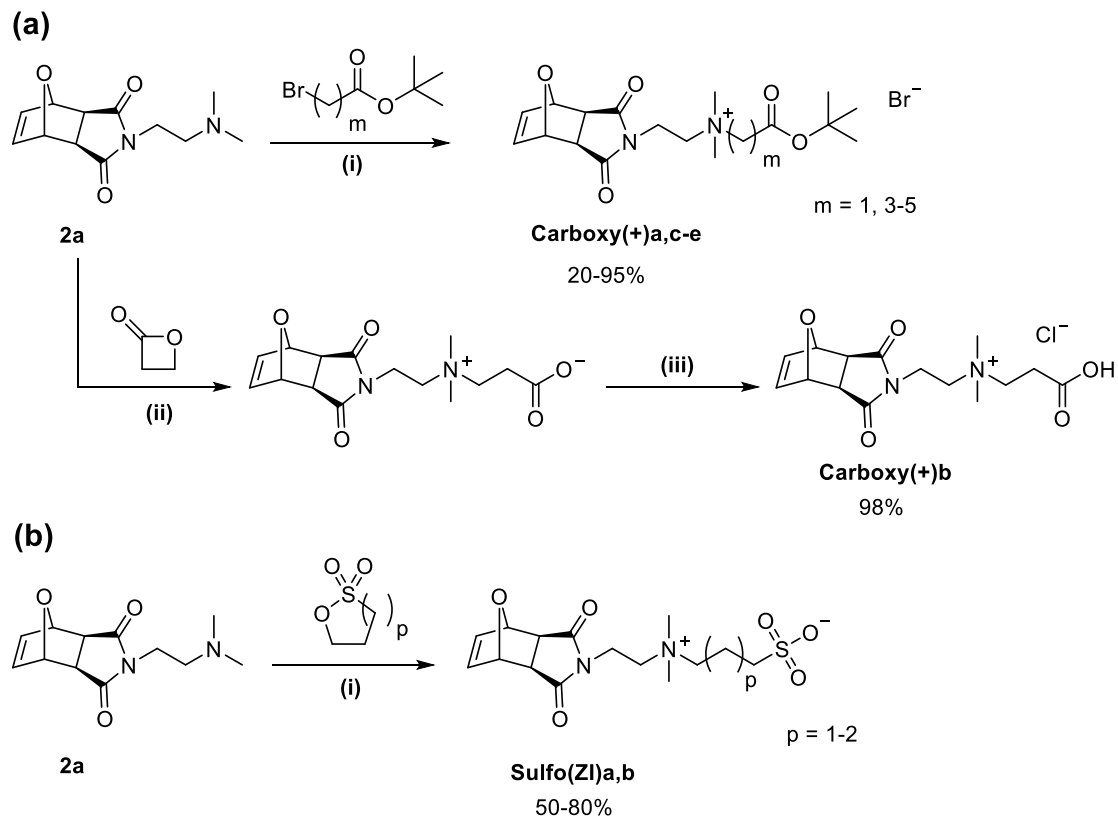


Figure 3.2: Synthesis of linear carboxy- and sulfobetaines: **(a)** (i) THF, 50 °C, 48 hours; (ii) THF, room temperature, overnight; (iii) 5.0 M HCl (aq), 30 minutes; **(b)** (i) acetonitrile, 1 wt % 1,3-dinitrobenzene, 50 °C, 48 hours.

Ruthenium-based catalysts are often incompatible with the carboxylate anion as it can complex with the catalyst and arrest polymerization.^{10,11} To avoid this problem, the **Carboxy** series was synthesized in a cationic, protected form (Figure 3.2a). Alkylation was achieved by nucleophilic substitution with *tert*-butyl bromoalkanoates. Post-polymerization, the *tert*-butyl protecting group was quantitatively cleaved under acidic conditions, which could be confirmed by IR spectroscopy (Figure 3.3).⁴ For the 2-carbon *tert*-butyl 3-bromopropionate, β -hydride elimination in the presence of weakly basic **2** to form an alkene was the dominant reaction and no desired product formed. In this case, a previously reported method² was employed to synthesize **C(+)****b**. First, β -propiolactone

was ring-opened by **2**, and then the resulting zwitterionic monomer was fully protonated under acidic conditions to ensure the cationic nature of the monomer. It was observed that the carboxybetaine monomers with longer alkyl chains exhibited similar solubility to the tertiary amine starting material and lower melting temperatures, making them difficult to isolate and purify. A 5-carbon spacer was found to be the longest chain that still yielded pure monomer using straightforward purification methods. Sulfobetaines are most easily obtained by the ring-opening of a sultone, of which propyl and butyl isomers are commercially available (Figure 3.2b). The sulfonate anion is fully compatible with Grubbs' catalysts and thus the monomers could be polymerized in the zwitterionic form without the need for post-polymerization modification.

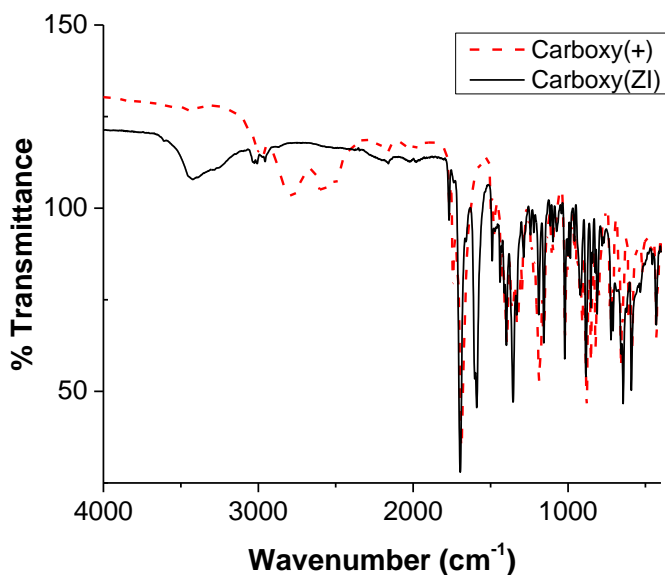
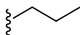
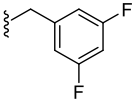
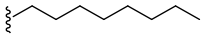
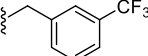
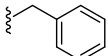
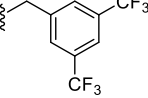
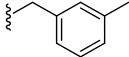

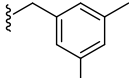
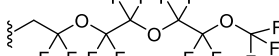
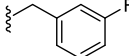
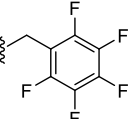


Figure 3.3: Representative FT-IR spectra of the cationic precursor **Carboxy(+)** and the deprotected zwitterionic **Carboxy(ZI)** monomers.

3.3.2 Amphiphilic dual-functional betaines

The versatility of this synthetic platform was perhaps best represented by the amphiphilic series, **Amph(+)**a-l. Amphiphilic materials contain both hydrophilic and hydrophobic (or lipophobic) moieties; these materials could be achieved here by choosing hydrophobic R groups. **Amph(+)**a,b and **j** were previously reported.^{1,7,8} The full set of hydrophobic substituents are shown in Table 3.2. Relative hydrophilicity, or hydrophobicity, is known to play a role in nonfouling properties,^{12,13} therefore it was advantageous to study both the effect of increasing hydrophobicity as well as the nature of the hydrophobic group. This was first done by extending the length of an alkyl R group from methyl (**C**₁(+)) to propyl (**Amph(+)**a) to octyl (**Amph(+)**b). Aromatic groups are seen in biologically relevant amphiphilic materials such as amino acids and (SM)AMPs,¹⁴ so a subset of the amphiphilic series was synthesized to contain benzyl (**Amph(+)**c), 3-methylbenzyl (**Amph(+)**d)), and 3,5-dimethylbenzyl (**Amph(+)**e) substituents.

Table 3.2: Summary of amphiphilic dual-functional betaine structures.

Polymer	R	X	Polymer	R	X
Amph(+a)		Br	Amph(+g)		OTs
Amph(+b)		Br	Amph(+h)		OTs
Amph(+c)		OTs	Amph(+i)		OTs
Amph(+d)		OTs	Amph(+j)		OTf
Amph(+e)		OTs	Amph(+k)		OTf
Amph(+f)		OTs	Amph(+l)		OTs

Fluorinated materials exhibit unique properties compared to their hydrocarbon counterparts, including exceptionally low surface energy.^{13,15} Many amphiphilic nonfouling materials have incorporated fluorine into their chemistries in unique ways, including hyperbranched polymers and perfluorinated networks. Due to limited solubility and challenging synthesis of fluorinated molecules, however, it can be difficult to systematically study to effects of fluorine in amphiphilic materials. To overcome these issues, a series of fluoro-substituted benzyl R groups were chosen, where both the position and amount of fluorine around the benzyl group could be easily varied with

commercially available reagents (**Amph(+)**f-i). These fluorinated monomers also had direct hydrocarbon controls in **Amph(+)**c-d. Finally, perfluorinated alkyl (**Amph(+)**j), ether (**Amph(+)**k), and benzyl (**Amph(+)**l) groups were also incorporated into the oxanorbornene platform as analogues to many of the perfluorinated groups found in the nonfouling literature.

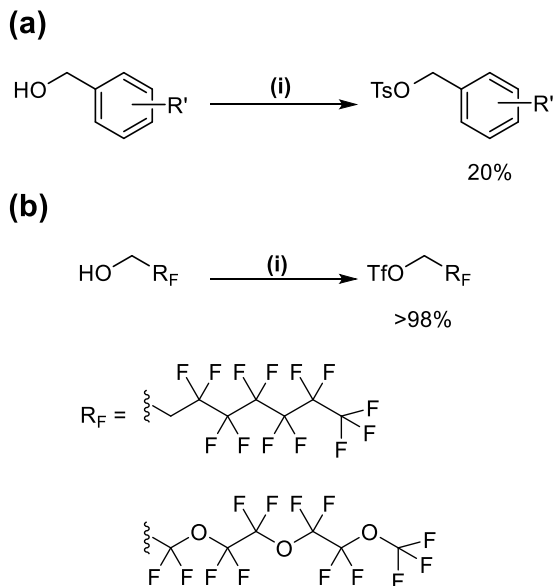


Figure 3.4: Synthesis of hydrophobe precursors. **(a)** (i) 4-toluenesulfonyl chloride, triethylamine, THF, 0 °C – room temperature, 3 hours; **(b)** trifluoromethanesulfonic anhydride, pyridine, DCM/dioxane, 30 minutes.

To synthesize the amphiphilic series, **2a** was again reacted with hydrophobes of the general form R-X at 50 °C for approximately 36 hours. For **Amph(+)**a and **Amph(+)**b, bromoalkanes were used. Yields were relatively low for these monomers, ~40%, due to the lower reactivity of the bromo leaving groups. To keep the same conditions for the benzyl series, **Amph(+)**c-i,l, the commercially available alcohols were purchased and converted to tosyl groups, which were then reacted with **2a** (Figure 3.4a). Interestingly, it was previously found that bromo and tosyl leaving groups were ineffectual for the perfluoroalkane moiety, most likely due to fluorine's strong electron-

withdrawing behavior. Thus, the perfluoroalkane and perfluoroether alcohols were converted to triflate groups as shown in Figure 3.4b¹⁶ and then reacted with **2a**. In the case of the tosyl and triflate reagents, yields of the resulting monomers were in the range of 80-90%.

The majority of the amphiphilic monomers precipitated out of either THF or diethyl ether as fine, off-white powders and were easily isolated by filtration. Two of the monomers, however, behaved differently during the purification process. **Amph(+)****k** could be precipitated out into diethyl ether from acetonitrile, but as a foaming solid instead of a powder. The monomer could be obtained in a more usable form after slow precipitation out of methanol. In this case, the fluid nature of the perfluoroether tail appeared to determine the physical properties of the final monomer.

Amph(+)**i** was unique in that it did not precipitate out of THF or diethyl ether, either at 50 °C or room temperature. Instead, it appeared to act as a molecular gelator in these solvents. After approximately 12 hours, the reaction in THF went from a clear, homogenous, freely flowing solution to a gelatinous solid. The gelled mixture could be redissolved in methanol or TFE, showing that the gel was physically and not chemically crosslinked. The monomer was ultimately purified by recrystallization from a TFE/diethyl ether mixture. While this monomer's behavior was puzzling, the strongly electron-withdrawing bis(trifluoromethyl) substituents were previously shown to influence the electronic properties of a similar oxanorbornene monomer.¹⁷ Molecular gelators are sensitive to structural changes, and the relationship between structure and gelation properties is often complex.¹⁸ Some sort of molecular interaction is required to drive the assembly though, and it is plausible that the electron-deficient benzyl

substituent in conjunction with the cationic group and hydrophobic norbornene moiety all contribute to a system where self-assembly can occur.

Many amphiphilic materials are characterized by ill-defined, heterogeneous structures, which makes it difficult to define structure-property relationships especially for nonfouling applications.¹³ The amphiphilic monomers described above are advantageous because of their well-defined structure. The nature and position of the hydrophobic group was known in relation to the charged group based on the synthetic scheme and characterization techniques such as NMR spectroscopy. Figure 3.5 shows representative ¹H NMR and ¹⁹F NMR spectra of monomer **Amph(+)****h**. The proton spectrum corroborated the structure while the fluorine spectrum confirmed the presence and nature of the fluorinated groups in the molecule.

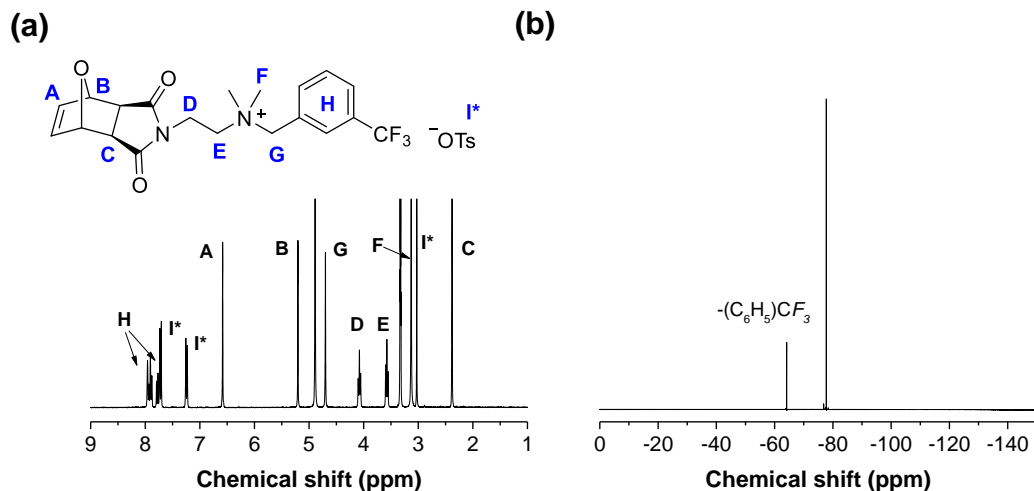


Figure 3.5: Representative NMR spectra in MeOD-d₄ of monomer **Amph(+)****h**. (a) ¹H NMR and (b) ¹⁹F NMR spectra (TFA used as standard).

3.4 Polymer synthesis

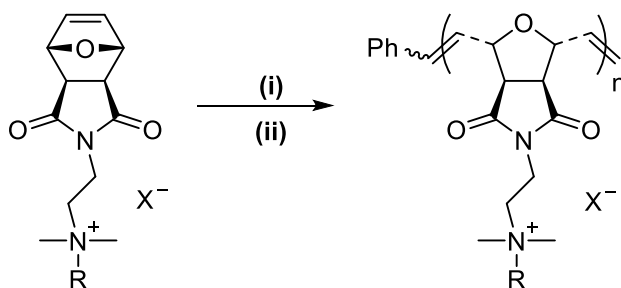


Figure 3.6: Representative polymerization conditions for the **C₁(+)**, **Carboxy(+)**, **Sulfo(ZI)**, and **Amph(+)** series: (i) Grubbs' 3rd generation catalyst, TFE/CH₂Cl₂, room temperature, 15-35 minutes; (ii) ethyl vinyl ether, room temperature, 1 hour.

Homopolymers of these monomers were obtained as shown in Figure 3.6.

Grubbs' 3rd generation catalyst was used due to its fast reaction kinetics, reasonable stability, and demonstrated compatibility with charged systems.¹⁻⁴ Due to the limited solubility of charged and zwitterionic molecules, 2,2,2-trifluoroethanol (TFE) was used to solvate the monomers. Previously TFE had been shown to be compatible with ROMP. Grubbs' 3rd catalyst was dissolved in dichloromethane (CH₂Cl₂), a good solvent for the catalyst. Quantitative conversion was achieved for all monomers, as verified by NMR spectroscopy, after 15 – 35 minutes based on the monomer. All polymerizations were quenched with ethyl vinyl ether, per the established procedure.

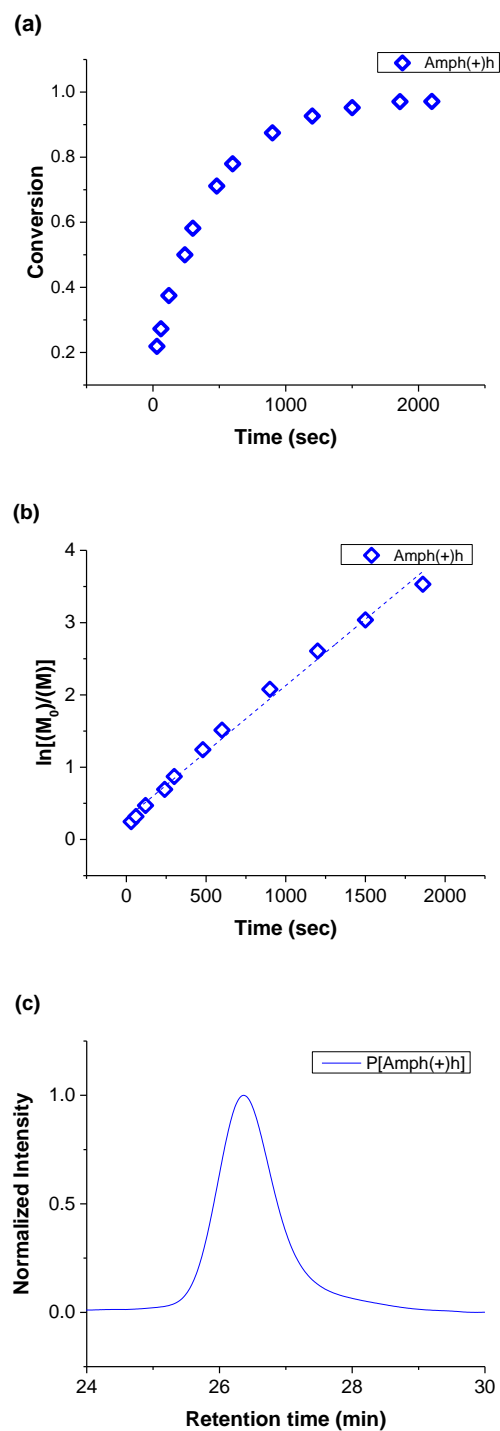


Figure 3.7: Kinetics for the homopolymerizations by ROMP of monomer **Amph(+h)**, where $[\text{Amph(+h)}]_0$ 80 mM and $[\text{monomer}]_0:[\text{catalyst}]_0 = 50:1$. **a.)** Conversion as a function of time as calculated from ^1H NMR spectra; **b.)** First-order time conversion with linear fit; **c.)** Representative GPC trace after 8 minutes (~70% conversion). 2,2,2-trifluoroethanol + 0.1% NaTFA was used as the eluent, with molecular weights calculated relative to PMMA standards.

Previously, it was verified that the carboxybetaines and sulfobetaines, as well as certain amphiphilic hydrocarbon-containing monomers, polymerized in a controlled fashion by ROMP. Similarly, it was confirmed here that the **C₁(+)** and fluorinated **Amph(+)** series also resulted in controlled polymerizations. As an example, the polymerization kinetics for **Amph(+)****h** – an asymmetrically substituted, fluorinated monomer – are shown in Figure 3.7. The targeted degree of polymerization was set at 50 and the initial monomer concentration of monomer was 80 mM. Figure 3.7a shows the monomer conversion as a function of time, which was calculated by ¹H NMR spectroscopy from the ratio of monomer to polymer alkene peaks. The monomer achieved quantitative conversion at 35 minutes and followed the expected timecourse. The ln[(M₀)/(M)] vs. time plot (Figure 3.7b) exhibited approximately linear behavior, indicating that this monomer followed a first order time conversion and polymerized in a controlled manner. A crude GPC trace in TFE (Figure 3.7c), taken when the polymerization had reached approximately 70% conversion, showed a symmetric distribution with minimal tailing and $\bar{D} \approx 1.07$. Because of the problems inherent in GPC with charged polymers, and the massive differences in solution properties between the uncharged PMMA standards and our oxanorbornene-based polymers, an accurate molecular weight could not be calculated from this method. Based on the monomers' first order time conversions and low PDIs, it was confirmed that well-defined dual-functional polymers were achieved by ROMP.

3.5 Experiment Procedures

3.5.1 Materials

All reagents were purchased from either Sigma-Aldrich, Alfa Aesar, Acros Organics, or Fisher Scientific in the highest purity available and used as received, unless otherwise noted. 4-(dimethylamino)butylamine, 5-(dimethylamino)amylamine, and 6-(dimethylamino)hexylamine were purchased from Matrix Scientific and used as received. 1,3-dinitrobenzene was obtained from Avocado Research Chemicals and used as received. 4-Bromobutanoic acid tert-butyl ester was purchased from Astatech, Inc. and used as received. 5-bromopentanoic acid tert-butyl ester and 6-bromohexanoic acid tert-butyl ester were synthesized as described below. Perfluoroether alcohol was purchased from Matrix Scientific and used as received. Tetrahydrofuran (THF, Fisher Scientific, HPLC grade) was distilled from sodium/benzophenone under nitrogen and dichloromethane (CH₂Cl₂, Fisher Scientific, ACS grade) was distilled from CaH₂ under nitrogen immediately prior to use. 2,2,2-trifluoroethanol (TFE, 99+%) was purchased from Alfa Aesar and used as received. Grubbs' 3rd generation catalyst (G3) was synthesized according to a previously reported procedure.¹⁹

3.5.2 Instrumentation and methodology

Nuclear magnetic resonance (NMR) spectra were obtained on a Bruker DPX-300 NMR spectrometer. Abbreviations for assignments are as follows: s: singlet; t: triplet; q: quartet; m: multiplet; comp: overlapping non-equivalent peaks; br: broad.

Mass spectral data were obtained at the University of Massachusetts, Mass Spectrometry Facility from a JEOL JMS 700 instrument (JEOL, Peabody, MA).

Gel permeation chromatography (GPC) traces were obtained on an Agilent 1260 series system with a refractive index detector, and a HFIP gel guard column (7 mm x 50 mm) and 3 HFIP gel columns (7mm x 300 mm) in series. The columns were incubated at

40 °C. 2,2,2-trifluoroethanol with 20 mM NaTFA was used as the eluent at a flow rate of 0.75 mL/min. Methanol was used as the flow marker. Molecular weight was calculated relative to poly(methyl methacrylate) standards.

3.5.3 Synthesis and characterization

exo-Oxanorbornene anhydride (1): was synthesized by a modified version of an established procedure.²⁰ Maleic anhydride (50.0 g, 0.51 mol) and furan (37 mL, 0.51 mol) were dissolved in 500 mL toluene. The reaction solution was allowed to stir for 72 hours, after which the precipitated *exo* product was isolated by filtration. The product was washed several times with excess toluene followed by hexanes, and dried under vacuum overnight to give an off-white powder. Yield and spectrographic data matched those reported in the literature.

¹H NMR (300 MHz, CDCl₃): δ (ppm) = 3.2 (s, 2H, -CH-C=O), 5.48 (s, 2H, -C-CH-O-), 6.6 (s, 2H, -CH=CH-).

2a was synthesized according to a previously published procedure.¹ Briefly, **1** (15.24 g, 0.09 mol) was added to 300 mL of a 1:1 MeOH:THF solution at 60 °C. After the solid had completely dissolved, *N,N*-dimethylethylenediamine (10 mL, 0.09 mol) was added drop-wise to the solution. The reaction was then allowed to stir overnight at 50 °C. The excess solvent was removed under reduced pressure to yield a light yellow, waxy solid. The final off-white, crystalline product was obtained after recrystallization from MeOH/hexanes (2:1). Yield and spectrographic data matched those reported in the literature.

2b-e were synthesized using a modified version of the procedure outlined above. **1** (1 equivalent) and the appropriate amine (1 equivalent: b: 3-(dimethylamino)propylamine; c: 4-(dimethylamino)butylamine; d: 5-(dimethylamino)amylamine; e: 6-(dimethylamino)hexylamine) were dissolved in 1:1 MeOH:THF at 60 °C, then stirred overnight at 50 °C. The solvent was evaporated off under reduced pressure, after which the yellow oil was taken up in chloroform and washed three times with saturated NaHCO₃. The organic layer was dried over Na₂SO₄ and the excess solvent was removed by rotary evaporation. The light yellow oil product was dried under high vacuum overnight and taken directly to the next step without further purification. Yields: 20-40%

2a: Data previously reported.¹ ¹H NMR (300 MHz, CDCl₃): δ (ppm) = 2.26 (s, 6H, -N(CH₃)₂), 2.42 (t, *J* = 6.8 Hz, 2H, -CH₂-CH₂-N(CH₃)₂), 2.87 (s, 2H, -CH-C=O), 3.60 (t, *J* = 6.9 Hz, -CH₂-CH₂-N(CH₃)₂), 5.27 (s, 2H, -C-CH-O-), 6.52 (s, 2H, -CH=CH-).

2b: ¹H NMR (300 MHz, CDCl₃): δ (ppm) = 1.72 (quintet, *J* = 7.2 Hz, 2H, -CH₂-CH₂-CH₂-), 2.19 (s, 6H, -N(CH₃)₂), 2.26 (m, 2H, -CH₂-CH₂-CH₂-), 2.83 (s, 2H, -CH-C=O), 3.53 (t, *J* = 7.2 Hz, 2H, -CH₂-CH₂-CH₂-), 5.26 (s, 2H, -C-CH-O-), 6.51 (s, 2H, -CH=CH-).

¹³C NMR (75 MHz, CDCl₃): δ (ppm) = 25.60, 37.21, 45.34, 47.39, 56.72, 80.90, 136.54, 176.27.

2c: ¹H NMR (300 MHz, CDCl₃): δ (ppm) = 1.42 (m, 2H, -CH₂-CH₂-CH₂-CH₂-), 1.57 (m, 2H, -CH₂-CH₂-CH₂-CH₂-), 2.18 (s, 6H, -N(CH₃)₂), 2.24 (m, 2H, -CH₂-CH₂-CH₂-CH₂-),

2.82 (s, 2H, -CH-C=O), 3.48 (t, $J = 7.2$ Hz, 2H, -CH₂-CH₂-CH₂-CH₂-), 5.24 (s, 2H, -C-CH-O-), 6.50 (s, 2H, -CH=CH-).

¹³C NMR (75 MHz, CDCl₃): δ (ppm) = 24.69, 25.48, 38.78, 45.43, 47.36, 59.09, 80.88, 136.52, 176.24.

2d: ¹H NMR (300 MHz, CDCl₃): δ (ppm) = 1.30 (m, 2H, -CH₂-CH₂-CH₂-CH₂-CH₂-), 1.48 (m, 2H, -CH₂-CH₂-CH₂-CH₂-CH₂-), 1.59 (m, 2H, -CH₂-CH₂-CH₂-CH₂-CH₂-), 2.21 (s, 6H, -N(CH₃)₂), 2.24 (m, 2H, -CH₂-CH₂-CH₂-CH₂-CH₂-), 2.84 (s, 2H, CH-C=O), 3.48 (t, $J = 7.4$ Hz, 2H, -CH₂-CH₂-CH₂-CH₂-CH₂-), 5.28 (s, 2H, -C-CH-O-), 6.52 (s, 2H, -CH=CH-).

¹³C NMR (75 MHz, CDCl₃): δ (ppm) = 24.59, 27.17, 27.54, 38.91, 45.44, 47.38, 59.58, 80.90, 136.54, 176.28.

2e: ¹H NMR (300 MHz, CDCl₃): δ (ppm) = 1.30-1.56 (m, 8H, -CH₂-CH₂-CH₂-CH₂-CH₂-CH₂-), 2.20 (s, 6H, -N(CH₃)₂), 2.22 (m, 2H, -CH₂-CH₂-CH₂-CH₂-CH₂-CH₂-), 2.83 (s, 2H, CH-C=O), 3.47 (t, $J = 7.4$ Hz, 2H, -CH₂-CH₂-CH₂-CH₂-CH₂-CH₂-), 5.26 (s, 2H, -C-CH-O-), 6.51 (s, 2H, -CH=CH-).

¹³C NMR (75 MHz, CDCl₃): δ (ppm) = 26.61, 26.96, 27.54, 38.93, 45.49, 47.38, 59.71, 80.89, 136.54, 176.28.

C1(+)a-e were synthesized according to the previously reported procedure.⁷ **2a-e** (1 equivalent) were dissolved in dry THF under N₂. The solution was cooled to 0 °C in an ice bath, and dimethyl sulfate (1.5 equivalents) was added drop-wise. After letting the reaction stir for 4 hours at room temperature, the precipitated product was filtered, rinsed with THF and dried under high vacuum. Yields: 95-98%.

C1(+)a: data previously reported.⁷ ¹H NMR (300 MHz, MeOD-d₄): δ (ppm) = 3.03 (s, 2H, -CH-C=O), 3.20 (s, 9H, -N(CH₃)₃), 3.60 (t, *J* = 6.6, 2H, -CH₂-CH₂-N(CH₃)₃), 3.70 (s, 3H, CH₃SO₄⁻), 3.97 (t, *J* = 6.5 Hz, 2H, -CH₂-CH₂-N(CH₃)₃), 5.22 (s, 2H, -C-CH-O-), 6.59 (s, 2H, -CH=CH-).

C1(+)b: ¹H NMR (300 MHz, MeOD-d₄): δ (ppm) = 2.09 (m, 2H, -CH₂-CH₂-CH₂-), 3.01 (s, 2H, -CH-C=O), 3.12 (s, 9H, -N(CH₃)₂), 3.28 (m, 2H, -CH₂-CH₂-CH₂-), 3.62 (t, *J* = 6.4 Hz, 2H, -CH₂-CH₂-CH₂-), 3.70 (s, 3H, CH₃SO₄⁻), 5.21 (s, 2H, -C-CH-O-), 6.59 (s, 2H, -CH=CH-).

¹³C NMR (75 MHz, MeOD-d₄): δ (ppm) = 21.28, 34.82, 52.13, 53.70, 63.74, 81.02, 136.20, 177.12.

HR-MS (ESI) *m/z*: calculated 265.1547, found 265.1543

C1(+)c: ¹H NMR (300 MHz, MeOD-d₄): δ (ppm) = 1.69 (m, 4H, -CH₂-CH₂-CH₂-CH₂-), 2.98 (s, 2H, -CH-C=O), 3.11 (s, 9H, -N(CH₃)₂), 3.36 (m, 2H, -CH₂-CH₂-CH₂-CH₂-), 3.58 (t, *J* = 6.2 Hz, 2H, -CH₂-CH₂-CH₂-CH₂-), 3.70 (s, 3H, CH₃SO₄⁻), 5.20 (s, 2H, -C-CH-O-), 6.58 (s, 2H, -CH=CH-).

¹³C NMR (75 MHz, MeOD-d₄): δ (ppm) = 19.25, 23.70, 36.90, 52.07, 53.69, 65.65, 80.99, 136.18, 177.33.

HR-MS (ESI) *m/z*: calculated 279.1703, found 279.1712

C1(+)d: ¹H NMR (300 MHz, MeOD-d₄): δ (ppm) = 1.34 (m, 2H, -CH₂-CH₂-CH₂-CH₂-CH₂-), 1.67 (m, 2H, -CH₂-CH₂-CH₂-CH₂-CH₂-), 1.82 (m, 2H, -CH₂-CH₂-CH₂-CH₂-CH₂-), 2.96 (s, 2H, -CH-C=O), 3.14 (s, 9H, -N(CH₃)₂), 3.28 (m, 2H, -CH₂-CH₂-CH₂-CH₂-

CH_2 -), 3.53 (t, $J = 6.8$ Hz, 2H, $-\text{CH}_2\text{-CH}_2\text{-CH}_2\text{-CH}_2\text{-CH}_2$ -), 3.70 (s, 3H, CH_3SO_4 -), 5.17 (s, 2H, $-\text{C-CH-O}$), 6.58 (s, 2H, $-\text{CH}=\text{CH}$ -).

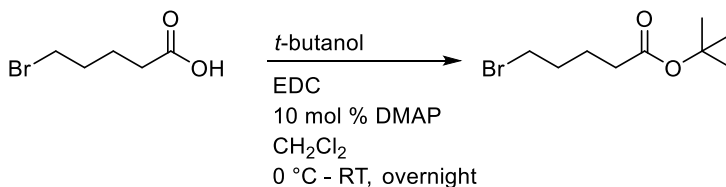
^{13}C NMR (75 MHz, MeOD- d_4): δ (ppm) = 21.81, 22.71, 26.45, 37.46, 52.05, 53.70, 66.20, 80.91, 136.22, 177.32.

HR-MS (ESI) m/z : calculated 293.1860, found 293.1859

C1(+)e: ^1H NMR (300 MHz, MeOD- d_4): δ (ppm) = 1.39-1.77 (m, 8H, $-\text{CH}_2\text{-CH}_2\text{-CH}_2\text{-CH}_2\text{-CH}_2\text{-CH}_2$ -), 2.94 (s, 2H, $-\text{CH-C=O}$), 3.13 (s, 9H, $-\text{N}(\text{CH}_3)_2$), 3.29 (m, 2H, $-\text{CH}_2\text{-CH}_2\text{-CH}_2\text{-CH}_2\text{-CH}_2$ -), 3.50 (t, $J = 6.9$ Hz, 2H, $-\text{CH}_2\text{-CH}_2\text{-CH}_2\text{-CH}_2\text{-CH}_2\text{-CH}_2$ -), 3.70 (s, 3H, CH_3SO_4 -), 5.17 (s, 2H, $-\text{C-CH-O}$), 6.57 (s, 2H, $-\text{CH}=\text{CH}$ -).

^{13}C NMR (75 MHz, MeOD- d_4): δ (ppm) = 22.23, 25.22, 25.46, 26.73, 37.81, 52.11, 53.69, 66.28, 80.89, 136.22, 177.29.

HR-MS (ESI) m/z : calculated 307.2016, found 307.2016

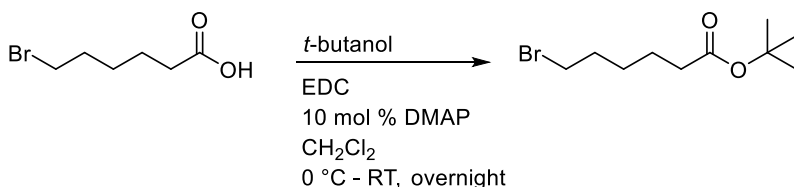


5-bromopentanoic acid tert-butyl ester: 5-bromovaleric acid (5.24 g, 29 mmol, 1 eq), *t*-butanol (3.22 g, 43 mmol, 1.5 eq) and 4-dimethylaminopyridine (DMAP, 0.52 g, 4.3 mmol, 10 mol %) were dissolved in 100 mL dry CH_2Cl_2 under N_2 in a clean, dry 3-neck round bottom flask. The solution was cooled in an ice bath and 1-ethyl-3-(3-dimethylaminopropyl)carbodiimide (EDC, 8.24 g, 43 mmol, 1.5 eq) dissolved in a minimum amount of CH_2Cl_2 was added drop-wise to the stirring solution. The reaction was allowed to stir overnight at room temperature, then washed with saturated NaHCO_3

and brine and dried over sodium sulfate. The excess solvent was evaporated off and the crude product was purified by silica gel column chromatography using 9:1 hexanes:ethyl acetate as the eluent. Yield: 44%

^1H NMR (300 MHz, CDCl_3): δ (ppm) = 1.46 (s, 9H, $-\text{COOC}(\text{CH}_3)_3$), 1.75 (m, 2H, $-\text{CH}_2-\text{CH}_2-\text{CH}_2-$), 1.89 (m, 2H, $-\text{CH}_2-\text{CH}_2-\text{CH}_2-\text{CH}_2-$), 2.26 (t, $J = 7.2$ Hz, 2H, $-\text{CH}_2-\text{Boc}$), 3.42 (t, $J = 6.6$ Hz, 2H, $\text{Br}-\text{CH}_2-$).

^{13}C NMR (75 MHz, CDCl_3): δ (ppm) = 23.65, 28.10, 32.01, 33.23, 34.53, 80.35, 172.54.



6-bromohexanoic acid tert-butyl ester: The same procedure as used to synthesize 5-bromopentanoic acid tert-butyl ester was used here, with 6-bromohexanoic acid (5.77 g, 30 mmol, 1 eq), *t*-butanol (3.25 g, 44 mmol, 1.5 eq), DMAP (0.53 g, 4.4 mmol, 10 mol %), and EDC (8.43 g, 44 mmol, 1.5 eq). Yield: 46%

^1H NMR (300 MHz, CDCl_3): δ (ppm) = 1.46 (s, 9H, $-\text{COOC}(\text{CH}_3)_3$), 1.49-1.87 (m, 6H, $-\text{CH}_2-\text{CH}_2-\text{CH}_2-\text{CH}_2-\text{CH}_2-$), 2.24 (m, 2H, $-\text{CH}_2-\text{Boc}$), 3.42 (t, $J = 6.8$ Hz, 2H, $\text{Br}-\text{CH}_2-$).

^{13}C NMR (75 MHz, CDCl_3): δ (ppm) = 24.22, 27.58, 28.11, 32.45, 33.67, 35.30, 80.17, 172.91.

Carboxy(+)**b** was synthesized as previously described² in its protonated form.

Carboxy(+)**a,c-e** were synthesized according to the previously described procedure.⁴ **2a**

(1 equivalent) was dissolved in dry THF. The appropriate bromide (1.5 equivalents; **a**: *tert*-butyl bromoacetate, **c**: 4-bromobutanoic acid *tert*-butyl ester, **d**: 5-bromopentanoic acid *tert*-butyl ester, **e**: 6-bromohexanoic acid *tert*-butyl ester) was added, and the reaction was allowed to stir for 36 hours at 50 °C. The resulting precipitate was then filtered, rinsed with excess dry THF and dried under high vacuum. Yields: 20-95%

Carboxy(+)**a**: $^1\text{H NMR}$ (300 MHz, MeOD- d_4): δ (ppm) = 1.56 (s, 9H, $-\text{COOC}(\underline{\text{C}}\text{H}_3)_3$), 3.04 (s, 2H, $-\underline{\text{C}}\text{H}-\text{C}=\text{O}$), 3.36 (s, 6H, $-\text{N}(\underline{\text{C}}\text{H}_3)_2$), 3.82 (m, 2H, $-\text{C}\underline{\text{H}}_2-\underline{\text{C}}\text{H}_2-\text{N}(\text{C}\underline{\text{H}}_3)_2$ -), 3.97 (t, $J = 6.8$ Hz, 2H, $-\underline{\text{C}}\text{H}_2-\text{C}\underline{\text{H}}_2-\text{N}(\text{C}\underline{\text{H}}_3)_2$ -), 4.38 (s, 2H, $-\text{N}(\text{C}\underline{\text{H}}_3)_2-\underline{\text{C}}\text{H}_2-\text{Boc}$), 5.22 (s, 2H, $-\text{C}-\underline{\text{C}}\text{H}-\text{O}-$), 6.59 (s, 2H, $-\underline{\text{C}}\text{H}=\underline{\text{C}}\text{H}-$).

$^{13}\text{C NMR}$ (75 MHz, MeOD- d_4): δ (ppm) = 26.80, 32.01, 51.28, 60.42, 61.54, 81.00, 85.13, 136.28, 163.44, 176.46.

HR-MS (FAB) m/z : calculated 351.1920, found 351.1907

Carboxy(+)**b**: data previously reported.² $^1\text{H NMR}$ (300 MHz, MeOD- d_4): δ (ppm) = 2.93 (t, 2H, $J = 7.7$ Hz, $-\underline{\text{C}}\text{H}_2\text{COOH}$), 2.96 (s, 2H, $-\underline{\text{C}}\text{H}-\text{C}=\text{O}$), 3.18 (s, 6H, $-\text{N}(\underline{\text{C}}\text{H}_3)_2$ -), 3.57 (t, 2H, $J = 6.7$ Hz, $-\text{C}\underline{\text{H}}_2-\underline{\text{C}}\text{H}_2-\text{N}(\text{C}\underline{\text{H}}_3)_2$ -), 3.72 (m, 2H, $-\underline{\text{C}}\text{H}_2-\text{C}\underline{\text{H}}_2-\text{COOH}$), 3.97 (t, 2H, $J = 6.7$, $-\underline{\text{C}}\text{H}_2-\text{C}\underline{\text{H}}_2-\text{N}(\text{C}\underline{\text{H}}_3)_2$ -), 5.23 (s, 2H, $-\text{C}-\underline{\text{C}}\text{H}-\text{O}-$), 6.59 (s, 2H, $-\underline{\text{C}}\text{H}=\underline{\text{C}}\text{H}-$).

Carboxy(+)**c**: data previously reported.⁴ $^1\text{H NMR}$ (300 MHz, MeOD- d_4): δ (ppm) = 1.45 (s, 9H, $-\text{COOC}(\underline{\text{C}}\text{H}_3)_3$), 1.99 (m, 2H, $-\text{C}\underline{\text{H}}_2-\underline{\text{C}}\text{H}_2-\text{C}\underline{\text{H}}_2-$), 2.35 (t, $J = 6.9$ Hz, 2H, $-\underline{\text{C}}\text{H}_2-\text{Boc}$), 2.98 (s, 2H, $-\underline{\text{C}}\text{H}-\text{C}=\text{O}$), 3.14 (s, 6H, $-\text{N}(\underline{\text{C}}\text{H}_3)_2$), 3.36 (m, 2H, $-\text{N}(\text{C}\underline{\text{H}}_3)_2-\underline{\text{C}}\text{H}_2$ -), 3.53 (t, $J = 6.7$ Hz, 2H, $-\text{C}\underline{\text{H}}_2-\underline{\text{C}}\text{H}_2-\text{N}(\text{C}\underline{\text{H}}_3)_2$ -), 3.93 (t, $J = 6.7$ Hz, 2H, $-\underline{\text{C}}\text{H}_2-\text{C}\underline{\text{H}}_2-\text{N}(\text{C}\underline{\text{H}}_3)_2$ -), 5.17 (s, 2H, $-\text{C}-\underline{\text{C}}\text{H}-\text{O}-$), 6.54 (s, 2H, $-\underline{\text{C}}\text{H}=\underline{\text{C}}\text{H}-$).

Carboxy(+)d: ^1H NMR (300 MHz, MeOD- d_4): δ (ppm) = 1.47 (s, 9H, $-\text{COOC}(\text{CH}_3)_3$), 1.64 (m, 2H, $-\text{CH}_2-\text{CH}_2-\underline{\text{CH}_2}-\text{CH}_2-$), 1.83 (m, 2H, $-\text{CH}_2-\underline{\text{CH}_2}-\text{CH}_2-\text{CH}_2-$) 2.37 (t, $J = 7.2$ Hz, 2H, $-\underline{\text{CH}_2}-\text{Boc}$), 3.03 (s, 2H, $-\underline{\text{CH}}-\text{C}=\text{O}$), 3.16 (s, 6H, $-\text{N}(\text{CH}_3)_2$), 3.41 (m, 2H, $-\text{N}(\text{CH}_3)_2-\underline{\text{CH}_2}-$), 3.58 (m, 2H, $-\text{CH}_2-\underline{\text{CH}_2}-\text{N}(\text{CH}_3)_2-$), 3.95 (t, $J = 6.7$ Hz, 2H, $-\underline{\text{CH}_2}-\text{CH}_2-\text{N}(\text{CH}_3)_2-$), 5.22 (s, 2H, $-\text{C}-\underline{\text{CH}}-\text{O}-$), 6.59 (s, 2H, $-\underline{\text{CH}}=\underline{\text{CH}}-$).

^{13}C NMR (75 MHz, MeOD- d_4): δ (ppm) = 21.33, 21.58, 26.99, 32.11, 34.02, 50.41, 59.71, 63.81, 80.35, 80.98, 136.30, 172.71, 176.56.

HR-MS (FAB) m/z : calculated 393.2389, found 393.2361

Carboxy(+)e: ^1H NMR (300 MHz, MeOD- d_4): δ (ppm) = 1.42-1.83 (m, 6H, $-\text{CH}_2-\underline{\text{CH}_2}-\underline{\text{CH}_2}-\underline{\text{CH}_2}-\text{Boc}$), 1.47 (s, 9H, $-\text{COOC}(\text{CH}_3)_3$), 2.31 (t, $J = 7.2$ Hz, 2H, $-\underline{\text{CH}_2}-\text{Boc}$), 3.04 (s, 2H, $-\underline{\text{CH}}-\text{C}=\text{O}$), 3.17 (s, 6H, $-\text{N}(\text{CH}_3)_2$), 3.41 (m, 2H, $-\text{N}(\text{CH}_3)_2-\underline{\text{CH}_2}-$), 3.56 (m, 2H, $-\text{CH}_2-\underline{\text{CH}_2}-\text{N}(\text{CH}_3)_2-$), 3.95 (t, $J = 6.8$ Hz, 2H, $-\underline{\text{CH}_2}-\text{CH}_2-\text{N}(\text{CH}_3)_2-$), 5.22 (s, 2H, $-\text{C}-\underline{\text{CH}}-\text{O}-$), 6.59 (s, 2H, $-\underline{\text{CH}}=\underline{\text{CH}}-$).

^{13}C NMR (75 MHz, MeOD- d_4): δ (ppm) = 21.86, 24.16, 25.26, 26.95, 32.00, 34.58, 50.30, 59.56, 63.97, 80.13, 80.98, 136.27, 173.22, 176.48.

HR-MS (FAB) m/z : calculated 407.2546, found 407.2519

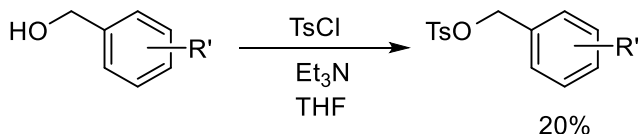
Sulfo(ZI)a was synthesized according to a previously reported procedure.²

Briefly, **2a** (2 g, 8.5 mmol) was dissolved in acetonitrile dried over Na_2SO_4 . 1,3-propanesultone (0.89 mL, 10.2 mmol) and 1 wt % 1,3-dinitrobenzene were added, and the reaction was allowed to stir for 36 hours at 50 °C. The resulting precipitate was then filtered, rinsed with excess dry acetonitrile followed by dry THF and dried under high vacuum. Yield: 86%.

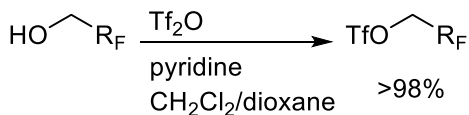
Sulfo(ZI)b was synthesized as above, using 1,4-butanedisulfone (1.04 mL), according to a previously reported procedure.⁴ Yield: 60%.

Sulfo(ZI)a: data previously reported.² ¹H NMR (300 MHz, D₂O): δ (ppm) = 2.18 (m, 2H, -CH₂-CH₂-CH₂-SO₃⁻), 2.92 (t, J = 7.1 Hz, 2H, -N(CH₃)₂-CH₂-CH₂-CH₂-), 3.12 (s, 6H, -N(CH₂)₃-), 3.50 (comp, 4H, -CH₂-CH₂-N(CH₃)₂ and -CH₂-CH₂-CH₂-SO₃⁻), 3.92 (t, J = 7.2 Hz, 2H, -CH₂-CH₂-N(CH₃)₂), 5.29 (s, 2H, -C-CH-O), 6.56 (s, 2H, -CH=CH-).

Sulfo(ZI)b: data previously reported.⁴ ¹H NMR (300 MHz, D₂O): δ (ppm) = 1.83 (m, 2H, -CH₂-CH₂-CH₂-CH₂-), 1.98 (m, 2H, -CH₂-CH₂-CH₂-CH₂-), 3.02 (m, 2H, -N(CH₃)₂-CH₂-CH₂-CH₂-CH₂-), 3.19 (s, 6H, -N(CH₃)₂-), 3.23 (s, 2H, -CH-C=O), 3.46 (m, 2H, -CH₂-CH₂-CH₂-CH₂-SO₄), 3.58 (t, 2H, -CH₂-CH₂-N(CH₃)₂, J = 7.0 Hz), 4.01 (t, 2H, -CH₂-CH₂-N(CH₃)₂, J = 7.0 Hz), 5.38 (s, 2H, -C-CH-O-), 6.66 (s, 2H, -CH=CH-).



The appropriate benzyl alcohol (1 eq) and triethylamine (1.5 eq) were dissolved in dry THF. 4-toluenesulfonyl chloride (1.2 eq) in dry THF was added dropwise to the solution at 0 °C. The reaction was allowed to warm to room temperature and the solution was stirred for 3 hours. The precipitate was filtered off, and the excess solvent was removed under reduced pressure. The final product was isolated by column chromatography (3:7 ethyl acetate:hexanes). Yields were approximately 20%.



Triflates were synthesized according to a previously published procedure.¹⁶

Amph(a-i,l): 2a (1.5 g, 1 eq) and the appropriate R-OTs reagent (1.2 eq) were dissolved in 25 mL dry THF and stirred at 50 °C for 36-48 hours.⁸ The precipitated product was filtered and washed with excess THF, then dried under high vacuum. Yields were approximately 80-90%

Amph(j-k): 2a (1.5 g, 1 eq) and R-OTf reagent (1.2 eq) were dissolved in 25 mL acetonitrile (dried over sodium sulfate) and stirred 50 °C for 48 hours. The product was precipitated out into anhydrous diethyl ether, filtered, and dried under high vacuum. Yields were approximately 80-90%.

Amph(+a): previously reported in Ref. 1. ¹H NMR (300 MHz, MeOD-d₄): δ (ppm) = 1.04 (t, *J* = 7.35, 3H, -CH₂CH₂CH₃), 1.85 (m, 2H, -CH₂CH₂CH₃), 3.03 (s, 2H, -CH-C=O), 3.38 (m, 2H, -CH₂CH₂CH₃), 3.54 (t, *J* = 6.88, 2H, -CH₂-CH₂-N(CH₃)₃), 3.95 (t, *J* = 6.78, 2H, -CH₂-CH₂-N(CH₃)₃), 5.22 (s, 2H, -C-CH-O-), 6.59 (s, 2H, -CH=CH-).

Amph(+b): previously reported in Ref. 7. ¹H NMR (300 MHz, MeOD-d₄): δ (ppm) = 0.93 (m, 3H, -CH₂CH₂(CH₂)₅CH₃), 1.37 (m, 10H, -CH₂CH₂(CH₂)₅CH₃), 1.80 (m, 2H, -CH₂CH₂(CH₂)₅CH₃), 3.03 (s, 2H, -CH-C=O), 3.39 (m, 2H, -CH₂CH₂(CH₂)₅CH₃), 3.53 (t, *J* = 6.88, 2H, -CH₂-CH₂-N(CH₃)₃), 3.94 (t, *J* = 6.88, 2H, -CH₂-CH₂-N(CH₃)₃), 5.22 (s, 2H, -C-CH-O-), 6.59 (s, 2H, -CH=CH-).

Amph(+c): ¹H NMR (300 MHz, MeOD-d₄): δ (ppm) = 2.38 (s, 3H, CH₃(C(C₂H₂)(C₂H₂)C)SO₃⁻), 3.02 (s, 2H, -CH-C=O), 3.10 (s, 6H, -N(CH₃)₃), 3.55 (t, *J* = 6.88 Hz, 2H, -CH₂-CH₂-N(CH₃)₃), 4.06 (t, *J* = 6.78 Hz, 2H, -CH₂-CH₂-N(CH₃)₃), 4.59 (s,

2H, -CH₂(C₆H₅)), 5.21 (s, 2H, -C-CH-O-), 6.58 (s, 2H, -CH=CH-), 7.25 (d, *J* = 8.29 Hz, 2H, CH₃(C(C₂H₂)(C₂H₂)C)SO₃⁻), 7.58 (comp, 5H, -CH₂(C₆H₅)), 7.72 (d, *J* = 8.29 Hz, 2H, CH₃(C(C₂H₂)(C₂H₂)C)SO₃⁻).

¹³C NMR (75 MHz, MeOD-d₄): δ = 19.90, 32.10, 68.03, 81.01, 125.56, 126.99, 128.42, 129.02, 130.72, 132.83, 136.25, 140.25, 142.24, 176.52.

HR-MS (ESI) *m/z*: calculated 327.1703, found 327.1696

Amph(+)d: ¹H NMR (300 MHz, MeOD-d₄): δ (ppm) = 2.38 (s, 3H, CH₃(C(C₂H₂)(C₂H₂)C)SO₃⁻), 2.43 (s, 3H, -CH₂(C₆H₄)CH₃), 3.02 (s, 2H, -CH-C=O), 3.09 (s, 6H, -N(CH₃)₃), 3.52 (t, *J* = 6.88 Hz, 2H, -CH₂-CH₂-N(CH₃)₃), 4.06 (t, *J* = 6.78 Hz, 2H, -CH₂-CH₂-N(CH₃)₃), 4.55 (s, 2H, -CH₂(C₆H₄)CH₃), 5.20 (s, 2H, -C-CH-O-), 6.58 (s, 2H, -CH=CH-), 7.24 (d, *J* = 8.10 Hz, 2H, CH₃(C(C₂H₂)(C₂H₂)C)SO₃⁻), 7.38-7.48 (comp, 4H, -CH₂(C₆H₄)CH₃), 7.72 (d, *J* = 8.10 Hz, 2H, CH₃(C(C₂H₂)(C₂H₂)C)SO₃⁻).

¹³C NMR (75 MHz, MeOD-d₄): δ = 19.89, 32.08, 59.70, 67.96, 81.01, 125.55, 126.86, 128.41, 128.87, 129.80, 131.37, 133.31, 136.25, 139.28, 140.24, 142.22, 176.51.

HR-MS (ESI) *m/z*: calculated 341.1860, found 341.1850

Amph(+)e: ¹H NMR (300 MHz, MeOD-d₄): δ (ppm) = 2.38 (comp, 3H + 6H, CH₃(C(C₂H₂)(C₂H₂)C)SO₃⁻ + -CH₂(C₆H₃)(CH₃)₂), 3.02 (s, 2H, -CH-C=O), 3.08 (s, 6H, -N(CH₃)₃), 3.49 (t, *J* = 6.97 Hz, 2H, -CH₂-CH₂-N(CH₃)₃), 4.04 (t, *J* = 6.88 Hz, 2H, -CH₂-CH₂-N(CH₃)₃), 4.49 (s, 2H, -CH₂(C₆H₃)(CH₃)₂), 5.19 (s, 2H, -C-CH-O-), 6.57 (s, 2H, -CH=CH-), 7.22 (comp, 2H + 3H, CH₃(C(C₂H₂)(C₂H₂)C)SO₃⁻ + -CH₂(C₆H₃)(CH₃)₂), 7.72 (d, *J* = 8.29 Hz, 2H, CH₃(C(C₂H₂)(C₂H₂)C)SO₃⁻).

¹³C NMR (75 MHz, MeOD-d₄): δ = 19.81, 32.10, 59.52, 67.92, 81.00, 125.56, 126.77, 128.44, 130.41, 132.09, 136.25, 139.02, 140.25, 142.28, 176.50.

HR-MS (FAB) m/z : calculated 355.1936, found 355.2023

Amph(+)f: ^1H NMR (300 MHz, MeOD- d_4): δ (ppm) = 2.38 (s, 3H, $\text{CH}_3(\text{C}(\text{C}_2\text{H}_2)(\text{C}_2\text{H}_2)\text{C})\text{SO}_3^-$), 3.02 (s, 2H, $-\text{CH}-\text{C}=\text{O}$), 3.11 (s, 6H, $-\text{N}(\text{CH}_3)_3$), 3.56 (t, $J = 6.78$ Hz, 2H, $-\text{CH}_2-\text{CH}_2-\text{N}(\text{CH}_3)_3$), 4.05 (t, $J = 6.69$ Hz, 2H, $-\text{CH}_2-\text{CH}_2-\text{N}(\text{CH}_3)_3$), 4.61 (s, 2H, $-\text{CH}_2(\text{C}_6\text{H}_3)(\text{CH}_3)_2$), 5.20 (s, 2H, $-\text{C}-\text{CH}-\text{O}-$), 6.57 (s, 2H, $-\text{CH}=\text{CH}-$), 7.24 (d, $J = 8.10$ Hz, 2H, $\text{CH}_3(\text{C}(\text{C}_2\text{H}_2)(\text{C}_2\text{H}_2)\text{C})\text{SO}_3^-$), 7.31-7.60 (comp, 4H, $-\text{CH}_2(\text{C}_6\text{H}_4)\text{F}$), 7.72 (d, $J = 8.10$ Hz, 2H, $\text{CH}_3(\text{C}(\text{C}_2\text{H}_2)(\text{C}_2\text{H}_2)\text{C})\text{SO}_3^-$).

^{13}C NMR (75 MHz, MeOD- d_4): $\delta = 19.92, 32.07, 60.15, 67.01, 80.99, 117.49, 117.77, 119.47, 119.76, 125.56, 128.47, 128.89, 129.26, 129.37, 130.89, 131.00, 136.25, 140.28, 142.30, 161.13, 164.41, 176.53$.

^{19}F NMR (282 MHz, MeOD- d_4): $\delta = -112.95$.

HR-MS (FAB) m/z : calculated 345.1609, found 345.1593

Amph(+)g: ^1H NMR (300 MHz, MeOD- d_4): δ (ppm) = 2.38 (s, 3H, $\text{CH}_3(\text{C}(\text{C}_2\text{H}_2)(\text{C}_2\text{H}_2)\text{C})\text{SO}_3^-$), 3.03 (s, 2H, $-\text{CH}-\text{C}=\text{O}$), 3.14 (s, 6H, $-\text{N}(\text{CH}_3)_3$), 3.57 (t, $J = 6.88$ Hz, 2H, $-\text{CH}_2-\text{CH}_2-\text{N}(\text{CH}_3)_3$), 4.07 (t, $J = 6.78$ Hz, 2H, $-\text{CH}_2-\text{CH}_2-\text{N}(\text{CH}_3)_3$), 4.61 (s, 2H, $-\text{CH}_2(\text{C}_6\text{H}_3)\text{F}_2$), 5.21 (s, 2H, $-\text{C}-\text{CH}-\text{O}-$), 6.59 (s, 2H, $-\text{CH}=\text{CH}-$), 7.26 (d, $J = 7.91$ Hz, 2H, $\text{CH}_3(\text{C}(\text{C}_2\text{H}_2)(\text{C}_2\text{H}_2)\text{C})\text{SO}_3^-$), 7.30 (comp, 3H, $-\text{CH}_2(\text{C}_6\text{H}_3)\text{F}_2$), 7.72 (d, $J = 8.10$ Hz, 2H, $\text{CH}_3(\text{C}(\text{C}_2\text{H}_2)(\text{C}_2\text{H}_2)\text{C})\text{SO}_3^-$).

^{13}C NMR (75 MHz, MeOD- d_4): $\delta = 19.90, 31.99, 60.28, 66.30, 81.00, 106.11, 106.46, 115.86, 116.21, 125.55, 128.45, 130.53, 136.25, 140.28, 142.22, 161.45, 164.93, 176.52$.

^{19}F NMR (282 MHz, MeOD- d_4): $\delta = -109.35$

HR-MS (FAB) m/z : calculated 363.1594, found 363.1550

Amph(+h): ^1H NMR (300 MHz, MeOD- d_4): δ (ppm) = 2.38 (s, 3H, $\text{CH}_3(\text{C}(\text{C}_2\text{H}_2)(\text{C}_2\text{H}_2)\text{C})\text{SO}_3^-$), 3.03 (s, 2H, $-\text{CH}-\text{C}=\text{O}$), 3.13 (s, 6H, $-\text{N}(\text{CH}_3)_3$), 3.57 (t, $J = 6.88$ Hz, 2H, $-\text{CH}_2-\text{CH}_2-\text{N}(\text{CH}_3)_3$), 4.08 (t, $J = 6.88$ Hz, 2H, $-\text{CH}_2-\text{CH}_2-\text{N}(\text{CH}_3)_3$), 4.70 (s, 2H, $-\text{CH}_2(\text{C}_6\text{H}_4)\text{CF}_3$), 5.20 (s, 2H, $-\text{C}-\text{CH}-\text{O}-$), 6.58 (s, 2H, $-\text{CH}=\text{CH}-$), 7.24 (d, $J = 7.91$ Hz, 2H, $\text{CH}_3(\text{C}(\text{C}_2\text{H}_2)(\text{C}_2\text{H}_2)\text{C})\text{SO}_3^-$), 7.72 (d, $J = 8.29$ Hz, 2H, $\text{CH}_3(\text{C}(\text{C}_2\text{H}_2)(\text{C}_2\text{H}_2)\text{C})\text{SO}_3^-$), 7.78 (d, $J = 7.72$ Hz, 1H, $-\text{CH}_2(\text{C}_6\text{H}_4)\text{CF}_3$), 7.92 (comp, 3H, $-\text{CH}_2(\text{C}_6\text{H}_4)\text{CF}_3$).

^{13}C NMR (75 MHz, MeOD- d_4): $\delta = 19.89, 32.02, 60.17, 66.85, 81.01, 125.55, 127.49, 128.43, 129.49, 130.04, 131.50, 136.25, 136.67, 140.25, 142.22, 176.51$.

^{19}F NMR (282 MHz, MeOD- d_4): $\delta = -64.13$.

HR-MS (ESI) m/z : calculated 395.1577, found 395.1586

Amph(+i): ^1H NMR (300 MHz, MeOD- d_4): δ (ppm) = 2.38 (s, 3H, $\text{CH}_3(\text{C}(\text{C}_2\text{H}_2)(\text{C}_2\text{H}_2)\text{C})\text{SO}_3^-$), 3.03 (s, 2H, $-\text{CH}-\text{C}=\text{O}$), 3.17 (s, 6H, $-\text{N}(\text{CH}_3)_3$), 3.59 (t, $J = 6.88$ Hz, 2H, $-\text{CH}_2-\text{CH}_2-\text{N}(\text{CH}_3)_3$), 4.10 (t, $J = 6.88$ Hz, 2H, $-\text{CH}_2-\text{CH}_2-\text{N}(\text{CH}_3)_3$), 4.80 (s, 2H, $-\text{CH}_2(\text{C}_6\text{H}_3)(\text{CF}_3)_2$), 5.20 (s, 2H, $-\text{C}-\text{CH}-\text{O}-$), 6.58 (s, 2H, $-\text{CH}=\text{CH}-$), 7.24 (d, $J = 8.10$ Hz, 2H, $\text{CH}_3(\text{C}(\text{C}_2\text{H}_2)(\text{C}_2\text{H}_2)\text{C})\text{SO}_3^-$), 7.71 (d, $J = 7.91$ Hz, 2H, $\text{CH}_3(\text{C}(\text{C}_2\text{H}_2)(\text{C}_2\text{H}_2)\text{C})\text{SO}_3^-$), 8.28 (comp, 3H, $-\text{CH}_2(\text{C}_6\text{H}_3)(\text{CF}_3)_2$).

^{13}C NMR (75 MHz, MeOD- d_4): $\delta = 19.89, 31.93, 60.27, 65.79, 81.01, 124.78, 125.53, 130.08, 132.14, 135.45, 136.24, 140.25, 142.20, 176.47$.

^{19}F NMR (282 MHz, MeOD- d_4): $\delta = -64.30$.

HR-MS (FAB) m/z : calculated 463.1530, found 463.1467

Amph(+j): previously reported in Ref. 8. ^1H NMR (300 MHz, MeOD- d_4): δ (ppm) = 2.98-2.83 (m, 2H, $-\text{CH}_2-\text{CH}_2-\text{R}_f$), 3.02 (s, 2H, $-\text{CH}-\text{C}=\text{O}$), 3.25 (s, 6H, $-\text{N}(\text{CH}_3)_3$), 3.60 (t,

$J = 6.6$ Hz, 2H, $-\text{CH}_2-\underline{\text{CH}}_2-\text{N}(\text{CH}_3)_3$), 3.85 (t, $J = 8.7$ Hz, 2H, $-\underline{\text{CH}}_2-\text{CH}_2-\text{R}_f$), 3.95 (t, $J = 6.8$ Hz, 2H, $-\underline{\text{CH}}_2-\text{CH}_2-\text{N}(\text{CH}_3)_3$), 5.20 (s, 2H, $-\text{C}-\underline{\text{CH}}-\text{O}-$), 6.57 (s, 2H, $-\underline{\text{CH}}=\underline{\text{CH}}-$).

Amph(+)k: ^1H NMR (300 MHz, DMF- d_7): δ (ppm) = 3.09 (s, 2H, $-\underline{\text{CH}}-\text{C}=\text{O}$), 3.52 (s, 6H, $-\text{N}(\underline{\text{CH}}_3)_3$), 3.78 (t, $J = 6.95$ Hz, 2H, $-\text{CH}_2-\underline{\text{CH}}_2-\text{N}(\text{CH}_3)_3$), 3.98 (br, 2H), 4.07 (t, $J = 6.95$ Hz, 2H, $-\underline{\text{CH}}_2-\text{CH}_2-\text{N}(\text{CH}_3)_3$), 4.17 (br, 2H), 5.22 (s, 2H, $-\text{C}-\underline{\text{CH}}-\text{O}-$), 6.65 (s, 2H, $-\underline{\text{CH}}=\underline{\text{CH}}-$).

^{13}C NMR (75 MHz, DMF- d_7): $\delta = 32.49, 43.21, 47.95, 51.49, 54.83, 60.85, 63.71, 64.58, 81.17, 119.46, 123.73, 136.85, 170.94, 176.72$.

^{19}F NMR (282 MHz, DMF- d_7): $\delta = -55.68, -66.48, -78.64, -88.77, -90.78$.

HR-MS (FAB) m/z : calculated 617.1020, found 617.0981

Amph(+)l: ^1H NMR (300 MHz, MeOD- d_4): δ (ppm) = 2.39 (s, 3H, $\underline{\text{CH}}_3(\text{C}(\text{C}_2\text{H}_2)(\text{C}_2\text{H}_2)\text{C})\text{SO}_3^-$), 3.04 (s, 2H, $-\underline{\text{CH}}-\text{C}=\text{O}$), 3.19 (s, 6H, $-\text{N}(\underline{\text{CH}}_3)_3$), 3.78 (t, $J = 6.31$ Hz, 2H, $-\text{CH}_2-\underline{\text{CH}}_2-\text{N}(\text{CH}_3)_3$), 4.07 (t, $J = 6.12$ Hz, 2H, $-\underline{\text{CH}}_2-\text{CH}_2-\text{N}(\text{CH}_3)_3$), 4.80 (s, 2H, $-\underline{\text{CH}}_2(\text{C}_6\text{F}_5)$), 5.23 (s, 2H, $-\text{C}-\underline{\text{CH}}-\text{O}-$), 6.59 (s, 2H, $-\underline{\text{CH}}=\underline{\text{CH}}-$), 7.25 (d, $J = 7.91$ Hz, 2H, $\text{CH}_3(\text{C}(\text{C}_2\text{H}_2)(\text{C}_2\text{H}_2)\text{C})\text{SO}_3^-$), 7.71 (d, $J = 8.10$ Hz, 2H, $\text{CH}_3(\text{C}(\text{C}_2\text{H}_2)(\text{C}_2\text{H}_2)\text{C})\text{SO}_3^-$).

^{13}C NMR (75 MHz, MeOD- d_4): $\delta = 19.89, 32.38, 55.62, 61.51, 81.07, 125.53, 128.38, 136.26, 140.22, 142.18, 176.54$.

^{19}F NMR (282 MHz, MeOD- d_4): $\delta = -137.70, -150.68, -162.57$.

HR-MS (FAB) m/z : calculated 417.1238, found 417.1244

Representative polymerization procedure: Monomer and G3 were weighed into separate clean, dry Schlenk flasks under N_2 . The monomer was then dissolved in 3 mL 2,2,2-trifluoroethanol and the catalyst was dissolved in 2 mL dry CH_2Cl_2 . Both solutions were subjected to 3 freeze-pump-thaw cycles and warmed to room temperature.

Using a nitrogen-purged syringe, the monomer solution was added to the catalyst solution. The polymerization was allowed to proceed for 30 minutes at room temperature under N₂. To quench the reaction, 1.5 mL ethyl vinyl ether was added and the solution was stirred for an additional hour. The polymer was then precipitated out into anhydrous diethyl ether, isolated by vacuum filtration and dried under high vacuum overnight. Yields were greater than 90% for all polymers.

3.6 Conclusions

Improved nonfouling materials are critical to combat biofouling's detrimental effects. Previously, we had reported on the use of novel zwitterionic ROMP polymers for nonfouling applications. These polymers included linear carboxybetaine and sulfobetaine side chain chemistries, as well as the dual-functional betaines. Here, that chemistry was expanded in order to better understand this ROMP system, specifically to determine the effect of zwitterionic interchange distance on a functionalized surface's properties. Carboxybetaine, sulfobetaine, and methyl dual-functional series were synthesized so as to vary the distance between charged groups. The modular nature of the oxanorbornene imide monomer allowed for a wide range of zwitterionic chemistries to be achieved through basic synthetic methods, which is a major advantage of this ROMP-based platform.

3.7 References

(1) Rankin, D. A.; P'Pool, S.J.; Schanz, H-J.; Lowe, A. B. The Controlled Homogeneous Organic Solution Polymerization of New Hydrophilic Cationic *exo*-7-Oxanorbornenes via ROMP with RuCl₂(PCy₃)₂CHPh in a Novel 2,2,2-Trifluoroethanol/Methylene Chloride Solvent Mixture. *J. Polym. Sci.: Part A* **2007**, *45*, 2113-2128.

- (2) Rankin, D. A.; Lowe, A. B. New Well-Defined Polymeric Betaines: First Report Detailing the Synthesis and ROMP of Salt-Responsive Sulfopropylbetaine- and Carboxyethylbetaine-*exo*-7-oxanorbornene Monomers. *Macromolecules* **2008**, *41*, 614-622.
- (3) Rankin, D. A.; Schanz, H-J. Effect of the Halide Counterion in the ROMP of *exo*-Benzyl-[2-(3,5-dioxo-10-oxa-4-azatricyclo[5.2.1.0^{2,6}]dec-8-en-4-yl)ethyl]dimethylammonium Bromide/Chloride. *Macromol. Chem. Phys.* **2007**, *208*, 2389-2395.
- (4) Colak, S.; Tew, G. N. Synthesis and Solution Properties of Norbornene Based Polybetaines. *Macromolecules* **2008**, *41*, 8436-8440.
- (5) Lowe, A.B.; McCormick, C. L. Synthesis and Solution Properties of Zwitterionic Polymers. *Chem. Rev.* **2002**, *102*, 4177-41895.
- (6) Laschewsky, A. Structures and Synthesis of Zwitterionic Polymers. *Polymers* **2014**, *6*, 1544-1601.
- (7) Colak, S.; Tew, G. N. Dual-Functional ROMP-Based Betaines: Effect of Hydrophilicity and Backbone Structure on Nonfouling Properties. *Langmuir* **2012**, *28*, 666-675.
- (8) Colak, S.; Tew, G. N. Amphiphilic Polybetaines: The Effect of Side-Chain Hydrophobicity on Protein Adsorption. *Biomacromolecules* **2012**, *13*, 1233-1239.
- (9) Kumara Swamy, K. C.; Bhuvan Kumar, N. N.; Pavan Kumar, K.V. P. Mitsunobu and Related Reactions: Advances and Applications. *Chem. Rev.* **2009**, *109*, 2551-2651.
- (10) Lienkamp, K.; Kins, C. F.; Alfred, S. F.; Madkour, A. E.; Tew, G. N. Water-Soluble Polymers from Acid-Functionalized Norbornenes. *J. Polym. Sci.: Part A* **2009**, *47*, 1266-1273.
- (11) Stubenrauch, K.; Moitzi, C.; Fritz, G.; Glatter, O.; Trimmel, G.; Stelzer, F. Precise Tuning of Micelle, Core, and Shell Size by the Composition of Amphiphilic Block Copolymers Derived from ROMP Investigated by DLS and SAXS. *Macromolecules* **2006**, *39*, 5865-5874.
- (12) Banerjee, I.; Pangule, R. C.; Kane, R. S. Antifouling Coatings: Recent Developments in the Design of Surfaces That Prevent Fouling by Proteins, Bacteria, and Marine Organisms. *Adv. Mater.* **2011**, *23*, 690-718.
- (13) Callow, J. A.; Callow, M. E. Trends in the development of environmentally friendly fouling-resistant marine coatings. *Nat. Commun.* **2011**, DOI: 10.1038/ncomms1251.

- (14) Hancock, R. E.; Lehrer, R. Cationic peptides: a new source of antibiotics. *Trends Biotechnol.* **1998**, *16*, 82-88.
- (15) Pagliaro, M.; Ciriminna, R. New fluorinated functional materials. *J. Mater. Chem.*, **2005**, *15*, 4981-4991.
- (16) Briza, T.; Kvicala, J.; Paleta, O.; Cermak, J. Preparation of bis(polyfluoroalkyl)cyclopentadienes, new highly fluorophilic ligands for fluorour biphase catalysis. *Tetrahedron* **2002**, *58*, 3841-3846.
- (17) deRonde, B. M.; Birke, A.; Tew, G. N. Design of Aromatic-containing Cell Penetrating Peptide Mimics with Structurally Modified π -electronics. *Chem.: Eur. J.* **2015**, *21*, 3013-3019.
- (18) Banerjee, S.; Das, R. K.; Maitra, U. Supramolecular gels 'in action'. *J. Mater. Chem.* **2009**, *19*, 6649-6687.
- (19) Love, J. A.; Morgan, J. P.; Trnka, T. M.; Grubbs, R. H. A Practical and Highly Active Ruthenium-Based Catalyst that Effects the Cross Metathesis of Acrylonitrile. *Angew. Chem. Int. Ed.* **2002**, *41*, 4035-4037.
- (20) Mantovani, G.; Lecolley, F.; Tao, L.; Haddleton, D. M.; Clerx, J.; Coernelissen, J. L. M.; Velonia, K. Design and Synthesis of N-Maleimido-Functionalized Hydrophilic Polymers via Copper-Mediated Living Radical Polymerization: A Suitable Alternative to PEGylation Chemistry. *J. Am. Chem. Soc.* **2005**, *127*, 2966-2973.

CHAPTER 4

NORBORNENE-BASED POLYMERS FOR SURFACE MODIFICATION

4.1 Introduction

The polybetaines described in the previous chapter were envisaged as nonfouling materials. To practically employ them in that capacity, a method was devised to create functionalized surfaces from these polymers. This chapter summarizes the synthesis and characterization of copolymers containing the oxanorbornene imide betaines and 5-(bicycloheptenyl)-triethoxysilane.¹ The siloxane groups could condense on oxidized surfaces to create a covalently anchored coating. Random and block copolymers were both explored, as well as polymers with varying amounts of siloxane repeat units. The resulting coatings were characterized by AFM and water contact angle analysis. Finally, the optimal coating composition to minimize protein adsorption was determined. Generally, it was found that well-defined copolymers were easily obtained by ROMP, despite the fact that the block copolymers were difficult to characterize due to their solution properties. Coatings from the random copolymers were relatively homogeneous and of intermediate wettability, while the block copolymers produced unique surface features. Even though the block copolymer coatings were more hydrophilic than their random copolymer counterparts, they exhibited significantly higher levels of protein adsorption. The optimal polymer composition that minimized protein adsorption while still creating a robust surface was determined to be a random copolymer with approximately 16% siloxane content. Briefly, functionalization of surfaces other than silica or glass was explored as well for potential future applications.

4.2 General Approach

Polybetaines have found great potential as nonfouling materials, but again the radical polymerization systems lack chemical diversity. Our oxanorbornene-based polybetaines, on the other hand, contained a multitude of functionalities that made them intriguing candidates for nonfouling coatings.^{1,2} In addition to the linear and dual-functional zwitterion chemistries, the olefinic oxanorbornene backbone was unique compared to many of the existing nonfouling polymers' scaffolds. Coatings functionalized surfaces are logical and easily screened applications for nonfouling polymers. Previously, surface-grafted polyzwitterion brushes comprised some of the most efficient nonfouling surfaces due to both their hydrophilicity and the entropic penalty required to compress extended chains in an aqueous environment.³⁻⁶ In contrast to many CRP techniques, however, surface-initiated ROMP is especially challenging to employ.⁷ In fact, many methods of functionalizing surfaces by ROMP produce bulk coatings, where the surface is first functionalized with a monomeric tether and then submerged in a solution containing the catalyst and additional free monomer.

We previously devised a strategy to create robust coatings from water-soluble oxanorbornene-based polymers, which produce bulk coatings but allow for greater control of the polymer precursor.^{1,2} By copolymerizing charged monomers with 5-(bicycloheptenyl)-triethoxysilane in a ratio of 5:1, the incorporated siloxane side chain could hydrolyze to form intra- and intermolecular crosslinks. Additionally, the siloxane condensed onto oxidized surfaces such as silicon wafers and glass slides, forming a covalent tether between the surface and the bulk coating. It was shown that these random copolymers produced coatings that could withstand use in an aqueous environment,

specifically on timescales appropriate for biological testing, and that the zwitterionic component was sufficient to reduce nonspecific fouling.

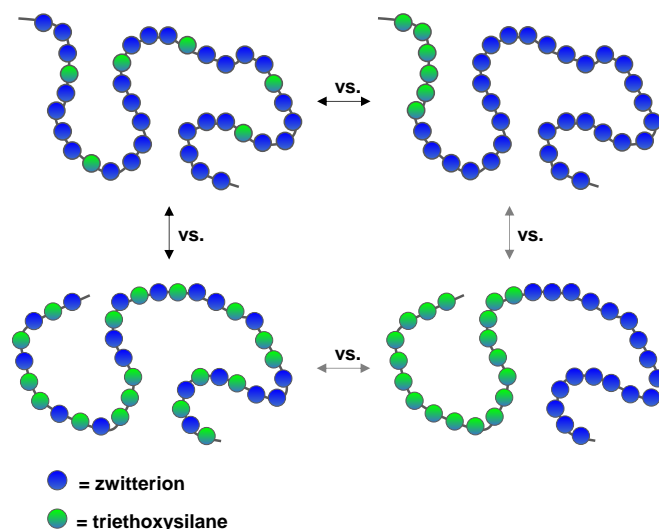


Figure 4.1: Schematic representation of random and block copolymers containing zwitterionic and siloxane-containing side chains for surface modification.

We were interested, however, in a more systematic study of the role of the siloxane-containing repeat unit. To this end, a library of model polymers was synthesized to ascertain the effects of polymer composition and repeat unit sequence on the final coatings as represented in Figure 4.1. The sulfobetaine monomer **Sulfo(ZI)b** was chosen as the model zwitterionic component due to its intrinsic zwitterionic nature and its lack of post-polymerization functionalization reactions. The effect of copolymer type, or the arrangement of repeat units along the polymer chain, was studied by comparing random to block copolymers, which were both easily obtained by ROMP. The effect of polymer composition was studied by varying the ratio of zwitterionic to siloxane-containing repeat units in the polymers. In this chapter's nomenclature, the prefix **rP** refers to random copolymers while **bP** refers block copolymers; the numerical subscripts refer to the number of zwitterionic and siloxane repeat units, respectively.

4.3 Polymer Synthesis and Characterization

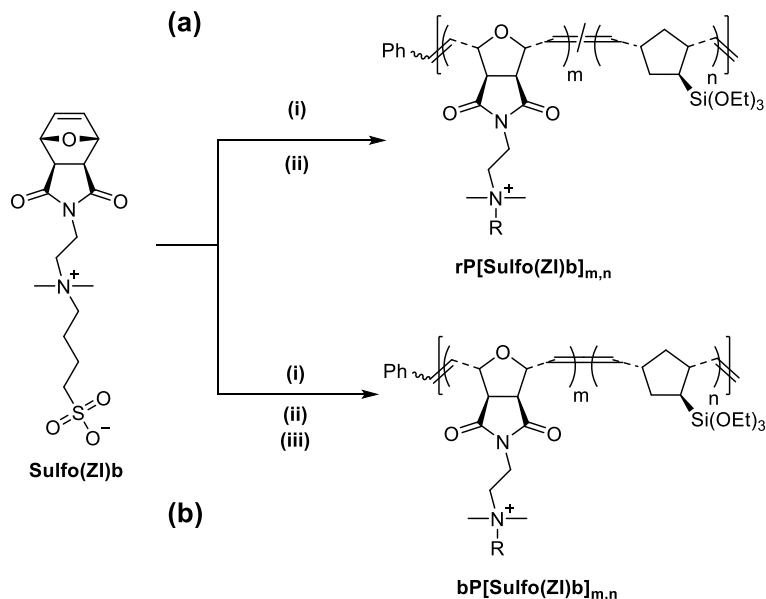


Figure 4.2. Synthesis of model sulfobetaine polymers for surface modification. **(a)** Random copolymers: (i) 5-(bicycloheptenyl)-triethoxysilane, G3, CH₂Cl₂/TFE, room temperature, 30 minutes; (ii) ethyl vinyl ether, room temperature, 1 hour; **(b)** Block copolymers: (i) G3, CH₂Cl₂/TFE, room temperature, 15 minutes; (ii) 5-(bicycloheptenyl)-triethoxysilane, CH₂Cl₂, room temperature, 10 minutes; (iii) ethyl vinyl ether, room temperature, 1 hour.

As shown in Figure 4.2, all copolymers were synthesized using Grubbs' 3rd generation catalyst in a mixture of CH₂Cl₂ and TFE. In general, the polymerizations were complete within a half hour or less. Random copolymers (Figure 4.2a) were synthesized by the addition of catalyst to a solution containing both zwitterionic and siloxane-containing polymers and then quenched with ethyl vinyl ether per the standard procedure. For the block copolymers (Figure 4.2b), the monomers were polymerized sequentially: the zwitterionic block was polymerized first, then the siloxane monomer was added. The siloxane monomer was known to polymerize in an uncontrolled fashion, thus its addition after the zwitterionic block. Likewise, higher order copolymers such as

triblocks were not pursued due to the siloxane monomer's uncontrolled polymerization. The degree of polymerization was held constant at 36 for a series of both the random and the block copolymers, to match previously published reports on nonfouling polymers.^{1,2} A longer random copolymer (125 repeat units) and block copolymer (80 repeat units) were synthesized to show that high molecular weight polymers could be polymerized with good control by this method as well. The random copolymer (**rP[Sulfo(ZI)b]_{100,25}**) was not intended for nonfouling applications, however, and so will not be discussed further. Both series of random and block copolymers were synthesized with varying ratios of zwitterionic to siloxane repeat units (Table 4.1), ranging from approximately 8-50 mol %.

Table 4.1: Compositional characterization of random and block polymers by NMR spectroscopy

Polymer	Theoretical		Calculated ^a		mol % Si
	m	n	m ^b	n	
rP[Sulfo(ZI)b] _{33,3}	33	3	33	3.5	8.3
rP[Sulfo(ZI)b] _{30,6}	30	6	30	6.5	16.7
rP[Sulfo(ZI)b] _{18,18}	18	18	N. D.	N. D. ^c	50.0
rP[Sulfo(ZI)b] _{100,25}	100	25	100	26	20.0
bP[Sulfo(ZI)b] _{33,3}	33	3	N. D.	N. D.	8.3
bP[Sulfo(ZI)b] _{30,6}	30	6	N. D.	N. D.	16.7
bP[Sulfo(ZI)b] _{18,18}	18	18	N. D.	N. D.	50
bP[Sulfo(ZI)b] _{70,10}	70	10	N. D.	N. D.	12.5

^a calculated by ¹H NMR spectroscopy in D₂O with trace sodium bromide; ^b assumed to be equal to the theoretical value due to the low resolution of the phenyl endgroup; ^c N. D. = not determined.

Because of the charged nature of these polymers in addition to the hydrolytically unstable triethoxysilane pendant groups, GPC was not used as a characterization technique. Instead, ¹H NMR spectroscopy was used exclusively. Deuterium oxide with trace amounts of sodium bromide was used as the solvent. In this solvent system, the

phenyl endgroup was not typically visible, thus endgroup analysis could not be used to calculate molecular weight or the total number of repeat units in the polymer chain. The crude NMR spectra indicated quantitative conversion, so for simplicity's sake it was assumed that the number of zwitterionic repeat units in the final polymer was equal to the theoretical value. The number of siloxane repeat units in the final polymers was calculated by taking the ratios of the peaks corresponding to the $-\text{Si}(\text{OCH}_2\text{CH}_3)_3$ and $-\text{N}(\text{CH}_3)_2$ or $-\text{CH}_2\text{CH}_2\text{CH}_2\text{CH}_2-$ groups. In the case of $\text{rP}[\text{Sulfo}(\text{ZI})\text{b}]_{18,18}$, NMR spectra could only be obtained at low resolution due to the polymer's insolubility in D_2O , thus the repeat unit ratios could not be quantitatively calculated.

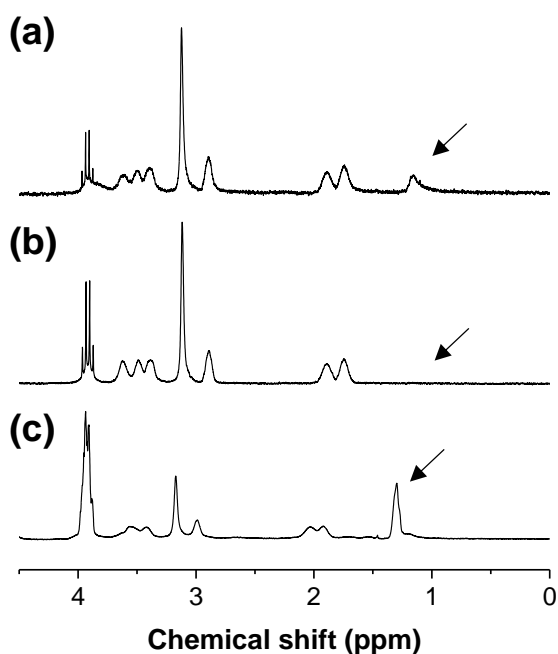


Figure 4.3: Representative NMR spectra of (a) $\text{rP}[\text{Sulfo}(\text{ZI})\text{b}]_{30,6}$ in $\text{D}_2\text{O}/\text{NaBr}$; (b) $\text{bP}[\text{Sulfo}(\text{ZI})\text{b}]_{30,6}$ in $\text{D}_2\text{O}/\text{NaBr}$; and (c) $\text{bP}[\text{Sulfo}(\text{ZI})\text{b}]_{30,6}$ in TFE-d_3 . Arrows indicate $-\text{Si}(\text{OCH}_2\text{CH}_3)_3$ peak shifts.

While it was found that the composition of the random copolymers were in good agreement with their theoretical feed ratios, the siloxane peaks were not visible for the

block copolymers and so the ratios of the repeat units were not calculated (Table 4.1). Although an in-depth study of the polymers' solution properties was not done, it was assumed that the block copolymers aggregated in aqueous solutions due to the hydrophobic block based on NMR spectroscopy data. In fact, methacrylate-based copolymers comprised of zwitterionic and triethoxysilane-containing blocks had been used previously to form vesicles, indicating that these monomer chemistries can drive self-assembly under the proper conditions. As shown in Figure 4.3a, peaks from both the zwitterionic block and the triethoxysilane block (indicated with an arrow) of **rP[Sulfo(ZI)b]_{30,6}** were observed in the spectrum when the polymer was dissolved in D₂O/NaBr. On the other hand, the peak corresponding to the methyl protons of the triethoxysilane group were absent from the spectrum of **bP[Sulfo(ZI)b]_{30,6}** in D₂O/NaBr (Figure 4.3b). When the block copolymer was dissolved in TFE-d₃, however, the siloxane peaks were again visible (Figure 4.3c). Clearly, the siloxane groups were present in the block copolymer, but not visible in the NMR spectrum in D₂O. This observation suggested that the hydrophobic blocks aggregated together, thus shielding the triethoxysilane protons. Because no residual monomer was observed in the crude polymers' NMR spectra after the completion of each block, it appeared that each step of the reaction went to completion and that the theoretical feed ratio was a good approximation of the polymers' true composition. Even though TFE-d₃ was a good (or better) solvent for both blocks of the copolymers, its cost made it impractical to use frequently. Additionally, model spectra of the random copolymers in D₂O and TFE-d₃ seemed to suggest that the peak integrations in TFE-d₃ were off to such an extent that the ratios of the repeat units could not be accurately calculated in this way either.

4.4 Surface Functionalization and Coating Characterization

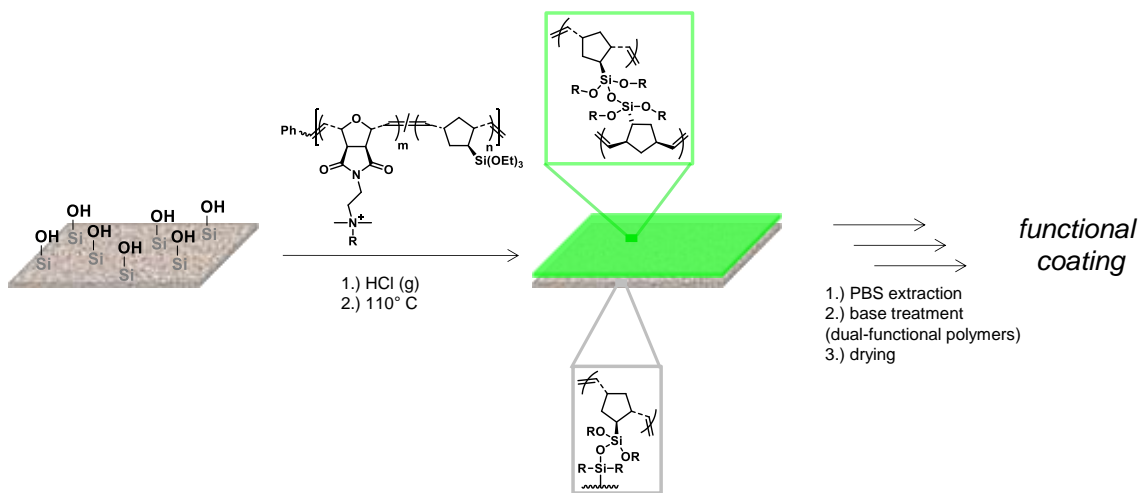


Figure 4.4: General procedure for coating preparation on silicon wafers.

To create coatings from these polymers, a multistep curing process was used (Figure 4.4).¹ First, a clean silicon wafer was spin-cast with a solution of the polymer in TFE. Next, the surfaces were exposed to gaseous HCl to hydrolyze the siloxane groups. Finally, the surfaces were heated at 110 °C for several hours. After condensation, a tightly crosslinked network containing both intra- and intermolecular crosslinks bound to the silicon surface was achieved. To remove any residual polymer from the coatings, the surfaces were soaked in PBS for several hours and then rinsed with RO water to remove excess salt. In the case of the dual-functional polymers, the surfaces were then soaked in a base solution for 20 minutes to ring-open the imide group. For the sulfobetaine series, however, this step was unnecessary and the samples were directly dried under high vacuum overnight.

Atomic force microscopy (AFM) was used to first elucidate the surface topographies of the resulting coatings. Figure 4.5 shows height images of the random copolymer series. On the **rP[Sulfo(ZI)b]_{33,3}** surface (Figure 4.5a), small defects were visible across the coating. These holes measured about 25 nm and were observed across entire samples. The **rP[Sulfo(ZI)b]_{30,6}** and **rP[Sulfo(ZI)b]_{18,18}** surfaces (Figures 4.5b and c, respectively), on the other hand, appeared smooth with no visible defects. The **rP[Sulfo(ZI)b]_{18,18}** surface, with the highest siloxane content, had the least variance across the surface by direct inspection, possibly a result of tighter crosslinking. From these images, it appeared that **rP[Sulfo(ZI)b]_{33,3}** contained too little siloxane to create a homogeneous coating, giving rise to dewetting effects and delamination.

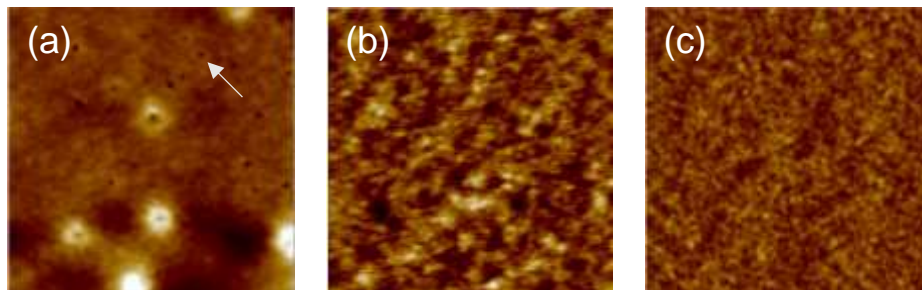


Figure 4.5. AFM tapping mode height images of (a) **rP[Sulfo(ZI)b]_{33,3}**; (b) **rP[Sulfo(ZI)b]_{30,6}**; and (c) **rP[Sulfo(ZI)b]_{18,18}**. All images represent a 1 μm x 1 μm x 7.5 nm area.

Even though the random and block copolymers contained the same chemical functionalities, the topographies of their coatings vastly differed. As seen in Figure 4.6, all block copolymer coatings exhibited rougher surfaces with striking bulbous features. The surface functionalized with **bP[Sulfo(ZI)b]_{33,3}** containing the least amount of siloxane (Figure 4.6a) had the most homogeneous surface. Increasing the siloxane content of the polymer coating to 16% and 50% (**bP[Sulfo(ZI)b]_{30,6}** and **bP[Sulfo(ZI)b]_{18,18}**) saw the formation of more well-defined, pebble-like surface features

in Figures 4.6b and c. The discernable surface characteristics of these block copolymer surfaces are in contrast to those of the random copolymer surfaces, which were largely featureless and homogeneous. The surface roughnesses, as tabulated in Table 4.2, corroborated these observations. Based on the molecular weights of the polymers, it is unlikely that they could undergo well-defined self-assembly. Based on the NMR spectra, however, we believe that these polymers do aggregate in solution. The topography of these surfaces may be a result of the perseveration of the aggregates during the coating and curing processes, an effect that was not expected to be present in the random copolymers.

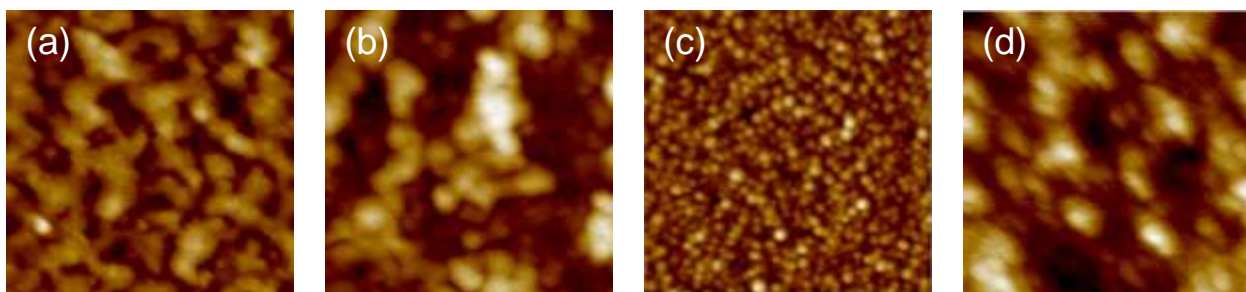


Figure 4.6: AFM tapping mode height images of (a) **bP[Sulfo(ZI)b]_{33,3}**; (b) **bP[Sulfo(ZI)b]_{30,6}**; (c) **bP[Sulfo(ZI)b]_{18,18}**; and (d) **bP[Sulfo(ZI)b]_{70,10}**. All images represent a 1 μm x 1 μm x 30 nm area.

Other qualitative differences were observed between coatings from the random and block copolymers. At the same casting solution concentration (usually 1w/v %), the thicknesses of the random copolymer coatings as measured by ellipsometry were approximately twice those of the block copolymers. This discrepancy was most likely a result of the differing topographies of the surfaces. Ellipsometry calculates the thickness of a coating as the average over an area. In the case of the block copolymer surfaces, which are clearly rougher, the calculated thickness can be thought of as the median height

of the surface features. The block copolymer surfaces had a tendency to delaminate around the edges of the silicon wafer samples as well. Increasing the casting solution concentration did little to alleviate this effect; in fact, it may have exacerbated it. No such problem was observed with the random copolymers. Block copolymers with a block that selectively interacts with a substrate can be used to achieve high graft density and good stability.⁸ Prior to curing, the siloxane-containing block of these polymers is non-selective for silica, and may even be sequestered further in the interior of aggregates, thus lowering the efficiency of the adherent block. Delamination would be symptomatic of fewer bonds being formed on the substrate.

Static water contact angle measurements were made to determine the relative hydrophilicities of the resulting surfaces (Table 4.2). Values were similar for the **rP[Sulfo(ZI)b]_{33,3}** and **rP[Sulfo(ZI)b]_{30,6}** surfaces (58° and 54°), implying that the surfaces were similarly hydrophilic. The static water contact angle increased greatly for the **rP[Sulfo(ZI)b]_{18,18}** surface to 69°, as expected due to the decreased zwitterionic content of the polymer. In general, the contact angles for the block copolymer series were less than those for the random copolymer series (<50° vs. >50°), again implying that the random copolymer surfaces were more hydrophilic, or more wettable. This effect was accounted for by the greater concentration of zwitterionic groups at the coating's interface due to the mobility of the zwitterionic block. It was also possible, however, that the block copolymers were less efficient at covering the substrate, and the greater wettability of these surfaces is due in part to the silica substrate's contribution. No clear trend was observed between the length of the zwitterionic block and the water contact angle for the block copolymer series, however, which may be due to the complex

nature of the surface chemistry after curing as discussed in the previous paragraph. Furthermore, silanol groups or SiO₂ resulting from the curing process may have increased the surfaces' wettabilities as well but would adversely affect the coatings' nonfouling properties. It was difficult to deconvolute the contributions of different hydrophilic surface groups, however, so wettability was assumed to be mainly influenced by the zwitterionic content.

Table 4.2: Surface properties of random and block copolymers.

Polymer	Roughness (nm)^a	Static water contact angle (°)^b	Γ_{Fibrinogen} (ng/mm²)^c
rP[Sulfo(ZI)b] _{33,3}	0.66	58	0.35 ± 0.32
rP[Sulfo(ZI)b] _{30,6}	0.29	54	1.03 ± 0.23
rP[Sulfo(ZI)b] _{18,18}	0.38	69	3.20 ± 1.19
bP[Sulfo(ZI)b] _{34,2}	1.88	44	12.56 ± 0.39
bP[Sulfo(ZI)b] _{30,6}	5.10	51	18.04 ± 2.76
bP[Sulfo(ZI)b] _{18,18}	3.45	33	5.04 ± 2.47
bP[Sulfo(ZI)b] _{70,10}	2.25	45	1.06 ± 0.29

^a root mean squared (rms) roughness calculated by the manufacturer's software based on a 1 μm x 1 μm image area; ^b water contact angles measured by the sessile drop technique; ^c fibrinogen adsorption measured by ellipsometry.

4.5 Protein Adsorption

Finally, protein adsorption was measured for all surfaces as a screening test for nonfouling efficacy. One of the simplest metrics for quantifying the nonfouling performance of a given coating is measuring the amount of irreversible protein adsorption on the surface. Fibrinogen – a large, negatively charged protein – was chosen as a model protein due to its frequent use in the literature. While adsorption of a single protein is a gross oversimplification of the actual processes that occur in biological environments, it still provides an easily accessible method for comparing the nonfouling efficacies of a

number of coatings. Here, ellipsometry was used to measure the thickness of the adsorbed protein layer in the dry state after a given surface's exposure to fibrinogen.⁹

The final amount of protein (Γ) was calculated from the following equation:

$$\Gamma(\text{ng}/\text{mm}^2) = h \times d$$

where h equals the measured thickness of the protein layer, and d equals the value for protein density as taken from the literature.^{10,11} Tabulated values can be found in Table 4.2.

Fibrinogen adsorption for the random and block copolymer series are given in Figure 4.7. A clean silica surface was used as the control. In the case of the random copolymer series, there was a clear trend between increasing siloxane content of the polymer and increasing protein adsorption. The **rP[Sulfo(ZI)b]_{33,3}** surface exhibited the least amount of protein adsorption at 0.35 ng/mm², but also with a large variance between samples as reflected in the large standard deviation. The **rP[Sulfo(ZI)b]_{30,6}** surface had an intermediate amount of protein adsorption (1.03 ng/mm²), which was greater than the **rP[Sulfo(ZI)b]_{33,3}** surface but still less than the bare silica control. The surface functionalized with the polymer with the highest siloxane content, **rP[Sulfo(ZI)b]_{18,18}**, exhibited the greatest amount of protein adsorption (3.20 ng/mm²), on par with the silica control. In general, the fibrinogen adsorption positively correlated with the static water contact angle measurements for these surfaces. The most hydrophobic surface, **rP[Sulfo(ZI)b]_{18,18}**, exhibited the highest amount of protein adsorption, as would be expected due to the decreased zwitterionic content of the polymer. The **rP[Sulfo(ZI)b]_{33,3}** surface looked especially promising due to its low degree of protein adsorption, however results were inconsistent for these surfaces as denoted by the large

error. It was thought that the high variance for these surfaces was due to the presence of the dewetting defects seen in the AFM images (Figure 4.5) or poor surface stability during the assay due to the lower degree of crosslinking.

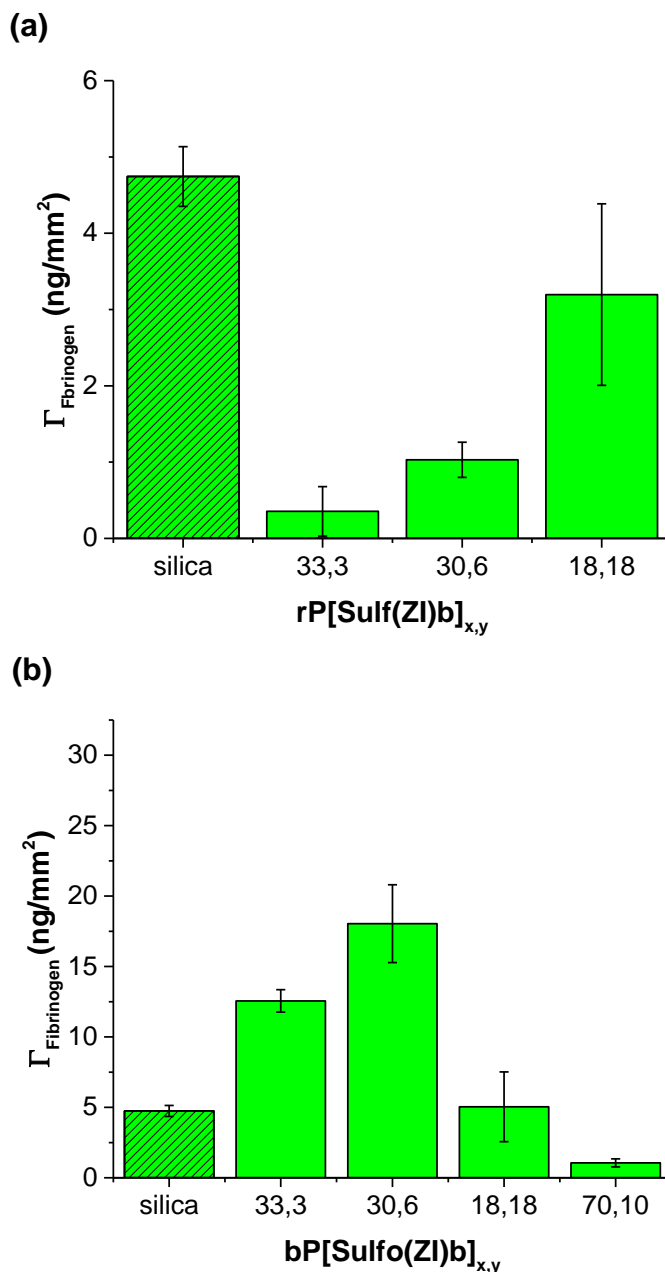


Figure 4.7: Fibrinogen adsorption on (a) random, and (b) block copolymer surfaces. A silica surface (shaded bar) was used as a control. Error bars represent \pm standard deviation, based on at least 3 independent measurements.

In contrast to the random copolymer surfaces, the block copolymer surfaces typically exhibited protein adsorption levels greater than the silica control. Fibrinogen adsorption was approximately 12 ng/mm² and 25 ng/mm² for the **bP[Sulfo(ZI)b]_{34,2}** and **bP[Sulfo(ZI)b]_{30,6}** surfaces, respectively – an extraordinarily high amount. Interestingly, fibrinogen adsorption decreased for the **bP[Sulfo(ZI)b]_{18,18}** surface to approximately 5 ng/mm². When the total polymer length increased to 80 repeat units at 12% siloxane (**bP[Sulfo(ZI)b]_{70,10}**), fibrinogen adsorption decreased further to 1.09 ng/mm², on the order of the block copolymer surfaces.

The block copolymer coatings with the lowest amounts of siloxane most likely suffered from poor surface coverage or poor anchorage, so that there was incomplete zwitterionic coverage of the substrate¹² or even delamination during the assay. The presumed dynamic nature of the brush-like surface may have also trapped or further interacted with the protein, resulting in high levels of adsorption. The **bP[Sulfo(ZI)b]_{18,18}** surface likely improved surface coverage of the polymer due to the increased number of potential crosslink sites, but still did not contain enough zwitterionic units to reduce protein adsorption below the silica control. Increasing the length of the block copolymer and specifically the zwitterionic block, in the case of the **bP[Sulfo(ZI)b]_{70,10}** surface, may have increased the zwitterionic surface coverage compared to the shorter block copolymers. The longer zwitterionic tail could compensate for any bare patches, thus creating a denser zwitterionic surface.¹³ This effect resulted in the decreased protein adsorption. Contact angle did not strongly correlate with protein adsorption in the case of the block copolymers, which was not wholly unsurprisingly due to the complex surface chemistry of these materials and the nature of biofouling.

Based on the protein fouling results, it appeared that the random copolymers produced the best nonfouling surfaces. We thought, however, that a mixed surface combining both random and block copolymers might boost the nonfouling efficiency of the surface by fully covering the underlying substrate while still allowing for the zwitterionic brush architecture.¹⁴ The **rP[Sulfo(ZI)b]_{30,6}** and **bP[Sulfo(ZI)b]_{70,10}** polymers were selected based on their nonfouling performances. The polymers were mixed in solution in ratios of 3:7, 1:1, and 7:3 and surfaces were prepared as before. Surfaces with the greatest block copolymer content (3:7 **rP[Sulfo(ZI)b]_{30,6}** : **bP[Sulfo(ZI)b]_{70,10}**) consistently delaminated and so were not pursued further. AFM images of the remaining two formulations are shown in Figure 4.8. Both surfaces appeared fairly homogenous and without obvious defects. The image in Figure 4.8a, however, contained several indistinct globular surface features that looked similar to those found on the pure block copolymer surfaces. These features disappeared on the surface in Figure 4.8b, however, indicating that the relative ratios of block and random copolymers did influence surface topography and that characteristics of the pure surfaces were somewhat maintained in the mixtures.

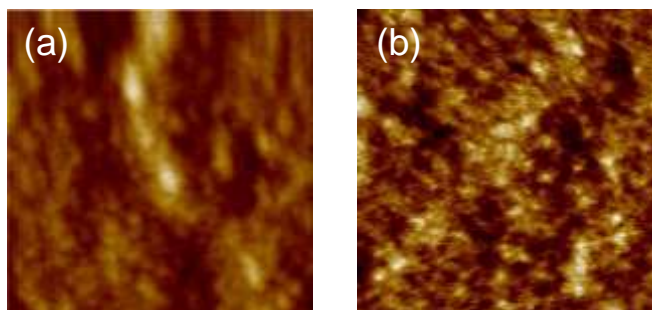


Figure 4.8: AFM height images of (a) 1:1 **rP[Sulfo(ZI)b]_{30,6}**:**bP[Sulfo(ZI)b]_{70,10}**; and (b) 7:3 **rP[Sulfo(ZI)b]_{30,6}**:**bP[Sulfo(ZI)b]_{70,10}**. All images represent a 1 μm x 1 μm x 5 nm area.

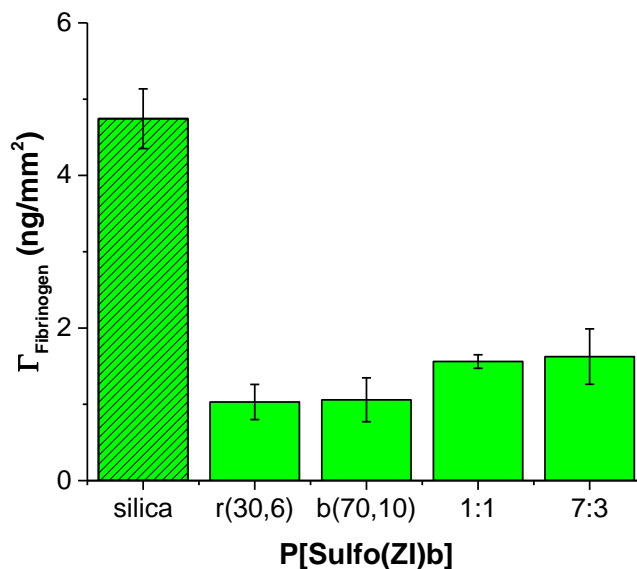


Figure 4.9: Fibrinogen adsorption on random copolymer, block copolymer and mixed surfaces. A silica surface (shaded bar) was used as a control. Error bars represent \pm standard deviation, based on at least 3 independent measurements.

Fibrinogen adsorption for the mixed surfaces, as well as for the pure random and block copolymer surfaces for comparison, are given in Figure 4.9. All surfaces and compositions decreased fibrinogen adsorption compared to the silica control. However, all surfaces performed similarly within error, exhibiting approximately 1 – 1.5 ng/mm² adsorbed fibrinogen. The presumed presence of both a tightly crosslinked network and free polymer chains did not appear to influence the nonfouling performance positively, if at all. Thus, the mixed surfaces were not considered to be appropriate nonfouling materials.

Based on the surface characterization of the random and block copolymer surfaces, it was clear that both the polymer repeat unit sequence and overall composition greatly influenced surface properties. Based on the fibrinogen adsorption studies, it was found that the polymer composition could be tuned to minimize protein adsorption.

Overall surface coverage and zwitterionic content appeared to be the factors that influenced nonfouling efficacy the greatest. In the case of the random copolymers, minimal adsorption occurred on the **rP[Sulfo(ZI)b]**_{33,3} surface, or the surface with the least amount of siloxane. The longest block copolymer, **bP[Sulfo(ZI)b]**_{70,10}, produced the most efficient nonfouling surface. Because of the practical issues associated with the block copolymers in general (delamination and difficulty characterizing the polymer precursors), and **rP[Sulfo(ZI)b]**_{33,3} (delamination and dewetting, as well as poor reproducibility), **rP[Sulfo(ZI)b]**_{30,6} was considered to contain the best polymer composition for screening tests. Thus, a ratio of 30:6 zwitterionic:siloxane-containing repeat units in a random distribution was selected for the nonfouling polymers in Chapters 5 and 6.

4.6 PDMS Functionalization

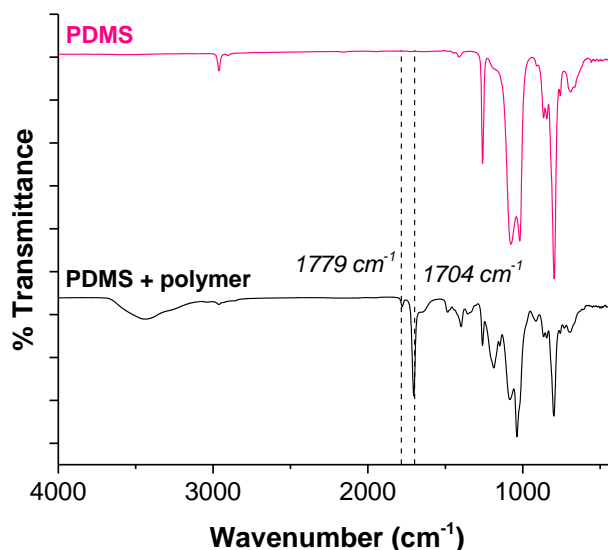


Figure 4.10: Grazing angle FT-IR spectra of PDMS substrate (top line, magenta), and oxidized PDMS functionalized with **rP[Sulfo(ZI)b]**_{30,6} (bottom line, black). Dotted lines highlight characteristic imide frequencies at 1779 cm⁻¹ and 1704 cm⁻¹.

While silicon-containing substrates such as silicon wafers and glass slides are useful for batch processing of coatings and their subsequent testing, more varied substrates are also of interest. In some cases, specific substrates are required for specialized assays or testing procedures, for instance high through-put antibacterial testing.¹⁵ Additionally, the underlying substrate can potentially affect the coatings' properties and behavior, thus offering another parameter in creating high performance materials.^{6,16} To this end, we were interested in the copolymers' ability to coat other oxidized surfaces.

Polydimethylsiloxane (PDMS), as well as other elastomeric substrates, are often used as foul-release materials.⁶ The low moduli of the elastomers promote weak adhesion between a foulant and the substrate, and make removal of foulant easier. Foul-release materials, however, do not typically deter the settlement of foulants. Thus, methods to incorporate nonfouling properties into elastomers like PDMS are of great interest to create high performance materials. PDMS is easily oxidized by chemical or physical methods such as oxygen plasma treatment to create synthetic handles on the surface. In this case, the glassy surface of oxidized PDMS could be functionalized with our siloxane-containing polymers much in the same manner as silicon wafers or glass slides.

Table 4.3: Experimental parameters to prepare functionalized PDMS surfaces

Plasma treatment time (minutes)	Casting solution concentration (w/v%)
1	1
5	2
10	5
15	---

Sylgard 184 was purchased and cured according to the manufacturer's instructions. Samples approximately 1 cm x 1 cm x 1.5 μm is size were cut out and pressed onto glass slide coverslips for easy handling. Different plasma exposure times and polymer solution concentrations (Table 4.3) in all combinations were screened. FT-IR was used to confirm the presence of the polymer coating after curing and extraction steps. Figure 4.10 shows the IR spectra of PDMS before and after polymer functionalization. The characteristic imide peak was clearly visible in the spectrum of the functionalized PDMS, indicating the presence of the ROMP backbone and thus successful functionalization.

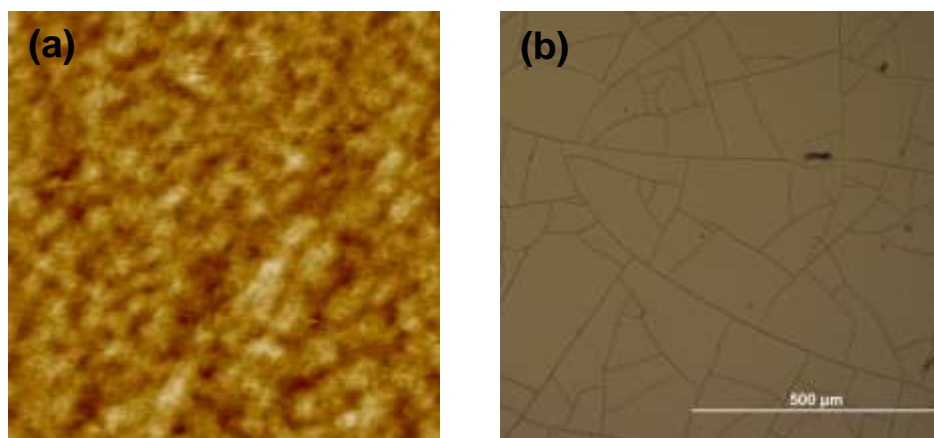


Figure 4.11: Surface characteristics of functionalized PDMS by (a) AFM and (b) optical microscopy images. The AFM image represents a 1 μm x 1 μm x 5 nm area.

While AFM showed a microscopically uniform polymer surface, it was clear from optical microscopy (and even the naked eye) that the functionalized surface suffered from defects on the macroscopic level. Cracks were visible on all surfaces regardless of casting solution concentration and plasma treatment time. The issue most likely arose due to the difference in moduli between the brittle, glassy surface and the soft bulk PDMS substrate. As the cracking could interfere with protein adsorption assays and

other characterization techniques, PDMS was not explored further as a substrate. Likewise, cursory exploration of polystyrene and polypropylene substrates revealed that the polymers would not adhere to the oxidized surfaces, making silica and glass the best substrates for these polymers.

4.7 Experimental Procedures

4.7.1 Materials

All reagents were purchased from either Sigma-Aldrich, Alfa Aesar, Acros Organics, or Fisher Scientific in the highest purity available and used as received, unless otherwise noted. 1,3-dinitrobenzene was obtained from Avocado Research Chemicals and used as received. 5-(bicycloheptenyl)triethoxysilane was purchased from Gelest Inc. and used as received. Tetrahydrofuran (THF, Fisher Scientific, HPLC grade) was distilled from sodium/benzophenone under nitrogen and dichloromethane (CH₂Cl₂, Fisher Scientific, ACS grade) was distilled from CaH₂ under nitrogen immediately prior to use. 2,2,2-trifluoroethanol (TFE, 99+%) was purchased from Alfa Aesar and used as received. Grubbs' 3rd generation catalyst (G3) was synthesized according to a previously reported procedure.¹⁷ Fibrinogen was purchased from Calbiochem as a lyophilized powder. Phosphate buffered saline (PBS, 0.01M) was purchased from Sigma Aldrich free of serum proteins as a powder and reconstituted in distilled water prior to use. Sylgard 184 was purchased from Dow Corning and prepared according to the supplier's instructions.

4.7.2 Instrumentation and methodology

Nuclear magnetic resonance (NMR) spectra were obtained on a Bruker DPX-300 NMR spectrometer. Abbreviations for assignments are as follows: s: singlet; t: triplet; q: quartet; m: multiplet; comp: overlapping non-equivalent peaks; br: broad.

Grazing angle Fourier transform infrared (FT-IR) spectra for the coatings were obtained on a Thermo Scientific Nicolet 6700 spectrometer with a Harrick germanium attenuated total reflection (ATR) attachment and N₂-cooled MCT/A. Clean silica wafers were used to collect the background spectra. Coating thicknesses of ~1 μm (5 wt/v % polymer/TFE casting solution) were used to improve signal intensity.

Optical microscopy images were taken on an Olympus BX51 microscope (Optical Analysis Corp. Nashua, NH).

Water contact angles were measured using a Rame-Hart telescopic goniometer and a Gilmont syringe with a 24-gauge flat-tipped needle filled with Milli-Q water. Reported values are the average of at least 6 measurements on three unique surfaces.

Polymer thickness measurements were made on a LSE model Gaertner Scientific Stokes Ellipsometer, with an angle of incidence of 70° from the normal and a 6328 Å HeNe laser, assuming a thin film model. A refractive index of 1.5 was assumed for the polymer layer. Reported values are the average of five measurements on three unique surfaces.

Atomic force microscopy (AFM) images were obtained in tapping mode on a Veeco Dimension 3100 instrument with a Nanoscope III controller with the manufacturer's software. Silicon cantilevers with a spring constant of 0.58 N/m were used. Root mean squared (rms) roughness values were calculated by the manufacturer's software on a 1 μm x 1 μm image.

4.7.3 Synthesis and characterization

Monomer **Sulfo(ZI)b** was synthesized as described in Chapter 2. Yields and spectroscopic data matched those previously reported.¹

Representative polymerization procedure: Monomer **Sulfo(ZI)b** (0.3 g, 0.8 mmol, 30 equivalents) and 5-(bicycloheptenyl)-triethoxysilane **3** (42 μ L, 0.16 mmol, 6 equivalents) were weighed into a clean, dry Schlenk flask under N₂, while G3 (0.024 g, 0.028 mmol, 1 equivalent) was weighed into a second Schlenk flask under N₂. The monomers were then dissolved in 3 mL 2,2,2-trifluoroethanol plus 1 mL dry CH₂Cl₂ and the catalyst was dissolved in 2 mL dry CH₂Cl₂. Both solutions were subjected to three freeze-pump-thaw cycles and warmed to room temperature. Using a nitrogen-purged syringe, the monomer solution was added to the catalyst solution. The polymerization was allowed to proceed for 30 minutes at room temperature under N₂. To quench the reaction, 1.5 mL ethyl vinyl ether was added and the solution was stirred for an additional hour. The polymer was then precipitated out into anhydrous diethyl ether, isolated by vacuum filtration and dried under high vacuum overnight. In the case of the block copolymers, the polymer solid was isolated by centrifugation after precipitation. Yields were greater than 90% for all polymers. The polymer was stored at -20 °C while not in use.

rP[Sulfo(ZI)b]: ¹H NMR (300MHz, D₂O + NaBr): δ (ppm) = 1.15 (br, 9H), 1.74 (br, 2H), 1.89 (br, 2H), 2.90 (br, 2H), 3.12 (br, 6H), 3.40 (br, 2H), 3.49 (br, 2H), 3.61 (br, 2H), 3.91 (q, $J = 9.1$ Hz, 6H), 4.65 (br, 1H), 5.03 (br, 1H), 5.90 (br, *cis*, 1H), 6.09 (br, *trans*, 1H).

4.7.4 Coating preparation

Casting solutions were prepared as 1 wt/v % polymer solutions (0.01g/1mL) in 2,2,2-trifluoroethanol and filtered through 0.45 μ m PTFE filters. Silicon wafers were cut

into 1.5 x 1.5 cm substrates, cleaned with piranha solution for 30 minutes, rinsed with RO water and dried under N₂ immediately before use. The polymer solutions were spin-cast onto the silicon substrates at 3000 rpm for 30 seconds. After drying under vacuum overnight, the samples were placed in a sealed desiccator containing concentrated HCl for 1 hour, then heated at 110 °C for 3 hours to complete the curing process. Any remaining free polymer was extracted from the coating by soaking the samples in PBS for several hours; the samples were rinsed with RO water to remove any buffer salts and dried under N₂ then overnight under high vacuum. The initial thicknesses of the coatings were measured by ellipsometry. AFM and contact angle measurements were taken on freshly prepared surfaces.

4.7.5 Protein adsorption measurements

Fibrinogen solutions (0.5 mg/mL) in PBS buffer were prepared directly before use at room temperature. The samples were placed in individual wells of a 12-well cell culture plate and soaked in PBS buffer for two hours to fully hydrate the surfaces. The coatings were transferred to a clean plate and approximately 3 mL of protein solution were added to each well. The plate was then incubated for two hours at 37 °C. Excess PBS was used to flood the wells to sufficiently dilute the protein, after which the samples were removed from the wells and rinsed further with RO water. The coatings were first dried under a stream of N₂ then overnight under high vacuum. To quantify protein adsorption, the thickness of the adsorbed protein layer was measured by ellipsometry using the published refractive index value of 1.405 for fibrinogen.^{1,9-11} By applying the following equation:

$$\Gamma(\text{ng}/\text{mm}^2) = h \times d$$

where h equals the measured thickness of the protein layer, and d equals fibrinogen density given in the literature^{1,9-11} as 1.085 g/cm³, the amount of adsorbed protein (I) was calculated.

4.7.6 PDMS functionalization

Sylgard 184 was purchased and cured according to the manufacturer's instructions. Samples approximately 1 cm x 1 cm x 1.5 μ m is size were cut out and pressed onto glass slide coverslips for easy handling. The samples were placed in a glass dish and exposed to oxygen plasma for the given amount of time. Immediately after, the polymer solution was spin-cast onto the surface at 3000 rpm for 30 seconds. After drying under vacuum overnight, the samples were placed in a sealed desiccator containing concentrated HCl for 1 hour, then heated at 110 °C for 3 hours to complete the curing process. Any remaining free polymer was extracted from the coating by soaking the samples in PBS for several hours; the samples were rinsed with RO water to remove any buffer salts and dried under N₂ then overnight under high vacuum.

4.8 Conclusions

A series of model random and block copolymers were synthesized which incorporated the sulfobetaine **Sulfo(ZI)b** and the commercially available 5-(bicycloheptenyl)-triethoxysilane monomers. These polymers were designed for surface functionalization, where the triethoxysilane groups from the 5-(bicycloheptenyl)-triethoxysilane repeat unit could hydrolyze to form covalently anchored coatings. Both the amount of siloxane and its position within the polymers were varied to find the optimal polymer composition for nonfouling coatings. The random and block copolymer series exhibited unique solution and surface properties. It was found, in general, that

random copolymers formed the most homogeneous, robust coatings. Despite the literature precedence for highly efficient coatings from block copolymers, the **bP[Sulfo(ZI)b]** series was found to be prone to surface defects and high levels of protein adsorption. The best polymer for screening nonfouling surfaces was determined to be **rP[Sulfo(ZI)b]_{30,6}**, or a random copolymer with approximately 16 mol % siloxane repeat units, based on durability and fibrinogen adsorption. While it was found that this polymer chemistry was broadly applicable for coating surfaces other than silica or glass, non-glassy substrates required further optimization and thus were not pursued further.

4.9 References

- (1) Colak, S.; Tew, G. N. Dual-Functional ROMP-Based Betaines: Effect of Hydrophilicity and Backbone Structure on Nonfouling Properties. *Langmuir* **2012**, *28*, 666-675.
- (2) Colak, S.; Tew, G. N. Amphiphilic Polybetaines: The Effect of Side-Chain Hydrophobicity on Protein Adsorption. *Biomacromolecules* **2012**, *13*, 1233-1239.
- (3) Chen, S.; Li, L.; Zhao, C.; Zheng, J. Surface hydration: Principles and applications toward low-fouling/nonfouling biomaterials. *Polymer* **2012**, *51*, 5283-5293.
- (4) Chen, S.; Jiang, S. A New Avenue to Nonfouling Materials. *Adv. Mater.* **2008**, *20*, 335-338.
- (5) Chang, Y.; Liao, S.; Higuchi, A.; Ruaan, R.; Chu, C.; Chen, W. A Highly Stable Nonbiofouling Surface with Well-Packed Grafted Zwitterionic Polysulfobetaine for Plasma Protein Repulsion. *Langmuir* **2008**, *24*, 5453-5458.
- (6) Callow, J. A.; Callow, M. E. Trends in the development of environmentally friendly fouling-resistant marine coatings. *Nat. Commun.* **2011**, DOI: 10.1038/ncomms1251.
- (7) Weck, M.; Jackiw, J. J.; Rossi, R. R.; Weiss, P. S.; Grubbs, R. H. Ring-Opening Metathesis Polymerization from Surfaces. *J. Am. Chem. Soc.* **1999**, *121*, 4088-4089.
- (8) Balastre, M.; Li, F.; Schorr, P.; Yang, J.; Mays, J. W.; Tirrell, M. V. A Study of Polyelectrolyte Brushes Formed from the Adsorption of Amphiphilic Diblock Copolymers Using Surface Forces Apparatus. *Macromolecules* **2002**, *35*, 9480-9486.

- (9) Elwing, H. Protein absorption and ellipsometry in biomaterial research. *Biomaterials* **1998**, *19*, 397-406.
- (10) Voros, J. The Density and Refractive Index of Adsorbing Protein Layers. *Biophys. J.* **2004**, *87*, 553-561.
- (11) Sharma, S.; Johnson, R. W.; Desai, T. A. Evaluation of the Stability of Nonfouling Ultrathin Poly(ethylene glycol) Films for Silicon-Based Microdevices. *Langmuir* **2004**, *20*, 348-356.
- (12) Huang, C-J.; Li, Y.; Krause, J. B.; Brault, N. D.; Jiang, S. Internal Architecture of Zwitterionic Polymer Brushes Regulates Nonfouling Properties. *Macromol. Rapid Commun.* **2012**, *33*, 1003-1007.
- (13) Gunkel, G.; Weinhart, M.; Becherer, T.; Haag, R.; Huck, W. T. S. Effect of Polymer Brush Architecture on Antibiofouling Properties. *Biomacromolecules* **2011**, *12*, 4169-4172.
- (14) Wang, Y.; Finlay, J. A.; Betts, D. E.; Merkel, T. J.; Luft, J. C.; Callow, M. E.; Callow, J. A.; DeSimone, J. M. Amphiphilic Co-networks with Moisture-Induced Surface Segregation for High-Performance Nonfouling Coatings. *Langmuir* **2011**, *27*, 10365-10369.
- (15) Mussard, W.; Kebir, N.; Kriegel, I.; Esteve, M.; Semetey. Facile and Efficient Control of Bioadhesion on Poly(dimethylsiloxane) by Using a Biomimetic Approach. *Angew. Chem. Int. Ed.* **2011**, *50*, 10871-10874.
- (16) Keefe, A. J.; Brault, N. D.; Jiang, S. Suppressing Surface Reconstruction of Superhydrophobic PDMS Using a Superhydrophilic Zwitterionic Polymer. *Biomacromolecules* **2012**, *13*, 1683-1687.
- (17) Love, J. A.; Morgan, J. P.; Trnka, T. M.; Grubbs, R. H. A Practical and Highly Active Ruthenium-Based Catalyst that Effects the Cross Metathesis of Acrylonitrile. *Angew. Chem. Int. Ed.* **2002**, *41*, 4035-4037.

CHAPTER 5

NONFOULING PROPERTIES OF HYDROPHILIC BETAINES: EFFECT OF INTERCHARGE DISTANCE

5.1 Introduction

Chapter 5 describes the nonfouling properties of the **C₁(ZI)**, **Carboxy(ZI)**, and **Sulfo(ZI)** series. In addition to quantifying these polymers' behavior as nonfouling materials, these hydrophilic betaines could be used to study the effect of intercharge distance on their nonfouling properties. Monomer and polymer syntheses were previously outlined in Chapters 3 and 4. The intercharge distance was varied by systematically altering the length of the alkyl chain between the cationic and anionic moieties in the linear carboxybetaine and sulfobetaine series, and between the oxanorbornene backbone and the cationic moiety in the dual-functional series. A comparison between the carboxybetaine and dual-functional series allowed us to study the effect of charge position within each repeat unit. While similar studies had been performed on polymer brush surfaces, this was the first in-depth study for oxanorbornene-based polymers.

5.2 General Approach

It was shown above in Chapter 3 that we could synthesize an extremely diverse set of polyzwitterions based on oxanorbornene monomers. The dual-functional zwitterions, comprising the **C₁(ZI)** and **Amph(ZI)** series, especially represented novel structures. Due to the novelty of our oxanorbornene-based platform, it lacked the breadth

of available research for the (meth)acrylate/acrylamide systems. For instance, Jiang and coworkers studied the effect of the spacer group length between the charged groups for carboxybetaine acrylamide surface-grafted brushes,¹ where the alkyl chain was varied from methyl to pentyl. Relative fibrinogen adsorption, as measured by surface plasmon resonance (SPR) spectroscopy, was similar for the 1-, 2-, and 3-carbon spacer surfaces, but increased noticeably on the 5-carbon spacer surface. It was also found that fibrinogen adsorption was dependent on the pH of the environment, as well as the solution's ionic strength, because of the pH-sensitive nature of the carboxylate group.

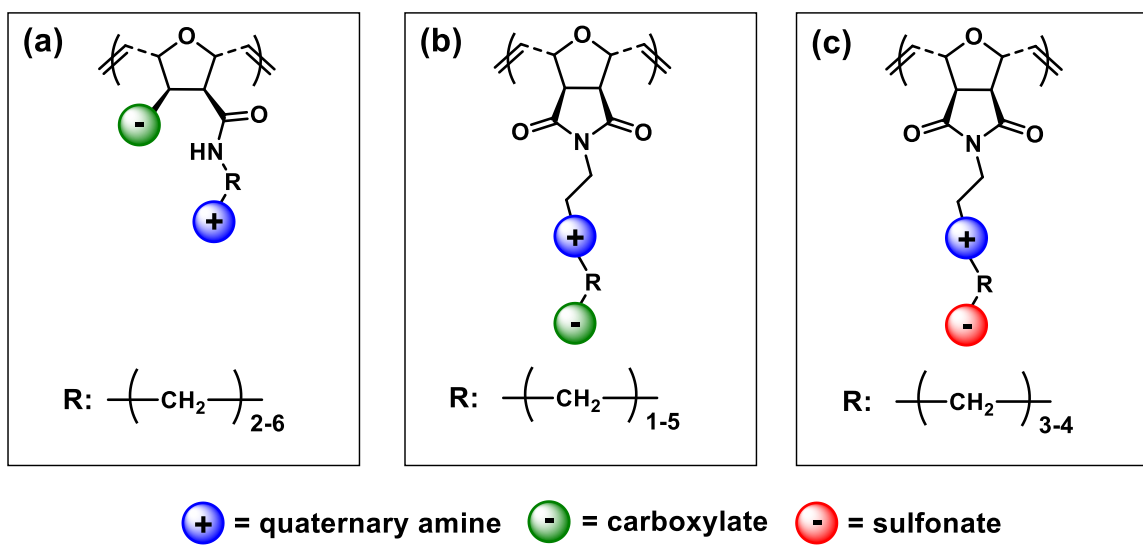


Figure 5.1: Polymers used to study the effect of charge distribution on oxanorbornene-based (a) dual-functional betaines, (b) carboxybetaines, and (c) sulfobetaines.

The modular nature of our chemistry platform was well-suited to structure-property relationship studies. Due to their similar zwitterionic chemistries and analogous structures in the literature, the hydrophilic linear (**Carboxy(ZI)** and **Sulfo(ZI)**) and dual-functional (**C₁(ZI)**) betaines were compared here as shown in Figure 5.1. (The **Amph(ZI)** series is discussed later in Chapter 6.) Specifically, the effect of interchange

distance on different betaines could be studied by comparing the **C₁(ZI)**, **Carboxy(ZI)**, and **Sulfo(ZI)** series in the same manner as the carboxybetaine acrylamide brushes discussed above. The length of the alkyl spacer between the imide backbone and the quaternary amine was varied from 2 to 6 carbons for the dual-functional methyl surface (Figure 5.1a). The spacers between the cationic and anion groups for the **Carboxy(ZI)** and **Sulfo(ZI)** series were varied between 1 to 5, and 3 to 4 carbons, respectively (Figure 5.1b and c). In addition to synthetic viability, the spacer lengths of the dual-functional and carboxybetaines were chosen to correlate with one another as closely as possible.

5.3 Coating Preparation and Characterization

5.3.1 Polymer Synthesis

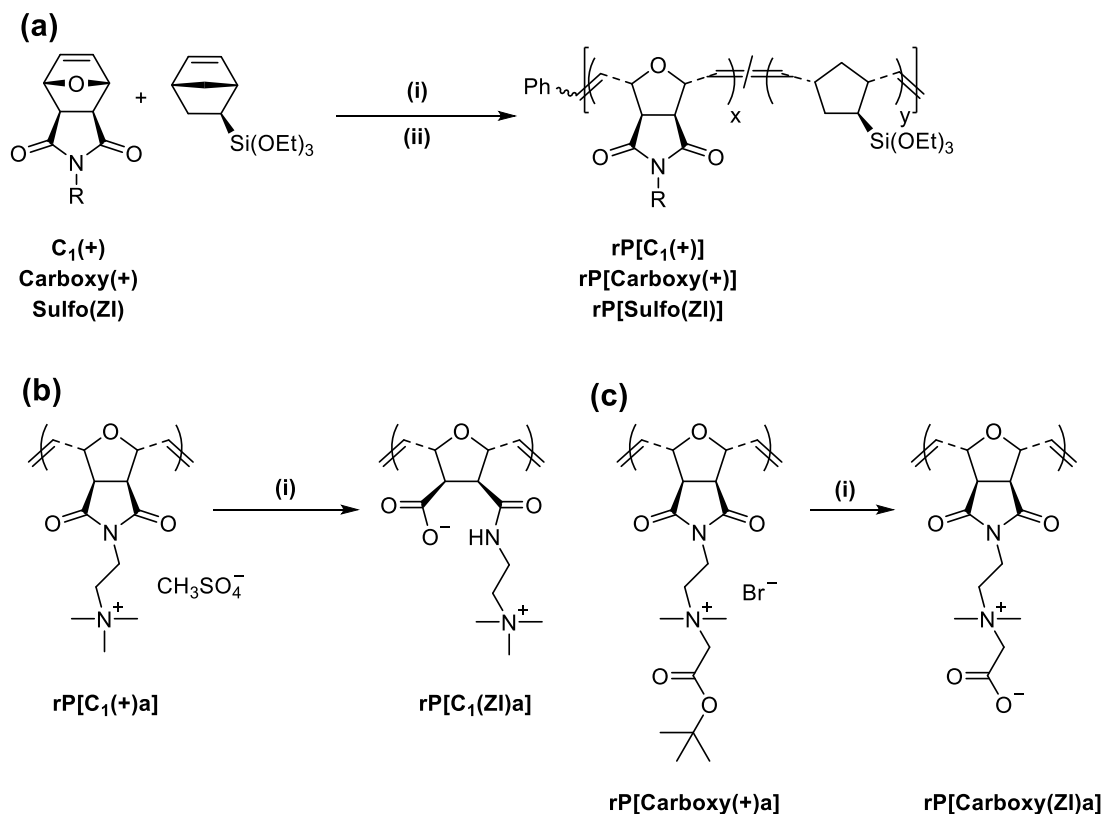


Figure 5.2: Polymerization of the **C₁(ZI)**, **Carboxy(ZI)**, and **Sulfo(ZI)** series and representative post-polymerization functionalization reactions: **(a)** (i) Grubbs' 3rd generation catalyst, TFE/CH₂Cl₂, room temperature, 30 minutes; (ii) excess ethyl vinyl ether, room temperature, 1 hour; **(b)** (i) 0.1 M NaOH, 20 minutes; **(c)** (i) HCl (g), overnight.

As discussed in Chapter 4, the charged monomers were randomly copolymerized with 5-(bicycloheptenyl)-triethoxysilane so that $x = 30$ and $y = 6$ to create polymers for functionalizing silica substrates (Figure 5.2a). These polymers are denoted here with the prefix **rP** to denote the random copolymerization with the siloxane monomer. The polymerizations were carried out in a mixture of TFE and CH₂Cl₂ to fully solubilize all components. Quantitative conversion for all polymers was achieved in 15-25 minutes. Because of the hydrolytic instability of the siloxane groups, as well as the highly charged content of the polymers, GPC was not a viable characterization technique, therefore ¹H NMR was used exclusively to characterize these precursor polymers. Table 5.1 summarizes the polymers' calculated compositions, where the molecular weights (M_n) ranged from 12 – 16.5 kDa and siloxane contents ranged from 16-23 mol %.

Table 5.1: Composition and molecular weight characterization of hydrophilic polymers by NMR spectroscopy

Polymer	x ^a	y ^b	M _n (kDa) ^c	mol % Si
rP[C₁(+)a]	30	8.2	13.0	21.5
rP[C₁(+)b]	30	8.9	13.6	22.9
rP[C₁(+)c]	30	5.7	13.2	16.0
rP[C₁(+)d]	30	7.1	14.0	19.1
rP[C₁(+)e]	30	8.7	14.8	22.5
rP[Carboxy(+)a]	30	5.8	14.4	16.2
rP[Carboxy(+)b]	30	8.1	12.4	21.3
rP[Carboxy(+)c]	30	8.2	15.9	21.5
rP[Carboxy(+)d]	30	9.1	16.5	23.3
rP[Carboxy(+)e]	30	7.2	16.5	19.4
rP[Sulfo(ZI)a]	30	6.2	12.3	17.1
rP[Sulfo(ZI)b]	30	6.8	12.9	18.5

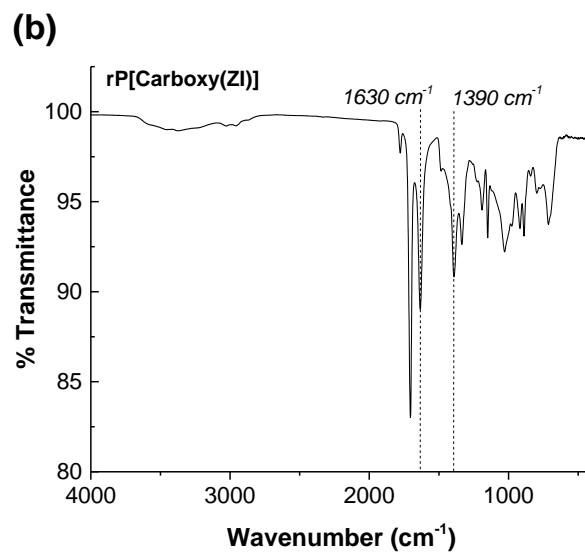
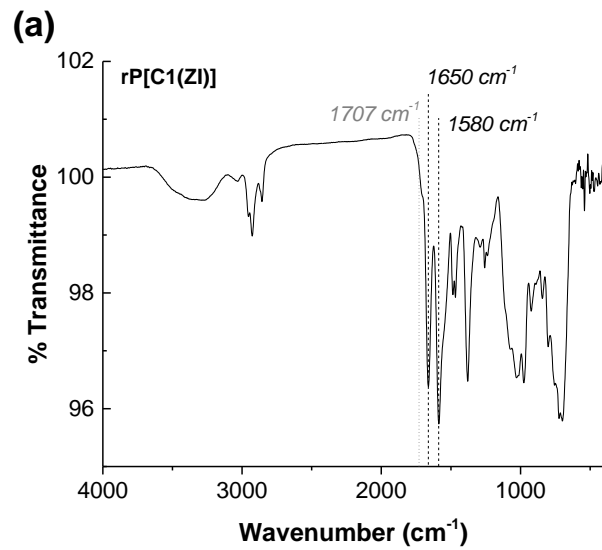
^a number of charged repeat units assumed to be 30 due to the low resolution of the phenyl endgroup; ^b number of siloxane repeat units as calculated by ¹H NMR spectroscopy from the ratio of the peaks corresponding to -N(CH₃)₂ and -Si(OCH₂-CH₃); ^c calculated from the x and y values given in the table and the monomers' known molecular weights.

5.3.2 Surface Characterization

Coatings were prepared as described in Chapter 4.^{2,3} The dual-functional and carboxybetaine surfaces were converted post-polymerization to the fully zwitterionic forms by either base or acid treatment (Figure 5.2b-c). After soaking the **rP[C₁(+)a-e]** surfaces in a 0.1 M NaOH solution for 20 minutes, the imide group ring-opened to form an anionic carboxylate group and an amide containing the cationic side chain. FT-IR spectra before and after base treatment showed that the strong imide peak at 1707 cm⁻¹ weakened and additional peaks appeared at 1650 and 1580 cm⁻¹ corresponding to the newly formed carboxylate and amide groups (Figure 5.3a). It should be noted that the IR

spectrum of the final surface still shows residual imide groups, implying that some cationic repeat units remain in the coating. This result is in contrast to that obtained from ring-opening the imide in solution, where the reaction is fast (on the order of minutes or less) and quantitative. Because the siloxane crosslinks are themselves base-sensitive, increasing the exposure time and the base concentration caused the coating to delaminate. We assumed, however, that the majority of the cationic repeat units were sequestered in the interior of the network due to the limited diffusion of the aqueous solution, and that their presence would not have a significant impact on the coatings' presumed zwitterionic nature.

FT-IR spectroscopy was also used to confirm the cleavage of the *tert*-butyl groups on the carboxylate polymers after acid treatment. In this case, the ester peak at 1720 cm^{-1} disappeared and gave rise to acid peaks at 1630 and 1390 cm^{-1} (Figure 5.3b). The sulfobetaine moiety required no further modification. Imide carbonyl (1707 cm^{-1}) and sulfonate (1395 and 1187 cm^{-1}) stretching frequencies in the IR spectra (Figure 5.3c) for the **rP[Sulfo(ZI)a-b]** surfaces were in agreement with the assumed zwitterionic surface chemistry.



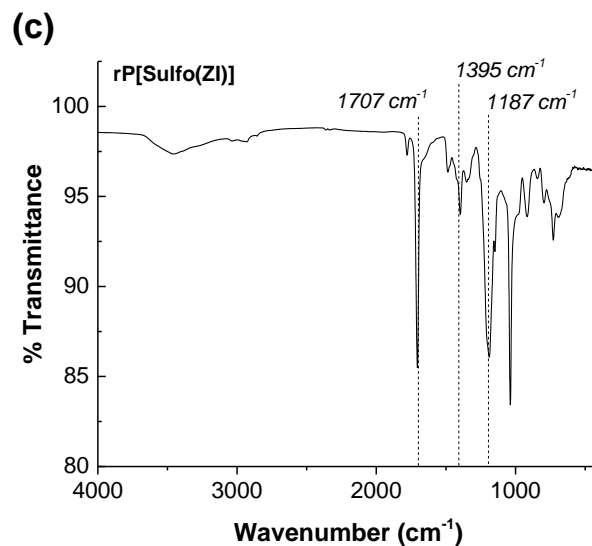


Figure 5.3: Representative FT-IR spectra of the cured and post-functionalized (a) **rP[C₁(ZI)**], (b) **rP[Carboxy(ZI)]** and (c) **rP[Sulfo(ZI)]** surfaces. Characteristic peaks corresponding to imide (1707 cm⁻¹), amide (1580 cm⁻¹), carboxylic acid (1650/1630 and 1390 cm⁻¹) and sulfonate (1395 and 1187 cm⁻¹) functional groups are marked with the dotted lines.

In addition to FT-IR, all coatings were characterized by several other surface-sensitive techniques in order to ascertain the influence of the coating chemistry on surface properties, and to correlate physical surface properties to the coatings' nonfouling performance. AFM showed that all surfaces exhibited similar topography. Roughnesses ranged from approximately 0.3 – 0.5 nm (Table 5.2) and no significant surface features or defects were visible. The lack of unique discernable surface characteristics within the polymer series was not wholly surprising as all the polymers were structurally and chemically similar. Likewise, the tightly cross-linked coatings would not be expected to undergo or allow for extensive rearrangement that would manifest itself in AFM images. One exception, however, was the sulfobetaine series. While the height images for both **rP[Sulfo(ZI)a]** and **rP[Ssulfo(ZI)b]** surfaces appeared nearly identical, the phase images were differentiated by the degree of phase separation. The **rP[Sulfo(ZI)a]** surface

appeared homogenous across a given sample, whereas weak phase separation was noticeable for the **rP[*S*sulfo(*ZI*)*b*]** surface (Figure 5.4).

Table 5.2: Surface properties of hydrophilic zwitterionic coatings

Polymer	Intercharge distance (Å) ^a	Roughness (nm) ^b	Water contact angle (°) ^c			Γ _{Fibrinogen} (ng/mm ²) ^e
			θ _{Advancing}	θ _{Receding}	θ _{Static}	
rP[C₁(+)a]	N/A	0.5	47 ± 2	12 ± 2	48 ± 2	0.53 ± 0.07
rP[C₁(+)b]	N/A	0.2	41 ± 3	16 ± 2	42 ± 3	0.50 ± 0.11
rP[C₁(+)c]	N/A	0.2	40 ± 2	≤ 10 ^d	38 ± 4	0.79 ± 0.32
rP[C₁(+)d]	N/A	0.2	70 ± 2	17 ± 1	65 ± 2	0.64 ± 0.37
rP[C₁(+)e]	N/A	0.2	68 ± 2	≤ 10	65 ± 2	1.30 ± 0.41
rP[Carboxy(+)a]	2.67	0.3	54 ± 3	11 ± 2	54 ± 3	0.34 ± 0.13
rP[Carboxy(+)b]	3.75	0.4	64 ± 2	≤ 10	64 ± 2	2.31 ± 0.22
rP[Carboxy(+)c]	4.96	0.4	49 ± 4	26 ± 2	50 ± 4	0.84 ± 0.26
rP[Carboxy(+)d]	6.43	0.5	41 ± 3	≤ 10	39 ± 2	0.46 ± 0.19
rP[Carboxy(+)e]	7.64	0.2	45 ± 2	≤ 10	43 ± 3	0.23 ± 0.16
rP[Sulfo(<i>ZI</i>)a]	5.29	0.3	56 ± 3	≤ 10	50 ± 4	0.59 ± 0.2
rP[Sulfo(<i>ZI</i>)b]	6.62	0.3	61 ± 2	≤ 10	54 ± 7	1.03 ± 0.08

^a values calculated by Spartan 2004 software; ^b root mean squared (rms) roughness calculated by the manufacturer's software based on a 1 μm x 1 μm image area; ^c water contact angles measured by the sessile drop technique; ^d angles approximately equal to 10° were too small to measure accurately; ^e fibrinogen adsorption measured by ellipsometry.

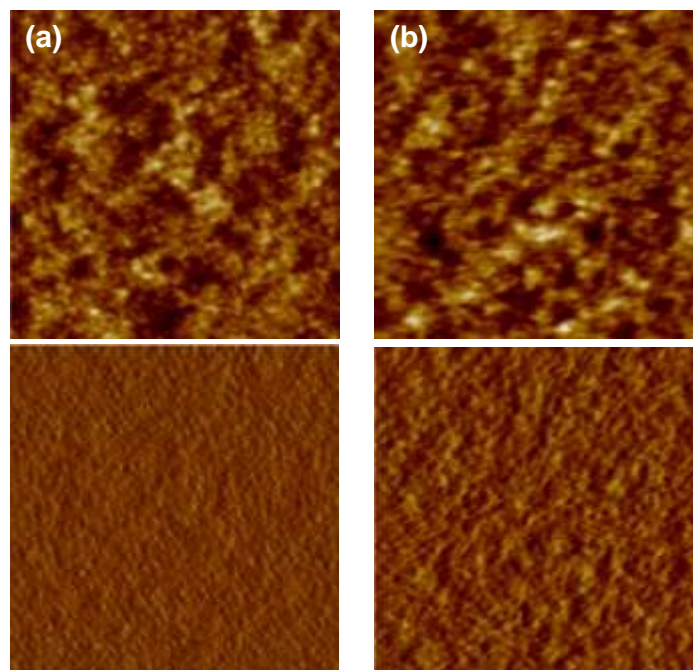


Figure 5.4: Representative tapping mode AFM height (top) and phase (bottom) images of (a) **rP[Sulfo(ZI)a]** and (b) **rP[Sulfo(ZI)b]** surfaces. Images represent a 1 μm x 1 μm area, where the z axis is 5 nm for the height images.

We had expected that the zwitterions (both linear and dual-functional) with longer alkyl spacers would be more hydrophobic than those with shorter alkyl spacers, due to both the increased distance between the charges and the added hydrophobicity from increasing the carbon content. Intercharge distances were calculated for the linear betaines to quantify the effect of increasing the alkyl spacer length (Table 5.2). For the **rP[Carboxy(ZI)]** and **rP[Sulfo(ZI)]** series, the intercharge distances increased linearly from 2.67 to 7.64 \AA and 5.29 to 6.62 \AA , respectively. To determine the relative wettabilities of each of the surfaces, water contact angle measurements were used. Although contact angles can be influenced by other surface properties such as roughness, rearrangement and defects,^{4,5} the lack of physical features in the AFM images implied that water contact angle would be an adequate method to compare nominal hydrophilicities.

Within the dual-functional series, the **rP[C₁(ZI)a-c]** surfaces all had similar advancing water contact angles, $41^\circ \leq \theta_A \leq 47^\circ$ (Table 5.2), implying that the surfaces were similarly hydrophilic. The advancing water contact angle increased, however, for both **rP[C₁(ZI)d]** and **rP[C₁(ZI)e]** to approximately 70° , which may be accounted for by the increased hydrophobic alkyl content. For the carboxybetaine series, the **rP[Carboxy(ZI)b]** surface had the largest measured advancing water contact angle (64°). The **rP[Carboxy(ZI)a]** and **rP[Carboxy(ZI)c]** surfaces had advancing water contact angles near 50° , while those for **rP[Carboxy(ZI)d]** and **rP[Carboxy(ZI)e]** were 41° and 45° , respectively. Despite the expectation that the contact angle would correlate with the interchange distance, the greatest advancing water contact angle for the carboxybetaine series was observed for the surface functionalized with **rP[Carboxy(ZI)b]**, containing the intermediate ethylene spacer. Advancing water contact angles for **rP[Sulfo(ZI)a]** and **rP[Sulfo(ZI)b]** were measured to be 56° and 61° , respectively, indicating that the surfaces' wettabilities were comparable. In general, all surfaces exhibited advancing water contact angles between 40° and 70° . Likewise, static contact angles for all surfaces were comparable to the advancing contact angles, while the degrees of hysteresis (the difference between advancing and receding contact angles) were similar for all surface chemistries (Table 5.2).

While the water contact angles implied that all of the surfaces were intermediately hydrophilic, similar charged polymer coatings were reported to exhibit superhydrophilicity.⁶ In our case, the hydrophobic backbone and comparatively large intramolecular spacing between the zwitterionic side chains, in addition to the presence of the siloxane-containing repeat unit, likely contributed to these surfaces' wettabilities.

Additionally, there was no clear trend between the measured contact angle and the theoretical interchange distances. It is possible that the structures here do not cover a wide enough range of charge distributions, thus the surfaces' wettabilities all fall in the same range and no trend can be discerned. It may also be possible that the charged moieties behave differently than expected because of intra- or intermolecular interactions based on spacer length, and so their behavior is more complex than can be deconvoluted from their contact angles.

5.4 Protein Adsorption

We expected that, in general, the zwitterionic surfaces with longer theoretical interchange distances or larger alkyl contents would exhibit larger amounts of protein adsorption due to the greater hydrophobic component. Carboxylates and carboxybetaines are pH-sensitive, however, so the **rP[C₁(ZI)]** and **rP[Carboxy(ZI)]** series may be affected by additional factors. Previous calculations on carboxybetaine surfactants showed that increasing the distance between the quaternary amine and the carboxylic acid increases the *pK_a* of the acid.⁷ This effect was also seen in polycarboxybetaines, although the formation of intramolecular ion pairs within the repeat units was found to influence the polymers' solution properties and electrostatic interactions as well.^{8,9} If the zwitterionic moieties in these bulk coatings behave the same way, extending the alkyl spacer length increases the *pK_a* of the **rP[Carboxy(ZI)]** carboxylate groups. Fibrinogen adsorption would then increase due to the reduction in zwitterionic character.^{1,10} Our dual-functional series decoupled the positive and negative charges by placing them on individual side chains, so that extending the quaternary amine side chain should not appreciably impact the electronic properties of the pH-sensitive carboxylic acid. Thus, it

was not necessarily clear that the linear and dual-functional series should behave similarly, even though they contain the same functional groups.

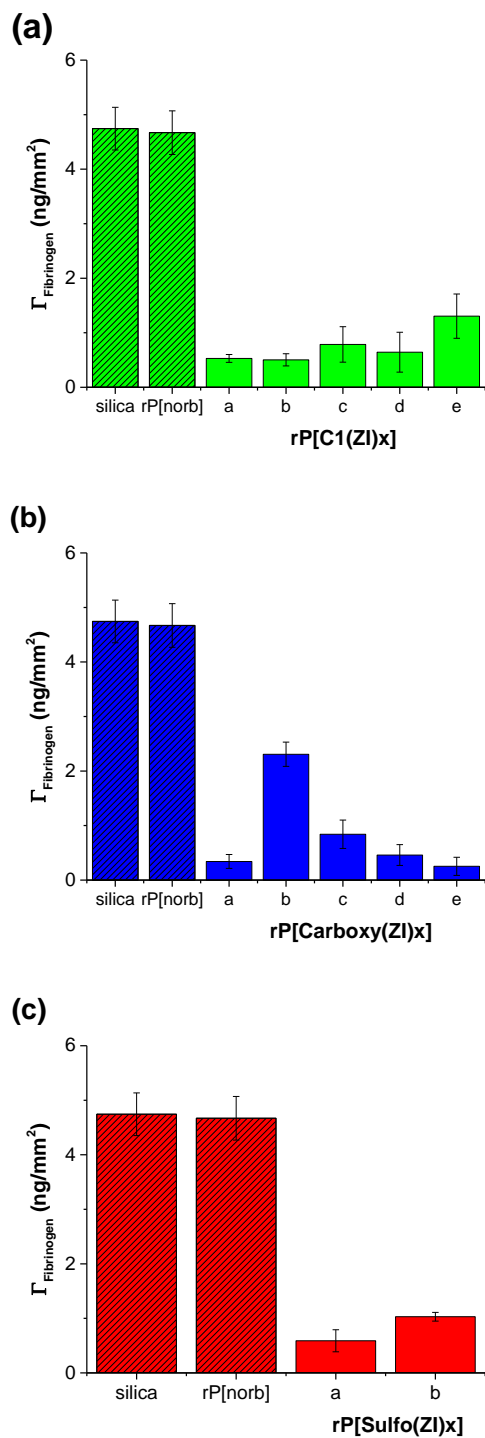


Figure 5.5: Fibrinogen adsorption as measured by ellipsometry for the (a) rP[C₁(ZI)] series; (b) rP[Carboxy(ZI)] series; and (c) rP[Sulfo(ZI)] series. Controls are indicated

by the shaded bars. Error bars represent \pm standard deviation, based on at least 3 independent measurements.

Fibrinogen adsorption data is given in Figure 5.5 for all surfaces. Silica and an uncharged oxanorbornene polymer (structure given in **5.6 Experimental** procedures section) were used as controls. In the case of the dual-functional series, all surfaces appeared to behave similarly, where $\Gamma_{\text{Fibrinogen}}$ ranged from 0.5 – 1.3 ng/mm² (Figure 5.5a). Surfaces coated in **rP[C₁(ZI)a-d]** performed almost identically, where $\Gamma_{\text{Fibrinogen}} \approx 0.5$ ng/mm². Any differences between **rP[C₁(ZI)a-e]**, however, were subtle when taking into account error. As shown in Figure 5.5b, the protein adsorption trend for the carboxybetaine series was somewhat more complex. The **rP[Carboxy(ZI)a]** surface was expected to have the least amount of adsorbed fibrinogen, while the **rP[Carboxy(ZI)e]** surface was expected to have the most, with a positive correlation between increasing spacer length and increasing protein adsorption. Instead, with the exception of **rP[Carboxy(ZI)b]**, all surfaces performed similarly, with $\Gamma_{\text{Fibrinogen}} \approx 0.2 - 0.8$ ng/mm². The greatest amount of adsorbed fibrinogen (2.3 ng/mm²) was seen on the **rP[Carboxy(ZI)b]** surface, which also had the highest water contact angle among the carboxybetaine series. For the **rP[Sulfo(ZI)a]** surface, $\Gamma_{\text{Fibrinogen}} = 0.56$ ng/mm², whereas $\Gamma_{\text{Fibrinogen}} = 1.03$ ng/mm² for the **rP[Sulfo(ZI)b]** surface (Figure 5.5c). The shorter interchange distance on the **rP[Sulfo(ZI)a]** surface appeared to correlate with the lower amount of fibrinogen adsorption compared to the **rP[Sulfo(ZI)b]** sample. With so few samples, however, it is difficult to determine if a robust trend exists within the sulfobetaine series. Overall, the dual-functional, carboxybetaine, and sulfobetaine surfaces all showed decreased amounts of fibrinogen adsorption when compared to the silica control surface. These results demonstrated both the importance of a charge-

neutral surface in preventing protein adsorption as well as the efficacy of our zwitterionic ROMP system.

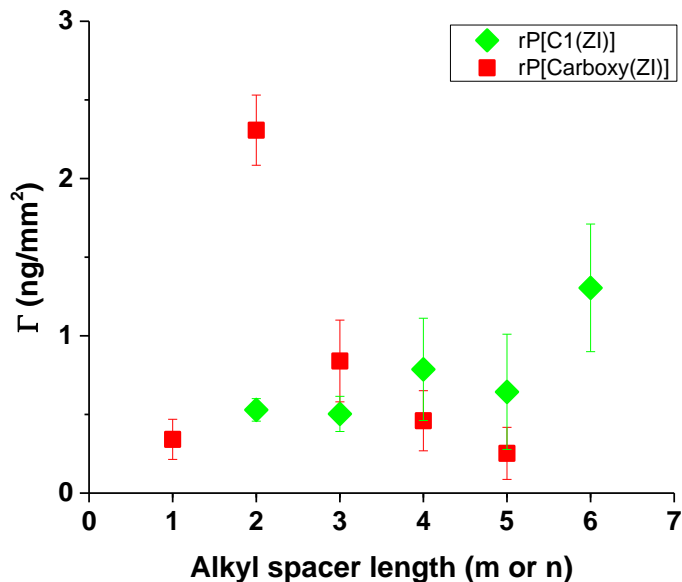


Figure 5.6: Fibrinogen adsorption vs. alkyl spacer length (**m** or **n**) for **rP[C1(ZI)]** (green diamonds) and **rP[Carboxy(ZI)]** (red squares) surfaces.

Despite the differences in the nature of the zwitterionic functionality found in the **rP[C1(ZI)]** and **rP[Carboxy(ZI)]** series, their fouling behavior was generally similar. Figure 5.6 shows fibrinogen adsorption versus the length of the alkyl chain attached to the cationic group (**m** and **n**), where the similarities between the fouling behaviors of the **rP[C1(ZI)]** and **rP[Carboxy(ZI)]** series are more apparent. As **n** increased from 2 to 5 carbons, fibrinogen adsorption (approximately 0.5 ng/mm²) remained essentially constant for the **rP[C1(ZI)]** series. Fouling approximately doubled to 1.3 ng/mm² when **m** = 6; however, within error, there was a gradual increase in fouling across the entire series. On the other hand, within the **rP[Carboxy(ZI)]** series, maximum fouling occurred on the **rP[C1(ZI)b]** surface (2.3 ng/mm²). Adsorption on surfaces where **m** ≠ 2 was again comparable both within the series and to the **rP[C1(ZI)]** series. Therefore, it appeared

that the amount of adsorbed fibrinogen on the **rP[Carboxy(ZI)b]** surface was anomalously high, as was the surface's water contact angle. We hypothesize that this behavior was observed with the ethylene spacer because it allowed for the most stable cyclized conformation of the pendant chain to create an ion pair.^{8,9} As previously noted, a cyclic ion pair increased the hydrophobicity of a polycarboxybetaine in solution, which correlates to the high water contact angle on the **rP[Carboxy(ZI)b]** surface.¹¹ More in-depth surface characterization, however, is necessary to better understand this phenomenon. The comparison between the linear and dual-functional betaines implies that the placement of the charged moieties within the polymer has a subtle effect on the nonfouling properties of the resulting surface.

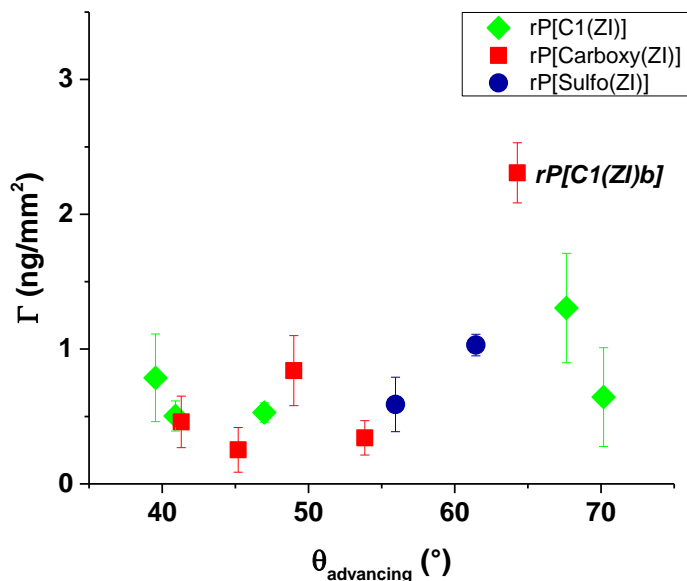


Figure 5.7: Fibrinogen adsorption vs. advancing water contact angle for **rP[C1(ZI)]** (green diamonds), **rP[Carboxy(ZI)]** (red squares), and **rP[Sulfo(ZI)]** (blue circles) surfaces.

Hydrophilic surfaces are thought to diminish irreversible protein adhesion by supporting a stable water layer, which shields the underlying surface from hydrophobic

and electrostatic interactions.¹²⁻¹⁸ It would be expected, then, that more hydrophilic surfaces would adsorb less protein than more hydrophobic surfaces when the surface chemistry is similar. To determine if this trend held true for our oxanorbornene-based platform, protein adsorption was plotted as a function of advancing water contact angle for the **rP[C1(ZI)]**, **rP[Carboxy(ZI)]**, and **rP[Sulfo(ZI)]** series (Figure 5.7). Most values tended to cluster around low contact angles ($40^\circ - 55^\circ$) and $\Gamma_{\text{Fibrinogen}} < 1 \text{ ng/mm}^2$, where the **rP[Carboxy(ZI)]** surface was again observed to be anomalous with higher fouling than the contact angle would suggest. Within error, the majority of the surfaces exhibited comparable fouling regardless of wettability. Interestingly, the nature of the charged groups did not appear to influence the trend either, as most surfaces from all three series were similar.

It has been shown for surface-initiated carboxybetaine brushes that increasing the atomic distance between the quaternary amine and carboxylate group resulted in higher levels of fibrinogen fouling.¹ This effect was exacerbated at low pH levels, due to the increased cationic nature of the surface and subsequent electrostatic interactions between the polymer chains and the protein. Previous work with the dual functional series also implied that increasing surface wettability by increasing the hydrophilicity of the quaternary amine's substituent lead to a decrease in protein adsorption.² The oxanorbornene-based polymers explored here, however, showed that their nonfouling properties were largely independent of both the interchange distance of the zwitterionic functional groups and the surfaces' relative wettabilities. Although a range of surface wettabilities ($40^\circ < \theta_A < 70^\circ$) was achieved by varying the distance between cation and anion, as well as the type of charged species, the majority of the surfaces still exhibited

similar levels of protein adsorption ($0.5 \text{ ng/mm}^2 < \Gamma_{\text{Fibrinogen}} < 1.0 \text{ ng/mm}^2$). The synthesized zwitterions were limited to some extent by synthetic viability. It is possible that a stronger correlation between surface wettability, or hydrophilicity, and protein adsorption would have been observed with a broader range of zwitterions. The contribution of the oxanorbornene backbone and the bulk nature of the polymer coatings may also largely contribute to the resulting surfaces' nonfouling properties, so that small changes in the zwitterion chemistry have less of an impact on the surface properties. Regardless, the fact that these materials' fouling properties are largely independent of their surface properties is contrary to some other zwitterionic nonfouling systems. This property, however, may be advantageous. While none of the surfaces tested here suppressed protein adsorption below the 0.1 ng/mm^2 threshold, many performed reasonably well ($\sim 0.5 \text{ ng/mm}^2$).

5.5 Experimental Procedures

5.5.1 Materials

All reagents were purchased from either Sigma-Aldrich, Alfa Aesar, Acros Organics, or Fisher Scientific in the highest purity available and used as received, unless otherwise noted. 4-(dimethylamino)butylamine, 5-(dimethylamino)amylamine, and 6-(dimethylamino)hexylamine were purchased from Matrix Scientific and used as received. 1,3-dinitrobenzene was obtained from Avocado Research Chemicals and used as received. 4-Bromobutanoic acid tert-butyl ester was purchased from Astatech, Inc. and used as received. 5-(bicycloheptenyl)triethoxysilane (**3**) was purchased from Gelest Inc. and used as received. 5-bromopentanoic acid tert-butyl ester and 6-bromohexanoic acid tert-butyl ester were synthesized as described below. Tetrahydrofuran (THF, Fisher

Scientific, HPLC grade) was distilled from sodium/benzophenone under nitrogen and dichloromethane (CH_2Cl_2 , Fisher Scientific, ACS grade) was distilled from CaH_2 under nitrogen immediately prior to use. 2,2,2-trifluoroethanol (TFE, 99+%) was purchased from Alfa Aesar and used as received. Grubbs' 3rd generation catalyst (G3) was synthesized according to a previously reported procedure.¹⁹ Fibrinogen was purchased from Calbiochem as a lyophilized powder. Phosphate buffered saline (PBS, 0.01M) was purchased from Sigma Aldrich free of serum proteins as a powder and reconstituted in distilled water prior to use.

5.5.2 Instrumentation and methodology

Nuclear magnetic resonance (NMR) spectra were obtained on a Bruker DPX-300 NMR spectrometer. Abbreviations for assignments are as follows: s: singlet; t: triplet; q: quartet; m: multiplet; comp: overlapping non-equivalent peaks; br: broad.

Gel permeation chromatography (GPC) traces were obtained on an Agilent 1260 series system with a refractive index detector, and a HFIP gel guard column (7 mm x 50 mm) and 3 HFIP gel columns (7mm x 300 mm) in series. The columns were incubated at 40 °C. 2,2,2-trifluoroethanol with 20 mM NaTFA was used as the eluent at a flow rate of 0.75 mL/min. Methanol was used as the flow marker. Molecular weight was calculated relative to poly(methyl methacrylate) standards.

Grazing angle Fourier transform infrared (FT-IR) spectra for the coatings were obtained on a Thermo Scientific Nicolet 6700 spectrometer with a Harrick germanium attenuated total reflection (ATR) attachment and N_2 -cooled MCT/A. Clean silica wafers were used to collect the background spectra. Coating thicknesses of $\sim 1 \mu\text{m}$ (5 wt/v % polymer/TFE casting solution) were used to improve signal intensity

Water contact angles were measured using a Rame-Hart telescopic goniometer and a Gilmont syringe with a 24-gauge flat-tipped needle filled with Milli-Q water. Reported values are the average of at least 6 measurements on three unique surfaces.

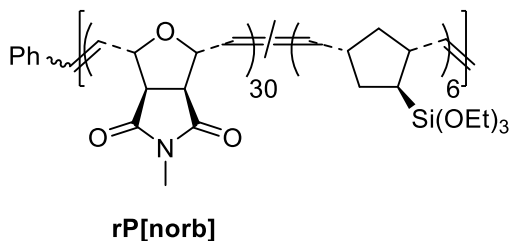
Polymer thickness measurements were made on a LSE model Gaertner Scientific Stokes Ellipsometer, with an angle of incidence of 70° from the normal and a 6328 \AA HeNe laser, assuming a thin film model. A refractive index of 1.5 was assumed for the polymer layer. Reported values are the average of five measurements on three unique surfaces.

Atomic force microscopy (AFM) images were obtained in tapping mode on a Veeco Dimension 3100 instrument with a Nanoscope III controller with the manufacturer's software. Silicon cantilevers with a spring constant of 0.58 N/m were used. Root mean squared (rms) roughness values were calculated by the manufacturer's software on a $1 \mu\text{m} \times 1 \mu\text{m}$ image.

Theoretical intercharge distances were calculated on the modeled side chains after energy minimization using Spartan 2004 software (Wavefunction, Inc., Irvine, CA).

5.5.3 Synthesis and characterization

Monomers **C1(+)**, **Carboxy(+)**, and **Sulfo(ZI)** were synthesized according to the procedures outlined in Chapter 3. **rP[norb]** was synthesized according to previously published procedures.^{2,20} Yields and spectroscopic data matched those reported.



Representative polymerization procedure: Monomer (**C₁(+)**a****) (0.3 g, 0.83 mmol, 30 equivalents) and 5-(bicycloheptenyl)-triethoxysilane (42 μ L, 0.16 mmol, 6 equivalents) were weighed into a clean, dry Schlenk flask under N₂, while G3 (0.024 g, 0.028 mmol, 1 equivalent) was weighed into a second Schlenk flask under N₂. The monomers were then dissolved in 3 mL 2,2,2-trifluoroethanol plus 1 mL dry CH₂Cl₂ and the catalyst was dissolved in 2 mL dry CH₂Cl₂. Both solutions were subjected to three freeze-pump-thaw cycles and warmed to room temperature. Using a nitrogen-purged syringe, the monomer solution was added to the catalyst solution. The polymerization was allowed to proceed for 30 minutes at room temperature under N₂. To quench the reaction, 1.5 mL ethyl vinyl ether was added and the solution was stirred for an additional hour. The polymer was then precipitated out into anhydrous diethyl ether, isolated by vacuum filtration and dried under high vacuum overnight. Yields were greater than 90% for all polymers. The polymer was stored at -20 °C while not in use.

rP[C₁(+)a**]:** data previously reported.² ¹H NMR (300MHz, DMSO-d₆): δ (ppm) = 1.15 (br, 9H), 3.15 (br, 9H), 3.39 (s, 3H), 3.52 (comp, 4H), 3.76 (br, 2H), 4.48 (br, 1H), 4.90 (br, 1H), 5.41 (br, 1H), 5.57 (br, 1H), 5.79 (br, *cis*, 1H), 5.97 (br, *trans*, 1H), 7.39 (br m, 5H, phenyl endgroup).

rP[C₁(+)b**]:** ¹H NMR (300MHz, DMSO-d₆): δ (ppm) = 1.14 (br, 9H), 1.95 (br, 2H), 3.05 (br, 9H), 3.29 (br, 2H), 3.39 (s, 3H), 3.44 (br, 2H), 3.75 (br, 6H), 4.46 (br, 1H), 4.94 (br, 1H), 5.36 (br, 1H), 5.54 (br, 1H), 5.98 (br, *cis*, 1H), 6.12 (br, *trans*, 1H), 7.39 (br m, 5H, phenyl endgroup).

rP[C₁(+)c]: ¹H NMR (300MHz, DMSO-d₆): δ (ppm) = 1.15 (br, 9H), 1.51 (br, 2H), 1.68 (br, 2H), 3.05 (br, 9H), 3.30 (br, 2H), 3.39 (s, 3H), 3.43 (br, 2H), 3.75 (br, 6H), 4.42 (br, 1H), 4.88 (br, 1H), 5.40 (br, 1H), 5.55 (br, 1H), 5.77 (br, *cis*, 1H), 5.97 (br, *trans*, 1H), 7.37 (br m, 5H, phenyl endgroup).

rP[C₁(+)e]: ¹H NMR (300MHz, DMSO-d₆): δ (ppm) = 1.15 (br, 9H), 1.25 (br, 2H), 1.55 (br, 2H), 1.69 (br, 2H), 3.05 (br, 9H), 3.24 (br, 2H), 3.39 (s, 3H), 3.45 (br, 2H), 3.75 (br, 6H), 4.41 (br, 1H), 4.88 (br, 1H), 5.41 (br, 1H), 5.54 (br, 1H), 5.76 (br, *cis*, 1H), 5.97 (br, *trans*, 1H), 7.37 (br m, 5H, phenyl endgroup).

rP[C₁(+)e]: ¹H NMR (300MHz, DMSO-d₆): δ (ppm) = 1.14 (br, 9H), 1.29 (br, 4H), 1.51 (br, 2H), 1.66 (br, 2H), 3.05 (br, 9H), 3.27 (br, 2H), 3.38 (comp, 3H + 2H), 3.75 (br, 6H), 4.40 (br, 1H), 4.88 (br, 1H), 5.41 (br, 1H), 5.56 (br, 1H), 5.76 (br, *cis*, 1H), 5.97 (br, *trans*, 1H), 7.37 (br m, 5H, phenyl endgroup).

rP[Carboxy(+)a]: ¹H NMR (300MHz, MeOD-d₄): δ (ppm) = 1.25 (br, 9H), 1.58 (br, 9H), 3.47 (br, 6H), 3.57 (br, 2H), 3.89 (comp, 6H + 2H), 4.50 (br, 2H), 4.74 (br, 1H), 5.17 (br, 1H), 5.48 (br, 1H), 5.65 (br, 1H), 5.91 (br, *cis*, 1H), 6.14 (br, *trans*, 1H), 7.36 (br m, 5H, phenyl endgroup).

rP[Carboxy(+)b]: ¹H NMR (300MHz, D₂O): δ (ppm) = 1.05 (br, 9H), 2.83 (br, 2H), 3.09 (br, 6H), 3.46 (br, 2H), 3.58 (br, 2H), 3.85 (comp, 6H + 2H), 4.56 (br, 1H), 4.93 (br, 1H), 5.38 (br, 1H), 5.56 (br, 1H), 5.83 (br, *cis*, 1H), 6.03 (br, *trans*, 1H).

rP[Carboxy(+)c]: data previously reported.² ¹H NMR (300MHz, MeOD-d₄): δ (ppm) = 1.25 (br, 9H), 1.50 (br, 9H), 2.09 (br, 2H), 2.45 (br, 2H), 2.98 (br, 6H), 3.29 (br, 2H), 3.50 (br, 2H), 3.60 (br, 2H), 3.89 (m, 6H), 3.96 (br, 2H), 4.75 (br, 2H), 5.17 (br, 2H),

5.53 (br, 1H), 5.65 (br, 1H), 5.92 (br, *cis*, 1H), 6.12 (br, *trans*, 1H), 7.40 (br m, 5H, phenyl endgroup).

rP[Carboxy(+)]d: $^1\text{H NMR}$ (300MHz, MeOD- d_4): δ (ppm) = 1.24 (br, 9H), 1.48 (br, 9H), 1.68 (br, 2H), 1.86 (br, 2H), 2.37 (br, 2H), 3.27 (br, 2H), 3.52 (br, 2H), 3.66 (br, 2H), 3.87 (m, 6H), 3.98 (br, 2H), 4.71 (br, 2H), 5.12 (br, 2H), 5.50 (br, 1H), 5.64 (br, 1H), 5.92 (br, *cis*, 1H), 6.14 (br, *trans*, 1H), 7.35 (br m, 5H, phenyl endgroup).

rP[Carboxy(+)]e: $^1\text{H NMR}$ (300MHz, MeOD- d_4): δ (ppm) = 1.22 (br, 9H), 1.47 (comp, 9H + 2H), 1.68 (br, 2H), 1.87 (br, 2H), 2.32 (br, 2H), 3.27 (br, 2H), 3.50 (br, 2H), 3.69 (br, 2H), 3.87 (m, 6H), 3.99 (br, 2H), 4.72 (br, 1H), 5.13 (br, 1H), 5.50 (br, 1H), 5.61 (br, 1H), 5.91 (br, *cis*, 1H), 6.12 (br, *trans*, 1H), 7.35 (br m, 5H, phenyl endgroup).

rP[Sulfo(ZI)a]: $^1\text{H NMR}$ (300MHz, $\text{D}_2\text{O} + \text{NaBr}$): δ (ppm) = 1.12 (br, 9H), 2.14 (br, 2H), 2.86 (br, 2H), 3.12 (br, 6H), 3.47 (comp, 2H + 2H), 3.55 (br, 2H), 3.89 (q, $J = 9.2$ Hz, 6H), 4.61 (br, 1H), 4.98 (br, 1H), 5.84 (br, *cis*, 1H), 6.04 (br, *trans*, 1H).

rP[Sulfo(ZI)b]: data previously reported.² $^1\text{H NMR}$ (300MHz, $\text{D}_2\text{O} + \text{NaBr}$): δ (ppm) = 1.15 (br, 9H), 1.74 (br, 2H), 1.89 (br, 2H), 2.90 (br, 2H), 3.12 (br, 6H), 3.40 (br, 2H), 3.49 (br, 2H), 3.61 (br, 2H), 3.91 (q, $J = 9.1$ Hz, 6H), 4.65 (br, 1H), 5.03 (br, 1H), 5.90 (br, *cis*, 1H), 6.09 (br, *trans*, 1H).

5.5.4 Coating preparation

Casting solutions were prepared as 1 wt/v % polymer solutions (0.01g/1mL) in 2,2,2-trifluoroethanol and filtered through 0.45 μm PTFE filters. Silicon wafers were cut into 1.5 x 1.5 cm substrates, cleaned with piranha solution for 30 minutes, rinsed with RO water and dried under N_2 immediately before use. The polymer solutions were spin-cast onto the silicon substrates at 3000 rpm for 30 seconds. After drying under vacuum

overnight, the samples were placed in a sealed desiccator containing concentrated HCl for 1 hour, then heated at 110 °C for 3 hours to complete the curing process. Any remaining free polymer was extracted from the coating by soaking the samples in PBS for several hours; the samples were rinsed with RO water to remove any buffer salts and dried under N₂ then overnight under high vacuum. Dual-functional surfaces (**rP[C₁(+)a-e]**) were converted to the zwitterionic form (**rP[C₁(ZI)a-e]**) by soaking in 0.1 M NaOH for twenty minutes, rinsing with RO water and drying overnight under vacuum. Deprotection of the **rP[Carboxy(+)]** surfaces was ensured by soaking the surfaces in 4 M HCl/dioxane overnight, rinsing with ethanol and RO water and drying under N₂ then under high vacuum overnight. The initial thicknesses of the coatings were measured by ellipsometry. AFM and contact angle measurements were taken on freshly prepared surfaces.

5.5.5 Protein adsorption measurements

Fibrinogen solutions (0.5 mg/mL) in PBS buffer were prepared directly before use at room temperature. The samples were placed in individual wells of a 12-well cell culture plate and soaked in PBS buffer for two hours to fully hydrate the surfaces. The coatings were transferred to a clean plate and approximately 3 mL of protein solution were added to each well. The plate was then incubated for two hours at 37 °C. Excess PBS was used to flood the wells to sufficiently dilute the protein, after which the samples were removed from the wells and rinsed further with RO water. The coatings were first dried under a stream of N₂ then overnight under high vacuum. To quantify protein adsorption, the thickness of the adsorbed protein layer was measured by ellipsometry

using the published refractive index value of 1.405 for fibrinogen.^{2,20-22} By applying the following equation:

$$\Gamma(\text{ng/mm}^2) = h \times d$$

where h equals the measured thickness of the protein layer, and d equals fibrinogen density given in the literature^{2,20-22} as 1.085 g/cm³, the amount of adsorbed protein (Γ) was calculated.

5.6 Conclusions

Carboxybetaine, sulfobetaine, and methyl dual-functional series were synthesized so as to vary the distance between charged groups. The modular nature of the oxanorbornene imide monomer allowed for a wide range of zwitterionic chemistries to be achieved through basic synthetic methods, which is a major advantage of this ROMP-based platform. FT-IR was used to confirm the ring-opening of the dual-functional surfaces. AFM revealed that all surface chemistries resulted in smooth, homogenous coatings with no appreciable surface features. Surfaces functionalized with the zwitterionic polymers exhibited advancing water contact angles in the range of 40° - 70°. All surfaces reduced the amount of irreversible fibrinogen adsorption when compared to the silica control (< 4 ng/mm²), which showed that the zwitterionic content of the polymers, regardless of the interchange distance, was adequate to create a protective barrier on a surface. While it was thought that there would be a positive correlation between increasing the interchange distance of the zwitterionic groups and increasing protein adsorption, based on previous studies in zwitterionic acrylamide systems, no strong trend was observed for this ROMP system.

5.7 References

- (1) Zhang, Z.; Vaisocherova, H.; Cheng, G.; Yang, W.; Xue, H.; Jiang, S. Nonfouling Behavior of Polycarboxybetaine-Grafted Surfaces: Structural and Environmental Effects. *Biomacromolecules* **2008**, *9*, 2686-2692.
- (2) Colak, S.; Tew, G. N. Dual-Functional ROMP-Based Betaines: Effect of Hydrophilicity and Backbone Structure on Nonfouling Properties. *Langmuir* **2012**, *28*, 666-675.
- (3) Colak, S.; Tew, G. N. Amphiphilic Polybetaines: The Effect of Side-Chain Hydrophobicity on Protein Adsorption. *Biomacromolecules* **2012**, *13*, 1233-1239.
- (4) Gudipati, C. S.; Finlay, J. A.; Callow, J. A.; Callow, M. E.; Wooley, K. L. The Antifouling and Fouling-Release Performance of Hyperbranched Fluoropolymer (HBFP)-Poly(ethylene glycol) (PEG) Composite Coatings Evaluated by Adsorption of Biomacromolecules and the Green Fouling Alga *Ulva*. *Langmuir* **2005**, *21*, 3044-3053.
- (5) Gudipati, C. S.; Greenlief, C. M.; Johnson, J. A.; Prayongpan, P.; Wooley, K. L. Hyperbranched Fluoropolymer (HBFP) and Linear Poly(ethylene glycol) (PEG) Based Amphiphilic Crosslinked Networks as Efficient Anti-fouling Coatings: An insight into the surface compositions, topographies and morphologies. *J. Polym. Sci., Part A: Polym. Chem.* **2004**, *42*, 6193-6208.
- (6) Dong, H.; Ye, P.; Zhong, M.; Pietrasik, J.; Drumright, R.; Matyjaszewski, K. Superhydrophilic Surfaces via Polymer-SiO₂ Nanocomposites. *Langmuir* **2010**, *26*, 15567-15573.
- (7) Weers, J. G.; Rathman, J. F.; Axe, F. U.; Crichlow, C. A.; Foland, L. D.; Scheuing, D. R.; Wiersema, R. J.; Zielske, A. G. Effect of the intramolecular charge separation distance on the solution properties of betaines and sulfobetaines. *Langmuir* **1991**, *7*, 854-867.
- (8) Izumrudov, V. A.; Zelikin, A. N.; Zhiryakova, M. V.; Jaeger, W.; Bohrisch, J. Interpolyelectrolyte Reactions in Solutions of Polycarboxybetaines. *J. Phys. Chem. B* **2003**, *107*, 7982-7986.
- (9) Izumrudov, V. A.; Domashenko, N. I.; Zhiryakova, M. V.; Davydova, O. V. Interpolyelectrolyte Reactions in Solutions of Polycarboxybetaines, 2: Influence of Alkyl Spacer in the Betaine Moieties on Complexing with Polyanions. *J. Phys. Chem. B* **2005**, *109*, 17391-17399.
- (10) Chen, S.; Jiang, S. A New Avenue to Nonfouling Materials. *Adv. Mater.* **2008**, *20*, 335-338.

- (11) Yaroslavov, A. A.; Sitnikova, T. A.; Rakhnyanskaya, A. A.; Yu. A. Ermakov, T. C. Burova, V. Ya. Grinberg, Menger, F. M. Contrasting Behavior of Zwitterionic and Cationic Polymers Bound to Anionic Liposomes. *Langmuir* **2007**, *23*, 7539-7544.
- (12) Chen, S.; Li, L.; Zhao, C.; Zheng, J. Surface hydration: Principles and applications toward low-fouling/nonfouling biomaterials. *Polymer* **2012**, *51*, 5283-5293.
- (13) Song, W.; Mano, J. F. Interactions between cells or proteins and surfaces exhibiting extreme wettabilities. *Soft Matter* **2013**, *9*, 2985-2999.
- (14) Kane, R. S.; Deschatelets, R.; Whitesides, G. M. Kosmotropes Form the Basis of Protein-Resistant Surfaces. *Langmuir* **2003**, *19*, 2388-2391.
- (15) Holmlin, R. E.; Chen, X.; Chapman, R. G.; Takayama, S.; Whitesides, G. M. Zwitterionic SAMS that Resist Nonspecific Adsorption of Protein from Aqueous Buffer. *Langmuir* **2001**, *17*, 2841-2850.
- (16) Banerjee, I.; Pangule, R. C.; Kane, R. S. Antifouling Coatings: Recent Developments in the Design of Surfaces That Prevent Fouling by Proteins, Bacteria, and Marine Organisms. *Adv. Mater.* **2011**, *23*, 690-718.
- (17) Callow, J. A.; Callow, M. E. Trends in the development of environmentally friendly fouling-resistant marine coatings. *Nat. Commun.* **2011**, DOI: 10.1038/ncomms1251.
- (18) Yang, W. J.; Neoh, K-G.; Kang, E-T.; Teo, S. L-M.; Rittschof, D. Polymer brush coatings for combating marine biofouling. *Prog. Polym. Sci.* **2014**, *39*, 1017-1042.
- (19) Love, J. A.; Morgan, J. P.; Trnka, T. M.; Grubbs, R. H. A Practical and Highly Active Ruthenium-Based Catalyst that Effects the Cross Metathesis of Acrylonitrile. *Angew. Chem. Int. Ed.* **2002**, *41*, 4035-4037.
- (20) Kim, G.-C.; Jeong, J.-G.; Lee, N.-J.; Ha, C.-S.; Cho, W.-J. Synthesis and biological activities of endo-3,5-epoxy-1,2,3,6-tetrahydrophthalimide and its polymers. *J. Appl. Polym. Sci.* **1997**, *64*, 2605-2612.
- (21) Elwing, H. Protein absorption and ellipsometry in biomaterial research. *Biomaterials* **1998**, *19*, 397-406.
- (22) Voros, J. The Density and Refractive Index of Adsorbing Protein Layers. *Biophys. J.* **2004**, *87*, 553-561.
- (23) Sharma, S.; Johnson, R. W.; Desai, T. A. Evaluation of the Stability of Nonfouling Ultrathin Poly(ethylene glycol) Films for Silicon-Based Microdevices. *Langmuir* **2004**, *20*, 348-356.

CHAPTER 6

NONFOULING PROPERTIES OF AMPHIPHILIC BETAINES: EFFECT OF HYDROPHOBIC SUBSTITUENTS

6.1 Introduction

In Chapter 6, the nonfouling properties of the **Amph(ZI)** series are explored. Chapter 3 previously described the design rationale and synthesis of the **Amph(ZI)** series. Its structural diversity created a rich library of amphiphilic chemistries to explore in the context of nonfouling materials. More importantly, this series' utility as a set of foundational materials lay in its ability to systematically vary the hydrophobic component. Both hydrocarbon and fluorinated hydrophobes were incorporated into the betaines. Coatings were created from the copolymers as described in Chapter 4. Surface-sensitive techniques including FT-IR, AFM and contact angle analysis were used to characterize the resulting surfaces, while fibrinogen was used as a metric to compare the nonfouling performance of the amphiphilic zwitterionic surfaces to each other as well as to the more traditional hydrophilic zwitterionic surfaces. A variety of surface energies and surface topographies were achieved based on the hydrophobe. Loose structure-property relationships were determined for subsets of the amphiphilic series. Finally, sum frequency generation (SFG) spectroscopy was used to quantitatively understand the interfacial chemistry of model amphiphilic surfaces.

6.2 General Approach

The dual-functional **Amph(ZI)** series described in Chapter 3 was unique for several reasons. While synthetic amphiphilic materials are well-known, those containing

charged or zwitterionic groups as the hydrophilic component are rarer.¹⁻¹⁰ Furthermore, the ability to incorporate the hydrophobe into the betaine so that each polymeric repeat unit contained a hydrophobic and hydrophilic moiety was specifically enabled by our dual-functional chemistry.^{9,10} Additionally, the **Amph(ZI)** series contained both hydrocarbon (Figure 6.1a) and fluorinated (Figure 6.1b) hydrophobes on the same backbone, which theoretically would allow for a direct comparison of hydrophobic and lipophobic materials. Due to the library of structures we obtained, the **Amph(ZI)** series could be used to study not only the effect of relative hydrophobicity and lipophobicity on nonfouling materials, but the effect of the chemical structure of the hydrophobe as well. Here, we hoped that these polymers would allow us to study the nonfouling properties of amphiphilic zwitterionic surfaces in a methodical manner. The exact structures of the hydrophobes are reproduced below in Table 6.1 for clarity.

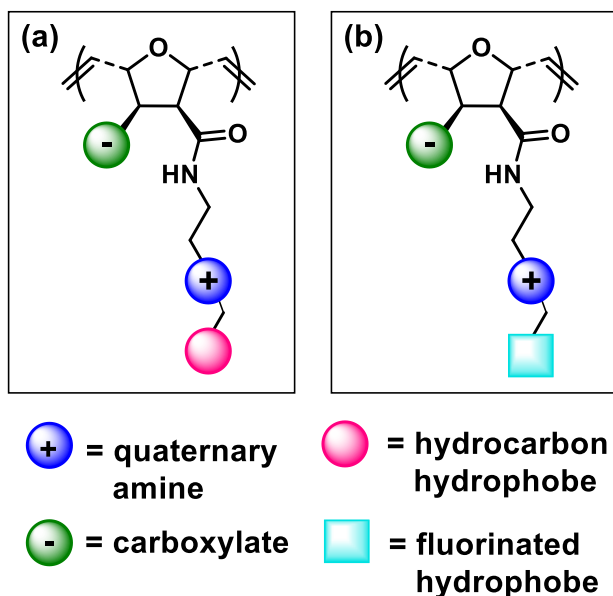
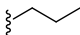
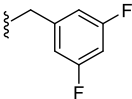
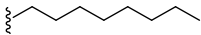
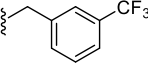
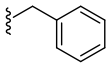
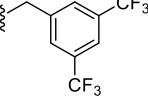
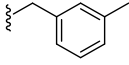
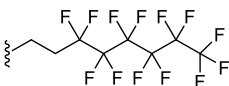
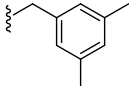
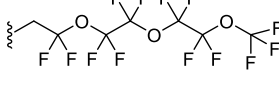
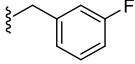
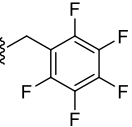


Figure 6.1: Polymers used to study the effect of amphiphilic structure on oxanorbornene-based dual-functional polybetaines: (a) hydrocarbon hydrophobic groups; and (b) fluorinated hydrophobic groups.

Table 6.1: Summary of amphiphilic dual-functional betaine structures.

Polymer	R	X	Polymer	R	X
Amph(+a)		Br	Amph(+g)		OTs
Amph(+b)		Br	Amph(+h)		OTs
Amph(+c)		OTs	Amph(+i)		OTs
Amph(+d)		OTs	Amph(+j)		OTf
Amph(+e)		OTs	Amph(+k)		OTf
Amph(+f)		OTs	Amph(+l)		OTs

6.3 Coating Preparation and Characterization

6.3.1 Polymer Synthesis

As in Chapter 5, the monomers were randomly copolymerized with 5-(bicycloheptenyl)-triethoxysilane in a ratio of 30 to 6 to create polymers for functionalizing silica substrates (Figure 6.2a). These polymers are denoted here with the prefix **rP** to denote the random copolymerization with the siloxane monomer. The polymerizations were carried out in a mixture of TFE and CH_2Cl_2 to fully solubilize all components. Quantitative conversion for all polymers was achieved in 15-35 minutes. Because of the hydrolytic instability of the siloxane groups, as well as the highly charged

content of the polymers, GPC was not a viable characterization technique, therefore ^1H NMR spectroscopy was used exclusively to characterize these precursor polymers. Table 6.2 summarizes the polymers' calculated compositions and siloxane contents, which ranged from 14-25 mol %.

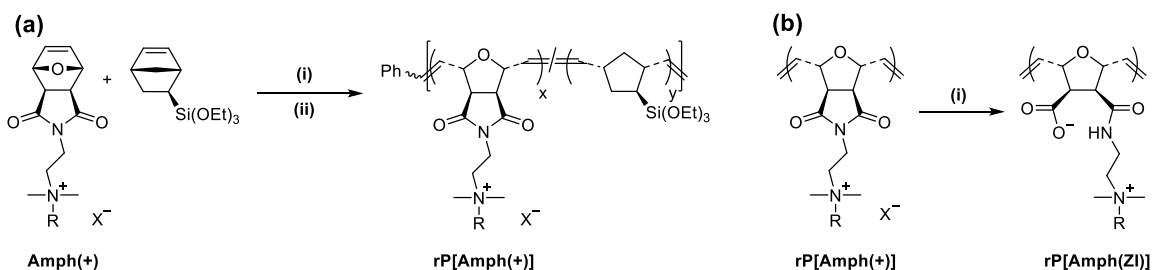


Figure 6.2: Polymerization of the **Amph(ZI)** series and representative post-polymerization functionalization reactions: **(a)** (i) Grubbs' 3rd generation catalyst, TFE/ CH_2Cl_2 , room temperature, 40 minutes; (ii) excess ethyl vinyl ether, room temperature, 1 hour; **(b)** (i) 1:1 0.2 M NaOH:DMF, 20 minutes.

Table 6.2: Composition and molecular weight characterization of amphiphilic polymers by NMR spectroscopy

Polymer	x^a	y^b	M_n (kDa) ^c	mol % Si
rP[Amph(+) a]	30	6.8	12.5	18.5
rP[Amph(+) b]	30	6.1	14.4	16.9
rP[Amph(+) c]	30	7.0	16.8	19.0
rP[Amph(+) d]	30	5.8	16.9	16.2
rP[Amph(+) e]	30	8.1	17.9	21.2
rP[Amph(+) f]	30	5.6	16.9	15.7
rP[Amph(+) g]	30	9.8	18.5	24.6
rP[Amph(+) h]	30	6.2	18.6	17.1
rP[Amph(+) i]	30	4.9	20.3	14.0
rP[Amph(+) j]	30	5.9	23.5	16.4
rP[Amph(+) k]	30	5.9	24.5	16.4
rP[Amph(+) l]	30	5.7	19.1	16.0

^a number of charged repeat units assumed to be 30 due to the low resolution of the phenyl endgroup; ^b number of siloxane repeat units as calculated by ^1H NMR spectroscopy from

the ratio of the peaks corresponding to $-\text{N}(\text{CH}_3)_2$ and $-\text{Si}(\text{OCH}_2\text{-CH}_3)$; ^c calculated from the x and y values given in the table and the monomers' known molecular weights.

6.3.2 Surface Characterization

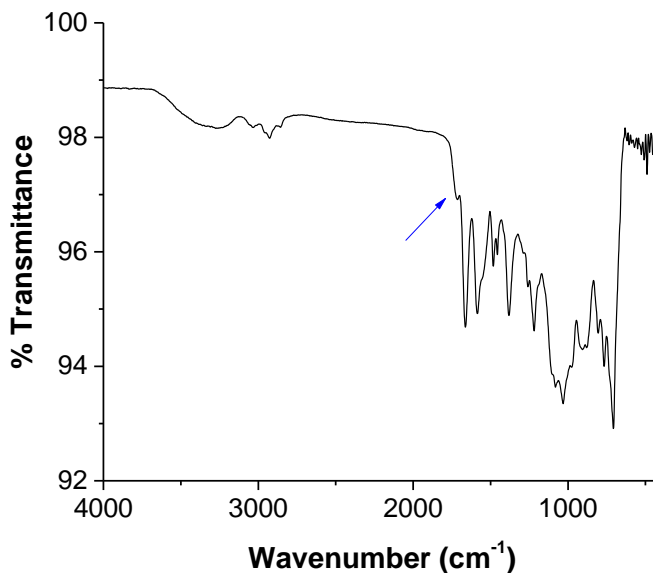


Figure 6.3: Representative FT-IR spectrum of **rP[Amph(ZI)c]**. The blue arrow highlights a weak peak corresponding to the imide carbonyl group at approximately 1700 cm^{-1} .

Coatings were prepared per the usual method. As with the **C₁(ZI)** series in Chapter 5, the polymers were ring-opened after surface functionalization (Figure 6.2b) which was confirmed by IR spectroscopy. Because of these polymers' increased hydrophobicity, the base solution was prepared in a mixture of water and DMF to better solubilize the imide. A representative IR spectrum for the **rP[Amph(ZI)c]** surface is given in Figure 6.3. As before, a residual imide peak was still visible after the base treatment. Based on the intensity of this peak, however, it appeared that more imide groups were present after base treatment in the amphiphilic dual-functional surfaces than in the hydrophilic dual-functional surfaces, most likely due to the reduced wettability of the more hydrophobic surfaces. Because the siloxane crosslinks are themselves base-

sensitive, increasing the exposure time and the base concentration caused the coating to delaminate. We assumed, however, that the majority of the cationic repeat units were sequestered in the interior of the network due to the limited diffusion of the aqueous solution, and that their presence would not have a significant impact on the coatings' presumed zwitterionic nature.

Further surface analysis was done by XPS. Two representative spectra for the **rP[Amph(ZI)c]** and **rP[Amph(ZI)l]** surfaces are given in Figures 6.4. In the **rP[Amph(ZI)c]** spectrum (Figure 6.4a), peaks corresponding to aromatic and alkyl carbons, oxygen, nitrogen, and silicon were all observed, as expected. In the **rP[Amph(ZI)l]** spectrum (Figure 6.4b), however, peaks corresponding to fluorine were clearly seen. This data showed that not only was the fluorinated moiety present in the precursor polymer, but also that it was present near the interface of the coating to interact with the environment.

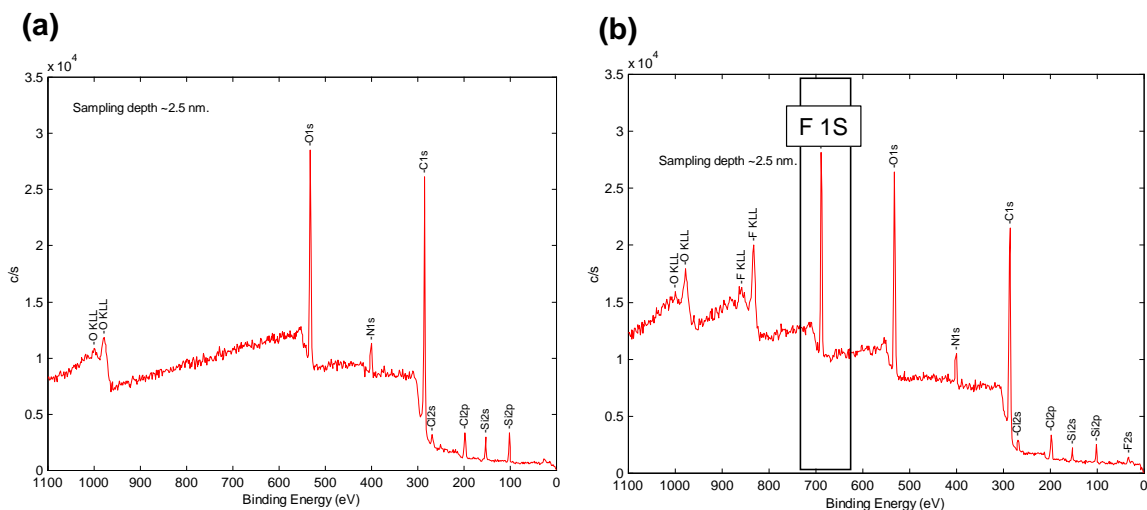


Figure 6.4. XPS spectra of (a) **sP[Amph(ZI)c]** and (b) **sP[Amph(ZI)l]**. A representative fluorine peak is highlighted in (b).

AFM was also used to compare the topographies of the amphiphilic surfaces (Figure 6.5). Many of the surfaces had similar appearances without distinguishing features. To some extent, this result was unexpected as amphiphilic materials are often characterized by dynamic, heterogeneous surfaces.¹⁻⁹ The **rP[Amph(ZI)i]** surface was one exception. A greater degree of heterogeneity was observed on its surface when compared to the other alkyl- and benzyl-containing surfaces. The **Amph(+i)** monomer possessed unique solution properties compared to the other benzyl-substituted monomers as well, which may have indicated additional interactions that manifested themselves in the surface topography. Also exceptional was the **sP[Amph(ZI)j]** surface, which was characterized by a high degree of roughness (5 nm). Generally, surface roughnesses ranged from 0.2 to 0.9 nm (Table 6.3), therefore any value greater than 1 nm was viewed as anomalous. Interestingly, the other perfluorinated surfaces (**sP[Amph(ZI)j]** – **sP[Amph(ZI)l]**) did *not* exhibit the same surface roughness, indicating that fluorine content is not the only factor influencing roughness or topography.

The phase images from AFM also gave some indication of phase separation on the surfaces. In general, a slightly higher level of phase separation was seen for these surfaces than for the hydrophilic zwitterionic surfaces. Representative images for **rP[Amph(ZI)c]** (benzyl) and **rP[Amph(ZI)l]** (pentafluorobenzyl) are given in Figure 6.6. There appeared to be little difference in phase separation by direct inspection between the hydrocarbon and fluorinated surfaces. As with the height images, it was expected that a greater degree of phase separation would be observed, especially for the fluorinated surfaces. In fact, there were few differences between the **Amph** surfaces and the **C₁**, **Carboxy**, and **Sulfo** surfaces.

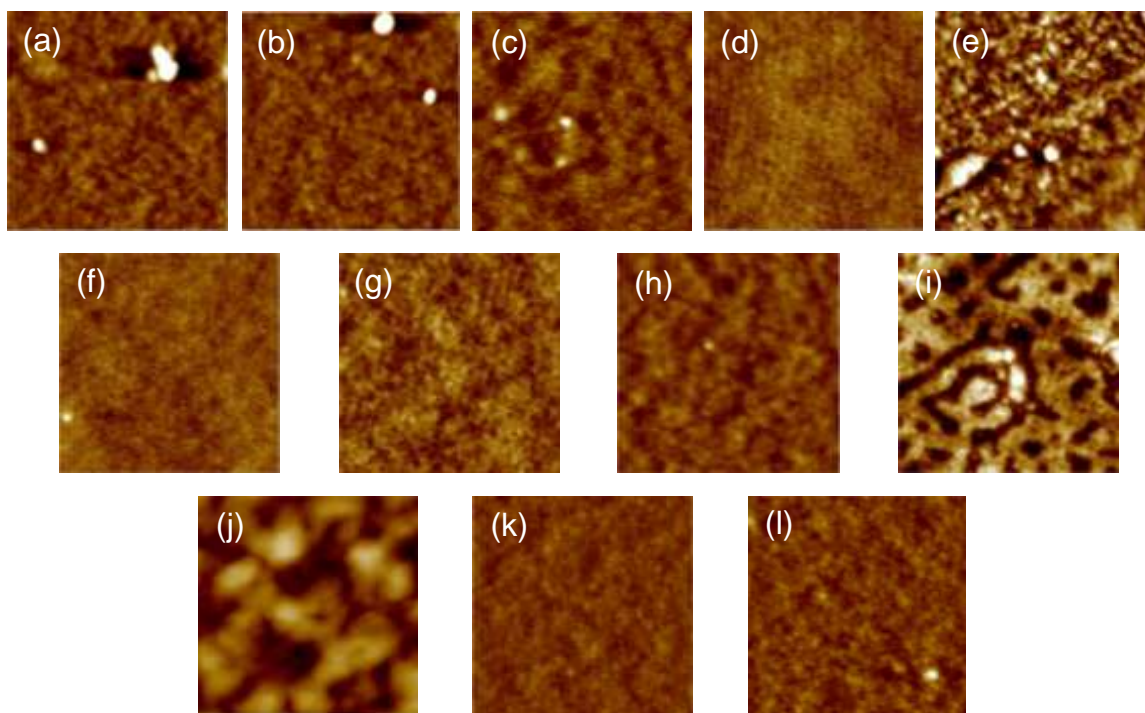


Figure 6.5: Tapping-mode AFM height images of zwitterionic, amphiphilic surfaces: **(a)** rP[Amph(ZI)a]; **(b)** rP[Amph(ZI)b]; **(c)** rP[Amph(ZI)c]; **(d)** rP[Amph(ZI)d]; **(e)** rP[Amph(ZI)e]; **(f)** rP[Amph(ZI)f]; **(g)** rP[Amph(ZI)g]; **(h)** rP[Amph(ZI)h]; **(i)** rP[Amph(ZI)i]; **(j)** rP[Amph(ZI)j]; **(k)** rP[Amph(ZI)k]; and **(l)** rP[Amph(ZI)l]. Images **(a)**-**(i)** and **(k)**-**(l)** represent a 1 μm x 1 μm x 5 nm area. Image **(j)** represents a 1 μm x 1 μm x 30 nm area.

The lack of unique discernable surface characteristics across the polymer series may be due to a strong contribution from the polymers' backbone. Likewise, the tightly cross-linked coatings may not allow for the hydrophobic side chains to extensively rearrange during the curing process. Many amphiphilic materials contain higher molecular weight segments of hydrophilic and hydrophobic macromolecules, as in amphiphilic conetworks and hyperbranched structures. Those materials have large domains that can separate and rearrange throughout the bulk material. Our polymers have small, discrete hydrophilic and hydrophobic moieties that are covalently bonded to one another within each repeat unit. This amphiphilic structure is on the monomer level,

which in conjunction with the tightly crosslinked nature of the final coatings, may produce domains that are too small to observe by AFM, or may help to homogenize the hydrophilic or hydrophobic components.

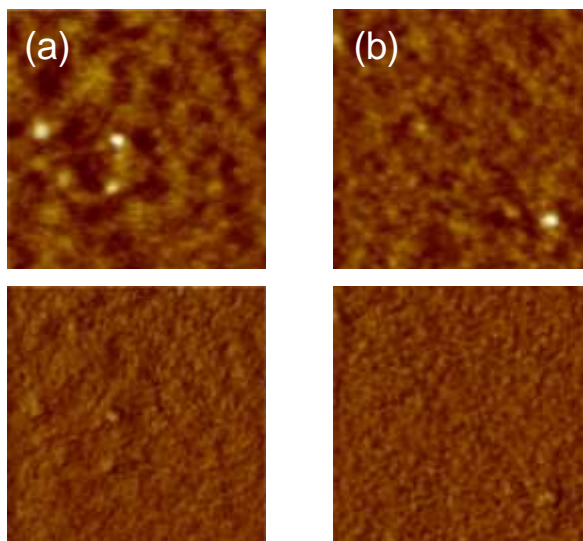


Figure 6.6: Tapping-mode AFM height (top) and phase (bottom) images of zwitterionic, amphiphilic surfaces: (a) **rP[Amph(ZI)c]**, and (b) **rP[Amph(ZI)l]**.

The water contact angles of these surfaces were measured to compare relative hydrophilicities, in the same manner as the hydrophilic surfaces in Chapter 5. Advancing water contact angles are reported in Table 6.3. Values ranged from 53° for the propyl surface (**rP[Amph(ZI)a]**) to 92° for the benzyl (**rP[Amph(ZI)c]**) surface. For amphiphilic surfaces, however, surface free energy may be a more appropriate metric for comparison than water contact angle. Hexadecane contact angles were also measured for all surfaces, and the surface free energies were calculated from the advancing water and advancing hexadecane contact angles, all tabulated in Table 6.3. Using hexadecane as the probe fluid measured the relative lipophilicity/lipophobicity of a surface. The smallest hexadecane contact angle (11°) was observed on the benzyl surface (**rP[Amph(ZI)c]**) whereas the highest contact angle (61°) was observed on the

perfluoroalkyl surface (**rP[Amph(ZI)j**). These results highlighted the difference between hydrophobicity and lipophobicity. Both **rP[Amph(ZI)c]** and **rP[Amph(ZI)j]** surfaces had approximately equal advancing water contact angles (90°) but vastly different hexadecane advancing contact angles. Even though both surfaces are hydrophobic, the fluorinated surface was more lipophobic. This discrepancy was further reflected in the surface free energies, where $\gamma_s = 73$ mN/m for the **rP[Amph(ZI)c]** surface and 22 mN/m for the **rP[Amph(ZI)j]** surface.

Table 6.3: Surface properties of amphiphilic zwitterionic coatings

Polymer	Roughness (nm) ^a	θ_{A,H_2O} (°) ^b	$\theta_{A,Hexadecane}$ (°) ^b	Surface free energy (mN/m) ^c			$\Gamma_{\text{Fibrinogen}}$ (ng/mm ²) ^d
				γ_s^d	γ_s^p	γ_s	
rPoly3(ZI)a	0.6	53 ± 1	14 ± 0	27	23	50	0.79 ± 0.07
rPoly3(ZI)b	0.6	62 ± 1	20 ± 0	26	26	52	4.18 ± 0.13
rPoly3(ZI)c	0.4	92 ± 2	11 ± 0	27	46	73	6.42 ± 0.47
rPoly3(ZI)d	0.3	63 ± 2	24 ± 1	17	25	42	17.40 ± 2.42
rPoly3(ZI)e	0.8	81 ± 5	23 ± 2	25	7	32	15.52 ± 0.29
rPoly3(ZI)f	0.3	65 ± 2	20 ± 2	15	26	41	9.00 ± 1.14
rPoly3(ZI)g	0.7	86 ± 4	26 ± 3	5	25	30	2.58 ± 0.23
rPoly3(ZI)h	0.3	80 ± 8	19 ± 3	26	7	33	8.00 ± 1.09
rPoly3(ZI)i	0.9	62 ± 2	21 ± 6	17	26	43	0.92 ± 0.31
rPoly3(ZI)j	5.9	88 ± 3	61 ± 2	15	7	22	0.03 ± 0.01
rPoly3(ZI)k	0.2	59 ± 1	21 ± 0	26	19	45	1.29 ± 0.73
rPoly3(ZI)l	0.3	61 ± 1	19 ± 0	26	18	44	0.84 ± 0.10

^a root mean squared (rms) roughness calculated by the manufacturer's software based on a 1 μm x 1 μm image area; ^b contact angles measured by the sessile drop technique; ^c calculated by the method given in refs. 4 and 5; ^d fibrinogen adsorption measured by ellipsometry.

6.4 Protein Adsorption

Fibrinogen adsorption was measured for these surfaces, as in Chapter 5, to compare the effect of the hydrophobes on the nonfouling properties of the surfaces (Table 6.3). These studies were done both as a probe of the surfaces' interfacial chemistries and

as a measure of their nonfouling efficacies. Fibrinogen adsorption spanned a large range for this series, from 0.03 ng/mm² up to 17 ng/mm². Several surfaces – **rP[Amph(ZI)a]**/propyl, **rP[Amph(ZI)i]**/3,5-bis(trifluoromethyl)benzyl, **rP[Amph(ZI)j]**/perfluoroalkyl, **rP[Amph(ZI)k]**/perfluoroether, and **rP[Amph(ZI)l]**/pentafluorobenzyl – performed on par with, or better than, the hydrophilic **C₁(ZI)**, **Carboxy(ZI)**, and **Sulfo(ZI)** surfaces. These amphiphilic surfaces were highly fluorinated, or in the case of **rP[Amph(ZI)a]**, contained a relatively small hydrophobic component that did not significantly increase the surface’s hydrophobicity over the **rP[C₁(ZI)a]** surface.

To better understand the protein adsorption trends, the amphiphilic series was broken down into several subsets. First, the propyl, octyl and benzyl surfaces (**rP[Amph(ZI)a]**, **rP[Amph(ZI)b]**, and **rP[Amph(ZI)c]**) were compared (Figure 6.7). The methyl dual-functional surface **rP[C₁(ZI)a]** was also included in this series, whereas silica and the **rP[norb]** surface were used as non-functionalized and uncharged controls, respectively. From Figure 6.7a, we can see that fibrinogen adsorption increased as the side chain increased from methyl to propyl to octyl to benzyl. The octyl and benzyl (**rP[Amph(ZI)b]**, and **rP[Amph(ZI)c]**) surfaces performed similarly to the silica and **rP[norb]** controls, despite their zwitterionic nature. When fibrinogen adsorption was plotted as a function of advancing water contact angle for these four zwitterionic surfaces, a clear positive correlation was observed. As the hydrophobicity of the surfaces increased, protein adsorption increased as well. This result was expected based on the theory that hydrophilicity is necessary to support a water layer at the interface, which shields hydrophobic as well as electrostatic interactions with the surface.^{10,11} This series

also demonstrated that hydrophobic side chains could negate the effect of the zwitterionic component. For this system, the octyl and benzyl side chains possessed the necessary hydrophobicity so that the **rP[Amph(ZI)b]** and **rP[Amph(ZI)c]** surfaces were no more effective than the negative controls.

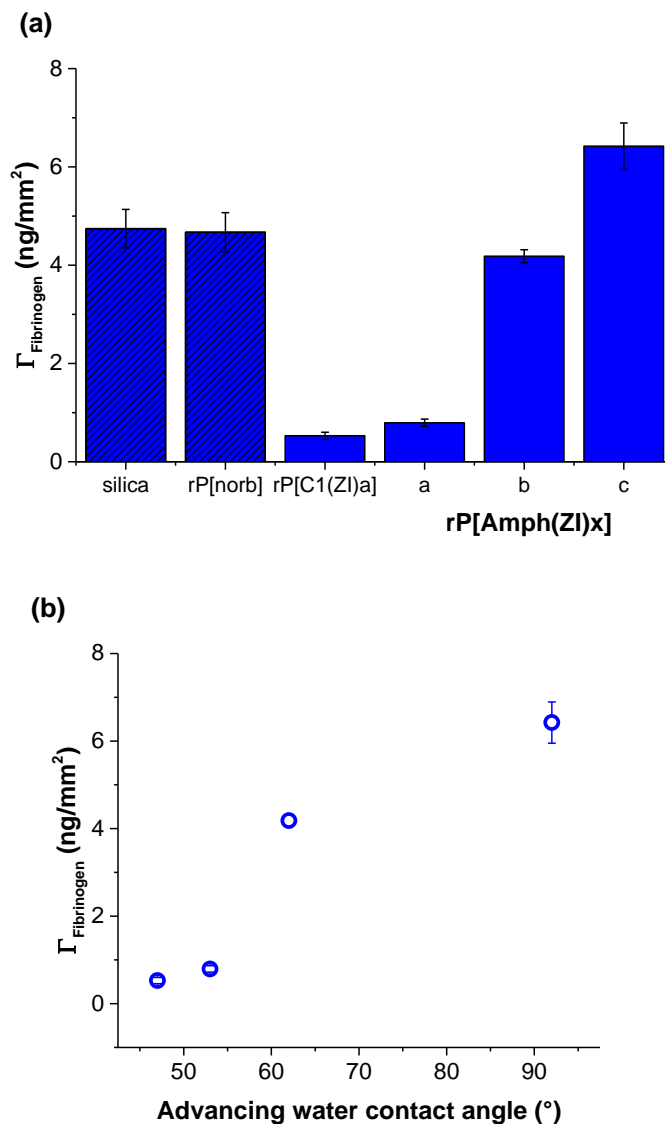
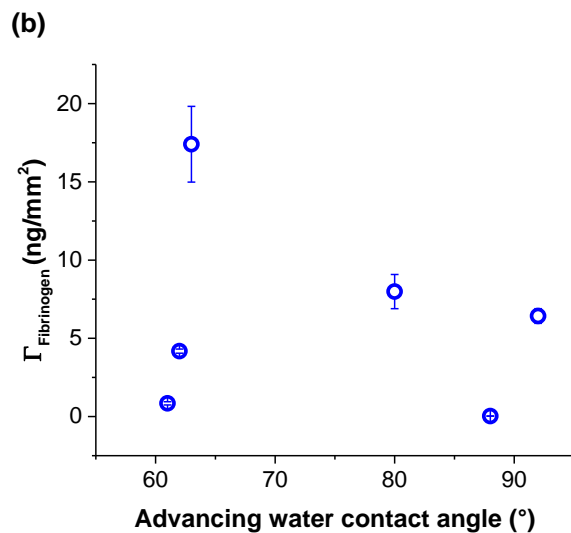
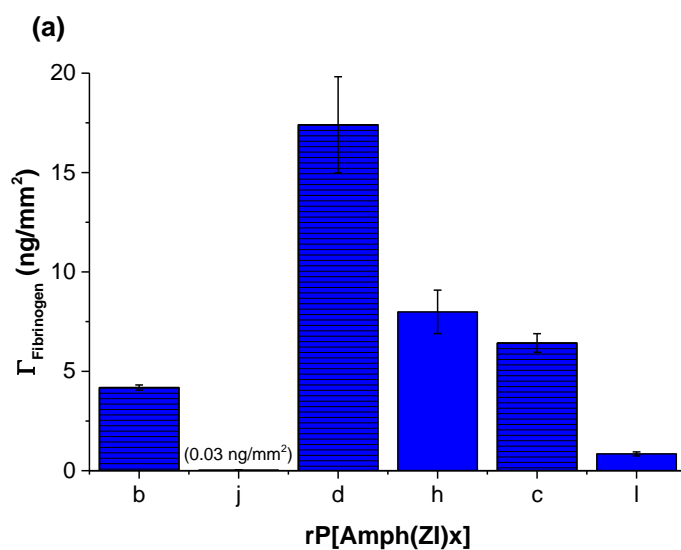


Figure 6.7: Nonfouling properties of **rP[Amph(ZI)a]**, **rP[Amph(ZI)b]**, and **rP[Amph(ZI)c]**: (a) fibrinogen adsorption, and (b) fibrinogen adsorption as a function of advancing water contact angle. Controls are indicated by the shaded bars. Error bars represent \pm standard deviation, based on at least 3 independent measurements.

Next, the effect of fluorination on various hydrophobes was studied by comparing the octyl and perfluoroalkyl (**rP[Amph(ZI)b** and **rP[Amph(ZI)j]**), 3-methylbenzyl and 3-trifluoromethylbenzyl (**rP[Amph(ZI)d** and **rP[Amph(ZI)h]**), and benzyl and pentafluorobenzyl (**rP[Amph(ZI)c** and **rP[Amph(ZI)l]**) surfaces (Figure 6.8). Several surfaces within this subset exhibited high levels of fibrinogen adsorption (Figure 6.8a), namely the **rP[Amph(ZI)c]**, **rP[Amph(ZI)d]** and **rP[Amph(ZI)h]** surfaces (unsubstituted and substituted, non-fluorinated benzyl groups). For all these surfaces, however, the nonfluorinated surfaces (shaded bars) consistently exhibited higher levels of protein adsorption than their fluorinated counterparts by approximately 5 ng/mm². In fact, the **sP[Amph(ZI)j]** surface with the perfluoroalkyl side chain had the lowest amount of protein adsorption out of all the **Amph(ZI)** surfaces, and even suppressed protein adsorption below the 0.1 ng/mm² threshold. While increased hydrophobicity was detrimental to a surface's nonfouling properties in the previous subset, here fluorination appeared to decrease protein adsorption within a hydrophobic series.

No trend was observed, however, when fibrinogen adsorption was plotted against advancing water contact angle (Figure 6.8b). As surface free energy is thought to be more indicative of amphiphilic materials' surface chemistry, fibrinogen adsorption was also plotted against surface free energy (Figure 6.8c).^{4,5} There was no general trend for this plot, meaning that surface free energy was not correlated with protein adsorption across the surfaces in this subset. It could be argued, however, that the plot contained two separate domains, both with a positive correlation between fibrinogen adsorption and surface free energy. To better understand this data, advancing water contact angle (open black bars) and surface free energy (solid blue bars) were plotted for the nonfluorinated

and nonfluorinated (shaded bars) surfaces in Figure 68.d. While no trend was again observed for the water contact angle values, it could be seen that the surface energies of the fluorinated surfaces were once again less than those of their nonfluorinated counterparts. For structurally similar hydrophobes – alkyl, aromatic, and substituted aromatic – the addition of fluorinated moieties reduced the surface free energy of the resulting coatings, and subsequently reduced protein adsorption as well.



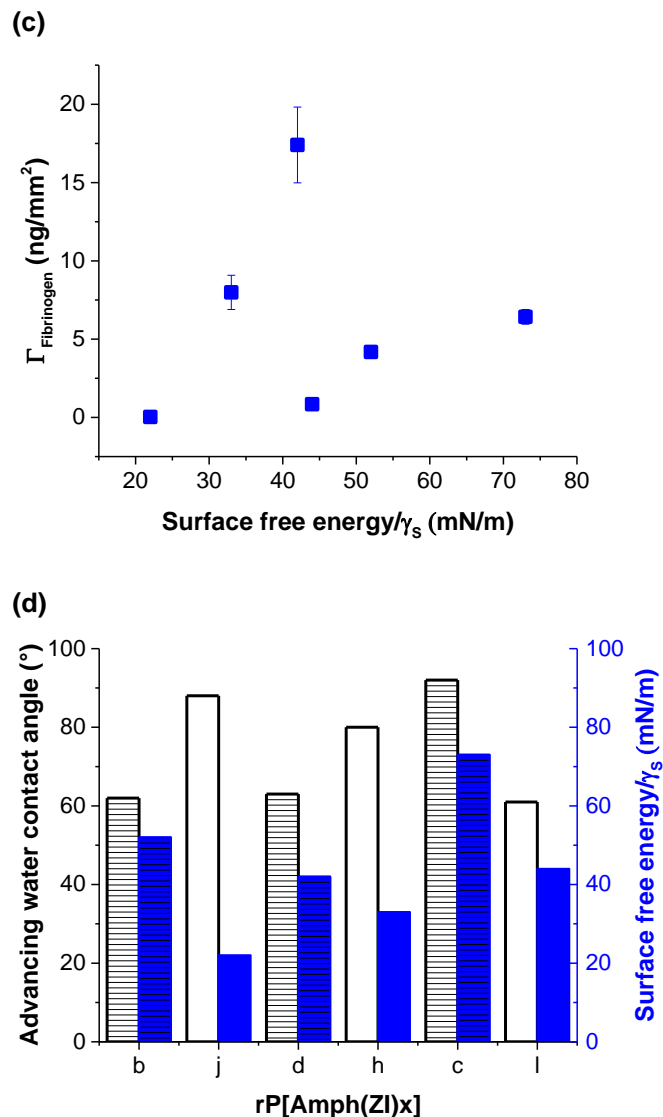


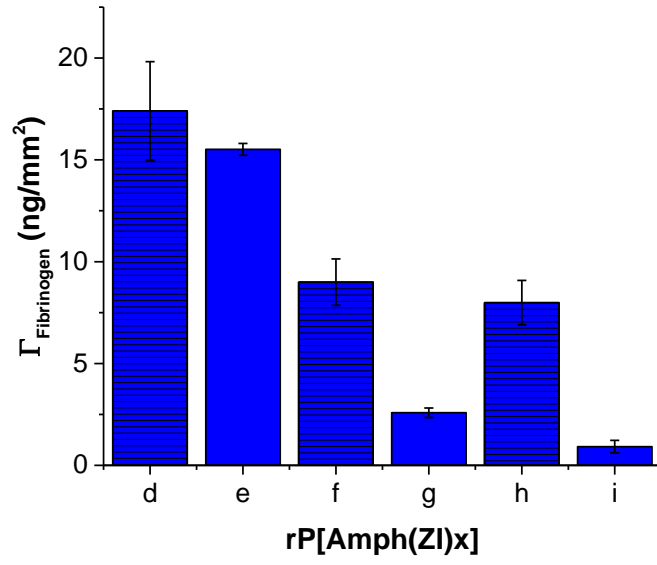
Figure 6.8: Nonfouling properties of rP[Amph(ZI)b], rP[Amph(ZI)g], rP[Amph(ZI)d], rP[Amph(ZI)h], rP[Amph(ZI)c], and rP[Amph(ZI)l]: (a) fibrinogen adsorption, (b) fibrinogen adsorption as a function of advancing water contact angle, (c) fibrinogen adsorption as a function of surface free energy, and (d) advancing water contact angle (open black bars) and surface free energy by surface (solid blue bars). Nonfluorinated surfaces are indicated by the shaded bars. Error bars represent \pm standard deviation, based on at least 3 independent measurements.

An interesting feature of the benzyl hydrophobes was that they allowed for both symmetric and asymmetric substituents (both hydrocarbon and fluorinated) around the aromatic ring. While this structural difference may seem minor, anything that effects the

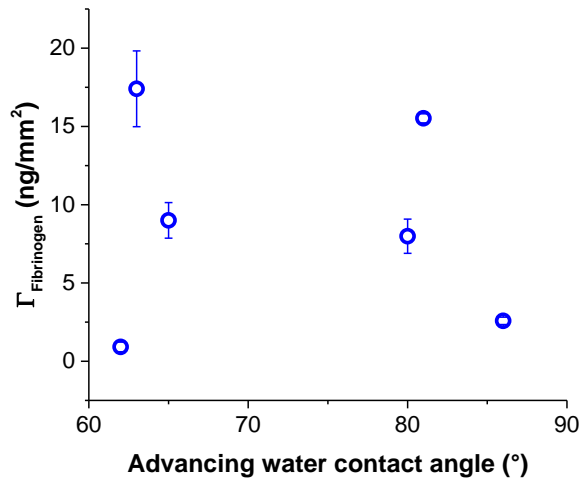
electronic properties around the ring or its interactions at the interface could potentially affect the nonfouling performance of the resulting surface. Thus, surfaces with asymmetrically substituted and symmetrically substituted benzyl groups were compared next in Figure 6.9. Fibrinogen adsorption for the 3-methylbenzyl and 3,5-dimethylbenzyl (**rP[Amph(ZI)d]** and **rP[Amph(ZI)e]**), 3-fluorobenzyl and 3,5-difluorobenzyl (**rP[Amph(ZI)f]** and **rP[Amph(ZI)g]**), and 3-trifluoromethylbenzyl and 3,5-bis(trifluoromethyl)benzyl (**rP[Amph(ZI)h]** and **rP[Amph(ZI)i]**) surfaces is shown in Figure 6.9a, where the surfaces with the asymmetrical benzyl hydrophobes are shaded.

Protein adsorption for the 3-methylbenzyl (**rP[Amph(ZI)d]**) and 3,5-dimethylbenzyl (**sr[Amph(ZI)e]**) surfaces exhibited similar amounts of fibrinogen adsorption, thus the position of the benzyl substituents did not appear to influence the nonfouling properties of these surfaces. Both of the methyl-substituted benzyl surfaces, however, adsorbed more fibrinogen (approximately 20 ng/mm²) than the unsubstituted benzyl surface (7 ng/mm²). For the fluorinated surfaces (**rP[Amph(ZI)f]** and **rP[Amph(ZI)g]**, and **rP[Amph(ZI)h]** and **rP[Amph(ZI)i]**), the position of substituents *did* make a difference, where the asymmetrically substituted surfaces adsorbed approximately 5 – 7 ng/mm² more protein than the symmetrically substituted surfaces.

(a)



(b)



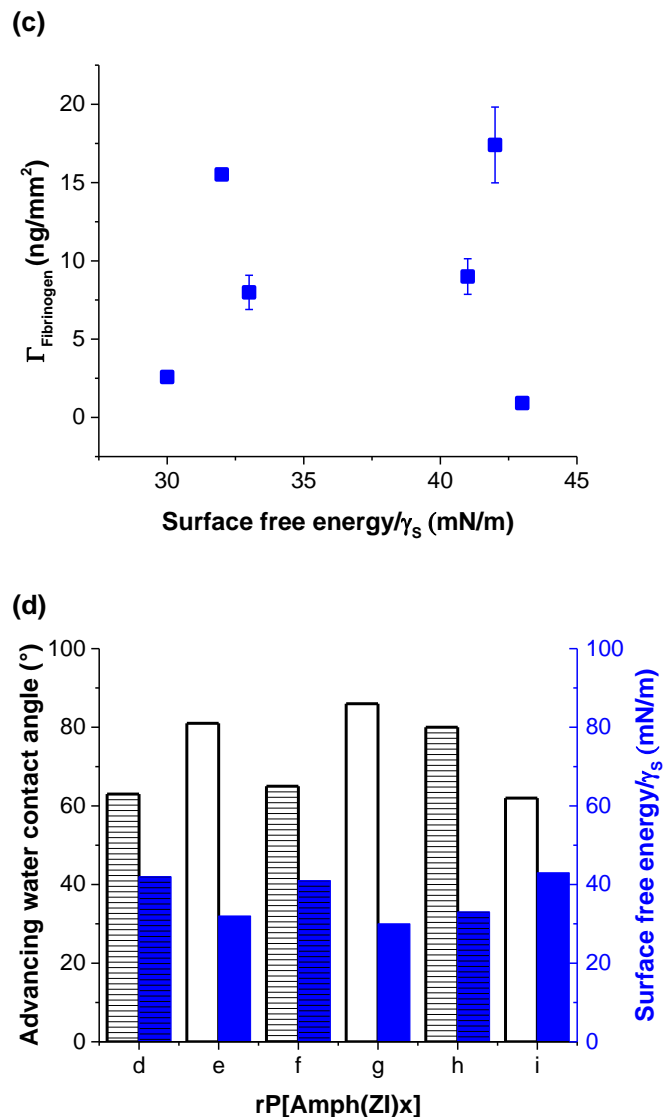


Figure 6.9: Nonfouling properties of rP[Amph(ZI)d], rP[Amph(ZI)e], rP[Amph(ZI)f], rP[Amph(ZI)g], rP[Amph(ZI)h], and rP[Amph(ZI)i]: (a) fibrinogen adsorption, (b) fibrinogen adsorption as a function of advancing water contact angle, (c) fibrinogen adsorption as a function of surface free energy, and (d) advancing water contact angle (open black bars) and surface free energy by surface (solid blue bars). Asymmetrically substituted benzyl surfaces are indicated by the shaded bars. Error bars represent \pm standard deviation, based on at least 3 independent measurements.

The cause for this discrepancy between the symmetric and asymmetric fluorinated benzyl surfaces was not readily apparent, so the surface properties for this group were more closely examined. There was no clear trend between either fibrinogen adsorption

and advancing water contact angle (Figure 6.9b), or fibrinogen adsorption and surface free energy (Figure 6.9c). For that matter, there was no general trend between the substituent positions and advancing water contact angle (open bars) or surface free energy (solid bars) in Figure 6.9d. The complex nature of this data speaks to both the intricacies of amphiphilic surfaces as well as nonfouling properties. A trend was been observed in the protein adsorption data, however it did not correlate with any of the other surface properties such as roughness or surface free energy. While it is possible that the complicated surface chemistry interacted with proteins in ways that were not observable through our other surface-sensitive characterization techniques, it is also possible that the trend was an over-extrapolation of the data. More in-depth surface characterization would be necessary to truly elucidate the interfacial chemistry for these benzyl-containing surfaces.

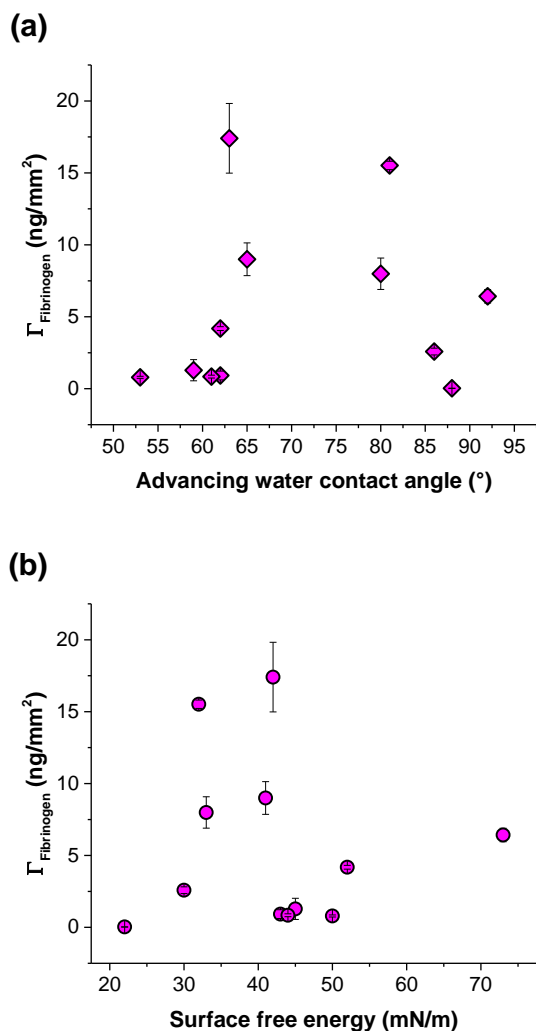


Figure 6.10: Fibrinogen adsorption as a function of (a) advancing water contact and (b) surface free energy for the **Amph(ZI)** series.

Finally, fibrinogen adsorption for the entire **Amph(ZI)** series was plotted as a function of advancing water contact angle (Figure 6.10a) and surface free energy (Figure 6.10b). In both cases, no trend was observed between protein and the given surface property across the entire series. We showed above that trends existed within smaller subsets of the series, but overall the series contained too many disparate chemistries to compare all the surfaces to one another.

6.5 Sum Frequency Generation Spectroscopy

While characterization techniques such as contact angle measurements and protein adsorption act as probes of the surfaces' properties, none of the above analyses could give an accurate picture of the **Amph(ZI)** series' surface chemistry. Fibrinogen adsorption gave some idea of the surfaces' interactions with an aqueous environment, but the biofouling process is influenced by many factors and the actual surface structure in water was still unknown. To better understand the surface chemistry of these amphiphilic surfaces, sum frequency generation (SFG) spectroscopy was employed.¹² With this nonlinear spectroscopy technique, an input signal consists of visible and IR beams that overlap at and reflect off of the sample's surface.¹³ The output signal contains molecular information about the surface. This technique is advantageous because a signal is only obtained from the surface, and not the bulk, so that phenomena like surface rearrangement in different environments can be observed. Furthermore, SFG spectroscopy can be easily employed in aqueous environments for *in situ* measurements, unlike other surface analytical techniques such as XPS.

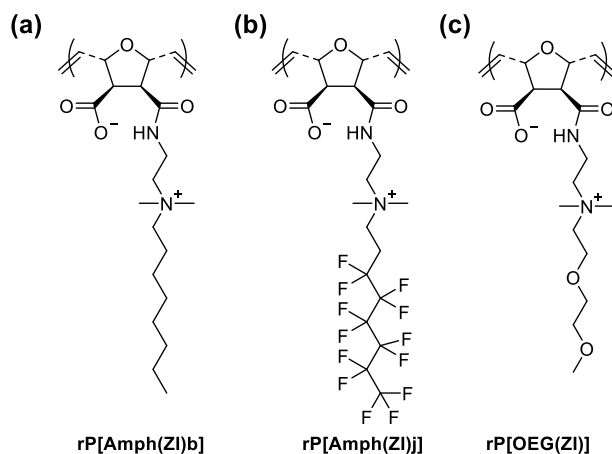


Figure 6.11: Structures of dual-functional betaines studied by SFG spectroscopy: (a) **rP[Amph(ZI)b]**, (b) **rP[Amph(ZI)j]**, and (c) **rP[OEG(ZI)]**.

While SFG spectroscopy is a powerful technique to study nonfouling materials, it is time-consuming and expensive to employ. Therefore, only a few of our surfaces were analyzed by SFG spectroscopy: **rP[Amph(ZI)b]**, **rP[Amph(ZI)j]** and a previously studied hydrophilic dual-functional surface containing an oligo(ethylene oxide) side chain, **rP[OEG(ZI)]**,¹⁰ for comparison. These structures are given in Figure 6.11. As shown above, the **rP[Amph(ZI)b]** and **rP[Amph(ZI)j]** surfaces both contained an octyl side chain but differed by the incorporation of fluorine into the **rP[Amph(ZI)j]** surface. This structural change had a huge impact on the calculated surface energies (52 vs. 22 mN/m) and fibrinogen adsorption (4 vs. 0.03 ng/mm²) for these surfaces. Clearly the fluorinated tail impacted the surface chemistry, but it was unknown how.

Spectra for these surfaces are shown in Figure 6.12, both in air (Figure 6.12a) and in D₂O (Figure 6.12b). Deuterium oxide was used instead of pure water to probe the surface structure in an aqueous environment to reduce interference from a strong water signal. Between 2700 and 3100 cm⁻¹, no signal was observed in air for the **rP[Amph(ZI)j]** surface. Peaks were observed at 2850 and 2880 cm⁻¹, and 2820 cm⁻¹ for the **rP[Amph(ZI)b]** and **rP[OEG(ZI)]** surfaces, respectively, that corresponded to –CH₂– and –CH₃, and –OCH₃ groups. From this data, it appeared that alkyl groups *were not* present at the air interface for the **rP[Amph(ZI)j]** surface, while the octyl and OEG side chains *were* present at the interface for the other surfaces.

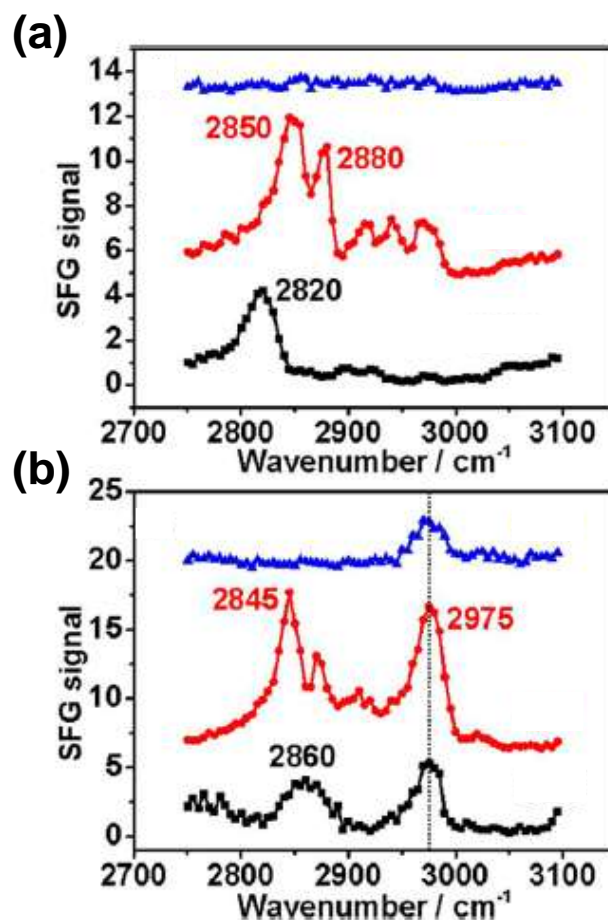


Figure 6.12: SFG spectra of **rP[OEG(ZI)]** (black line), **rP[Amph(ZI)b]** (red line), and **rP[Amph(ZI)j]** (blue line) (a) in air, and (b) in D₂O. The peak at 2975 cm⁻¹ corresponding to the quaternary amine group is highlighted with a dotted line. (Reproduced from Leng *et al*, ACS Macro Letters, 2013.)

When the surfaces were submerged in water, however, the SFG spectra clearly changed. A peak appeared at 2975 cm⁻¹ for all surfaces, which was assigned to the quaternary amine group (either -CH₂N- or -NCH₃). Whereas the cationic group was not observed in air, it appeared to migrate to the surfaces' interfaces in water for the hydrophilic, hydrophobic and lipophobic surfaces. Within this region, no other peaks were observed for the **rP[Amph(ZI)j]** surface. Peaks corresponding to the -CH₂-, -CH₃, and -OCH₃ groups were again observed in the spectra for the other two surfaces,

implying that the octyl and OEG side chains were again present at the surface and did not migrate due to the change in environment. While it was expected that the OEG side chain would be present at the surface in water due to its hydrophilicity, it was interesting to note that the octyl chain also remained at the surface despite its hydrophobicity.

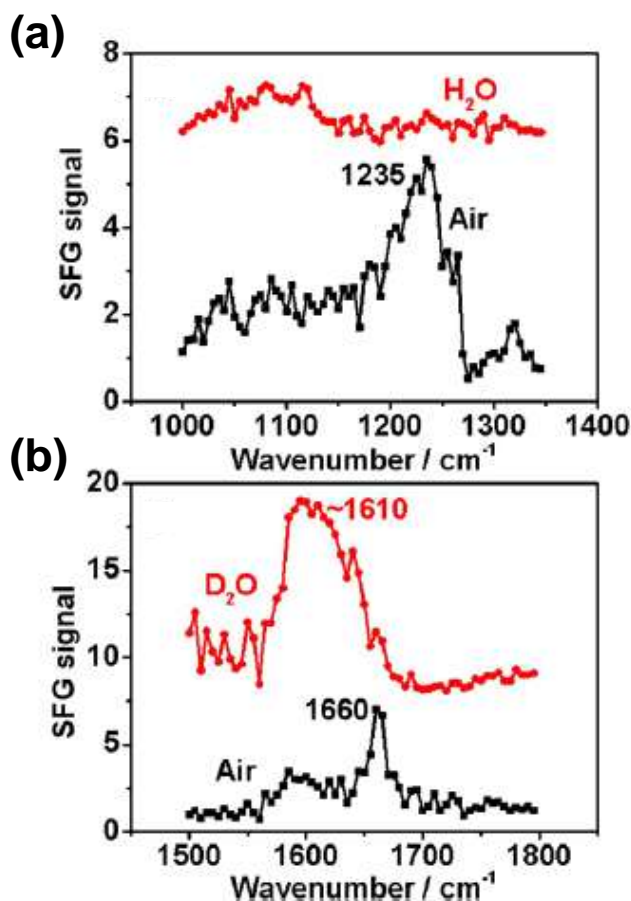


Figure 6.13: SFG spectra of **rP[Amph(ZI)j]** in air (black line) and in D₂O (red line) for the (a) C-F and (b) –C=O functional groups. (Reproduced from Leng *et al*, ACS Macro Letters, 2013.)

It was also important to understand the location of the fluorinated side chain in the **rP[Amph(ZI)j]** surface to truly understand the behavior of these materials. SFG spectra were thus obtained in the –CF (Figure 6.13a) and –C=O (Figure 6.13b) vibrational frequency regions both in air (black line) and in D₂O (red line). As shown in Figure

6.13a, a peak corresponding to the -CF group at 1235 cm^{-1} was observed in air but not in D_2O . Conversely, the carboxylate peak was visible in both the air and D_2O spectra (Figure 6.13b), although the peak experienced a red shift from air to water (1660 to 1610 cm^{-1}). The shift and increased intensity of the carboxylate peak in the presence of water indicated a more structured functional group, which could be a result of greater hydrogen bonding.

Taken together, the SFG spectra created a detailed picture of these surfaces' interfacial chemistries. When hydrated, the quaternary amine group migrated to the surface for all samples, regardless of surface chemistry. It appeared that the zwitterionic component was available at the interface for all the dual-functional betaines, meaning that it was available to interact with the environment including proteinaceous material. These surfaces, however, exhibited a range of protein adsorption values: $\Gamma_{\text{Fibrinogen}} = 0.04\text{ ng/mm}^2$ (**rP[OEG(ZI)]**), $\Gamma_{\text{Fibrinogen}} = 0.03\text{ ng/mm}^2$ (**rP[Amph(ZI)j]**) and $\Gamma_{\text{Fibrinogen}} = 4\text{ ng/mm}^2$ (**rP[Amph(ZI)b]**). Thus, the surfaces' properties appeared to be dictated primarily by the side chain chemistries. In the case of the **rP[OEG(ZI)]** surface, the OEG side chain was present at the interface regardless of environment. This surface's high efficacy was likely a result of its hydrophilicity ($\theta_{\text{A}} = 32^\circ$) due to the combined effect of the zwitterionic component and the readily available OEG side chain.

Similarly, the octyl side chain of the **rP[Amph(ZI)b]** surface was present at the interface both in air and in water. Despite the presence of the charged quaternary amine functionality in water, the **rP[Amph(ZI)b]** surface was relatively hydrophobic ($\theta_{\text{A}} = 62^\circ$) due to the octyl side chain's contribution to the interfacial chemistry. Its hydrophobicity was reflected in surface's protein adsorption ($\Gamma_{\text{Fibrinogen}} = 4\text{ ng/mm}^2$).

Based on the **rP[Amph(ZI)b]** and **rP[OEG(ZI)]**, it appeared that increasing hydrophobicity increased protein adsorption. The **rP[Amph(ZI)j]** surface performed on par with the **rP[OEG(ZI)]** surface in resisting protein adsorption, despite its advancing water contact angle of 88°. The SFG spectra provided the most insight into this phenomenon. Although the fluorinated side chain coated the surface in air due to its low surface energy, it migrated back into the bulk when the surface was placed in water. The hydrophobic component, therefore, was unavailable to interact with the proteins. Furthermore, as the fluorinated tails retreated into the bulk, the zwitterionic moieties became more prominent at the surface, which could reduce protein adsorption. This behavior appeared to mimic that observed in other amphiphilic materials by SFG or NEXAFS, such as the surface active block copolymers (SABC), where the perfluorinated side chain rearranged itself on the surface based on the interfacial environment.^{1,2,7,8} This result was interesting because our polymers contained a charged hydrophilic group instead of a PEG derivative, and a brittle, crosslinked network structure instead of the typically elastomeric nature of the SABCs.

Due to the involved nature of SFG spectroscopy, it was not feasible to study other amphiphilic surfaces, specifically those containing benzyl derivatives. The behavior seen in the **rP[Amph(ZI)j]** surface, however, could be extrapolated to the **rP[Amph(ZI)f-i]** surfaces. We hypothesized that the benzyl groups could freely rotate due to the methyl linkage between the hydrophobe and the quaternary amine. When exposed to water, the bulky, high surface energy benzyl group would be more likely to reorient itself on the surface rather than migrating into the bulk. The fluorinated substituents, however, could provide a driving force for the benzyl groups to migrate away from the interface. In the

case of the asymmetric substituents in the 3-position (**rP[Amph(ZI)f]** and **rP[Amph(ZI)h]** surfaces), the benzyl group could rotate so that the fluorinated moiety was positioned away from the water interface; the benzyl group would still be present in high concentrations at the interface however, like the octyl chains. When the benzyl groups contained fluorinated substituents in the 3 and 5 positions, it might be more favorable for the hydrophobe to migrate into the bulk and drive the zwitterionic groups up to the interface, as seen with the perfluoroalkyl chain. This change in surface chemistry could help resist protein adsorption when compared to the more hydrophobic interfaces. Again, this explanation for the trends seen with the **rP[Amph(ZI)f-i]** surfaces is conjecture based on limited SFG spectra. More in-depth surface analysis would be necessary to truly elucidate the surface chemistry for the entire **Amph(ZI)** series.

6.6 Experimental Procedures

6.6.1 Materials

All reagents were purchased from either Sigma-Aldrich, Alfa Aesar, Acros Organics, or Fisher Scientific in the highest purity available and used as received, unless otherwise noted. 5-(bicycloheptenyl)triethoxysilane (**3**) was purchased from Gelest Inc. and used as received. Tetrahydrofuran (THF, Fisher Scientific, HPLC grade) was distilled from sodium/benzophenone under nitrogen and dichloromethane (CH₂Cl₂, Fisher Scientific, ACS grade) was distilled from CaH₂ under nitrogen immediately prior to use. 2,2,2-trifluoroethanol (TFE, 99+%) was purchased from Alfa Aesar and used as received. Grubbs' 3rd generation catalyst (G3) was synthesized according to a previously reported procedure.¹⁴ Fibrinogen was purchased from Calbiochem as a lyophilized powder.

Phosphate buffered saline (PBS, 0.01M) was purchased from Sigma Aldrich free of serum proteins as a powder and reconstituted in distilled water prior to use.

6.6.2 Instrumentation and methodology

Nuclear magnetic resonance (NMR) spectra were obtained on a Bruker DPX-300 NMR spectrometer. Abbreviations for assignments are as follows: s: singlet; t: triplet; q: quartet; m: multiplet; comp: overlapping non-equivalent peaks; br: broad.

Grazing angle Fourier transform infrared (FT-IR) spectra for the coatings were obtained on a Thermo Scientific Nicolet 6700 spectrometer with a Harrick germanium attenuated total reflection (ATR) attachment and N₂-cooled MCT/A. Clean silica wafers were used to collect the background spectra. Coating thicknesses of ~1 μm (5 wt/v % polymer/TFE casting solution) were used to improve signal intensity.

Water and hexadecane contact angles were measured using a Rame-Hart telescopic goniometer and a Gilmont syringe with a 24-gauge flat-tipped needle filled with Milli-Q water. Reported values are the average of at least 6 measurements on three unique surfaces. Surface free energies were calculated according to the method given in refs. 4 and 5.

Polymer thickness measurements were made on a LSE model Gaertner Scientific Stokes Ellipsometer, with an angle of incidence of 70° from the normal and a 6328 Å HeNe laser, assuming a thin film model. A refractive index of 1.5 was assumed for the polymer layer. Reported values are the average of five measurements on three unique surfaces.

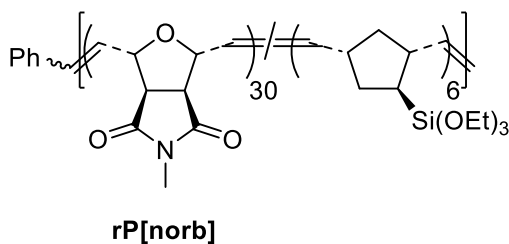
Atomic force microscopy (AFM) images were obtained in tapping mode on a Veeco Dimension 3100 instrument with a Nanoscope III controller with the manufacturer's software. Silicon cantilevers with a spring constant of 0.58 N/m were

used. Root mean squared (rms) roughness values were calculated by the manufacturer's software on a 1 μm x 1 μm image.

X-ray photoelectron spectroscopy (XPS) spectra were recorded on a Physical Electronics Quantum 2000 spectrometer with Al KR excitation at a spot size of 100 μm at 25 W. Spectra were obtained at 15° and 75° takeoff angles with respect to the plane of the sample surface.

6.6.3 Synthesis and characterization

Monomers **Amph(+)**a-**1** were synthesized according to the procedures outlined in Chapter 3. **rP[norb]** was synthesized according to previously published procedures.^{10,15} Yields and spectroscopic data matched those reported.



Representative polymerization procedure: Monomer (**Amph(+)**a) (0.41 g, 0.83 mmol, 30 equivalents) and 5-(bicycloheptenyl)-triethoxysilane (42 μL , 0.16 mmol, 6 equivalents) were weighed into a clean, dry Schlenk flask under N_2 , while G3 (0.024 g, 0.028 mmol, 1 equivalent) was weighed into a second Schlenk flask under N_2 . The monomers were then dissolved in 3 mL 2,2,2-trifluoroethanol plus 1 mL dry CH_2Cl_2 and the catalyst was dissolved in 2 mL dry CH_2Cl_2 . Both solutions were subjected to three freeze-pump-thaw cycles and warmed to room temperature. Using a nitrogen-purged syringe, the monomer solution was added to the catalyst solution. The polymerization was allowed to proceed for 30 minutes at room temperature under N_2 . To quench the reaction, 1.5 mL ethyl vinyl ether was added and the solution was stirred for an additional

hour. The polymer was then precipitated out into anhydrous diethyl ether, isolated by vacuum filtration and dried under high vacuum overnight. Yields were greater than 90% for all polymers. The polymer was stored at -20 °C while not in use.

rP[Amph(+)]a: ^1H NMR (300 MHz, MeOD- d_4): δ (ppm) = 1.07 (br, 3H), 1.24 (br, 9H), 1.88 (br, 2H), 3.26 (br, 6H), 3.46 (br, 2H), 3.68 (comp, 2H + 2H), 3.88 (q, $J = 9.23$ Hz, 6H), 3.99 (br, 2H), 4.75 (br, 1H), 5.22 (br, 1H), 5.52 (br, 1H), 5.62 (br, 1H), 5.92 (br, *cis*, 1H), 6.14 (br, *trans*, 1H), 7.37 (br m, 5H, phenyl endgroup).

rP[Amph(+)]b: ^1H NMR (300 MHz, MeOD- d_4): δ (ppm) = 0.94 (br, 3H), 1.24 (br, 9H), 1.35-1.43 (br, 10H), 1.84 (br, 2H), 3.25 (br, 6H), 3.56 (br comp, 2H + 2H + 2H), 3.88 (q, $J = 9.23$ Hz, 6H), 3.98 (br, 2H), 4.73 (br, 1H), 5.17 (br, 1H), 5.51 (br, 1H), 5.64 (br, 1H), 5.90 (br, *cis*, 1H), 6.14 (br, *trans*, 1H), 7.37 (br m, 5H, phenyl endgroup).

rP[Amph(+)]c: ^1H NMR (300 MHz, MeOD- d_4): δ (ppm) = 1.22 (br, 9H), 2.33 (s, 3H), 3.03 (br), 3.07 (br, 6H), 3.52 (br comp, 2H + 2H), 3.87 (br m, 6H), 4.05 (br, 2H), 4.58 (br comp, 2H + 1H), 5.09 (br, 1H), 5.44 (br, 1H), 5.55 (br, 1H), 5.81 (br, *cis*, 1H), 6.03 (br, *trans*, 1H), 7.20 (d, $J = 8.10$ Hz, 2H), 7.51 (br, 5H), 7.69 (d, $J = 8.10$ Hz, 2H).

rP[Amph(+)]d: ^1H NMR (300 MHz, MeOD- d_4): δ (ppm) = 1.20 (br, 9H), 2.32 (br comp, 3H + 3H), 3.00 (br, 6H), 3.55 (br comp, 2H + 2H), 3.88 (br m, 6H), 4.03 (br, 2H), 4.53 (br comp, 2H + 1H), 5.10 (br, 1H), 5.38 (br, 1H), 5.57 (br, 1H), 5.81 (br, *cis*, 1H), 6.03 (br, *trans*, 1H), 7.19 (d, $J = 7.91$ Hz, 2H), 7.35 (br, 4H), 7.68 (d, $J = 8.29$ Hz, 2H).

rP[Amph(+)]e: ^1H NMR (300 MHz, MeOD- d_4): δ (ppm) = 1.22 (br, 9H), 2.33 (br comp, 3H + 6H), 3.03 (br, 6H), 3.52 (br comp, 2H + 2H), 3.85 (br m, 6H), 4.05 (br, 2H), 4.58

(br comp, 2H + 1H), 5.10 (br, 1H), 5.41 (br, 1H), 5.60 (br, 1H), 5.81 (br, *cis*, 1H), 6.06 (br, *trans*, 1H), 7.18 (br comp, 2H + 3H), 7.68 (d, $J = 8.08$ Hz, 2H).

rP[Amph(+)]f: ^1H NMR (300 MHz, MeOD- d_4): δ (ppm) = 1.22 (br, 9H), 2.33 (br, 3H), 3.05 (br, 6H), 3.52 (br comp, 2H + 2H), 3.88 (q, $J = 9.29$ Hz, 6H), 4.05 (br, 2H), 4.60 (br comp, 2H + 1H), 5.11 (br, 1H), 5.43 (br, 1H), 5.58 (br, 1H), 5.82 (br, *cis*, 1H), 6.02 (br, *trans*, 1H), 7.20 (d, $J = 7.91$ Hz, 2H), 7.37 (br, 4H), 7.68 (d, $J = 8.10$ Hz, 2H).

rP[Amph(+)]g: ^1H NMR (300 MHz, MeOD- d_4): δ (ppm) = 1.23 (br, 9H), 2.34 (br, 3H), 3.09 (br, 6H), 3.52 (br comp, 2H + 2H), 3.87 (br m, 6H), 4.06 (br, 2H), 4.62 (br comp, 2H + 1H), 5.11 (br, 1H), 5.40 (br, 1H), 5.55 (br, 1H), 5.82 (br, *cis*, 1H), 6.03 (br, *trans*, 1H), 7.20 (comp, 2H + 3H), 7.67 (d, $J = 7.91$ Hz, 2H).

rP[Amph(+)]h: ^1H NMR (300 MHz, MeOD- d_4): δ (ppm) = 1.22 (br, 9H), 2.31 (br, 3H), 3.10 (br, 6H), 3.51 (br comp, 2H + 2H), 3.87 (br m, 6H), 4.09 (br, 2H), 4.65 (br comp, 2H + 1H), 5.11 (br, 1H), 5.40 (br, 1H), 5.59 (br, 1H), 5.82 (br, *cis*, 1H), 6.05 (br, *trans*, 1H), 7.19 (d, $J = 7.91$ Hz, 2H), 7.67 (d, $J = 7.54$ Hz, 2H), 7.87 (br, 4H).

rP[Amph(+)]i: ^1H NMR (300 MHz, MeOD- d_4): δ (ppm) = 1.22 (br, 9H), 2.30 (br, 3H), 3.10 (br, 6H), 3.51 (br, 2H), 3.70 (br, 2H), 3.87 (br m, 6H), 4.09 (br, 2H), 4.65 (br comp, 2H + 1H), 4.81 (br, 1H), 5.57 (br comp, 1H + 1H), 5.82 (br, *cis*, 1H), 6.05 (br, *trans*, 1H), 7.17 (d, $J = 8.10$ Hz, 2H), 7.66 (d, $J = 8.10$ Hz, 2H), 8.22-8.27 (br comp, 3H).

rP[Amph(+)]j: ^1H NMR (300 MHz, DMF- d_7): δ (ppm) = 1.24 (br, 9H), 3.13 (comp, 2H + 3H), 3.49 (br, 6H), 3.90 (br, 2H), 4.03 (br m, 6H), 4.13 (br, 2H), 4.60 (br, 1H), 5.12 (br, 1H), 5.58 (br, 2H), 5.82 (br, *cis*, 1H), 6.05 (br, *trans*, 1H), 7.40-7.55 (br m, 5H, phenyl endgroup).

rP[Amph(+)]k: ^1H NMR (300 MHz, DMF- d_7): δ (ppm) = 1.23 (br, 9H), 3.47 (br comp, 2H + 6H), 3.61-4.16 (br m, 2H + 2H + 6H + 2H + 2H), 5.17 (br comp, 1H + 1H), 5.58 (br comp, 1H + 1H), 5.89 (br, *cis*, 1H), 6.09 (br, *trans*, 1H), 7.40-7.55 (br m, 5H, phenyl endgroup).

rP[Amph(+)]l: ^1H NMR (300 MHz, MeOD- d_4): δ (ppm) = 1.23 (br, 9H), 2.36 (br, 3H), 3.19 (br, 6H), 3.56 (br, 2H), 3.88 (br comp, 6H + 2H), 4.08 (br, 2H), 4.61 (br, 1H), 4.76 (br, 2H), 5.09 (br, 1H), 5.41 (br, 1H), 5.61 (br, 1H), 5.84 (br, *cis*, 1H), 6.07 (br, *trans*, 1H), 7.19 (d, $J = 8.10$ Hz, 2H), 7.29-7.45 (br m, 5H, phenyl endgroup), 7.58 (d, $J = 7.91$ Hz, 2H).

6.6.4 Coating preparation

Casting solutions were prepared as 1 wt/v % polymer solutions (0.01g/1mL) in 2,2,2-trifluoroethanol and filtered through 0.45 μm PTFE filters. Silicon wafers were cut into 1.5 x 1.5 cm substrates, cleaned with piranha solution for 30 minutes, rinsed with RO water and dried under N_2 immediately before use. The polymer solutions were spin-cast onto the silicon substrates at 3000 rpm for 30 seconds. After drying under vacuum overnight, the samples were placed in a sealed desiccator containing concentrated HCl for 1 hour, then heated at 110 $^\circ\text{C}$ for 3 hours to complete the curing process. Any remaining free polymer was extracted from the coating by soaking the samples in PBS for several hours; the samples were rinsed with RO water to remove any buffer salts and dried under N_2 then overnight under high vacuum. The initial thicknesses of the coatings were measured by ellipsometry. AFM and contact angle measurements were taken on freshly prepared surfaces.

6.6.4 Protein adsorption measurements

Fibrinogen solutions (0.5 mg/mL) in PBS buffer were prepared directly before use at room temperature. The samples were placed in individual wells of a 12-well cell culture plate and soaked in PBS buffer for two hours to fully hydrate the surfaces. The coatings were transferred to a clean plate and approximately 3 mL of protein solution were added to each well. The plate was then incubated for two hours at 37 °C. Excess PBS was used to flood the wells to sufficiently dilute the protein, after which the samples were removed from the wells and rinsed further with RO water. The coatings were first dried under a stream of N₂ then overnight under high vacuum. To quantify protein adsorption, the thickness of the adsorbed protein layer was measured by ellipsometry using the published refractive index value of 1.405 for fibrinogen.^{10,16-18} By applying the following equation:

$$\Gamma(\text{ng}/\text{mm}^2) = h \times d$$

where h equals the measured thickness of the protein layer, and d equals fibrinogen density given in the literature^{10,16-18} as 1.085 g/cm³, the amount of adsorbed protein (Γ) was calculated.

6.6.5 Sum frequency generation spectroscopy

Right angle SiO₂ and CaF₂ prisms were purchased from Altos Photonics (Bozeman, MT). A layer of 100 nm SiO₂ was deposited onto each CaF₂ prism by an electron-beam deposition process using an SJ-26 Evaporator system at a pressure below 10⁻⁵ Torr. The deposition rate was 5 Å/s. The SiO₂ prisms and SiO₂ coated CaF₂ prisms were treated with O₂ plasma for 4 minutes in a PE-25-JW plasma cleaner (Plasma Etch, Carson City, NV). The amphiphilic polybetaine coatings were prepared according to the standard procedure. The **rP[OEG(ZI)]** and **rP[Amph(ZI)b]** coatings were prepared on

SiO₂ prisms, and the **rP[Amph(ZI)j]** coating was prepared on the SiO₂-coated CaF₂ prism. The thicknesses of the spin-coated films are around 30 nm, measured by a LSE model Gaertner Scientific Stokes Ellipsometer.

6.7 Conclusions

A novel series of amphiphilic zwitterionic polymers were synthesized for nonfouling applications. These amphiphilic materials contained alkyl, benzyl, and fluorinated hydrophobes. The dual-functional betaine chemistry as described in previous chapters gave rise to zwitterionic component. The modular nature of the oxanorbornene imide monomer allowed for a wide range of zwitterionic chemistries to be achieved through basic synthetic methods, which is a major advantage of this ROMP-based platform. FT-IR was used to confirm the ring-opening of the dual-functional surfaces. AFM revealed that among the amphiphilic chemistries, the 3,5-bis(trifluoromethyl)benzyl surface and perfluoroalkyl surface were the only surfaces that resulted in unique features and increased roughness (5 nm for the perfluoroalkyl surface). Water contact angles were measured to be in the range of 50° - 90° and surface free energies were calculated to be in the range of 20 – 70 mN/m where the perfluoroalkyl surface had the lowest surface energy and the benzyl surface had the greatest. The perfluoroalkyl surface also exhibited the lowest amount of fibrinogen adsorption (0.03 ng/mm²). Other benzyl derivative surfaces exhibited extraordinarily levels of protein fouling with greater than 10 ng/mm². While trends could be discerned within the benzyl subset regarding protein adsorption, overall there was no appreciable correlation throughout the **Amph(ZI)** series between any of the measured surface properties and protein adsorption. Sum frequency generation spectroscopy provided evidence that the fluorinated moieties rearranged on

the amphiphilic surfaces in response to changes in the environment, possibly influencing the nonfouling properties of the surfaces.

6.8 References

- (1) Callow, J. A.; Callow, M. E. Trends in the development of environmentally friendly fouling-resistant marine coatings. *Nat. Commun.* **2011**, DOI: 10.1038/ncomms1251.
- (2) Grozea, C. M.; Walker, G. C. Approaches in designing non-toxic polymer surfaces to deter marine biofouling. *Soft Matter* **2009**, *5*, 4088-4100.
- (3) Genzer, J.; Efimenko, K. Recent developments in superhydrophobic surfaces and their relevance to marine fouling: a review. *Biofouling* **2006**, *22*, 339-360.
- (4) Gudipati, C. S.; Finlay, J. A.; Callow, J. A.; Callow, M. E.; Wooley, K. L. The Antifouling and Fouling-Release Performance of Hyperbranched Fluoropolymer (HBFP)–Poly(ethylene glycol) (PEG) Composite Coatings Evaluated by Adsorption of Biomacromolecules and the Green Fouling Alga *Ulva*. *Langmuir* **2005**, *21*, 3044–3053.
- (5) Gudipati, C. S.; Greenlief, C. M.; Johnson, J. A.; Prayongpan, P.; Wooley, K. L. Hyperbranched Fluoropolymer (HBFP) and Linear Poly(ethylene glycol) (PEG) Based Amphiphilic Crosslinked Networks as Efficient Anti-fouling Coatings: An insight into the surface compositions, topographies and morphologies. *J. Polym. Sci., Part A: Polym. Chem.* **2004**, *42*, 6193-6208.
- (6) Wang, Y.; Finlay, J. A.; Betts, D. E.; Merkel, T. J.; Luft, J. C.; Callow, M. E.; Callow, J. A.; DeSimone, J. M. Amphiphilic Co-networks with Moisture-Induced Surface Segregation for High-Performance Nonfouling Coatings. *Langmuir* **2011**, *27*, 10365-10369.
- (7) Dimitriou, M. D.; Zhou, Z.; Yoo, H-S.; Killips, K. L.; Finlay, J. A.; Cone, G.; Sundaram, H, A.; Lynd, N. A.; Barteau, K. P.; Campos, L. M.; Fischer, D. A.; Callow, M. E.; Callow, J. A.; Ober, C. K.; Hawker, C. J.; Kramer, E. J. A General Approach to Controlling the Surface Composition of Poly(ethylene oxide)-Based Block Copolymers for Antifouling Coatings. *Langmuir* **2011**, *27*, 13762-13772.
- (8) Youngblood, J. P.; Andruzzi, L.; Ober, C. K.; Hexemer, A.; Kramer, E. J.; Callow, J. A.; Callow, M. E. Coatings based on side-chain ether-linked poly(ethylene glycol) and fluorocarbon polymers for the control of marine biofouling. *Biofouling* **2003**, *19*, 91-98.
- (9) Colak, S.; Tew, G. N. Amphiphilic Polybetaines: The Effect of Side-Chain Hydrophobicity on Protein Adsorption. *Biomacromolecules* **2012**, *13*, 1233-1239.

- (10) Colak, S.; Tew, G. N. Dual-Functional ROMP-Based Betaines: Effect of Hydrophilicity and Backbone Structure on Nonfouling Properties. *Langmuir* **2012**, *28*, 666-675.
- (11) Chen, S.; Li, L.; Zhao, C.; Zheng, J. Surface hydration: Principles and applications toward low-fouling/nonfouling biomaterials. *Polymer* **2012**, *51*, 5283-5293.
- (12) Leng, C.; Gibney, K. A.; Liu, Y.; Tew, G. N.; Chen, Z. In Situ Probing the Surface Restructuring of Antibiofouling Amphiphilic Polybetaines in Water. *ACS Macro Lett.* **2013**, *2*, 1011-1015.
- (13) Chen, Z.; Shen, Y. R.; Somorjai, G. A. Studies of polymer surfaces by sum frequency generation vibrational spectroscopy. *Annu. Rev. Phys. Chem.* **2002**, *53*, 437-465.
- (14) Love, J. A.; Morgan, J. P.; Trnka, T. M.; Grubbs, R. H. A Practical and Highly Active Ruthenium-Based Catalyst that Effects the Cross Metathesis of Acrylonitrile. *Angew. Chem. Int. Ed.* **2002**, *41*, 4035-4037.
- (15) Kim, G.-C.; Jeong, J.-G.; Lee, N.-J.; Ha, C.-S.; Cho, W.-J. Synthesis and biological activities of endo-3,5-epoxy-1,2,3,6-tetrahydrophthalimide and its polymers. *J. Appl. Polym. Sci.* **1997**, *64*, 2605-2612.
- (16) Elwing, H. Protein absorption and ellipsometry in biomaterial research. *Biomaterials* **1998**, *19*, 397-406.
- (17) Voros, J. The Density and Refractive Index of Adsorbing Protein Layers. *Biophys. J.* **2004**, *87*, 553-561.
- (18) Sharma, S.; Johnson, R. W.; Desai, T. A. Evaluation of the Stability of Nonfouling Ultrathin Poly(ethylene glycol) Films for Silicon-Based Microdevices. *Langmuir* **2004**, *20*, 348-356.

CHAPTER 7

CHARGED HYDROGELS FROM NORBORNENE-BASED POLYMERS

7.1 Introduction

Chapter 1 described the ring-opening reaction in oxanorbornene imides that occurred in the presence of strong bases. Chapters 2-6 subsequently detailed the synthesis and applications of dual-functional polybetaines resulting from the imide ring-opening to form a carboxylic acid in the presence of sodium hydroxide. The alternative ring-opening reaction, where a primary amine inserted into the imide ring to form two amide groups, was not pursued to an appreciable extent. For one, the resulting diamide polymers exhibited reduced solubility when compared to their imide precursors. An interesting materials application for this reaction, however, was discovered when oxanorbornene imide-based polymers were reacted with multifunctional amines in aqueous solutions. Due to the multiple reaction sites, these reactions resulted in networks. More specifically, when the oxanorbornene imide polymer was water-soluble, a hydrogel was formed.

ROMP had been used previously to create gels, often by copolymerizing mono- and difunctional alkenes,¹ or polymerizing monomers with functional groups that could be crosslinked by an orthogonal reaction.² This new approach utilizing the imide ring-opening reaction was advantageous for several reasons: gelation occurred quickly and spontaneously in water without the need for organic solvent exchange; no additional reagents or by-products were used or produced that need to be leached out; and water uptake, modulus and other physical properties could theoretically be tuned by the selection of the ROMP polymer. With the expanding interest in hydrogels as novel

biomaterials, especially gels with unique chemistries and properties, these ROMP-based networks appeared to be interesting additions to the field.

7.2 Hydrogel Synthesis

7.2.1 Polymer Precursor Synthesis

A series of hydrophilic polymers, given in Figure 7.1, were synthesized to study the formation and properties of these hydrogels. These polymers contained cationic (**Poly1** and **Poly2**) and zwitterionic (**Poly3** and **Poly4**) functionalities that would exhibit the polyelectrolyte and antipolyelectrolyte effects, respectively.⁴⁻¹¹ Furthermore, **Poly1** and **Poly3** contained pH-sensitive tertiary amine and carboxylate groups, respectively, which could potentially impart responsive properties to the gels. In the case of **Poly1**, increasing the pH of swelling solution from acidic to basic (as compared to the tertiary amine's pK_a value) was expected to deprotonate the amine. Because the polymer would then be uncharged, deswelling in water would occur. **Poly3** could transition from cationic to zwitterionic if the carboxylate group were protonated or deprotonated. This transition could potentially control the gels' swelling in electrolyte solutions. Polymers were synthesized as shown in Figure 7.1a, where monomers **1**, **2**, **3(+)**, and **4** were homopolymerized using Grubbs' 3rd generation catalyst in a TFE/CH₂Cl₂ mixture as described previously in Chapter 2.^{12,13} **Poly3** was synthesized in the protected, cationic form **Poly3(+)**, which was then deprotected under acidic conditions to give the zwitterionic form (Figure 7.1b).¹² The degree of polymerization was held constant at 75. High molecular weight polymers were assumed to crosslink more easily; however, solubility could decrease at longer polymer lengths, thus intermediate molecular weights

(<30 kDa) were chosen. Molecular weights were taken as the theoretical values based on complete conversion by ^1H NMR spectroscopy.

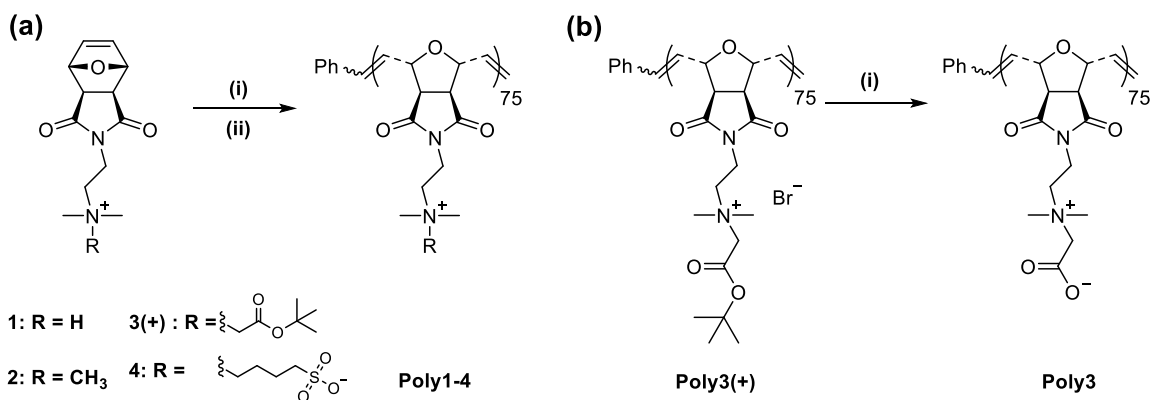


Figure 7.1: Synthesis of poly(oxanorbornene imide) polymer precursors. **(a)** (i) Grubbs' 3rd generation catalyst, TFE/CH₂Cl₂, room temperature, 30 minutes; (ii) ethyl vinyl ether, room temperature, 1 hour; **(b)** (i) 1:1 CH₂Cl₂:TFA, room temperature, overnight.

7.2.2 Gelation

Initially, small molecule diamines were used as potential crosslinkers for the precursor polymers. These primary amines included ethylene diamine, 1,6-diaminohexane, 1,8-diaminooctane, and 1,12-diaminododecane. **Poly2** and **Poly4** were chosen as model polymer chemistries to initially screen the diamines. The polymers were dissolved in pure water (**Poly2**) or 0.1 M NaCl (**Poly4**), and the diamines were dissolved in pure water. The diamine solution was then added to the polymer solution, mixed together by pipetting, and the reaction was allowed to stand. Regardless of the polymer concentration, diamine concentration, or ratio of amine to imide groups (1:10 up to several-fold excess amine), no consistent gelation occurred. It was hypothesized that larger diamines would promote network formation as the second amine's reactivity might be less affected after the first amine had reacted with the imide. None of the diamines up

to 1,12-diaminododecane, however, formed a network with the ROMP polymers. The imide groups' steric hindrance and reduced reactivity of the diamines were thought to prevent gelation.

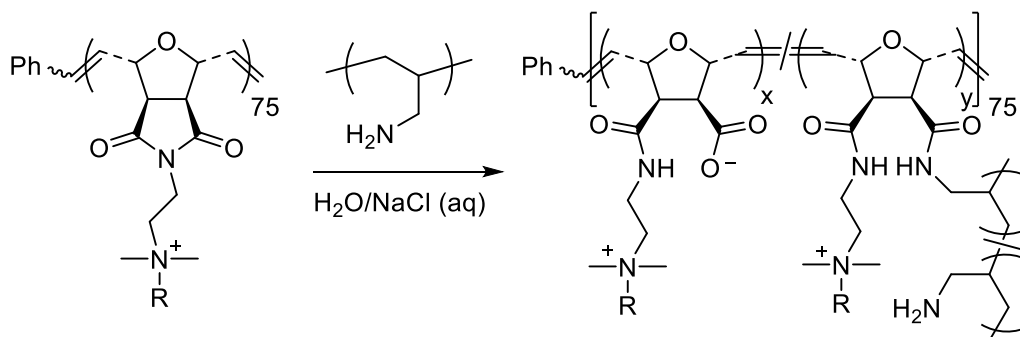


Figure 7.2: General gelation reaction between **Poly1-4** and PAA in water.

Because small molecule diamines did not result in gelation, a multifunctional polymeric amine was used instead (Figure 7.2). Poly(allylamine) (PAA), where $M_w \approx 15$ kDa, was purchased as an aqueous solution and used as received. ROMP polymers **Poly1-4** were dissolved in either pure water (**Poly1-2**) or 0.1 M NaCl (**Poly3-4**) at various concentrations and mixed with PAA in modified syringe molds. Most gels formed within five minutes, while many gelled in less than a minute. Table 7.1 summarizes the conditions that were screened for gel formation. It was found that **Poly1** did not form true gels at any of the given concentrations or amine ratios. While **Poly1** was freely soluble in water, an insoluble mass crashed out of solution when PAA was added. The pK_a of **Poly1**'s tertiary amine was estimated to be about 8.35 based on the titration of similar ROMP polymers,^{1b} while that of PAA's primary amine was taken to be 9.49 based on allylamine's pK_a .¹⁴ In distilled or reverse osmosis water, **Poly1** was assumed to be largely protonated, thus its solubility due to the overall cationic charge. Upon the addition of PAA, **Poly1** would be deprotonated and insoluble in aqueous

solution. While the polymers still appeared to crosslink, based on the precipitate's insolubility in water and organic solvents, homogeneous hydrogels could not be formed and so **Poly1** was not pursued further as a precursor polymer.

Table 7.1: Attempted gelation conditions between **Poly1-4** and PAA

[Poly] (g/mL)	[PAA]:[Poly] (mol:mol)	Poly1	Poly2	Poly3	Poly4
0.025	3:1	N. D.	-	+	+
0.025	1.5:1	N. D.	-	+	+
0.05	3:1	-	-	+	+
0.1	3:1	-	+	+	+
0.1	1.5:1	-	+	+	+
≤0.1	≤1:1	-	-	N. D.	-

(+) = gel formed; (-) = no gel formed; N. D. = not determined.

As shown in Table 7.1, **Poly2**, **Poly3**, and **Poly4** readily formed gels with PAA. In general, all polymers required a slight excess of amine to form a stable gel, regardless of the polymer precursor concentration. Gels formed when a larger excess (three-fold) of PAA was used as well, but not when the imide was in excess. A noticeable increase in solution viscosity, however, was observed when the ROMP polymer was only in slight excess. In the case of cationic **Poly2**, gels only formed when the polymer concentration was equal to or greater than 0.1 g/mL in the precursor solution. Interestingly, the zwitterionic **Poly3** and **Poly4** polymers formed gels at concentrations down to 0.025 g/mL, approximately four times more dilute than **Poly2**'s gelation threshold concentration. All polymers were the same length and similar molecular weights, so those properties were ruled out as factors contributing to the gelation discrepancies. The physical appearances of the cationic and zwitterionic gels differed as well. Whereas the

Poly2 gels were homogeneous and transparent (Figure 7.3a), the **Poly3** and **Poly4** gels were completely opaque (Figure 7.3b).

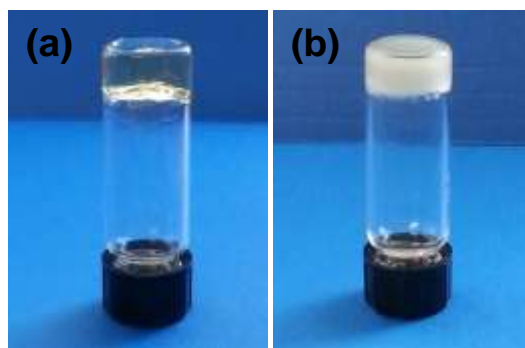


Figure 7.3: Resulting gels from (a) **Poly2/PAA** and (b) **Poly3/PAA**.

Opacity generally indicates a heterogeneous network structure. The zwitterionic gels were formed in salt solutions to ensure that the polymers were completely soluble in the precursor solutions. These solutions began to take on an opaque appearance shortly after PAA was added but prior to gel formation. Because polymer solubility decreases as molecular weight increases, it was thought that the zwitterionic polymers' increased molecular weight due to the formation of crosslinks prior to the gel point decreased their solubility in the electrolyte solution. Inter- and intramolecular interactions between the zwitterionic groups then increased as the overall solubility decreased and caused the polymers to collapse on themselves, which would increase the local concentration of the reactive groups. Gels could then form at lower overall concentrations. The opacity could be a result of a heterogeneous network as well as additional physical crosslinks between the zwitterionic side chains, such as those that form in ampholytic gels and saloplastics.^{15,16}

7.3 Gel Characterization

7.3.1 Network Chemistry

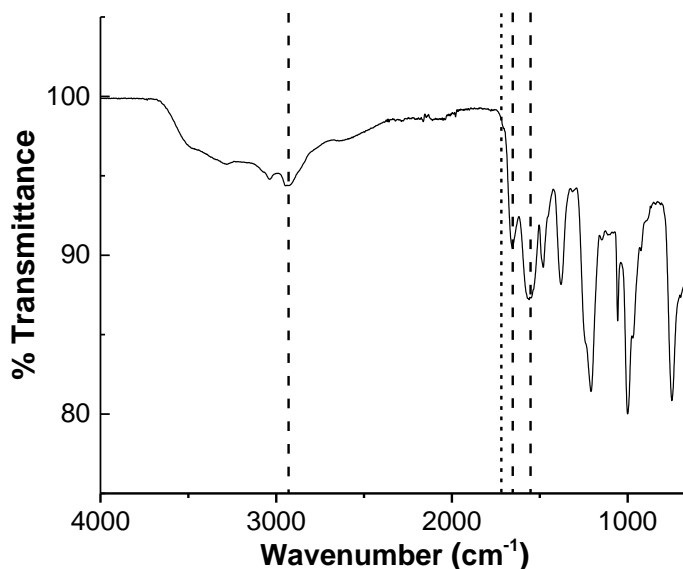


Figure 7.4: Representative IR spectrum of a dehydrated **Poly2**/PAA gel. Frequencies corresponding to imide groups (fine dotted line) and amide and carboxylate groups (bold dotted lines) are marked for clarity.

FT-IR spectroscopy was used to confirm the crosslinking reaction in the gels (Figure 7.4). A **Poly2**/PAA gel was prepared and residual unreacted material was extracted in pure water. The gel was then fully dried and analyzed. The FT-IR spectrum showed that imide groups (fine dotted line) were completely consumed, and only peaks from the ring-opened product – amide and carboxylate groups – were observed (bold dotted lines). Even though an excess of amine was used, not all the imide groups were converted to diamide crosslinks. As evidenced by the peak at approximately 1560 cm⁻¹, the remaining imide groups were ring-opened to form amide and carboxylate pairs. The relative intensities of the peaks, however, imply that the majority of the imide groups

were converted to diamide pairs. The change in solution pH due to the addition of PAA was most likely responsible for ring-opening the remaining imide groups during network formation. Other analytical techniques such as solid state NMR were attempted to better understand the molecular structure of the gels, but the gels were too highly hydrated and thus the relevant functional groups were too dilute to obtain any useful information.

7.3.2 Swelling Properties and Water Uptake

The swelling properties and water uptake of these hydrogels were measured at different salinities and pH values. Because the network structure of these gels were thought to be complex and heterogeneous, we had hoped to elucidate some of their structural aspects by indirectly observing their swelling behavior. Here, the swelling ratio Q was calculated as the ratio of the gels' swollen volume over the dry weight (V_s/W_d) and equilibrium water content $W.C.$ was calculated as $[(W_s - W_d)/W_s]*100$, where W_s was taken as the gel's swollen weight. These gels were found to be fragile and difficult to handle, making it difficult to obtain measurements and robust data.

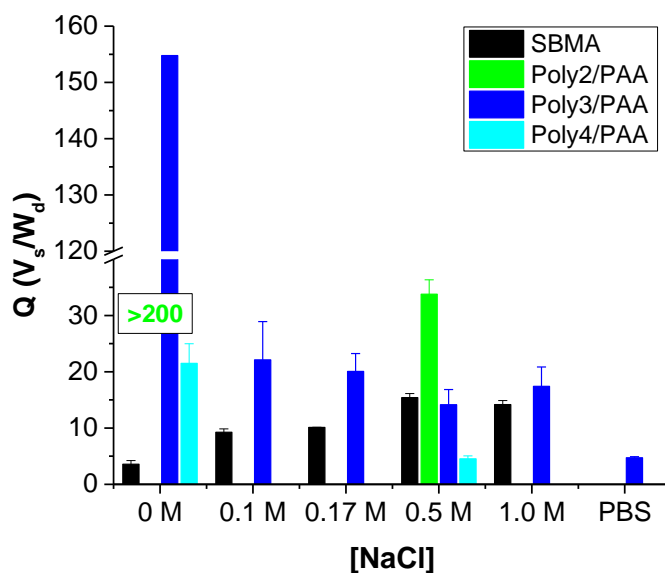


Figure 7.5: Swelling ratios of an **SBMA** control gel, and **Poly2/PAA**, **Poly3/PAA**, and **Poly4/PAA** gels (1/1.5 mol/mol) at varying salt concentrations. Error bars represent \pm standard deviation based on at least three samples, when available.

Figure 7.5 shows a plot of swelling ratios for gels swollen in aqueous solutions at different salinities. The pH of these solutions was approximately 5, except for the phosphate-buffered saline which was assumed to be neutral (7.4). The **Poly2/PAA**, **Poly3/PAA**, and **Poly4/PAA** gels were all synthesized at a molar ratio of 1:1.5 imide:amine. A control zwitterionic gel was synthesized by redox polymerization from sulfobetaine methacrylate (**SBMA**) and *N,N*-methylene(bisacrylamide) as the crosslinker. Clear, tacky gels were obtained from this chemistry. As the salt concentration of the swelling solution increased, the swelling ratio of the **SBMA** gels increased from 5 at 0 M NaCl (pure water) to 15 at 0.5 M and 1.0 M NaCl (black bars). Sulfobetaine polymers exhibit the antipolyelectrolyte effect, meaning they swell and take on an extended coil conformation in electrolyte solutions and collapse in pure water.^{6,7} This effect was

reflected in the swelling data, where the **SMBA** gels swelled more as the salt concentration of the solution increased.

The **Poly3/PAA** gels (blue bars) contained the carboxybetaine moiety, which also would be expected to exhibit the antipolyelectrolyte effect at this pH, however their swelling behavior was actually opposite that of the **SBMA** gels. In pure water, the **Poly3/PAA** gels swelled the most ($Q = 155$) and exhibited swelling ratios of around $Q = 20$ in the NaCl solutions. Interestingly, the **Poly3/PAA** gels deswelled even more in PBS at a salt concentration of approximate 0.1 NaCl and a pH of 7.4, even though at neutral pH the carboxybetaine groups should be zwitterionic and not cationic. These gels swelled the most in pure water, implying the polyelectrolyte effect. The **Poly4/PAA** gels containing the zwitterionic sulfobetaine group behaved similarly (cyan bars). In pure water $Q = 20$ whereas in 0.5 M NaCl $Q = 5$. While the swelling trend was similar to that of the **Poly3/PAA** gels, the actual swelling ratios were much smaller, which may imply a more tightly crosslinked network.

Based on the stoichiometry of the reaction, there was assumed to be an excess of cationic primary amines in the gel, which should be highly hydrated in pure water. The IR spectra of dried gels shows the presence of carboxylate groups, which were thought to be a result of imide groups ring-opening but not reacting to form a diamide with the PAA. Again, because quantitative characterization of the gel chemistry was extremely difficult, the exact nature of the charged functional groups was unknown. This swelling data strongly implied, however, that the gels contained an excess of cationic groups regardless of the zwitterionic polymer precursor. When a cationic precursor polymer was used, as in the case of the **Poly2/PAA** gels (green bar), the gels swelled so much in pure

water that they broke apart ($Q > 200$) and an accurate swelling ratio could not be calculated. When swollen in 0.5 M NaCl, however, the gels deswelled so that $Q = 35$. This behavior was in line with expectations due to the cationic nature of both **Poly2** and presumably the unreacted amine groups in PAA.

Equilibrium water content for almost all gels was above 90%, except for the **SBMA** gels in pure water and the **Poly2**/PAA gels in PBS, where W.C. = 70%. In salt water and pure water these gels are highly hydrated, which can be advantageous for many applications.³ Gel fractions (the amount of material incorporated into the network) were even more difficult to calculate due to the fragile nature of the gels. It was common to lose appreciable segments of the gel during the weighing and measuring processes as they came into contact with the weigh boats and calipers. A more delicate procedure would be advantageous to more accurately measure the physical properties of these gels. Likewise, an in-depth study on the effect of solution pH on swelling properties was not completed due to the gels' seeming instability in basic environments.

The swelling and solution properties of these gels failed to quantitatively define their chemical structure. All gels, regardless of the precursor polymer, swelled in pure water and deswelled in salt water. This behavior implied that the gels carried a net charge and were ampholytes in nature but the results were not necessarily conclusive.⁵⁻¹¹ Further characterization is needed to truly elucidate their chemistry. In the future, mechanical testing and more advanced analytical techniques would be necessary to characterize these gels.

7.4 Experimental Procedures

7.4.1 Materials

All reagents were purchased from either Sigma-Aldrich, Alfa Aesar, Acros Organics or Fisher Scientific in the highest purity available and used as received, unless otherwise noted. 1,3-dinitrobenzene was obtained from Avocado Research Chemicals and used as received. Poly(allylamine) (MW = 15,000 g/mol; 15% solids in water) was purchased from Polysciences, Inc. Tetrahydrofuran (THF, Fisher Scientific, HPLC grade) was distilled from sodium/benzophenone under nitrogen and dichloromethane (CH₂Cl₂, Fisher Scientific, ACS grade) was distilled from CaH₂ under nitrogen immediately prior to use. 2,2,2-trifluoroethanol (TFE, 99+%) was purchased from Alfa Aesar and used as received. Grubbs' 3rd generation catalyst (G3) was synthesized according to a previously reported procedure.¹⁷

7.4.2 Instrumentation and methodology

Nuclear magnetic resonance (NMR) spectra were obtained on a Bruker DPX-300 NMR spectrometer. Abbreviations for assignments are as follows: s: singlet; t: triplet; q: quartet; m: multiplet; comp: overlapping non-equivalent peaks; br: broad.

Fourier transform infrared (FT-IR) spectra were recorded by a PerkinElmer Spectrum 100 spectrometer with a universal ATR sampling accessory and ZnSe crystal.

7.4.3 Synthesis

Monomers **1**, **2**, **3(+)**, and **4** were synthesized as described in Chapter 2. Yields and spectroscopic data matched those reported.^{12,13}

Representative polymerization procedure: Monomer (**1**) (0.3 g, 0.80 mmol, 75 equivalents) was weighed into a clean, dry Schlenk flask under N₂, while G3 (0.0095 g,

0.01 mmol, 1 equivalent) was weighed into a second Schlenk flask under N₂. The monomer was then dissolved in 3 mL 2,2,2-trifluoroethanol plus 1 mL dry CH₂Cl₂ and the catalyst was dissolved in 2 mL dry CH₂Cl₂. Both solutions were subjected to three freeze-pump-thaw cycles and warmed to room temperature. Using a nitrogen-purged syringe, the monomer solution was added to the catalyst solution. The polymerization was allowed to proceed for 30 minutes at room temperature under N₂. To quench the reaction, 1.5 mL ethyl vinyl ether was added and the solution was stirred for an additional hour. The polymer was then precipitated out into anhydrous diethyl ether, isolated by vacuum filtration and dried under high vacuum overnight. Yields were greater than 90% for all polymers. The polymer was stored at -20 °C while not in use.

Poly3(+) deprotection procedure: The polymer was placed in a scintillation vial and was dissolved in a minimum amount of 1:1 CH₂Cl₂. The solution was stirred overnight at room temperature. The polymer was then precipitated out twice into anhydrous diethyl ether and dried under high vacuum. Deprotection was confirmed by ¹H NMR and IR spectroscopy.

7.4.4 Gel formation

Polymers were dissolved in either reverse osmosis water (**Poly1-2**) or 0.1 M NaCl (**Poly3-4**) at the given concentration. The polymer solution was added to a modified 3 mL syringe mold and the PAA solution (as received) as added. The reaction was then gently agitated to ensure complete mixing. A gel formed within a minute or so. The gels were allowed to sit undisturbed for approximately 5 minutes, and were then demolded into the swelling solution.

To form the **SBMA** gels, [2-(methacryloyl)ethyl]-dimethyl-(3-sulfopropyl)-ammonium hydroxide (sulfobetaine methacrylate/**SBMA**) was dissolved in 0.1 M NaCl at a concentration of approximately 0.25 g/mL. 1.5 mol % *N,N*-methylenebisacrylamide was added to the solution, which was allowed to stir for several minutes. 1 mol % ammonium persulfate and 1 v/v % tetraethylethylene diamine (TEMED) was added to the solution and agitated. The solution was then poured into modified syringe molds, which were allowed to set overnight. The gels were then demolded directly into the swelling solutions.

7.4.5 Swelling and water uptake measurements

The gels were placed into approximately 200 mL of the appropriate swelling solution. The swelling solution was changed 3 times daily for two weeks. At that time, the gels were removed from the swelling solution, gently blotted on a Kim Wipe, and then weighed and measured. Gels that had been swelled in an electrolyte solution were then placed in pure water (changed 3 times daily) for a week to dialyze out salts within the gels. The swollen gels were dried under a stream of nitrogen for several days, and then under high vacuum overnight. The dehydrated network was then weighed again and swelling ratios and water uptake were calculated.

7.5 Conclusions

The ring-opening reaction that was described in Chapter 1 was utilized here to create a novel set of hydrogels from poly(oxanorbornene imide)s. Cationic (**Poly1** and **Poly2**) and zwitterionic (**Poly3** and **Poly4**) precursor ROMP polymers were reacted in water with multifunctional poly(allylamine) to form networked structures. These hydrogels were advantageous because of their synthetic simplicity and lack of additional

reagents or potentially detrimental byproducts. While their structural heterogeneity made them difficult to characterize, it was apparent that the gels were highly hydrated and that they could incorporate a wide variety of chemical functionalities. In the future, additional characterization of these gels may better highlight their properties and their utility as charged materials.

7.6 References

- (1) (a) Zhang, K.; Cui, J.; Lackey, M.; Tew, G. N. Hydrogels Based on Living Ring-Opening Metathesis Polymerization. *Macromolecules*, 2010, **43**, 10246-10252. (b) Madkour, A. E.; Grolman, J. M.; Tew, G. N. Synthesis of hydrogels *via* ring-opening metathesis polymerization: factors affecting gelation. *Polym. Chem.* 2011, **2**, 114-119.
- (2) Zhang, K.; Lackey, M. A.; Wu, Y.; Tew, G. N. Universal Cyclic Polymer Templates. *J. Am. Chem. Soc.*, 2011, **133**, 6906-6909.
- (3) Burdick, J. A.; Murphy, W. L. Moving from Static to Dynamic Complexity in Hydrogel Design. *Nat. Commun.* **2012**, doi: 10.1038/ncomms2271.
- (4) Lowe, A.B.; McCormick, C. L. Synthesis and Solution Properties of Zwitterionic Polymers. *Chem. Rev.* **2002**, *102*, 4177-41895.
- (5) Kiatkamjornwong, S.; Phunchareon, P. Influence of reaction parameters on water adsorption of neutralized poly(acrylic acid-co-acrylamide) synthesized by inverse suspension polymerization. *J. Appl. Polym. Sci.* **1999**, *72*, 1349-1366.
- (6) Schosseler, F.; Ilmain, F.; Candau, S. J. Structure and Properties of Partially Neutralized Poly(acrylic acid) Gels. *Macromolecules*, **1991**, *24*, 225-234.
- (7) Zhang, Z.; Chao, T.; Jiang, S. Physical, chemical and chemical-physical double network of zwitterionic hydrogels. *J. Phys. Chem. B.* **2008**, *112*, 5327-5332.
- (8) Kabiri, K.; Faraji-Dana, S.; Zohuriaan-Mehr, M. J. Novel sulfobetaine-sulfonic acid-contained superswelling hydrogels. *Polym. Adv. Technol.* **2005**, *16*, 659-666.
- (9) Dogu, S.; Kilic, M.; Okay, O. Collapse of acrylamide-based polyampholyte hydrogels in water. *J. Appl. Polym. Sci.* **2009**, *113*, 1375-1382.
- (10) Am Ende, M. T.; Peppas, N. A. Transport of ionizable drugs and proteins in crosslinked poly(acrylic acid) and poly(acrylic acid-co-2-hydroxyethyl methacrylate) hydrogels. I. Polymer characterization. *J. Appl. Polym. Sci.* **1996**, *59*, 673-685.

- (11) Dobbins, S. C.; McGrath, D. E.; Bernards, M. T. Nonfouling Hydrogels Formed from Charged Monomer Subunits. *J. Phys. Chem. B.* **2012**, *116*, 14346-14352.
- (12) Colak, S.; Tew, G. N. Synthesis and Solution Properties of Norbornene Based Polybetaines. *Macromolecules* **2008**, *41*, 8436-8440.
- (13) Colak, S.; Tew, G. N. Dual-Functional ROMP-Based Betaines: Effect of Hydrophilicity and Backbone Structure on Nonfouling Properties. *Langmuir* **2012**, *28*, 666-675.
- (14) Hall, H. K. Correlation of the Base Strengths of Amines. *J. Am. Chem. Soc.* **1957**, *79*, 5441-5444.
- (15) Sun, T. L.; Kurokawa, T.; Kuroda, S.; Bin Ihsan, A.; Akasaki, T.; Sato, K.; Haque, Md. A.; Nakajima, T.; Gong, J. P. Physical hydrogels composed of polyampholytes demonstrate high toughness and viscoelasticity. *Nat. Mater.* **2013**, *12*, 932-937.
- (16) Porcel, C. H.; Schlenoff, J. B. Compact Polyelectrolyte Complexes: 'Saloplastic' Candidates for Biomaterials. *Biomacromolecules* **2009**, *10*, 2968-2975.
- (17) Love, J. A.; Morgan, J. P.; Trnka, T. M.; Grubbs, R. H. A Practical and Highly Active Ruthenium-Based Catalyst that Effects the Cross Metathesis of Acrylonitrile. *Angew. Chem. Int. Ed.* **2002**, *41*, 4035-4037.

BIBLIOGRAPHY

- Ahmed, S. R.; Bullock, S. E.; Cresce, S. V.; Kofinas, P. Polydispersity control in ring opening metathesis polymerization of amphiphilic norbornene diblock copolymers. *Polymer* **2003**, *44*, 4943-4948.
- Alberts, B.; Johnson, A.; Lewis, J.; Raff, M.; Roberts, K.; Walter, P. *Molecular Biology of the Cell*. 4th Ed. Garland Science, New York, **2002**.
- Am Ende, M. T.; Peppas, N. A. Transport of ionizable drugs and proteins in crosslinked poly(acrylic acid) and poly(acrylic acid-co-2-hydroxyethyl methacrylate) hydrogels. I. Polymer characterization. *J. Appl. Polym. Sci.* **1996**, *59*, 673-685.
- Balastre, M.; Li, F.; Schorr, P.; Yang, J.; Mays, J. W.; Tirrell, M. V. A Study of Polyelectrolyte Brushes Formed from the Adsorption of Amphiphilic Diblock Copolymers Using Surface Forces Apparatus. *Macromolecules* **2002**, *35*, 9480-9486.
- Banerjee, I.; Pangule, R. C.; Kane, R. S. Antifouling Coatings: Recent Developments in the Design of Surfaces That Prevent Fouling by Proteins, Bacteria, and Marine Organisms. *Adv. Mater.* **2011**, *23*, 690-718.
- Banerjee, S.; Das, R. K.; Maitra, U. Supramolecular gels 'in action'. *J. Mater. Chem.* **2009**, *19*, 6649-6687.
- Bartels, J. W.; Cheng, C.; Powell, K. T.; Xu, J.; Wooley, K. L. Hyperbranched Fluoropolymers and their Hybridization into Complex Amphiphilic Crosslinked Copolymer Networks. *Macromol. Chem. Phys.* **2007**, *208*, 1676-1687.
- Bielawski, C. W.; Grubbs, R. H. Living ring-opening metathesis polymerization. *Prog. Polym. Sci.* **2007**, *32*, 1-29.
- Bixler, G. D.; Bhushan, B. Biofouling: lessons from nature. *Phil. Trans. R. Soc. A* **370**, 2381-2417.
- Briza, T.; Kvicala, J.; Paleta, O.; Cermak, J. Preparation of bis(polyfluoroalkyl)cyclopentadienes, new highly fluorophilic ligands for fluorour biphasic catalysis. *Tetrahedron* **2002**, *58*, 3841-3846.
- Burdick, J. A.; Murphy, W. L. Moving from Static to Dynamic Complexity in Hydrogel Design. *Nat. Commun.* **2012**, doi: 10.1038/ncomms2271.
- Callow, J. A.; Callow, M. E. Trends in the development of environmentally friendly fouling-resistant marine coatings. *Nat. Commun.* **2011**, DOI: 10.1038/ncomms1251.

- Chang, Y.; Liao, S.; Higuchi, A.; Ruaan, R.; Chu, C.; Chen, W. A Highly Stable Nonbiofouling Surface with Well-Packed Grafted Zwitterionic Polysulfobetaine for Plasma Protein Repulsion. *Langmuir* **2008**, *24*, 5453-5458.
- Chen, S.; Jiang, S. A New Avenue to Nonfouling Materials. *Adv. Mater.* **2008**, *20*, 335-338.
- Chen, S.; Li, L.; Zhao, C.; Zheng, J. Surface hydration: Principles and applications toward low-fouling/nonfouling biomaterials. *Polymer* **2012**, *51*, 5283-5293.
- Chen, Z.; Shen, Y. R.; Somorjai, G. A. Studies of polymer surfaces by sum frequency generation vibrational spectroscopy. *Annu. Rev. Phys. Chem.* **2002**, *53*, 437-465.
- Colak, S.; Tew, G. N. Amphiphilic Polybetaines: The Effect of Side-Chain Hydrophobicity on Protein Adsorption. *Biomacromolecules* **2012**, *13*, 1233-1239.
- Colak, S.; Tew, G. N. Dual-Functional ROMP-Based Betaines: Effect of Hydrophilicity and Backbone Structure on Nonfouling Properties. *Langmuir* **2012**, *28*, 666-675.
- Colak, S.; Tew, G. N. Synthesis and Solution Properties of Norbornene Based Polybetaines. *Macromolecules* **2008**, *41*, 8436-8440.
- Cooper, B. M.; Chan-Seng, D.; Samanta, D.; Zhang, X.F.; Parelkar, S.; Emrick, T. Polyester-graft-phosphorylcholine prepared by ring-opening polymerization and click chemistry. *Chem. Commun.* **2009**, *7*, 815-817.
- Darouiche, R. O. Treatment of infections associated with surgical implants. *New Engl. J. Med.* **2004**, *350*, 1422-1429.
- deRonde, B. M.; Birke, A.; Tew, G. N. Design of Aromatic-containing Cell Penetrating Peptide Mimics with Structurally Modified π -electronics. *Chem.: Eur. J.* **2015**, *21*, 3013-3019.
- Dimitriou, M. D.; Zhou, Z.; Yoo, H-S.; Killips, K. L.; Finlay, J. A.; Cone, G.; Sundaram, H, A.; Lynd, N. A.; Barteau, K. P.; Campos, L. M.; Fischer, D. A.; Callow, M. E.; Callow, J. A.; Ober, C. K.; Hawker, C. J.; Kramer, E. J. A General Approach to Controlling the Surface Composition of Poly(ethylene oxide)-Based Block Copolymers for Antifouling Coatings. *Langmuir* **2011**, *27*, 13762-13772.
- Dobbins, S. C.; McGrath, D. E.; Bernards, M. T. Nonfouling Hydrogels Formed from Charged Monomer Subunits. *J. Phys. Chem. B.* **2012**, *116*, 14346-14352.
- Dogu, S.; Kilic, M.; Okay, O. Collapse of acrylamide-based polyampholyte hydrogels in water. *J. Appl. Polym. Sci.* **2009**, *113*, 1375-1382.

- Dong, H.; Ye, P.; Zhong, M.; Pietrasik, J.; Drumright, R.; Matyjaszewski, K. Superhydrophilic Surfaces via Polymer–SiO₂ Nanocomposites. *Langmuir* **2010**, *26*, 15567-15573.
- Elwing, H. Protein absorption and ellipsometry in biomaterial research. *Biomaterials* **1998**, *19*, 397-406.
- Estephan, Z. G.; Schlenoff, P. S.; Schlenoff, J. B. Zwitteration as an Alternative to PEGylation. *Langmuir* **2011**, *27*, 6794-6800.
- Genzer, J.; Efimenko, K. Recent developments in superhydrophobic surfaces and their relevance to marine fouling: a review. *Biofouling* **2006**, *22*, 339-360.
- González-Vera, J. A.; García-López, M. T.; Herranz, R. Regioselective Base-Promoted Nucleophilic Ring Opening of Spirocyclic 2,6-Dioxopiperazines: Synthesis of *N*-(1-Carboxycyclohexyl)amino Acid Derivatives. *Eur. J. Org. Chem.* **2007**, 548-554.
- Green, T. W.; Wuts, P. G. M. *Protective Groups in Organic Synthesis*. Wiley-Interscience, New York, **1999**, 564-566, 740-743.
- Grozea, C. M.; Walker, G. C. Approaches in designing non-toxic polymer surfaces to deter marine biofouling. *Soft Matter* **2009**, *5*, 4088-4100.
- Gudipati, C. S.; Finlay, J. A.; Callow, J. A.; Callow, M. E.; Wooley, K. L. The Antifouling and Fouling-Release Performance of Hyperbranched Fluoropolymer (HBFP)–Poly(ethylene glycol) (PEG) Composite Coatings Evaluated by Adsorption of Biomacromolecules and the Green Fouling Alga *Ulva*. *Langmuir* **2005**, *21*, 3044–3053.
- Gudipati, C. S.; Greenlief, C. M.; Johnson, J. A.; Prayongpan, P.; Wooley, K. L. Hyperbranched Fluoropolymer (HBFP) and Linear Poly(ethylene glycol) (PEG) Based Amphiphilic Crosslinked Networks as Efficient Anti-fouling Coatings: An insight into the surface compositions, topographies and morphologies. *J. Polym. Sci., Part A: Polym. Chem.* **2004**, *42*, 6193-6208.
- Gunkel, G.; Weinhart, M.; Becherer, T.; Haag, R.; Huck, W. T. S. Effect of Polymer Brush Architecture on Antibiofouling Properties. *Biomacromolecules* **2011**, *12*, 4169-4172.
- Hall, H. K. Correlation of the Base Strengths of Amines. *J. Am. Chem. Soc.* **1957**, *79*, 5441-5444.
- Hancock, R. E.; Lehrer, R. Cationic peptides: a new source of antibiotics. *Trends Biotechnol.* **1998**, *16*, 82-88.
- Harder, P.; Grunze, M.; Dahint, R.; Whitesides, G. M.; Laibinis, P. E. Molecular Conformation in Oligo(ethylene glycol)-Terminated Self-Assembled Monolayers on

Gold and Silver Surfaces Determine Their Ability to Resist Protein Adsorption. *J. Phys. Chem. B* **1998**, *102*, 426-436.

Harrison, D. B.; Feast, W. J. Aqueous ring-opening metathesis polymerizations of heteropolycyclic carboxylic acids with transition-metal chlorides. *Polymer* **1991**, *32*, 558-563.

Holmlin, R. E.; Chen, X.; Chapman, R. G.; Takayama, S.; Whitesides, G. M. Zwitterionic SAMS that Resist Nonspecific Adsorption of Protein from Aqueous Buffer. *Langmuir* **2001**, *17*, 2841-2850.

Huang, C.-J.; Li, Y.; Krause, J. B.; Brault, N. D.; Jiang, S. Internal Architecture of Zwitterionic Polymer Brushes Regulates Nonfouling Properties. *Macromol. Rapid Commun.* **2012**, *33*, 1003-1007.

Hucknall, A.; Rangarajan, S.; Chilkoti, A. In Pursuit of Zero: Polymer Brushes that Resist the Adsorption of Proteins. *Adv. Mater.* **2009**, *21*, 2441-2446.

Ishihara, K.; Aragaki, R.; Ueda, T.; Watanabe, A.; Nakabayashi, N. Reduced thrombogenicity of polymers having phospholipid polar groups. *J. Biomed. Mater. Res.* **1990**, *24*, 1069-1077.

Ishihara, K.; Oshida, H.; Endo, Y.; Ueda, T.; Watanabe, A.; Nakabayashi, N. Hemocompatibility of human whole blood on polymers with a phospholipid polar group and its mechanism. *J. Biomed. Mater. Res.* **1992**, *26*, 1543-1552.

Ishihara, K.; Ziats, N. P.; Tierney, B. P.; Nakabayashi, N.; Anderson, J. M. Protein adsorption from human plasma is reduced on phospholipid polymers. *J. Biomed. Mater. Res.* **1991**, *25*, 1397-1407.

Izumrudov, V. A.; Domashenko, N. I.; Zhiryakova, M. V.; Davydova, O. V. Interpolyelectrolyte Reactions in Solutions of Polycarboxybetaines, 2: Influence of Alkyl Spacer in the Betaine Moieties on Complexing with Polyanions. *J. Phys. Chem. B* **2005**, *109*, 17391-17399.

Izumrudov, V. A.; Zelikin, A. N.; Zhiryakova, M. V.; Jaeger, W.; Bohrisch, J. Interpolyelectrolyte Reactions in Solutions of Polycarboxybetaines. *J. Phys. Chem. B* **2003**, *107*, 7982-7986.

Kabiri, K.; Faraji-Dana, S.; Zohuriaan-Mehr, M. J. Novel sulfobetaine-sulfonic acid-contained superswelling hydrogels. *Polym. Adv. Technol.* **2005**, *16*, 659-666.

Kane, R. S.; Deschatelets, R.; Whitesides, G. M. Kosmotropes Form the Basis of Protein-Resistant Surfaces. *Langmuir* **2003**, *19*, 2388-2391.

- Katritzky, A. R.; Yao, J.; Qi, M.; Chou, Y.; Sikora, D. J.; Davis, S. Ring opening reactions of succinimides. *Heterocycles* **1998**, *48*, 2677-2691.
- Keefe, A. J.; Brault, N. D.; Jiang, S. Suppressing Surface Reconstruction of Superhydrophobic PDMS Using a Superhydrophilic Zwitterionic Polymer. *Biomacromolecules* **2012**, *13*, 1683-1687.
- Kiatkamjornwong, S.; Phunchareon, P. Influence of reaction parameters on water adsorption of neutralized poly(acrylic acid-co-acrylamide) synthesized by inverse suspension polymerization. *J. Appl. Polym. Sci.* **1999**, *72*, 1349-1366.
- Kim, G.-C.; Jeong, J.-G.; Lee, N.-J.; Ha, C.-S.; Cho, W.-J. Synthesis and biological activities of endo-3,5-epoxy-1,2,3,6-tetrahydrophthalimide and its polymers. *J. Appl. Polym. Sci.* **1997**, *64*, 2605-2612.
- Kratz, K.; Breitenkamp, K.; Hule, R.; Pochan, D.; Emrick, T. PC-Polyolefins: Synthesis and Assembly Behavior in Water. *Macromolecules* **2009**, *42*, 3227-3229.
- Kratz, K.; Xie, W.; Lee, A.; Freeman, B.D.; Emrick, T. Phosphorylcholine-Substituted ROMP Polyolefin Coatings Provide Fouling Resistance to Membrane Materials. *Macromol. Mater. Eng.* **2011**, *296*, 1142-1148.
- Krishnan, S.; Ayothi, R.; Hexemer, A.; Finlay, J. A.; Sohn, K. E.; Perry, R.; Ober, C. K.; Kramer, E. J.; Callow, M. E.; Callow, J. A.; Fischer, D. A. Anti-biofouling Properties of Comblike Block Copolymers with Amphiphilic Side Chains. *Langmuir* **2006**, *22*, 5075-5086.
- Kudaibergenov, S.; Jaeger, W.; Laschewsky, A. Polymeric Betaines: Synthesis, Characterization and Application. *Adv. Polym. Sci.* **2006**, *201*, 157-224.
- Kumara Swamy, K. C.; Bhuvan Kumar, N. N.; Pavan Kumar, K.V. P. Mitsunobu and Related Reactions: Advances and Applications. *Chem. Rev.* **2009**, *109*, 2551-2651.
- Laschewsky, A. Structures and Synthesis of Zwitterionic Polymers. *Polymers* **2014**, *6*, 1544-1601.
- Leng, C.; Gibney, K. A.; Liu, Y.; Tew, G. N.; Chen, Z. In Situ Probing the Surface Restructuring of Antibiofouling Amphiphilic Polybetaines in Water. *ACS Macro Lett.* **2013**, *2*, 1011-1015.
- Lewis, A. L. Phosphorylcholine-based polymers and their use in the prevention of biofouling. *Colloids Surf., B* **2000**, *18*, 261-275.
- Lienkamp, K.; Kins, C. F.; Alfred, S. F.; Madkour, A. E.; Tew, G. N. Water-Soluble Polymers from Acid-Functionalized Norbornenes. *J. Polym. Sci.: Part A* **2009**, *47*, 1266-1273.

- Love, J. A.; Morgan, J. P.; Trnka, T. M.; Grubbs, R. H. A Practical and Highly Active Ruthenium-Based Catalyst that Effects the Cross Metathesis of Acrylonitrile. *Angew. Chem. Int. Ed.* **2002**, *41*, 4035-4037.
- Lowe, A. B.; Billingham, N. C.; Armes, S. P. Synthesis of polybetaines with narrow molecular mass distribution and controlled architecture. *Chem. Comm.* **1996**, 1555-1556.
- Lowe, A. B.; McCormick, C. L. Synthesis and Solution Properties of Zwitterionic Polymers. *Chem. Rev.* **2002**, *102*, 4177-41895.
- Lowe, A. B.; Vamvakaki, M.; Wassall, M.A.; Wong, L.; Billingham, N. C.; Armes, S. P.; Lloyd, A.W. Well-defined sulfobetaine-based statistical copolymers as potential antibioadherent coatings. *J. Biomed. Mater. Res.* **2000**, *52*, 88-94.
- Lynch, A. S.; Robertson, G. T. Bacterial and Fungal Biofilm Infections. *Annu. Rev. Med.* **2008**, *59*, 415-428.
- Maddikeri, R. R.; Colak, S.; Gido, S. P.; Tew, G. N. Zwitterionic Polymersomes in an Ionic Liquid: Room Temperature TEM characterization. *Biomacromolecules* **2011**, *12*, 3412-3417.
- Madkour, A. E.; Grolman, J. M.; Tew, G. N. Synthesis of hydrogels via ring-opening metathesis polymerization: factors affecting gelation. *Polym. Chem.* **2011**, *2*, 114-119.
- Mantovani, G.; Lecolley, F.; Tao, L.; Haddleton, D. M.; Clerx, J.; Coernelissen, J. L. M.; Velonia, K. Design and Synthesis of N-Maleimido-Functionalized Hydrophilic Polymers via Copper-Mediated Living Radical Polymerization: A Suitable Alternative to PEGylation Chemistry. *J. Am. Chem. Soc.* **2005**, *127*, 2966-2973.
- Martinelli, E. Nanostructured films of amphiphilic fluorinated block copolymers for fouling release applications. *Langmuir* **2008**, *24*, 10365-10369.
- Matson, J. B.; Grubbs, R. H. ROMP-ATRP Block Copolymers Prepared from Monotelechelic Poly(oxa)norbornenes Using a Difunctional Terminating Agent. *Macromolecules* **2008**, *41*, 5626.
- Mosquera, V. X.; Perez-Alvarez, L.; Ricoy-Martinez, E.; Mosquera-Perez, I.; Castro-Beira, A.; Cuenca-Castillo, J.J. Initial Experience With Excimer Laser-Assisted Pacemaker and Defibrillator Lead Extraction. *Rev Esp Cardiol.* **2011**, *64*, 824-827.
- Mussard, W.; Kebir, N.; Kriegel, I.; Esteve, M.; Semetey. Facile and Efficient Control of Bioadhesion on Poly(dimethylsiloxane) by Using a Biomimetic Approach. *Angew. Chem. Int. Ed.* **2011**, *50*, 10871-10874.

Ostuni, E.; Chapman, R. G.; Holmlin, R. E.; Takayama, S.; Whitesides, G. M. A survey of Structure-Property Relationships of Surfaces that Resist the Adsorption of Protein. *Langmuir* **2001**, *17*, 5605–5620.

Page, K.; Wilson, M.; Parkin, I. P. Antimicrobial surfaces and their potential in reducing the role of the inanimate environment in the incidence of hospital-acquired infections. *J. Mater. Chem.* **2009**, *19*, 3819-3831.

Page, S.M.; Parelkar, S.; Gerasimenko, A.; Shin, D.Y.; Peyton, S.; Emrick, T. Promoting cell adhesion on slippery phosphorylcholine hydrogel surfaces. *J. Mater. Chem. B* **2014**, *2*, 620-624.

Pagliari, M.; Ciriminna, R. New fluorinated functional materials. *J. Mater. Chem.*, **2005**, *15*, 4981-4991.

Polzer, F.; Heigl, J.; Schneider, C.; Ballauff, M.; Borisov, O. Synthesis and Analysis of Zwitterionic Spherical Polyelectrolyte Brushes in Aqueous Solution. *Macromolecules* **2011**, *44*, 1654-1660.

Porcel, C. H.; Schlenoff, J. B. Compact Polyelectrolyte Complexes: ‘Saloplastic’ Candidates for Biomaterials. *Biomacromolecules* **2009**, *10*, 2968-2975.

Prime, K. L.; Whitesides, G. M. Adsorption of proteins onto surfaces containing end-attached oligo(ethylene oxide): a model system using self-assembled monolayers. *J. Am. Chem. Soc.* **1993**, *115*, 10714-10721.

Rankin, D. A.; Lowe, A. B. New Well-Defined Polymeric Betaines: First Report Detailing the Synthesis and ROMP of Salt-Responsive Sulfopropylbetaine- and Carboxyethylbetaine-*exo*-7-oxanorbornene Monomers. *Macromolecules* **2008**, *41*, 614-622.

Rankin, D. A.; P’Pool, S. J.; Schanz, H-J.; Lowe, A. B. The Controlled Homogeneous Organic Solution Polymerization of New Hydrophilic Cationic *exo*-7-Oxanorbornenes via ROMP with RuCl₂(PCy₃)₂CHPh in a Novel 2,2,2-Trifluoroethanol/Methylene Chloride Solvent Mixture. *J. Polym. Sci., Part A: Polym. Chem.* **2007**, *45*, 2113-2128.

Rankin, D. A.; Schanz, H-J. Effect of the Halide Counterion in the ROMP of *exo*-Benzyl-[2-(3,5-dioxo-10-oxa-4-azatricyclo[5.2.1.0^{2,6}]dec-8-en-4-yl)ethyl]dimethylammonium Bromide/Chloride. *Macromol. Chem. Phys.* **2007**, *208*, 2389-2395.

Rodriguez Emmenegger, C.; Brynda, E.; Riedel, T.; Sedlakova, Z.; Housak, M.; Alles, A. B. Interaction of Blood Plasma with Antifouling Surfaces. *Langmuir* **2009**, *25*, 6328-6333.

Rodriquez-Emmenegger, C.; Schmidt, B. V. K. J.; Sedlakova, Z.; Subr, V.; Alles, A. B.; Brynda, D.; Barner-Kowollik, C. Low Temperature Aqueous Living/Controlled (RAFT) Polymerization of Carboxybetaine Methacrylamide up to High Molecular Weights. *Macromol. Rapid Commun.* **2011**, *32*, 958-965.

Schitter, R. M. E.; Jocham, D.; Stelzer, F.; Moszner, N.; Völkel, T. J. New routes to polyelectrolytes and reactive polymers via ROMP. *J. Appl. Polym. Sci.* **2000**, *78*, 47-60.

Schosseler, F.; Imain, F.; Candau, S. J. Structure and Properties of Partially Neutralized Poly(acrylic acid) Gels. *Macromolecules*, **1991**, *24*, 225-234.

Sharma, S.; Johnson, R. W.; Desai, T. A. Evaluation of the Stability of Nonfouling Ultrathin Poly(ethylene glycol) Films for Silicon-Based Microdevices. *Langmuir* **2004**, *20*, 348-356.

Som, A.; Tezgel, A. O.; Gabriel, G. J.; Tew, G. N. Self Activation in De Novo Designed Mimics of Cell-Penetrating Peptides. *Angew Chem., Int. Ed.*, **2011**, *50*, 6147-6150.

Song, W.; Mano, J. F. Interactions between cells or proteins and surfaces exhibiting extreme wettabilities. *Soft Matter* **2013**, *9*, 2985-2999.

Stubenrauch, K.; Fritz-Popovski, G.; Ingolic, E.; Grogger, W.; Glatter, O.; Stelzer, F.; Trimmel, G. Microphase Separation Study of Amphiphilic ROMP Block Copolymers by SAXS and TEM. *Macromolecules* **2007**, *40*, 4592-4600.

Stubenrauch, K.; Moitzi, C.; Fritz, G.; Glatter, O.; Trimmel, G.; Stelzer, F. Precise Tuning of Micelle, Core, and Shell Size by the Composition of Amphiphilic Block Copolymers Derived from ROMP Investigated by DLS and SAXS. *Macromolecules* **2006**, *39*, 5865-5874.

Su, S. C. K.; Shafer, J. A. Effect of the imidazole group on the hydrolysis of N-[2-(4-imidazolyl)ethyl] phthalimide. *J. Org. Chem.* **1969**, *34*, 2911-2915.

Sun, T. L.; Kurokawa, T.; Kuroda, S.; Bin Ihsan, A.; Akasaki, T.; Sato, K.; Haque, Md. A.; Nakajima, T.; Gong, J. P. Physical hydrogels composed of polyampholytes demonstrate high toughness and viscoelasticity. *Nat. Mater.* **2013**, *12*, 932-937.

Tauhardt, L.; Pretzel, D.; Kempe, K.; Gottschaldt, M.; Pohlers, D.; Schubert, U. S. Zwitterionic poly(2-oxazoline)s as promising candidates for blood contacting applications. *Polym. Chem.* **2014**, *5*, 5751-5764.

Toomey, R.; Tirrell, M. Functional polymer brushes in aqueous media from self-assembled and surface-initiated polymers. *Annu. Rev. Phys. Chem.* **2008**, *59*, 493-517.

- Tsai, W. B.; Grunkemeier, J. M.; Horbett, T. A. Human plasma fibrinogen adsorption and platelet adhesion to polystyrene. *J. Biomed. Mater. Res.* **1999**, *44*, 130-139.
- Ueda, T.; Oshida, H.; Kurita, K.; Ishihara, K.; Nakabayashi, N. Preparation of 2-Methacryloyloxyethyl Phosphorylcholine Copolymers with Alkyl Methacrylates and Their Blood Compatibility. *Polym. J.* **1992**, *24*, 1259-1269.
- Ueda, T.; Watanabe, A.; Ishihara, K.; Nakabayashi, N. Protein adsorption on biomedical polymers with a phosphorylcholine moiety adsorbed with phospholipid. *J. Biomater. Sci., Polym. Ed.* **1992**, *3*, 185-194.
- Voros, J. The Density and Refractive Index of Adsorbing Protein Layers. *Biophys. J.* **2004**, *87*, 553-561.
- Wang, D. A.; Williams, C. G.; Li, Q. A.; Sharma, B.; Elisseff, J. H. Synthesis and characterization of a novel degradable phosphate-containing hydrogel. *Biomaterials* **2003**, *24*, 3969-3980.
- Wang, Y.; Finlay, J. A.; Betts, D. E.; Merkel, T. J.; Luft, J. C.; Callow, M. E.; Callow, J. A.; DeSimone, J. M. Amphiphilic Co-networks with Moisture-Induced Surface Segregation for High-Performance Nonfouling Coatings. *Langmuir* **2011**, *27*, 10365-10369.
- Weck, M.; Jackiw, J. J.; Rossi, R. R.; Weiss, P. S.; Grubbs, R. H. Ring-Opening Metathesis Polymerization from Surfaces. *J. Am. Chem. Soc.* **1999**, *121*, 4088-4089.
- Weers, J. G.; Rathman, J. F.; Axe, F. U.; Crichlow, C. A.; Foland, L. D.; Scheuing, D. R.; Wiersema, R. J.; Zielske, A. G. Effect of the intramolecular charge separation distance on the solution properties of betaines and sulfobetaines. *Langmuir* **1991**, *7*, 854-867.
- Worz, A.; Berchtold, B.; Moosmann, K.; Prucker, O.; Ruhe, J. Protein-resistant polymer surfaces. *J. Mater. Chem.* **2012**, *22*, 19547-19561.
- Xu, Y.; Takai, M.; Konno, T.; Ishihara, K. Microfluidic flow control on charged phospholipid polymer interface. *Lab Chip* **2007**, *7*, 199-206.
- Yang, W. J.; Neoh, K-G.; Kang, E-T.; Teo, S. L-M.; Rittschof, D. Polymer brush coatings for combating marine biofouling. *Prog. Polym. Sci.* **2014**, *39*, 1017-1042.
- Yaroslavov, A. A.; Sitnikova, T. A.; Rakhnyanskaya, A. A.; Yu. A. Ermakov, T. C. Burova, V. Ya. Grinberg, Menger, F. M. Contrasting Behavior of Zwitterionic and Cationic Polymers Bound to Anionic Liposomes. *Langmuir* **2007**, *23*, 7539-7544.
- Youngblood, J. P.; Andruzzi, L.; Ober, C. K.; Hexemer, A.; Kramer, E. J.; Callow, J. A.; Callow, M. E. Coatings based on side-chain ether-linked poly(ethylene glycol) and fluorocarbon polymers for the control of marine biofouling. *Biofouling* **2003**, *19*, 91.

Yu, B.; Lowe, A. B.; Ishihara, K. RAFT Synthesis and Stimulus-Induced Self-Assembly in Water of Copolymers Based on the Biocompatible Monomer 2-(Methacryloyloxy)ethyl Phosphorylcholine. *Biomacromolecules* **2009**, *10*, 950-958.

Zhang, K.; Cui, J.; Lackey, M.; Tew, G. N. Hydrogels Based on Living Ring-Opening Metathesis Polymerization. *Macromolecules*, 2010, **43**, 10246-10252.

Zhang, K.; Lackey, M. A.; Wu, Y.; Tew, G. N. Universal Cyclic Polymer Templates. *J. Am. Chem. Soc.*, 2011, **133**, 6906-6909.

Zhang, Z.; Chao, T.; Chen, S.; Jiang, S. Superlow Fouling Sulfobetaine and Carboxybetaine Polymers on Glass Slides. *Langmuir* **2006**, *22*, 10072-10077.

Zhang, Z.; Chao, T.; Jiang, S. Physical, chemical and chemical-physical double network of zwitterionic hydrogels. *J. Phys. Chem. B.* **2008**, *112*, 5327-5332.

Zhang, Z.; Chen, S.; Chang, Y.; Jiang, S. Surface Grafted Sulfobetaine Polymers via Atom Transfer Radical Polymerization as Superlow Fouling Coatings. *J. Phys. Chem. B* **2006**, *110*, 10799-10804.

Zhang, Z.; Chen, S.; Jiang, S. Dual-Functional Biomimetic Materials: Nonfouling Poly(carboxybetaine) with Active Functional Groups for Protein Immobilization. *Biomacromolecules* **2006**, *7*, 3311-3315.

Zhang, Z.; Cheng, G.; Carr, L. R.; Vaisocherova, H.; Chen, S.; Jiang, S. The hydrolysis of cationic polycarboxybetaine esters to zwitterionic polycarboxybetaines with controlled properties.

Zhang, Z.; Vaisocherova, H.; Cheng, G.; Yang, W.; Xue, H.; Jiang, S. Nonfouling Behavior of Polycarboxybetaine-Grafted Surfaces: Structural and Environmental Effects. *Biomacromolecules* **2008**, *9*, 2686-2692.